Communauté
UNIVERSITÉ Grenoble Alpes

THÈSE

Pour obtenir le grade de

DOCTEUR DE LA COMMUNAUTÉ UNIVERSITÉ GRENOBLE ALPES

Spécialité : **Biologie cellulaire**

Arrêté ministériel : 25 Mai 2016

Présentée par

Céline DESBOURDES

Thèse dirigée par **Pr. Uwe SCHLATTNER**
et codirigée par
Dr. Malgorzata TOKARSKA-SCHLATTNER et Dr. Mathieu BOISSAN

préparée au sein du
Laboratoire de Bioénergétique Fondamentale et Appliquée
et de **Ecole Doctorale de Chimie et Sciences du Vivant**

Nucleoside diphosphate kinase D: a dual function mitochondrial protein

Thèse soutenue publiquement le **28 Février 2017**,
devant le jury composé de :

M. Stefan NONCHEV
Prof., Université Grenoble-Alpes, Président
Mme Maja HERAK BOSNAR
Senior Scientific Associate, Ruder Bošković Institute, Rapporteur
M. Guy LENAERS
Directeur de Recherche, Université Angers, Rapporteur
Mme Marie-Lise LACOMBE
Directrice de recherche émérite, Université P. et M. Curie, Examinatrice
M. Eric FONTAINE
Prof., Université Grenoble-Alpes, Examinateur

Abstract : The nucleoside diphosphate kinases (NDPK) are essential for generation of nucleoside triphosphates (NTPs) using ATP and NDPs. The mitochondrial NDPK isoform (NDPK-D) located in the mitochondrial intermembrane space is found to have two modes of function. First, the phosphotransfer mode in which the protein has a kinase activity like other NDPK enzymes. In this mode, NDPK-D produces GTP for the optic atrophy 1 protein (OPA1), a GTPase involved in mitochondrial fusion, and ADP for the adenylate translocator (ANT) and the mitochondrial ATPase for ATP regeneration. The second mode of function is called lipid transfer and is related to the capacity of NDPK-D to bind anionic phospholipids, especially cardiolipin (CL). In this mode, the protein can cross-link the two mitochondrial membranes and transfer CL from the inner to the outer mitochondrial membrane, which can serve as a signal for mitophagy and apoptosis. This work aims to study these NDPK-D functions in more detail. With the use of HeLa cells stably expressing the wild-type, kinase inactive (H151N mutation) or lipid binding deficient (R90D mutation) NDPK-D and mouse lung epithelial cells, we show (i) the close proximity between NDPK-D and OPA1 that leads to GTP channeling from NDPK-D to OPA1, (ii) the essential role of NDPK-D for CL externalization to the mitochondrial surface during mitophagy, serving as a recognition signal for LC3-II-autophagosomes to eliminate damaged mitochondria, (iii) the possible inhibition of CL externalization due to the presence of NDPK-D/OPA1 complexes, and (iv) a pro-metastatic phenotype of HeLa cells expressing either of the NDPK-D mutants (H151N or R90D), characterized by high invasive and migratory potential, altered proteomic profile and changed mitochondrial network structure and function. Finally, a first bacterial expression and purification strategy for full-length OPA1 has been established for future in vitro studies of NDPK-D/OPA1 complexes.

Résumé : Les nucléosides diphosphate kinases (NDPK) sont essentielles pour la génération des nucléosides triphosphates (NTPs) en utilisant l'ATP et des NDPs. L'isoforme mitochondriale de NDPK (NDPK-D), située dans l'espace intermembranaire des mitochondries, possède deux modes de fonctionnement. Dans le premier mode ("phosphotransfert"), la protéine a une activité de kinase comme les autres enzymes NDPK. Dans ce mode de fonctionnement, NDPK-D produit du GTP pour la protéine optique atrophy 1 (OPA1), une GTPase impliquée dans la fusion des mitochondries, et de l'ADP pour le translocateur à adénine (ANT) et l'ATPase mitochondriale pour la régénération d'ATP. Le second mode de fonctionnement est appelé « transfert de lipide » et est lié à la capacité de la protéine à se lier aux phospholipides anioniques, particulièrement la cardiolipine (CL). Dans ce mode NDPK-D peut réticuler les deux membranes mitochondriales et transférer CL de la membrane interne vers la membrane externe des mitochondries, pouvant servir de signal pour la mitophagie et l'apoptose. Ce travail a pour objectif d'étudier plus en détails ces différentes fonctions de NDPK-D. En utilisant des cellules HeLa exprimant de façon stable la protéine sauvage, kinase inactive (mutation H151N) ou incapable de se lier aux lipides (mutation R90D) et des cellules épithéliales de poumons de souris, nous montrons (i) une grande proximité entre NDPK-D et OPA1 qui conduit au channeling de GTP par NDPK-D pour OPA1, (ii) le rôle essentiel de NDPK-D pour l'externalisation de CL vers la surface des mitochondries pendant la mitophagie, servant de signal de reconnaissance pour le complexe LC3-II-autophagosomes afin d'éliminer les mitochondries endommagées, (iii) la possible inhibition de l'externalisation de CL par la présence de complexes NDPK-D/OPA1, et (iv) un phénotype pro-métastatique des cellules HeLa exprimant la NDPK-D mutée (H151N ou R90D), caractérisé par un fort potentiel invasif et migratoire, un profil protéique altéré, et des modifications au niveau structural et fonctionnel du réseau mitochondrial. Finalement, une première stratégie d'expression et de purification de la protéine OPA1 entière a été établie pour de futures études in vitro des complexes NDPK-D/OPA1.

Acknowledgements

Ce travail n'aurait pu être possible sans le financement par la Fondation pour la recherche médicale (FRM) et la bourse Explo'ra Doc de la région Rhones-Alpes qui m'a été accordé pour les 6 mois passés aux Etats-Unis.

J'aimerais tout d'abord adresser mes remerciements à Mme Maja HERAK BOSNAR et M. Guy LENAERS, rapporteurs; Mme Marie-Lise LACOMBE et M. Eric FONTAINE, examinateurs ainsi qu'à M. Stefan NONCHEV, président du jury, pour avoir accepté d'évaluer ce travail de thèse et pour leurs commentaires constructifs.

Mes remerciements vont également au Pr. Uwe Schlattner, mon directeur de thèse et directeur du LBFA. Merci de m'avoir permis de travailler sur ce projet novateur, pour ton esprit scientifique aiguisé et pour avoir cru, souvent plus que moi, dans les résultats obtenus.

Merci également aux Dr. Malgorzata Tokarska-Schlattner et Dr. Mathieu Boissan, pour avoir codirigé cette thèse et pour vos remarques constructives.

Merci au Dr. VE Kagan de m'avoir accueillie dans son équipe pendant 6 mois et de m'avoir permis d'accéder à des techniques de pointes pour l'analyse des lipides. Merci à toute son équipe pour leur accueil, leur aide et tout le soutien dont ils ont fait preuve envers moi. Plus particulièrement, merci à Gaowei (mon papa), Valentina (ma maman), Anastasiia, Tamil et Dariush.

J'aimerais remercier également les personnes suivantes qui ont, par différentes manières, participés au succès de ce travail: Stéphane Attia pour les purifs de NDPK-D et nos discussions au labo; Cécile Cottet (responsable de la plateforme d'imagerie) pour ton aide, tes conseils; Frédérique Lamarche (responsable de la culture cellulaire) pour tes conseils et ton aide quand j'avais des doutes sur mes cellules; Martin Pelosse pour m'avoir lancée dans ce projet de thèse avec le clonage de OPA1 et d'avoir répondu à mes questions, même bêtes; Jean-Marc Moulis pour avoir pris du temps pour me conseiller et répondre à mes préoccupations scientifiques; Laurence Kay pour avoir partagé ton bureau avec moi pendant 2 ans et pour nos discussions qui m'ont bien souvent fait relativiser; Hervé pour ton oreille attentive quand j'en avais besoin ; merci aussi à Madeleine, Karine, Cindy et tous ceux que j'aurais pu oublier parce que sans vous le LBFA ne serait pas le LBFA.

Merci également à Gérard Larmurier, pour ton travail et ta disponibilité. Je te souhaite une bonne et heureuse retraite !
Merci à Sarah Hamant tout simplement parce que tu n'es pas une secrétaire comme les autres, que tu as toujours été disponible quand j'en avais besoin. Merci également d'avoir géré l'impression et l'envoi de ma thèse!
Je remercie les autres doctorants du labo qui sont plus que des collègues et qui ont su m'apporter leur soutien lorsque nécessaire. Merci à vous Adeline, Arthur, Charline, Clovis, Camille et Morgane!

Enfin, un immense merci à mes amis :
- la Mafia italienne (Antonino, Alessandra, Federica, Paolo, Giuseppe) et les français (Elise, Anaïs et David) merci encore car ces 6 mois à Pittsburgh auraient été différents si vous n'aviez pas été là.
- Arnaud, Thibault, Louise et Guillaume : parce que vous êtes vous et qu'on ne peut s'en passer ;)
- L'ECPM team : Marion, Isabelle, Irène, Quentin (bon anniversaire), Charlotte, Clémence… parce que Strasbourg un jour, Strasbourg toujours !

Un immense merci à ma famille et belle-famille pour leur soutien surtout les derniers mois si difficiles pour nous. Merci pour tout!
Enfin, merci à toi Olivier de croire en moi comme tu le fais. Sans toi je n'aurais pas réussi…

Contents

Chapter 1

General Introduction

1.1 Mitochondria: an overview

1.1.1 Origin of mitochondria

In 1967, Margulis formulated the endosymbiotic theory whereby mitochondria would derived from the uptake of a proteobacterium in a larger host cell more than 1.5 billion years ago (O'Rourke, 2010).

The first one to report mitochondria as subcelluluar structures was Altman in 1890 who called them "bioblast". The name mitochondrion coming from the greek "mitos" (thread) and "chondros" (granule) was introduced by Benda in 1898 based on their appearance (for review (Ernster and Schatz, 1981)).

The first isolation of mitochondria was achieved by Bensley and Hoerr in 1934 (Ernster and Schatz, 1981) and improved later by introducing differential centrifugation and the use of isotonic buffer (Claude, 1930s). In 1948, a hypertonic sucrose buffer were used by Hogeboom, Schneider and Palade allowing them to obtain well-shaped mitochondria. Some years later, the hypertonic buffer was changed for an isotonic sucrose buffer leading to a better cell sedimentation and reducing the inhibitory effect of sucrose on some enzymes. Since then, this procedure is used as a reference for mitochondrial isolation. The further elaboration of this technique allowed to determine the ultrastructure of mitochondria by electron microscopy. In parallel, Kennedy and Lehninger proofed that the Krebs cycle, ß-oxidation and oxidative phosphorylation (OXPHOS) occur in mitochondria.

1.1.2 Structure of mitochondria

Mitochondria are organelles present in all of the eukaryotic cells. Also called energy powerhouse of the cell because they transform energy into ATP needed by the cell,

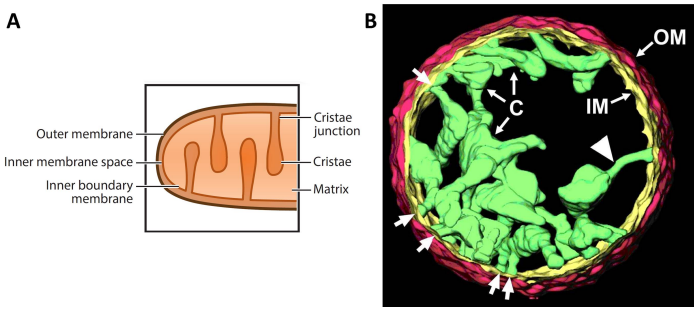

Figure 1.1 – Structure of mitochondria: **(A)** Schematic representation of a mitochondrion and its ultrastructure (taken from (Pernas and Scorrano, 2016)); **(B)** Electron tomography representation of an isolated mitochondrion from rat liver (taken from (Mannella et al., 2001)). OM: outer mitochondrial membrane, IM: inner mitochondrial membrane, C: cristae, unlabeled arrows indicate cristae junctions

mitochondria have their own DNA and ribosomes and can synthesize their own proteins. Mitochondria are round shaped organelles with a diameter of 0.5 to 1 µm and 1 to 10 µm length.

Mitochondria are made up of two membranes: the outer mitochondrial membrane (OMM) and the inner mitochondrial membrane (IMM), which one presents invaginations called cristae (Fig. 1.1). Both membranes delimit the mitochondrial intermembrane space (IMS). At the center of mitochondria, completely surrounded by IMM, is the matrix (Fig. 1.1.A).

1.1.2.1 Outer mitochondrial membrane

The outer mitochondrial membrane (OMM) constitutes the barrier which controls the diffusion of small molecules (ions, nucleotides or other metabolites) from the cytosol to the matrix through the voltage dependent anion channel (VDAC) (Cogliati et al., 2016) and protects the cell from toxic products like reactive oxygen species or mtDNA (Pernas and Scorrano, 2016) present in the matrix. The nuclear-encoded mitochondrial proteins are imported into mitochondria through the translocase of the outer membrane (TOM). Several other proteins involved in mitochondrial shape and fission/fusion dynamics (Mnf1& 2, Fis1) or apoptotic signaling (BAK) are also located at the OMM (Cogliati et al., 2016).

In addition, regions in the OMM interact with other organelles such as the endoplasmic reticulum (RE), leading to mitochondria-associated endoplasmic reticulum membranes (MAMs) structures, and with other mitochondria, forming intermitochondrial junctions (MJs) (Cogliati et al., 2016). The OMM interacts also with ribosomes or the nucleus (Pernas and Scorrano, 2016).

The lipid composition of the OMM is different from plasma membrane but similar to endoplasmic reticulum with a majority of phosphatidylcholine (PC), phosphatidylethanolamine (PE) and phosphatidylinositol (PI) (Horvath and Daum, 2013).

1.1.2.2 Inner membrane

The inner mitochondrial membrane hosts, among many other proteins, the electron transport chain and the ATP synthase as well as the adenine nucleotide transporter (ANT).

The particular lipid composition of the IMM is characterized by a high content of cardiolipin (18% of the total phospholipids, almost undetectable in OMM). In rat liver mitochondria, PC and PE represent respectively 40% and 34% of the total phospholipids (Horvath and Daum, 2013). The difference in cardiolipin (CL) contents between IMM and OMM allows the development of specific methods to measure cardiolipin externalization to the mitochondrial surface during mitophagy (Chu et al., 2013).

The IMM can be subdivided in three regions: the inner boundary membrane (IBM), the cristae junctions (CJs) and the cristae (cf Fig. 1.1.B).

IBM: the IMM is cross-linked to the OMM, through enzymes or protein complexes, in structures called contact sites. These sites are the location of protein import complexes, such as the translocase of the inner membrane (TIM), allowing the protein import from cytosol to the matrix. Contact sites can be involved in different functions such as energy transfer, protein import and apoptosis, but also in lipid transfer between IMM and OMM (Pernas and Scorrano, 2016).

CJs: Along the IMM, there are cristae which are bag-like structures separated from the IMS by narrow tubular junctions, the cristae junctions (CJs) (see Fig. 1.1.B). These junctions are 20 to 50 nm in diameter and limit the diffusion towards the IMS of important molecules and proteins for the OXPHOS system (Pernas and Scorrano, 2016; Cogliati et al., 2016).

Cristae: Cristae are the invaginations coming from CJs. They are the site of oxidative phosphorylation (OXPHOS) with a content in ATP synthase and complex III of 94% of the total and around 85% of total cytochrome C (Cogliati et al., 2016).

1.1.2.3 Intermembrane space

Due to the permeability of OMM to metabolites and proteins, the intermembrane space composition is chemically comparable to the cytoplasm in respect to low-molecular-weight solutes. For example in the liver, it has been estimated that 6% of the total mitochondrial protein is located in the intermembrane space (Alberts et al., 2002).

1.1.2.4 Matrix

The mitochondrial matrix is more viscous than the cellular cytoplasm. Enzymes, ribosomes, mtDNA and other metabolites (ATP, Mg^{2+}, Ca^{2+}, K^{+}...) compose the matrix. The matrix is the site of the Krebs cycle and the ß-oxidation of fatty acids.

1.1.3 Mitochondria: the energy powerhouse of the cell

Mitochondria are also called energy power house of the cell because they harbor the lasts steps in the respiratory cycle which produces ATP molecules needed for the cell to maintain its functions. Indeed, the glucose coming from the nutrients is degraded in pyruvate by the glycolysis process in cytosol. In aerobic condition, the pyruvate will enter mitochondria and will be converted to acetyl-coA. Acetyl-coA will then enter the Krebs cycle which is coupled to mitochondrial oxidative phosphorylation to give energy.

Pyruvate oxidation Glucose is converted to two molecules of pyruvate by glycolysis which occurs in the cytoplasm. Pyruvate molecules are transported into the mitochondrial matrix where they are converted into acetyl-coenzyme A (acetyl-CoA) by the pyruvate deshydrogenase according to the chemical reaction 1.1. The acetyl-CoA is then used in the Krebs cycle for $FADH_2$ and NADH production.

$$Pyruvate + NAD^{+} + CoA \longrightarrow acetyl - CoA + NADH + CO_2 \tag{1.1}$$

Krebs cycle After the transformation of glucose in pyruvate by glycolysis and the oxidation of pyruvate into acetyl-CoA, the third step for energy recovery from glucose is the Krebs cycle. This cycle occurs in the mitochondrial matrix during which acetyl-CoA is oxidized by a sequence of eight reactions (Fig. 1.2).

The Krebs cycle produces 2 **GTP** molecules per glucose like for glycolysis. However, the most important is the production, during glycolysis and Krebs cycle, of "high energy" electrons carried by NADH and $FADH_2$, which are then used in the oxidative phosphorylation for the principle mitochondrial ATP production.

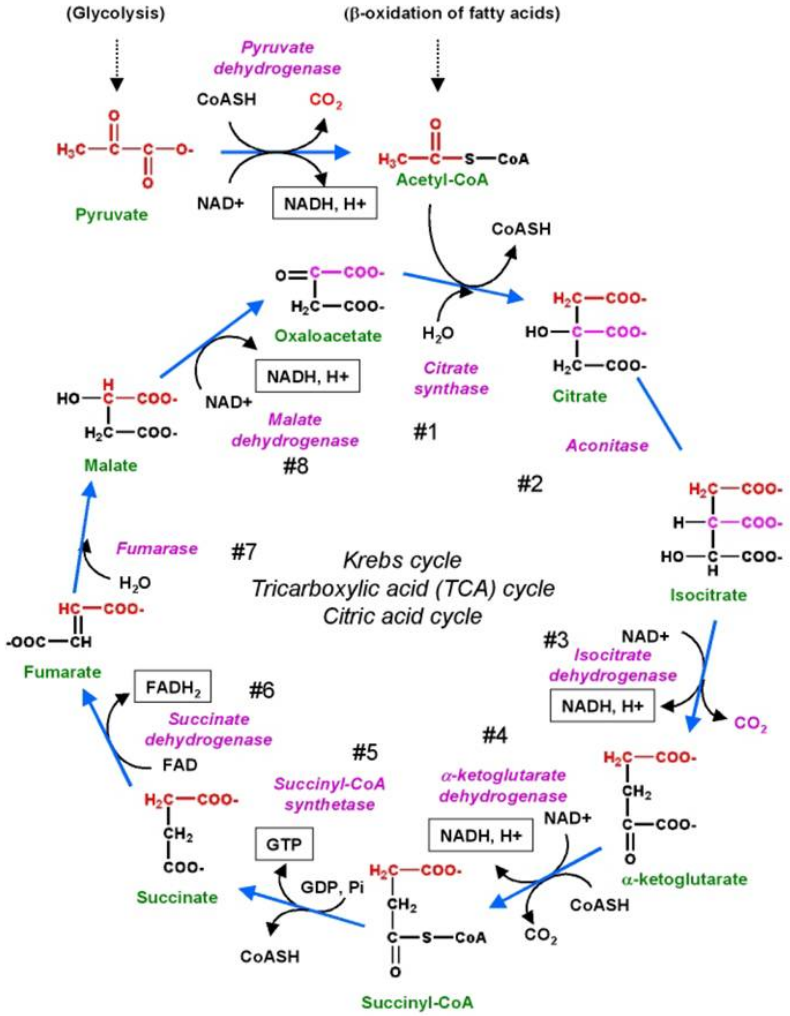

Figure 1.2 – Krebs cycle. (Figure taken from http://www.mikeblaber.org/oldwine/-BCH4053/ Lecture36)

Oxidative phosphorylation The high-energy electrons carried by NADH and $FADH_2$ and produced during glycolysis and Krebs cycle, are oxidized by the mitochondrial electron transport chain (ETC). Four multi-protein complexes are embedded in the IMM and constitute the ETC. Three of them are proton-pumping enzymes (complex I, III and IV) which generate proton motive force by pumping H^+ out of the matrix and thus driving the ATP synthase. The ubiquinone (Q) and soluble cytochrome c are used for electron transport between the different membrane-embedded complexes (Fig. 1.3). NADH enters in the ETC by complex I (NADH-ubiquinone oxidoreductase) and $FADH_2$ by succinate-quinone oxidoreductase (complex II). Both of them reduce Q to ubiquinol (QH_2). QH_2 is then used by complex III (cytochrom c oxidase) for cytochrome c reduction. Complex IV uses cytochrome c for final oxygen reduction into h_2 (Fig. 1.3, complex IV).

The proton re-entry from the IMS back to the matrix along the proton gradient drives the complex V (ATP synthase) leading to the production of ATP molecules (Fig. 1.3, complex V).

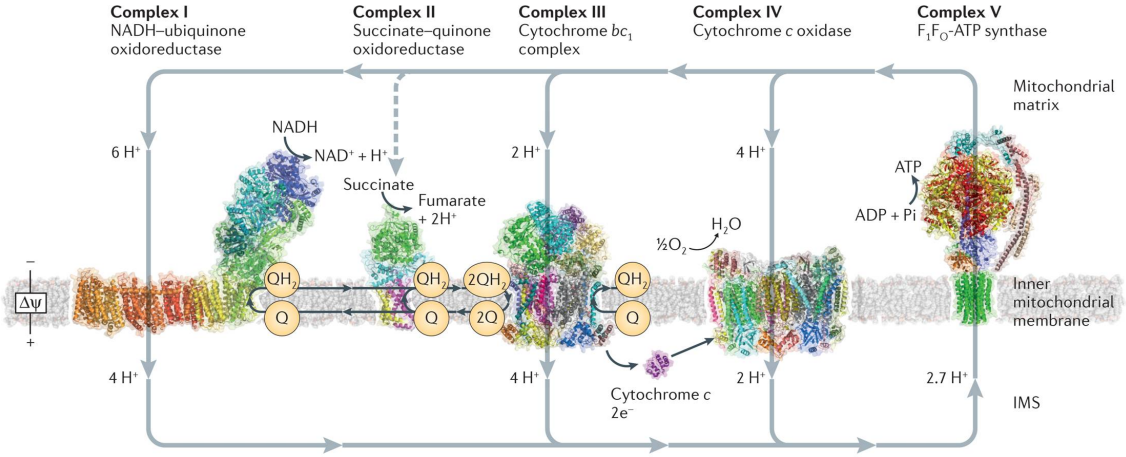

Figure 1.3 – The mitochondrial electron transport chain and ATP synthase. Q: ubiquinone, QH_2: ubiquinol, IMS: intermembrane space, $\Delta\Psi$: mitochondrial membrane potential. (Figure taken from (Sazanov, 2015))

1.1.4 Mitochondrial lipid synthesis

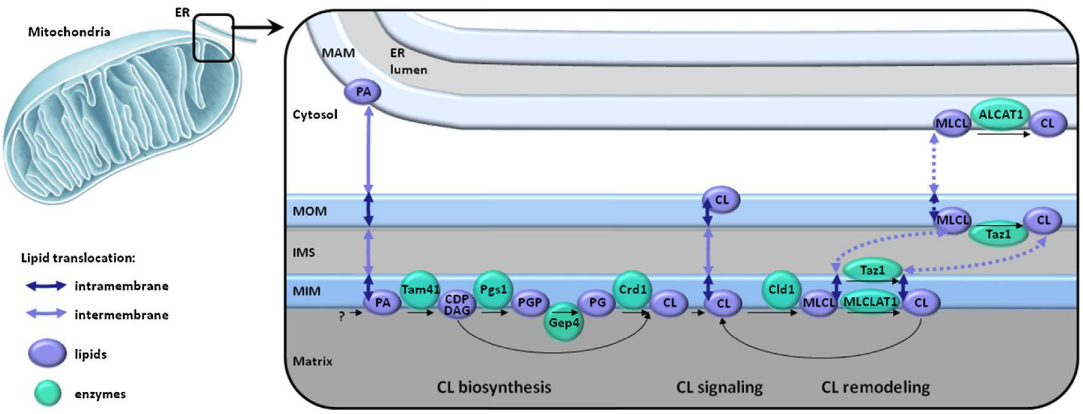

Figure 1.4 – Mitochondrial phospholipids synthesis pathway and CL remodeling. MOM: mitochondrial outer membrane (OMM); MIM: mitochondrial inner membrane (IMM) (Figure taken from (Schlattner et al., 2014))

Mitochondrial membranes have a specific lipid composition. Most of the lipids are synthesized in the endoplasmic reticulum (ER) and transported to mitochondria by interaction between ER and OMM in structures called mitochondria associated membranes (MAMs). However, phospholipids such as PE, PA, PG and CL are directly produced by mitochondria (Horvath and Daum, 2013; Osman et al., 2011). As shown in figure 1.4, the majority of CL is synthesized in the IMM using phosphatidic acid (PA) coming from ER via phosphatidylglycerol (PG) as an intermediate. Phosphatidylethanolamine (PE) is produced by conversion of phosphatidylserine (PS) imported from ER.

1.1.5 Mitochondrial dynamics

Mitochondria are dynamic organelles involved in several cellular processes. They can fuse and form long filaments, or undergo fission, leading to isolated round mitochondria. This dynamic behavior normally maintains a balance between fusion and fission that depends on a specific metabolic demand. Mitochondrial fusion and fission are drived by large GTPase proteins belonging to the dynamin family, all well conserved between yeast, mammals and flies.

Fission Fission is the process by which one mitochondria will be divided in two or more daughter mitochondria. In mammals, the fission is achieved by the cytosolic dynamin-related protein 1 (Drp1) and the mitochondrial fission protein 1 (Fis1) located at the OMM facing the cytosol (Chan, 2006). For a successful fission, cytoplasm, cytoskeletal and organellar elements need to be coordinated. The three steps of fission

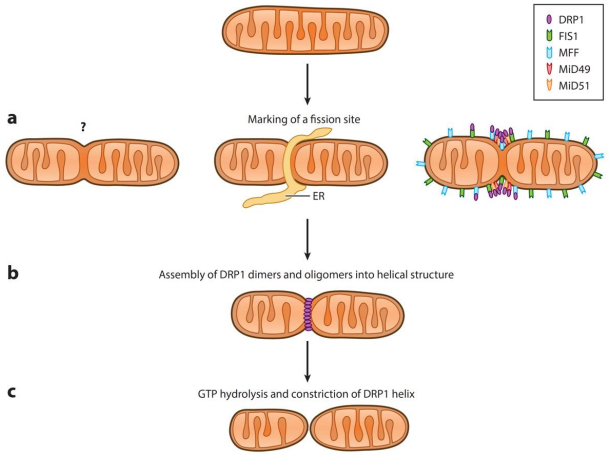

Figure 1.5 – Mitochondrial fission process. ER: endoplasmic reticulum; Drp1, Fis1, MFF, MiD49 and MiD51, profusion proteins described in the text (Figure taken from (Pernas and Scorrano, 2016))

are the following (Fig. 1.5): *(i)* marking of fission site; (ii) dimer/oligomers of Drp1 combine around the marked fission site into an helical-shaped superstructure; (iii) fission of the mitochondria by tightening of the Drp1 helix using GTP hydrolysis.

The Drp1 assembly is facilitated by closely associated ER. Indeed, division of mitochondria occurs at the ER-mitochondria contact sites and data support the model in which ER supported by cytoskeletal machinery begin to tighten mitochondria, therefore helping to recruit Drp1 (Pernas and Scorrano, 2016).

Other proteins might be involved in Drp1 recruitment on the OMM. How these proteins work with the cytoskeletal machinery and ER for Drp1 recruitment and fission is not yet understood. However, proteins have been localized in mammalian mitochondria: mitochondrial fission factor (MFF), mitochondrial dynamics proteins 49 kDa and 51 kDa (MiD49 and MiD51), and fission 1 (Fis1). Fis1 knock-down induces elongation whether its overexpression induces fragmentation. MFF is involved in the steady-state recruitment of Drp1, independently of Fis1. Knock-down of MFF leads to elongation and decrease of Drp1 recruitment at the mitochondrial surface; its overexpression induces mitochondrial fragmentation. MiD49 and 51 specifically recruit Drp1 to mitochondria and not to peroxisome like Fis1 and MFF can do. MiD51 activates or inhibits fission according to cytosolic demand. For MiD49, it is not clear whether it is a profusion or profission factor but it is suggested to work like MiD51.

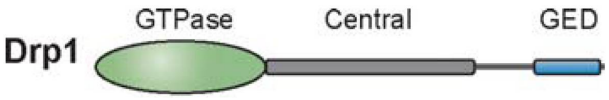

Figure 1.6 – Schematic structure of Drp1 fission protein. . GED: GTPase effector domain. (Figure taken from (Chan, 2006))

The dynamin related protein 1 (Drp1) identified as a key player in mitochondrial

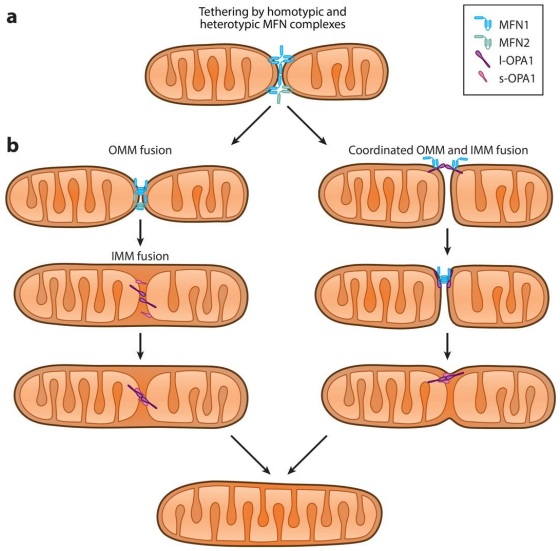

Figure 1.7 – Mitochondrial fusion process. Mfn1, Mfn2 and s-/l-OPA1 are pro-fusion proteins described in the text. (Figure taken from (Pernas and Scorrano, 2016))

fission is mainly found in the cytosol. Drp1 has the typical GTPase domain conserved within the dynamin family at its N-terminus and a GTPase effector domain at its C-terminus (fig. 1.6). Drp1 is the only known protein driving fission, and thus it is interesting that in Drp1$^{-/-}$ mouse embrionic fibroblast (MEF) cells mitochondrial fission still occurs (Pernas and Scorrano, 2016). This suggests the presence of another fission machinery.

Fusion Mitochondrial fusion allows mitochondria to exchange mtDNA, metabolites, lipids or proteins depending on the cellular demand. In mammals, fusion of mitochondria is performed by Mitofusin 1 and 2 (Mfn1 and 2) for the OMM and OPA1 for the IMM (Chan, 2006; Pernas and Scorrano, 2016). The steps for mitochondrial fusion are the following (Fig. 1.7): (i) two mitochondria are coming in close proximity, (ii) once in contact, Mfn1&2 form homotypic or heterotypic oligomers between mitochondria and mediate OMM fusion, (iii) IMM fusion occurs via OPA1 which depends on inner membrane potential. It is not known if IMM and OMM fusion occur independently or simultaneously *in vivo*. Moreover, OPA1 is required on only one IMM unlike Mgm1 (yeast homolog of OPA1) which is required on both IMM for a successful fusion.

Mitofusins are large GTPases proteins from the dynamin family located at the OMM. They have a GTPase domain at their N-terminus, hydrophobic heptad repeat (HR) regions and a transmembrane domain which orients the GTPase domain to the cytosolic side (Fig. 1.8). Cells lacking one of the Mfn protein have a loss of mitochondrial fusion and a fragmented mitochondrial network. If both Mfn are knocked-down, cells have no mitochondrial fusion resulting in fragmented mitochondria and poor mitochondrial function (Chen et al., 2005). It seems also that Mfn1 and Mfn2 have similar function.

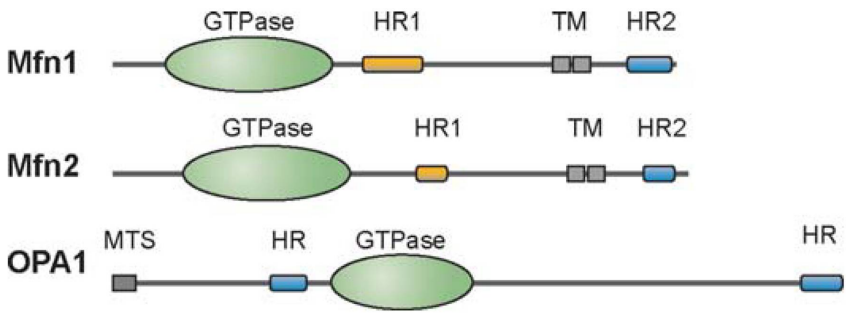

Figure 1.8 – Mitochondrial fusion proteins. Mfn1 and Mfn2 are involved in OMM fusion whereas OPA1 is involved in IMM fusion. TM: transmembrane domain, HR: heptad repeat region, MTS: mitochondrial targeting sequence.(Figure taken from (Chan, 2006))

Indeed, overexpression of one of the Mfn protein in cells can rescue the mitochondrial fusion defect due to the loss of the other Mfn homolog.

OPA1 is a GTPase which belongs to the dynamin family. Localized at the IMM, the protein has a transmembrane domain at its N-terminus, which allows the protein to be anchored in the IMM and exposing the GTPase domain towards the intermembrane space (Fig. 1.8). OPA1 will be described more in detail in the following section 1.2.

1.1.6 Mitophagy and Apoptosis

Mitophagy Mitophagy is the specific autophagic process whereby damaged mitochondria are removed or degraded. This process was first observed by electron microscopy in mammalian cells. During mitophagy, mitochondria are sequestered into vesicles (lysosomes) coated with the autophagosome marker LC3 (microtubule-associated protein light chain 3). Mitophagy helps to recycle and maintain a pool of healthy mitochondria in cells according to the metabolic demand. Different stimuli can initiate mitophagy in mammals: nutrient deprivation or starvation (by inhibition of the mTOR pathway), mitochondrial DNA damage, inhibition of the respiratory chain, mitochondrial membrane depolarization, photo-damage, ROS overproduction and mitochondrial dynamics (fission/fusion) (Deas et al., 2011; Zhang, 2015). Different mediators are involved in mitophagy induction, such as cardiolipin (Chu et al., 2013) or the choline dehydrogenase (CHDH) (Zhang, 2015), but most of all the best studied PINK1/Parkin pathway.

The PINK1-Parkin pathway is depicted in Figure 1.9. The PTEN-induced kinase 1 (PINK1) has a mitochondrial targeting sequence which targets the protein to mitochondria. In normal conditions, PINK1 imported to IMM through translocases TOM, is cleaved by the rhomboid-like protease (PARL) and then degraded by proteasome. In contrast, e.g in a depolarized mitochondria, PINK1 import and PARL activity are inhibited, thus, PINK1 accumulates at the OMM and recruits the cytosolic E3 ubiquitin

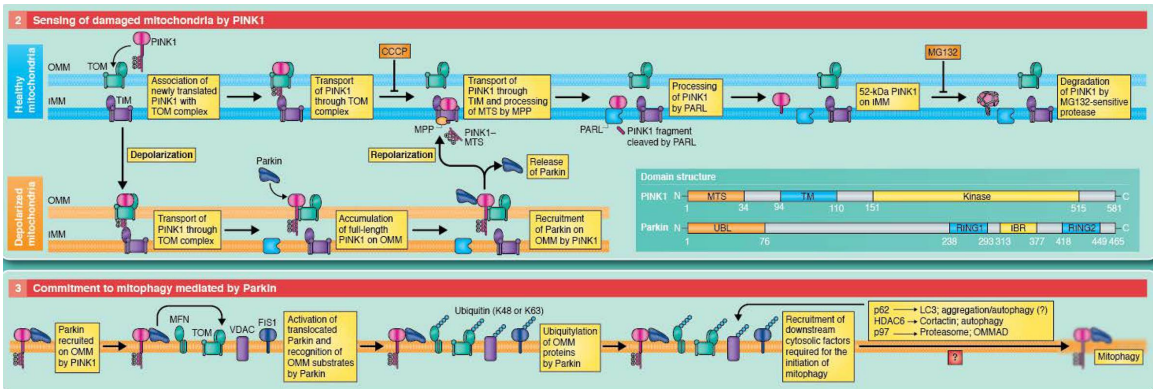

Figure 1.9 – Mitophagy process description with the PINK-Parkin pathway. (Figure taken from (Jin and Youle, 2012))

ligase, Parkin (Jin and Youle, 2012). The recruited Parkin ubiquitilates OMM proteins such as the voltage-dependant anion channel (VDAC), Mfn1-2, TOM, Fis1 and mitochondrial Rho GTPase (MIRO1-2). Ubiquitinated OMM proteins will then interact with LC3-II on the autophagosomal membrane and direct the mitochondria towards the lysosomes.

In addition, other receptors such as NIX, BNIP3 and FUNDC1, localized at the OMM, are found to recruit LC3-II coated lysosomes.

Apoptosis Apoptosis, the programmed cell death, naturally occurs during embryonic development, tissue homeostasis or immune system response. Deregulation of the apoptotic pathway can lead to uncontrolled cell proliferation leading to cancer, autoimmune and neurodegenerative diseases. Apoptosis can follow two pathways, the extrinsic pathway which is initiated by the binding of a specific ligand on a death receptor anchored in the cell membrane. This induces the activation of caspase 8 and initiates apoptosis (Parsons and Green, 2010). The second pathway is called intrinsic pathway due to involvement of mitochondria.

The intrinsic pathway is the mitochondrial mediated apoptotic pathway initiated by stimuli such as DNA damage, chemotherapeutic agents or growth-factor privation (Wang and Youle, 2009; Parsons and Green, 2010). The critical step in this intrinsic pathway is the permeabilization of the OMM (MOMP). Indeed, MOMP allows release of pro-apoptotic proteins such as cytochrome C and Smac/DIABLO (second mitochondria derived activator of caspase/direct inhibitor of apoptosis-binding protein) from the IMS to the cytoplasm for downstream caspase activation. Once released in the cytosol, cyt C will be engaged in formation of the apoptosome complex with dATP, Apaf-1 and the initiator caspase 9 (Fig. 1.10). This structure acts as a platform for caspase 9 activation which will then activate effector caspase by cleavage. Without efficient MOMP, cyt c would not be released in cytoplasm and thus caspases could

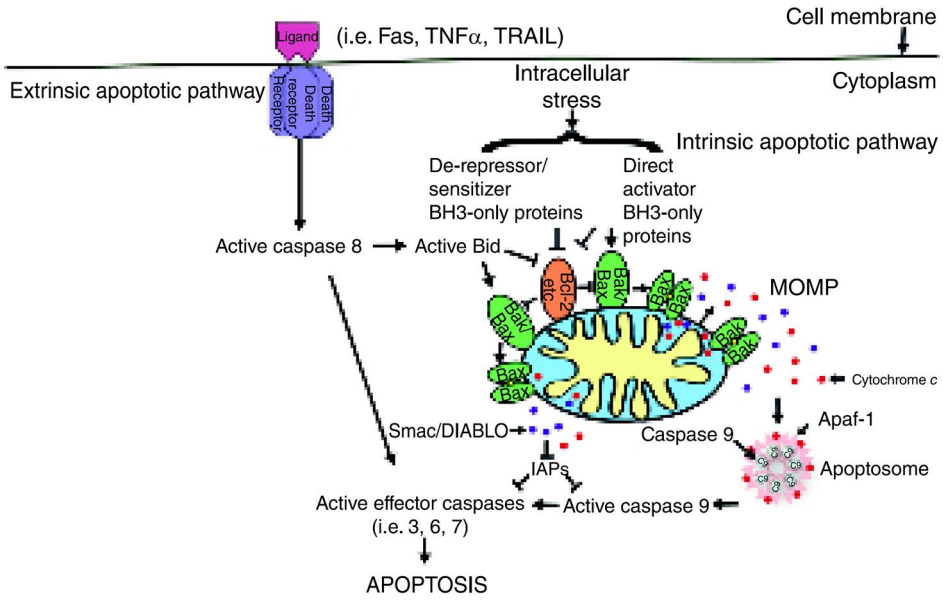

Figure 1.10 – Apoptotic pathways. Extrinsic (on the left) and intrinsic pathways on the right are depicted. (Figure taken from (Parsons and Green, 2010))

not be activated. Thus apoptosis could not take place. The release of Smac/DIABLO protein helps for activation of caspases 9 and effector. Indeed, it will neutralize the inhibitor of apoptosis proteins (IAPs) by binding, thus allowing caspase 9 to be activated and avoiding the inhibition of caspase effectors by IAPs. Moreover, other factors such as mitochondrial dynamics, bioenergetics state or cristae remodeling play a role in MOMP as well as the global physiological state of mitochondria.

As mentioned before, MOMP is a crucial step for irreversible induction of apoptosis. MOMP is regulated by proteins from the Bcl-2 family. These Bcl-2 proteins can be divided into three groups: pro-apoptotic , anti-apoptotic and BH3-only members (Fig. 1.11). BH3-only proteins are pro-apoptotic proteins regulating the other two classes of the Bcl-2 family by binding. Proteins of the anti-apoptotic class bind and sequester pro-apoptotic proteins thus inhibiting MOMP and cyt C release. BH3-only and pro-apoptotic members are both pro-apoptotic and mainly cytosolic except the Bak protein localizing also to OMM (Fig. 1.10). In presence of apoptotic stimuli, Bak forms a complex with Bax on OMM, thus permeabilizing OMM e.g. by forming pores. IMS proteins are released in the cytosol and caspase activation is initiated. BH3-only proteins do not permeabilize OMM but are thought to activate Bak/Bax directly or by inhibiting the anti-apoptotic members.

These BH3-only proteins respond to an intracellular stress triggered e.g. by growth-factor withdrawal or DNA damage to initiate the apoptotic pathway.

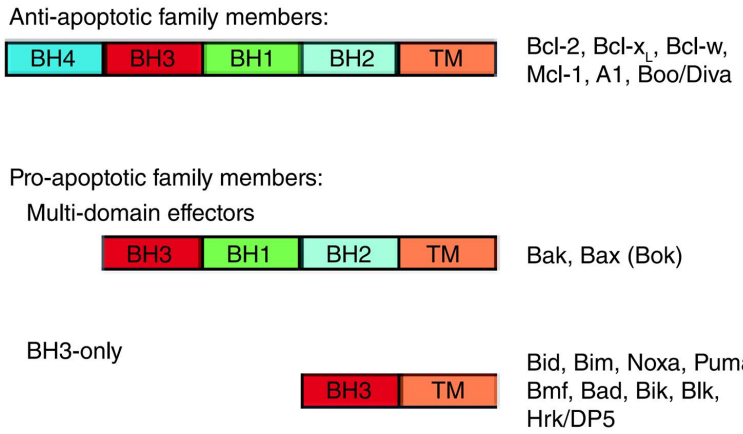

Figure 1.11 – Bcl-2 protein family. Bcl-2 proteins family members can be organized in three groups of proteins: anti-apoptotic, pro-apoptotic and BH3-only members. BH, BH homology domains; TM, transmembrane domain. (Figure taken from (Parsons and Green, 2010))

Once OMM is permeabilized and the mitochondrial membrane potential is lost, also ROS production increases. Reorganisation of cristae due to OPA1 cleavage can affect MOMP process. Also, fission/fusion of mitochondria could affect MOMP due to interaction of Bcl-2 family members with proteins of the fission/fusion machinery during apoptosis.

1.2 OPA1: GTPase involved in mitochondrial dynamics

The optic atrophy 1 protein (OPA1) is a mitochondrial GTPase which belongs to the dynamin family. The protein is involved in mitochondrial dynamics, mitochondrial bioenergetics and mutation in its gene leads to a mitochondrial disease.

1.2.1 OPA1 muations: ADOA disease

OPA1 is an ubiquitous protein with a tissue specific expression profile. Indeed the highest expression levels are found in brain, testis, skeletal muscle and retina (Delettre et al., 2001). Mutations in the opa1 gene leads to the autosomal dominant optic atrophy (ADOA), a hereditary optic neuropathy with a frequency ranging from 1:12000 to 1:50000. ADOA is characterized by the degeneration of the optic nerve due to loss of retinal ganglion cells leading to blindness (Delettre et al., 2000).

1.2.2 OPA1 processing during mitochondrial life

OPA1 is encoded by the *opa1* gene constituted of 31 exons, 3 of which are alternatively spliced (exons 4, 4b and 5b). The alternative splicing of the *opa1* gene leads to eights

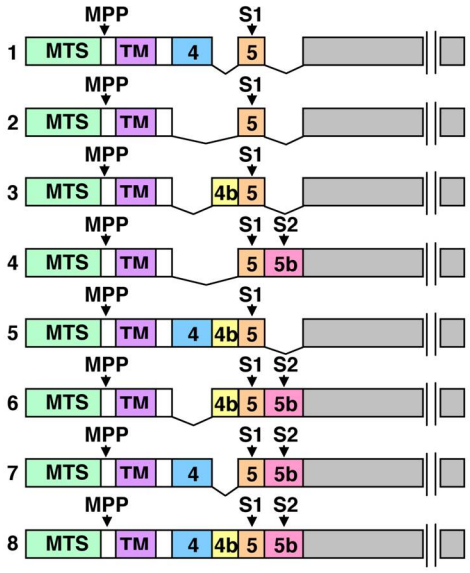

Figure 1.12 – OPA1 alternatively spliced variants. MTS: mitochondrial targeting sequence, MPP: cleavage site of the MPP protease, TM: transmembrane domain, 4, 4b and 5b are the alternatively spliced exons, S1 and S2 are the cleavage sites for OMA1 and YME1L respectively. (Figure taken from (Song et al., 2007))

mRNAs (Delettre et al., 2001; Song et al., 2007) (Fig. 1.12). All the OPA1 isoforms are composed of a mitochondrial targeting sequence at the N-terminus, followed by a transmembrane domain, the well conserved GTPase domain, a middle domain and a GTPase effector domain which allows intra- or inter-OPA1 interactions. OPA1 is anchored in the IMM by its N-terminus transmembrane domain facing the intermembrane space, and seems to be mostly concentrated close to cristae invaginations (Olichon et al., 2002).

During mitochondrial life, long (l-OPA1) isoforms can be cleaved at two sites into short (s-OPA1) isoforms. While l-OPA1 is anchored in the IMM, s-OPA1 is soluble in the mitochondrial intermembrane space. Splice variants and proteolytic cleavage generally leads to (at least) five apparent OPA1 bands between 84 and 96 kDa on Western blots. These bands correspond to two long isoforms (l-OPA1) and three short one (s-OPA1) (Ishihara et al., 2006; Griparic et al., 2007). Cleavage of l-OPA1 isoforms is performed at two distinct sites, S1 (exon 5) and S2 (exon 5b), by different enzymes (fig. 1.12). S1 cleavage is proposed to be performed by OMA1 or PARL (Belenguer and Pellegrini, 2013) whereas the cleavage at S2 might be performed by a i-AAA protease, YME1L (Wai and Langer, 2016; Anand et al., 2014). The proteolytic cleavage at S1 is enhanced by CCCP treatment without increasing S2 cleavaged products. This means cleavage at the two sites can be differentially regulated e.g. collapse of the inner mitochondrial membrane potential induces l-OPA1 cleavage at S1 (Song et al., 2007) (Fig.1.13).

Olichon et al. investigated the role of the alternatively spliced exons in the *opa1*

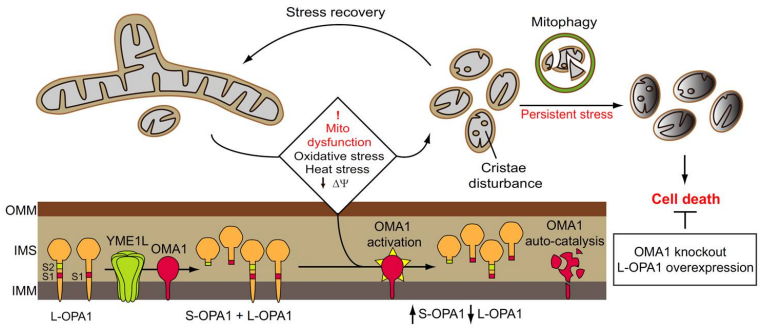

Figure 1.13 – Relation between mitochondrial fragmentation and OPA1 degradation. (Figure taken from (MacVicar and Langer, 2016))

gene (Olichon et al., 2007). For exon4, they showed that a siOPA1 with ex4 leads to mitochondrial fragmentation and mitochondrial membrane potential dissipation without cyt C release. They conclude that ex4 variants are needed for mitochondrial fusion. At the same time they excluded exons 4b and 5b from any involvement in regulating inner mitochondrial membrane potential and fusion.

By contrast, exons 4b and 5b were involved in pro-apoptotic pathways. OPA1 containing exon 5b might have a specific conformation which allows sequestration of cyt C. Variants with the exons 4b and 5b have the specific capacity to trap cyt c inside mitochondria and especially within cristae.

The underlying hypotesis is that proteins containing domain 5b can form an homopolymerizing coiled-coil structure which, by higher order assembly, might maintain the cristae junction tight and thus cyt C inside the cristae. OPA1 variants with domain 4b might regulate the complex formation involving domain 5b OPA1. Since domain 4b is also a target of pro-apoptotic proteins such as tBid or Bik, it could be involved in disassembling the OPA1 complex, leading to cyt C release into the IMS (Olichon et al., 2007).

Finally, several studied agree that l-OPA1 is involved in mitochondrial fusion, while s-OPA1 may have a role in fission due to colocalization of s-OPA1 with the fission machinery in OMM (Anand et al., 2014; Ishihara et al., 2006; MacVicar and Langer, 2016).

1.3 Nucleoside Diphosphate Kinase D: a multifunctional protein

Nucleoside diphosphate kinase was first discovered in 1953 in yeast and pigeon breast muscle (Lacombe et al., 2000). Activity measurements of the protein revealed variation depending on the tissue and the cellular compartment analyzed. The highest activity

was found in cytoplasm but some was also detected in nuclei, mitochondria or associated to membranes (Jacobus W and Evans, 1977).

In 1990, the primary structure for NDPK were reported for the first time for *Myxoccus xanthus*, *Dictyostelium* and rat (Lacombe et al., 2000). This helped to discover that the product of two regulatory genes, independently isolated, are NDP kinases. One is involved in mammalian tumor malignancy (*nm23*) and the other one, *awd*, is essential for *Drosophila* development. The human NDPK isoforms were discovered by a large cDNA screening and by similarity to the first discovered isoforms.

1.3.1 NDPK family

Nucleosides diphosphates kinases are ubiquitous enzymes belonging to the class of transferases (EC 2.7.4.6). They catalyze the transfer of γ -phosphate between nucleoside tri- and diphosphates following the reaction 1.2.

$$ATP + NDP \rightleftharpoons ADP + NTP \tag{1.2}$$

To date, 10 human isoforms of NDPK are identified but they do not all present a NDP kinase activity. As shown in Tables 1.1 and 1.2, NDPK isoforms can be organized in two groups (Boissan et al., 2009; Lacombe et al., 2000): the first one is composed of the isoforms A to D (H1 to H4), which are proteins sharing a high sequence identity (58 to 88%, Table 1.1) and presenting NDPK activity. The second group (Nm23-H5 to H9) contains proteins which share a lower sequence identity with group I and between each other (22 to 44%, Table 1.1), with no NDPK activity except for H6. Group II proteins are mainly found in testis, while group I proteins are ubiquitous.

NDPKs proteins have regulatory functions in differentiation, normal and tumor development (reviewed in (Boissan et al., 2009)). For example, NDPK-A and B are highly expressed in tumors. It has been shown that the decrease of NDPK-A expression correlates with the increase of the metastatic potential in melanomas and in breast, liver, ovary and colon carcinomas (Milon et al., 1997).

Table 1.1 – Human NDPK/Nm23 isoforms with their percentage of identity.(taken from (Boissan et al., 2009)

Group I				Group II							
	H2	H3	H4	H5	H6	H7A	H7B	H8A	H8B	H8C	H9
H1	**88**	**67**	**58**	*32*	*31*	*31*	*29*	*NS*	*22*	*28*	*30*
H2	**100**	**65**	**59**	*34*	*33*	*30*	*29*	*NS*	*22*	*28*	*29*
H3		**100**	**61**	*30*	*37*	*29*	*29*	*28*	*25*	*26*	*30*
H4			**100**	*32*	*31*	*29*	*28*	*NS*	*25*	*24*	*26*
H5				*100*	*40*	*44*	*27*	*31*	*35*	*34*	*38*
H6					*100*	*38*	*29*	*31*	*32*	*32*	*35*
H7/A						*100*	*29*	*33*	*36*	*31*	*34*
H7/B							*100*	*NS*	*22*	*33*	*34*
H8/A								*100*	*NS*	*22*	*38*
H8/B									*100*	*26*	*33*
H8/C										*100*	*31*

Group I and II Nm23/NDPKs are represented in bold and italic values, respectively.Values represent the % identity between the NDPK domains of each protein. XRP2 protein, which possesses one partial NDPK domain missing the catalytic histidine and presenting 25 and 21% identity with Nm23-H2 and Nm23-H6, respectively, and no significant homology with the other isoforms, was not included in the table. The various isoforms are indicated as H1 to H10. NS: non significant

Table 1.2 – NDPK family characteristics.(taken from (Lacombe et al., 2000))

Isoform	Size (aa)	Mass (Da)	p*I*	Locus	Tissular expression[b]	Subcellular localization[c]	NDPK activity	Comments
Nm23-H1	152	17,149	5.83	17q21.3	Ubiquitous[1] (kidney, liver, intestine, brain)	Cytoplasmic	Yes	Overexpressed in tumors; inverse correlation with metastatic potential
Nm23-H2	152	17,298	8.52	17q21.3	Ubiquitous[2] (heart, liver, pancreas, kidney)	Cytoplasmic, nuclear	Yes	Overexpressed in tumors; transcription factor (PuF) for c-*myc* proto-oncogene
Nm23-H3	168	18,903	6.91	16q13[a]	Ubiquitous[1] (pituitary gland, cerebellum, adrenal gland)	Cytoplasmic	Yes	Overexpression suppresses granulocyte differentiation and induces apoptosis of myeloid cells. N-terminus of 17 aa
Nm23-H4	187	20,659	10.3	16p13.3	Ubiquitous[2] (prostate, liver, heart)	Mitochondrial	Yes	Associated with mitochondrial membranes (contact sites?); N-terminus of 33 aa
Nm23-H5	212	24,236	5.89	5q21.3	Testis (traces in brain and kidney)[2]	Nd[d]	Not found	Expressed in male germinal cells C-extension of 51 aa
Nm23-H6	186	21,142	8.51	3p21.3	Ubiquitous (skeletal muscle, placenta)[2] (kidney, heart, spleen)[3]	Mitochondrial, Cytoplasmic	Yes	A role in regulation of cell growth and cell cycle progression?
Nm23-H7	376	42,492	6.03	1q24	Mainly in testis,[3] (also in liver, heart, brain, ovary, small intestine, and spleen)	Nd[d]	Nd	Duplicated NDP kinase domain. N-terminus of 85 aa
Nm23-H8	588	67,270	4.9	7	Mainly in testis[3]	Nd[d]	Nd	N-terminal thioredoxin domain; triplicated NDP kinase domain; human dynein IC1 equivalent?

[a] Another chromosomal localization was reported in 16p13.3 (GenBank acc. no: AL031718).
[b] The tissular expression was analyzed by hybridization of specific probes to the Human RNA Master blot (1) and to Northern blot (MTN blot) (2), both available from Clontech, and by RT-PCR (3). Tissues which present the highest expression are indicated in parenthesis.
[c] Chromosomal localizations of *nm23*-H1 to -H8 genes were reported by Varesco *et al.* (1992), Backer *et al.* (1993), Martinez *et al.* (1997), Milon *et al.* (1997), Munier *et al.* (1998), Mehus *et al.* (1999), and Tsuiki *et al.* (1999), Mehus and Lambeth (1999), and Mehus and Lambeth, unpublished, based on high throughput genomic DNA sequence from chromosome 7.
[d] nd, not determined.

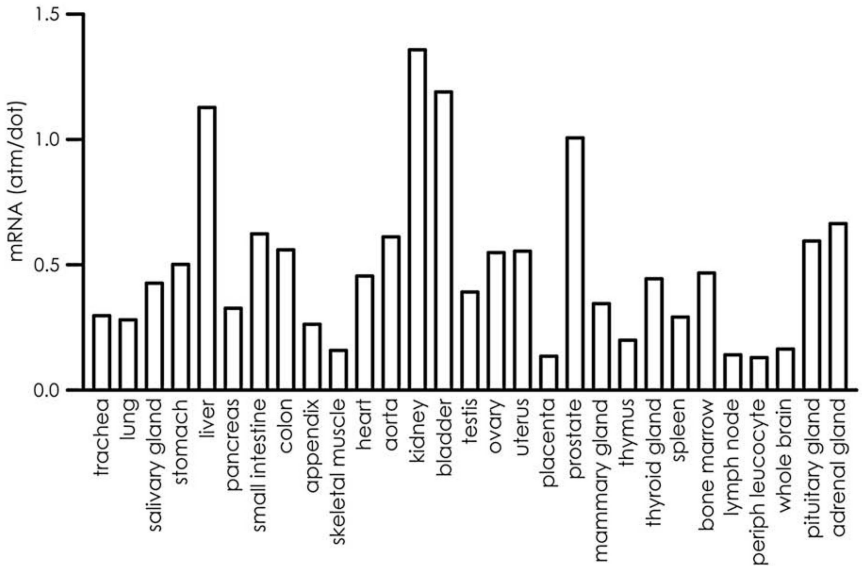

Figure 1.14 – Expression level of NDPK-D in human tissues. (taken from (Lacombe et al., 2009))

1.3.2 NDPK-D

The nucleoside diphosphate kinase D (NDPK-D), also called Nm23-H4 for non metastatic protein 23 human isoform 4 was first described in 1997 ((Milon et al., 1997)). It is a 20 kDa protein (mainly localized in the mitochondrial intermembrane space) and the only isoform within the NDPK family with a classical mitochondrial targeting sequence of 33 amino acids at its N-terminus, localizing the protein exclusively in mitochondria (Milon et al., 2000; Tokarska-Schlattner et al., 2008; Boissan et al., 2009). Sharing 56% and 55% identity with NDPK-A and NDPK-B respectively, NDPK-D belongs to the group I of NDPK isoforms (Table 1.1) and presents a NDP kinase activity. Indeed, the protein possesses the critical His151, that is transiently phosphorylated during phosphotransfer, and other conserved residues characteristic for the active site of NDPK proteins (Lys45, Tyr85, Phe33, Arg121, Thr127, Arg138, Asn148, Glu162), involved in nucleotide binding and catalysis (Milon et al., 1997).

NDPK-D: an ubiquitous protein. As mentioned above, NDPK-D belongs to group I of NDPK family and is probably expressed in every tissue. However, the expression level of this NDPK isoform depends on the tissue as shown in figure 1.14. The highest level of NDPK-D is found in kidney, liver, bladder and prostate (Milon et al., 1997; Lacombe et al., 2009).

NDPK-D structure. NDPK-D, like the other isoforms of group I, forms a hexameric complex ((Milon et al., 2000)) (fig. 1.15). Comparison of the amino acid sequences reveals some differences between NDPK-D and NDPK-A or B. Near the conserved

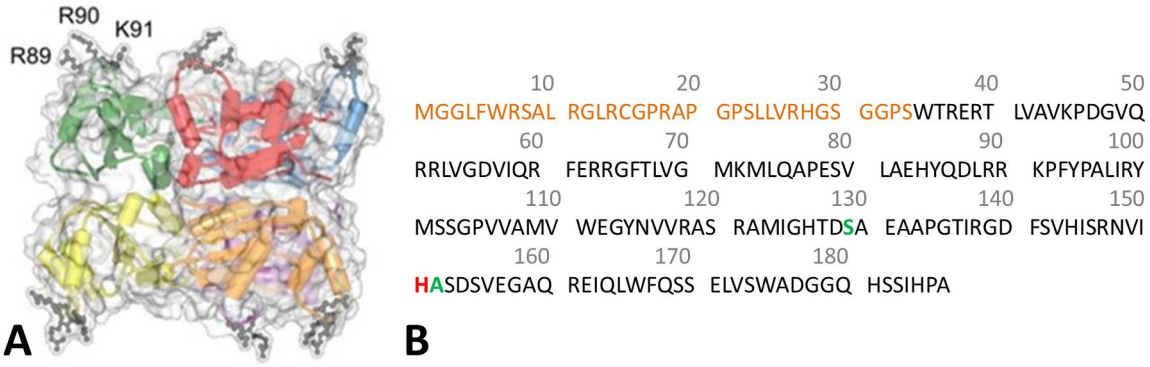

Figure 1.15 – Structural insight of NDPK-D with **(A)** Hexameric structure of the protein (figure taken from (Schlattner et al., 2013a), PDB:1EHW) and **(B)** Amino acid sequence of the protein with the amino acids from the MTS labeled in orange, the conserved His151 labeled in red and the changed Ser129, Al152 labeled in green. R89, R90 and K91 correspond to cationic amino acids involved in to anionic phospholipids binding.

His151 (H red in fig. 1.15.B), a glycine is changed into an alanine at position 152 (green A in fig. 1.15.B). This leads to a modification of the initial consensus motif NXXHGSD, present in A and B isoforms, to NXXHASD in NDPK-D (Milon et al., 2000). The serine 129 (green S in fig. 1.15.B) present in NDPK-D is replaced by a proline in NDPK-A and B. This modification is equivalent to the K-pn mutation in *awd* gene in Drosophilla (Milon et al., 1997) which is known to destabilize the intersubunit interaction within the hexamers.Indeed, its mutation to Proline greatly stabilize the protein ((Milon et al., 2000)). At the C-terminus of the protein, a YE motif conserved in other isoforms and involved in the stabilization of the hexameric structure of the protein is neither present in NDPK-D. Moreover, a cationic triad (R89, R90 and K91 in fig.1.15.A) has been identified in each NDPK-D monomer. This motif is exposed to the top and bottom faces of the hexameric structure of the protein (fig.1.15.A) and identified to interact with anionic lipids from membranes (Tokarska-Schlattner et al., 2008).

Phosphotransfer activity. NDPK-D, due to its location in the IMS, uses mitochondrially generated ATP for the generation of other NTPs, especially GTP when considering the nucleotide composition of the compartiment (Lacombe et al., 2000). Indeed, ANT continuously provides ATP into the IMS, driving the phosphotransfer activity of NDPK-D towards ATP consumption. ADP produced is then reimported by ANT into the matrix for rephosphorylation, stimulating respiration. Co-immunoprecipitation experiments revealed an interaction between NDPK-D and OPA1 (Schlattner et al., 2013a). Since NDPK-D can produce GTP, it has been postulated that the kinase could directly fuel OPA1 with GTP. In addition, the phosphotransfer activity of the protein is dependent on the lipid binding state of the protein (Schlattner et al., 2013a). Indeed,

when the protein binds cardiolipin-membranes on both of the two opposite lipid binding faces (see below), phosphotransfer activity is completely inhibited. However, when the protein is only bound to membranes with one of its binding faces, kinase activity occurs as well as the stimulation of the respiration. Experimentally, the lipid binding deficient mutant of the protein (R90D mutation) is less efficient in stimulating respiration even though it has the same NDP kinase activity (Tokarska-Schlattner et al., 2008).

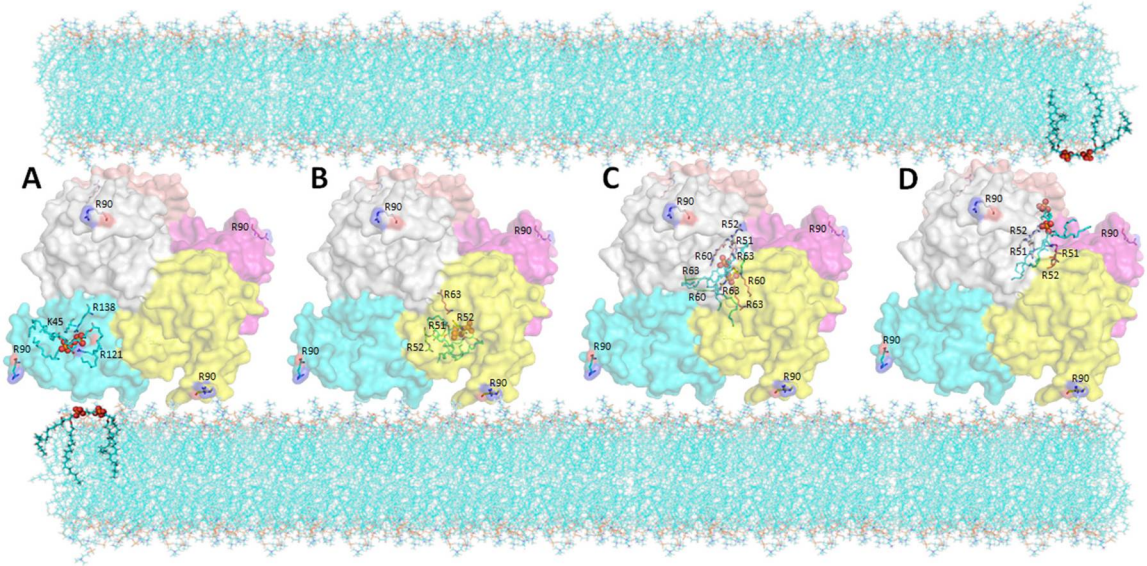

Figure 1.16 – Molecular modeling of cardiolipin-binding sites in Nm23-H4 and putative lipid transfer mechanisms. Colors of the NM23-H4 hexamer (1EHW) indicate the different chains (A–D, surface representation). Arg-90 is highlighted in all structures. CL is indicated in green, with phosphates highlighted as red spheres. Arginine and lysine residues within 5 Å of the CL phosphates are shown. (Figure taken from (Schlattner et al., 2013a))

Lipid transfer activity. In cells, NDPK-D is found associated to mitochondrial membranes (Milon et al., 2000; Tokarska-Schlattner et al., 2008). *In vitro* experiments show that NDPK-D is able to bind to and to transfer anionic lipids between membranes. The protein can cross-link two membranes, without fusing them, and transfer lipids between them (intermembrane lipid transfer) (Epand et al., 2007; Tokarska-Schlattner et al., 2008). However, both membranes need to contain cardiolipin for the transfer to occur. Probably, cardiolipin has to mediate an initial cross-linking step before anionic lipids can be transferred.

Furthermore, HeLa cells expressing the wild-type protein show mitochondrial accumulation of Bax and an increased sensitivity to apoptosis when cells are treated with rotenone. In cells expressing a lipid binding-deficient mutant of NDPK-D (i.e. carrying the mutation R90D), this accumulation and sensitivity to apoptosis is less important (Schlattner et al., 2013a). This shows that NDPK-D-mediated cardiolipin transfer between IMM and OMM is involved in pro-apoptotic signaling. When the protein is unable to bind to membranes and intermembrane CL transfer does not occur, this

protects cells against apoptosis. CL transfer to OMM is also a pro-mitophagic signal as the externalized CL at the mitochondrial surface is recognized by LC3-autophagosome (Chu et al., 2013).

Finally, in its lipid transfer function and under mitophagic stress, NDPK-D transfers cardiolipin to the OMM which is then exposed to the mitochondrial surface, through flippases action, and acts as an "eat-me" signal for the autophagic machinery.

Computational modeling and molecular docking allowed the elaboration of a model for the CL transfer between membranes (Fig. 1.16) (Schlattner et al., 2013a). Docking revealed cardiolipin binding pockets in the hexameric structure of the protein. This could allow the transfer of CL from sites to sites (see A, B, C and D in Fig. 1.16) until OMM. In addition, computational modeling based on dynamics calculations revealed that the loop containing the Arg90 residue, involved in cardiolipin binding, is the most flexible within the hexamer. A rotary wheel movement of the hexamer might allow CL transfer from IMM to OMM.

Bifunctional nanoswitch model. Due to its dual activity, NDPK-D is supposed to work according to a bifunctional nanoswitch model ((Schlattner et al., 2015)). In its phosphotransfer mode, NDPK-D provides GTP into IMS and directly for OPA1 and stimulates respiration through ADP regeneration. In the lipid transfer mode, the protein cross-links IMM and OMM allowing CL transfer from IMM to OMM.

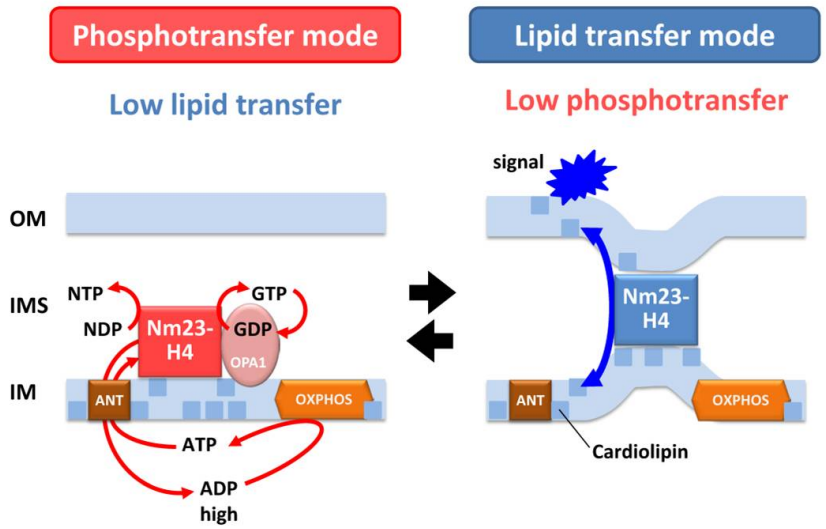

Figure 1.17 – Model for the dual function of NDPK-D/NM23-H4 (bifunctional nanoswitch). In phosphotransfer mode (left, elements in red/brown/orange), the hexameric NDPK-D only binds to one membrane, mainly the mitochondrial inner membrane (IMM), and thus maintains phosphotransfer activity. Since there is no bridging to the mitochondrial outer membrane (OMM), lipid transfer activity is low or absent. In this mode, NDPK-D regenerates NTP (mainly GTP) in the intermembrane space (IMS), in particular for local use, e.g., by the interacting GTPase OPA1. NDPK-D also channels ADP via ANT into the matrix space for stimulation of oxidative phosphorylation (OXPHOS) and ATP regeneration. In the lipid transfer mode (right, elements in light and dark blue), the symmetrical NDPK-D hexamers are fully membrane-bound, i.e., attached simultaneously to IMM and OMM. This cross-linking inhibits phosphotransfer activity, but allows for intermembrane lipid transfer, in particular of cardiolipin. Final migration of cardiolipin (or oxidized cardiolipin) to the mitochondrial surface is suggested to serve as a signal for mitophagy or apoptosis. The mechanism responsible for switching between the two modes is currently unknown, but may depend on the availability/accessibility of cardiolipin and other anionic phospholipids in the IMM outer leaflet and the OMM inner leaflet, or interacting proteins like OPA1. (Figure taken from (Schlattner et al., 2015))

The trigger which allows to switch between the two functional modi of the protein could be the degree of membrane binding of the protein. When NDPK-D is unbound to membrane or by only bound on one of the binding faces of the hexamer, the protein is in the phosphotransfer mode (Fig. 1.17, left side). When the protein is bound simultaneously to two membranes by its two binding faces, the protein is phosphotransfer inactive and the lipid transfer mode is active (Fig. 1.17, right side).

Chapter 2

Bacterial expression of NDPK-D and OPA1

Note: Expression of OPA1 is a manuscript in preparation. C.D. was responsible for the entire work on OPA1 expression and purification.

2.1 Introduction and objectives

As detailed in the general introduction, NDPK-D has a dual function (Schlattner et al., 2013a). In the phosphotransfer mode, NDPK-D produces GTP. It is supposed that this GTP is used primarily for the mitochondrial GTPase OPA1, as immunoprecipitation experiments show an interaction between both proteins (Schlattner et al., 2013a), and further evidence could be provided within this thesis (Chapter 3). OPA1 is involved in mitochondrial inner membrane fusion and cristae maintenance (Pernas and Scorrano, 2016; Wai and Langer, 2016). The second NDPK-D function in intermembrane lipid transfer may also be linked to OPA1. As we show in this thesis (Chapter 3), this function can lead to externalization of cardiolipin (CL) at the mitochondrial surface during mitophagy, a process involving an early cleavage of OPA1.

To gain more insight into the OPA1/NDPK-D interaction by *in vitro* experiments, our goal was to express and purify both proteins. NDPK-D expression and purification has already been achieved (Milon et al., 2000). For OPA1, only the soluble GTPase domain has been recombinantly expressed and purified (Ban et al., 2010; Griparic and Van Der Bliek, 2005; Pernas and Scorrano, 2016). However, for our study we also need the full-length protein including the transmembrane domain to test both for their interaction with NDPK-D. This chapter first presents the expression and purification of NDPK-D as established in the laboratory. It then gives a detailed description of the set-up and optimization for OPA1 expression and purification. Further, the methods used to characterize the recombinant OPA1 are explained.

2.2 Material and methods

2.2.1 Culture media

E. coli cultures were grown in Luria broth (LB, Sigma, France) medium containing 10 g/l NaCl, 10 g/l tryptone and 5 g/l of yeast extract in distilled water. The solid form for culture dishes was obtained by addition of 1.5 % (w/v) Agar (Eurobio, France). If needed, the following antibiotics were added at the indicated concentrations: ampicillin (100 mg/l), kanamycin (50 mg/l) and chloramphenicol (45 mg/l).

2.2.2 Bacterial strains

E. coli BL21 Star™(DE3) and BL21CodonPlus-(DE3)-RIPL were used for expression of recombinant proteins; BL21CodonPlus-(DE3)-RIPL with the additional rare codon tRNAs provided was in particular used for expression of the insoluble form of OPA1 recombinant.*E. coli* BL21-(DE3)-RIL were used for expression of recombinant NDPK-D. *E. coli* MACH1 was used for plasmid preparations. Every *E.coli* strain listed were purchased chemically competent (see Table2.1 for more information).

Table 2.1 – Characteristics of the bacterial strains used in the study.

Strain	Genotype	Manufacturer
BL21 Star (DE3)	F^- ompT hsdSB (rB^-mB^-) gal dcm rne131 (DE3)	Invitrogen
BL21CodonPlus-(DE3)-RIPL	F^- ompT hsdS(rB^- mB^-) dcm^+ Tetr gal λ(DE3) endA Hte [argU proL Cam^r] [argU ileY leuW Strep/Specr]	Agilent technologies
BL21CodonPlus-(DE3)-RIL	F^- ompT hsdS(rB^- mB^-) dcm^+ Tetr gal λ(DE3) endA Hte [argU ileY leuW Cam^r]	Agilent technologies
MACH1	F^- Φ80(lacZ) ΔM15 ΔlacX74 hsdR(rK^-mK^+) ΔrecA1398 endA1 tonA	Invitrogen

2.2.3 Transformation

E. coli MACH1 (200 µl) were transformed with plasmid as follows: 15 µl of ligation mix or 100 ng of purified plasmid were added to 200 µl bacteria and incubated 30 min on ice. The tube was then warmed up at 42°C in a water bath for 1 min and cooled down on ice for 2 min. Then LB medium (800 µl) without antibiotics was added and the tube

was incubated 1h at 37°C while shaking. After incubation, the tube was centrifuged at 700 g for 4 min. The supernatant was discarded and the pellet was re-suspended in 100 µl LB, plated on a LB/Ampicillin agar plate and incubated overnight at 37°C.

E. coli BL21 Star™(DE3) (100 µl) were transformed with pACE-10His-Opa1(2.1.C) vector (see section2.2.5.3 for description) as follows: 45 ng plasmid was added to bacteria and incubated 30 min on ice and then 30 sec at 42°C in a water bath before cooling down the tube on ice for 2 min. Then, LB medium (800 µl) without antibiotics was added and the tube was incubated 1h at 37°C while shaking. After incubation, the tube was centrifuged at 700 g for 4 min. The supernatant was discarded and the pellet was re-suspended in 100 µl LB, plated on a LB/Ampicillin agar plate and incubated overnight at 37°C.

E. coli BL21CodonPlus-(DE3)-RIPL (100 µl) were transformed with 45- ng of plasmid, according to the manufacturer's protocol (*Agilent Technologies*).

E. coli BL21-(DE3)-RIL (100 µl) were transformed with pET-28b vector containing NDPK-D cDNA (Milon et al., 2000) and carrying resistance to kanamycin with the same protocol as for textitE. coli BL21 Star™(DE3) except that bacteria were plated on a LB/kanamycin/chloramphenicol agar plate.

2.2.4 Recombinant NDPK-D

2.2.4.1 NDPK-D expression

The gene corresponding to the human NDPK-D wild-type protein, lacking the first 33 amino acids corresponding to the mitochondrial targeting peptide and carrying a His-tag at its N-terminus (Milon et al., 2000) is inserted in the bacterial plasmid pET-28b. In these plasmids, the inserted gene is under the control of the T7 promoter (Studier and Moffatt, 1986) which is inhibited by the repressor LacI. The addition of isopropyl ß-D-1-thiogalactopyranoside (IPTG) in the culture medium allows gene transcription and thus the production of the desired protein. The plasmid transformed into *E. coli* BL21-(DE3)-RIL (see section 2.2.3 for protocol) was grown at 37°C in LB medium supplemented with kanamycin and chloramphenicol. The expression of the protein was induced with 0.5 mM IPTG for 3h at 37°C. After expression, bacteria were centrifuged at 4000 rpm (rotor JS-4 Beckman coulter, 4050 g) for 45 min at 4°C, the pellet, washed with 150 mM NaCl solution, centrifuged again at 4000 rpm (rotor JS-4 Beckman, 4050 g) for 15 min at 4°C, is stored at -20°C until use.

2.2.4.2 NDPK-D purification

NDPK-D purification included three steps and two affinity chromatography steps with Blue Sepharose and NiNTA.

Lysis The bacterial pellets were re-suspended with 40 ml lysis buffer (10 mM Tris-HCl pH 7, 100 mM NaCl, 1 mM EDTA, protease inhibitor cocktail) supplemented with 1 µl/40 ml Benzonase and sonicated with a tip sonicator for 10 times 20 sec at 70% cycle and 70% power, on ice. The lysate was then centrifuged at 25 000 g (rotor JA-20, Beckmann) for 1h at 4°C. The supernatant was immediately used for chromatography.

Blue Sepharose chromatography. The Blue Sepharose 6 Fast Flow (*GE Healthcare Life Sciences*) matrix was manually packed into a 10 ml column and used in an Äkta system. The column was equilibrated with equilibration buffer (10 mM Tris pH7, 20 mM NaCl, 1 mM DTT, 0.1 mM EDTA). The lysate was diluted 5 times with equilibration buffer without NaCl in order to decrease the salt concentration to 20 mM. The injection of the diluted lysate ($\simeq$ 100 ml) was performed at a flow rate of 0.5 ml/min. The column was then washed with 50 ml equilibration buffer and elution was performed with 30 ml elution buffer (10 mM Tri-HCl pH8, 50 mM NaCl, 5 mM $MgCl_2$, 3 mM ATP, 0.1 mM EDTA, 1 mM DTT). 3 ml fractions were collected and loaded on SDS-PAGE. Fractions containing NDPK-D were pooled and used for NiNTA chromatography.

NiNTA affinty chromatography. The NiNTA Superflow matrix (*Qiagen*) was manually packed into a 10 ml column connected to an Äkta system. The resin was equilibrated with equilibration buffer (10 mM Tris pH 8, 50 mM NaCl) before injection of the fractions from Blue Sepharose at a flow rate of 1 ml/min. The flow-through was collected and elution was performed by applying a gradient from 0 to 100% elution buffer (10 mM Tris pH 8, 50 mM NaCl, 1 mM DTT, 200 mM imidazole) over 20 min at 1 ml/min and collecting 1 ml fractions. Samples of fractions were loaded on SDS-PAGE to check the efficiency of the purification process.

2.2.5 Recombinant OPA1

2.2.5.1 Reagents and molecular cloning kits

Primers used for amplification and sequencing were synthetized by Eurogentech (Belgium). Restriction enzymes, Phusion polymerase, dNTP, BSA and buffers were from NEBiolabs. Commercial kits used for plasmid extraction or purification were from Macherey-Nagel (Tab.2.2). DNA length marker (Generuler 1 kb DNA ladder) was from Thermo Scientific.

Table 2.2 – Commercial kits used for molecular cloning steps

Product	Purpose	Manufacturer
PCR clean-up Gel extraction	PCR product purification and DNA extraction from agarose gel	Macherey-Nagel
NucleoSpin plasmid	Plasmid extraction and purification from bacteria	Macherey-Nagel

Antiprotease cocktail (cOmplete tablets-EDTA free, 1 tabs per 50 ml of solution) was from Roche. Lysozyme was from Sigma and Benzonase® was from Merck. The NiNTA affinity resin was from Qiagen (NiNTA Superflow).

2.2.5.2 Agarose gel electrophoresis

Agarose gels containing 1% Agarose in 1x TAE buffer (40 mM Tris-Acetate pH 8,3 and 1 mM EDTA) were used for DNA plasmid analysis. Ethidium bromide was added to the gel at a final concentration of 0.05 µl/ml in order to visualize DNA bands with UV light. DNA samples and DNA ladder were mixed with 6x loading dye (10 mM Tris-HCl pH7.6, 0.03% Xylene cyanol FF, 0.03% bromophenol blue, 60 mM EDTA and 60% glycerol) before loading. Gels were run at 50V for 1h in 1x TAE buffer.

2.2.5.3 OPA1 plasmid

The OPA1 gene sequence used in this study corresponds to the mitochondrial precursor of splice variant 1 (registered as O60313 in the Uniprot database, see fig.1.12). The origin was introduced into the bacterial vector pACE-10His of the ACEMBL expression system which adds an N-terminal 10x His-tag to the inserted protein which is cleavable by TEV protease. This yielded the OPA1 vector pACE-10His-OPA1(2.1.C) (Fig.2.1). pACE-10His plasmids carry ampicillin resistance for selection, and protein expression is under control of the T7 promotor and the lacO repressor, thus inducible by IPTG.

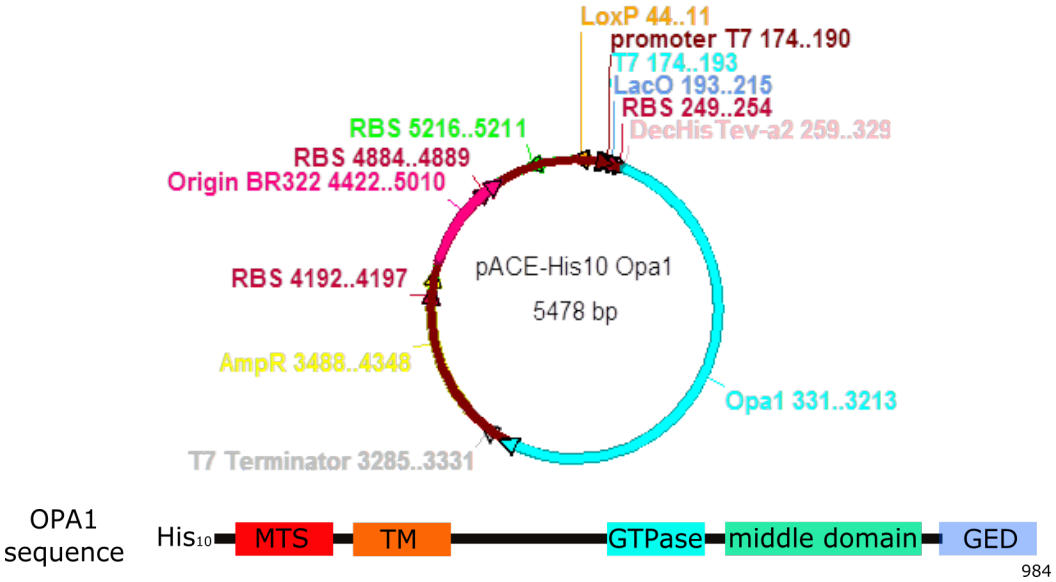

Figure 2.1 – OPA1 plasmid pACE-10His-Opa1(2.1.C). Top: Plasmid map of pACE-10His-OPA1. Bottom: Schematic representation of the domain structure of this OPA1 protein. His_{10}: 10 histidin tag, MTS, red: mitochondrial targeting sequence, TM, orange: transmembrane domain, GTPase, turquoise: GTPase domain, GED, light blue: GTPase effector domain.

2.2.5.4 Plasmid construction

The OPA1 sequence from mammalian vector pMSCV-OPA1 (from addgene) was subcloned into the microbial vector pACE-His10a2-T172A using conventional molecular biology methods (Sambrook et al., 1989). This procedure is summarized in the following steps:

PCR The opa1 cDNA from pMSCV-OPA1 was amplified by a polymerase chain reaction (PCR) using two primers (Table 2.3). The PCR reaction mix contained: 1 µl pMSCV-OPA1 at 53.5 ng/l, 1 µl of each primers, 1 µl dNTP, 10 µl buffer 5x (High fidelity or GC Phusion), 0.5 µl Phusion® High fidelity DNA polymerase, 35.5 µl sterilized water. The PCR reaction was run according to the program shown in Table 2.4, and PCR efficiency checked on 1% Agarose gel electrophoresis. DNA fragments were purified with the "PCR clean-up-Gel extraction" kit following the manufacturer's protocol *(Macherey-Nagel)* and eluted with 25 µl of NE buffer.

Table 2.3 – PCR primers used for opa1 amplification. In bolt: restrictions sites ; underlined: nucleotides that hybridize; T_m: hybridization temperature

Primers	**Length (bp)**	**T_m (°C)**	**Quantity (nmol)**
attat**catatg**tggcgactacgtcggg	19	60	13.3
ata**ctcgag**ttatttctcctgatgaagagcttcaatgaaagc	33	61	12.9

Table 2.4 – PCR conditions

Denaturation	**Denaturation**	**Annealing**	**Elongation**	**Final elongation**	**Final hold**
98°C	98°C	59°C	72°C	72°C	4°C
30 sec	30 sec	30 sec	1 min 20 sec	10 min	∞
	x 30 cycles				

Digestion The opa1 cDNA and the plasmid pACE-10His were digested by restriction enzymes Nde1 and Xho1 to prepare them for ligation. The digestion was performed overnight at room temperature for opa1 and at 37°C for pACE-10Hisa2-T172A (an available, unrelated pACE-10His expression plasmid) with a mix as indicated in Table 2.5. Two lots of pACE-10Hisa2-T172A have been used independently for a higher yield.

Table 2.5 – Composition of the restriction digest for opa1 gene and pACE-His10a2-T172A

opa1 gene	**pACE-10Hisa2-T172A** (lot1)	**pACE-10Hisa2-T172A** (lot2)
10 µl DNA at 282 ng/µl	20 µl DNA at 143 ng/µl	11 µl DNA at 433 ng/µl
5 µl BSA 10x	5 µl BSA 10x	5 µl BSA 10x
5 µl Neb4 buffer	5 µl Neb4 buffer	5 µl Neb4 buffer
2.5 µl Nde1	5 µl Nde1	2.5 µl Nde1
2.5 µl Xho1	5 µl Xho1	2.5 µl Xho1
25 µl H_2O	10 µl H_2O	24 µl H_2O

The opa1 digest was cleaned with "PCR clean-up-Gel extraction" kit and eluted with 20 µl buffer. The digest of the bacterial vector was separated on 1% Agarose gel. The bands corresponding to the backbone size were excised and processed using the "PCR clean-up-Gel extraction" kit in order to extract the pACE-10His backbone from the agarose gel.

Ligation Purified opa1 cDNA and pACE-10His backbone were ligated to obtain the pACE-10His-OPA1 plasmid. Each reaction mix (see Table 2.6) was run at room temperature for 3h. Half of the reaction mixture was then transformed into *E. coli* MACH1

which were plated on LB/Ampicillin agar plates and grown overnight at 37°C. The second half of the reaction was left overnight at room temperature and only then transformed into *E. coli* MACH1 and processed like above.

Table 2.6 – Composition of the ligation mix

pACE-10His (lot1)	**pACE-10His** (lot2)
10 µl backbone at 35 ng/µl	14 µl backbone at 57.5 ng/µl
7 µl opa1 gene at 125 ng/µl	10 µl opa1 gene at 125 ng/µl
2 µl ligase	2 µl ligase
2 µl buffer	2 µl buffer

Colony growth and selection Each colony on the agar plate was labeled and then transferred and grown in 10 ml LB/Ampicillin medium overnight at 37°C, shaking at 200 rpm. Each culture was processed for plasmid extraction with the "NucleoSpin plasmid" kit according to the manufacturer protocol *(Macherey-Nagel)*, using 2 x 25 µl elution buffer (AE buffer) per culture. Concentration and purity of each plasmid sample were checked by absorbance measurements at 230, 260 and 280 nm and comparing absorbance ratio ($\frac{A_{260}}{A_{280}}$; $\frac{A_{260}}{A_{230}}$) with a nanospectrophotometer (Nanodrop).

Control digest and sequencing Plasmids of all positive clones were digested with EcoR1, using 200 ng plasmid with 0.5 µl EcoR1 in 1 µl EcoR1 buffer and H_2O in a final volume of 10 µl. The reaction was run at 37°C for 2h, and products were separated on 1% Agarose gel. Characteristic bands from an EcoR1 digest of pACE-10His-OPA1 are found at 1900 bp and 3218 bp. Based on these results, 2-3 clones were selected for sequencing. Sequencing primers given in Table 2.7 were solubilized in sterilized pure water at a final concentration of 100 µM. Sequencing was performed by the GATC Biotech company. Primers and samples were prepared according to their recommendations.

Table 2.7 – Primers used for sequencing pACE-10His-OPA1

Name	**Sequence**
Opa1-seq1	tgataccggaccttagtgaatataaatggattg
Opa1-seq2	tataatacgcaagatcatctgccacgg
Opa1-seq3	tacagacttggtcagtcaaatggacc
Opa1-seq4	attgggaggaaatccttcaacaatctttg
Opa1-seq5	acccaagaacagtgtgttcacaatg
Opa1-seq6	acttgatgctttcattgaagctcttcatc
Opa1-seq7	cccgacgtagtcgccacatatg

2.2.5.5 Expression of recombinant OPA1

OPA1 expression was performed in two different *E.coli* strains, BL21Star (DE3), is a standard strain used for T7-driven protein expression, BL21CodonPlus-(DE3)-RIPL contains plasmids providing extra copies of rare bacterial tRNA genes (argU, proL, ileY and leuW), which often improves expression of human genes that frequently contain such rare codons (differences in codon usage). The same protocol was applied for both bacterial strains. After transformation with pACE-10His-OPA1, a pre-culture was grown with a single colony in LB medium (125 ml) supplemented with ampicillin overnight at 37°C, shaking at 200 rpm. This culture was then used to inoculate a larger volume of LB+Ampicillin medium (2x400 ml) in order to get an OD_{600} of 0.1 in the final volume. Bacteria were grown at 37°C, shaking at 200 rpm, until an OD_{600} of about 0.8-1.0. At this time, expression is induced with 0.5 mM IPTG and culture continued for 4h at 37°C or 21h at 16°C, always shaking at 200 rpm. Cultures were centrifuged at 4000 rpm (4050 g, rotor JS-4, Beckman) for 30 min at 4°C. The pellet was washed with PBS and centrifuged 4000 rpm (4050 g, rotor JS-4, Beckman) for 30 min at 4°C. Pellets were frozen at -20°C until use.

2.2.5.6 Purification of OPA1 soluble fragment

Lysis The *E. coli* BL21(DE3) pellet (from 200 ml culture volume) was lysed with 30 ml lysis buffer (50 mM Hepes pH 8, 100 mM NaCl, 2 mM ß-mercaptoethanol, 1 mg/ml lysozyme, 1 µl benzonase and antiprotease cocktail) on ice for 10 min. Then, bacteria were sonicated three times 1 min with a tip sonicator at 80% cycle and 80% power. The lysate was centrifuged at 20 000 rpm (rotor JA-20, Beckman, 48380 g) for 1h at 4°C. The supernatant was kept and processed by NiNTA affinity resin.

NiNTA affinity chromatography All the following steps were performed in a glass column (2.5 cm x 30 cm) operated in gravity mode. 6 ml NiNTA resin 50 % (v/v) slurry in ethanol was washed with water and equilibrated with 10 ml lysis buffer. The lysate was then incubated with the resin for 2h at 4°C in the glass column under constant shaking at 180 rpm (horizontal shaker). After incubation, the flow-through was collected, and the resin washed with 50 ml wash buffer (5 mM imdazole, 50 mM Hepes pH8, 100 mM NaCl, 2 mM ß-mercaptoethanol and antiprotease cocktail). Then, bound proteins were eluted by adding three times 3 ml of 20 mM imidazole buffer (20 mM imdazole, 50 mM Hepes pH 8, 100 mM NaCl, 2 mM ß-mercaptoethanol and antiprotease cocktail), and all eluted fractions collected. Fractions were then resolved on a 10% SDS-PAGE and analyzed by Western blot for OPA1.

2.2.5.7 Solubilization and purification of OPA1 from insoluble material

Lysis The *E. coli* BL21CodonPlus-(DE3)-RIPL pellet (200 ml culture volume) was lysed with 30 ml lysis buffer (50 mM Tris pH 8, 100 mM NaCl, 2 mM ß-mercaptoethanol, 1 mg/ml lysozyme, 1 µl benzonase and antiprotease cocktail) on ice for 30 min to allow a good digestion by benzonase and lysozyme . Then, bacteria were sonicated three times 1 min with a tip sonicator at 70% cycle and 50% power. The lysate was centrifuged at 4000 rpm (rotor JS-4, Beckman, 4050 g) for 30 min at 4°C (Jevševar et al., 2005). The supernatant was discarded, and the pellet washed with 45 ml PBS and centrifuged at 4000 rpm (rotor JS-4, Beckman, 4050 g) for 30 min at 4°C. The supernatant was again discarded and the pellet kept for the following steps.

Screening for solubilisation agent The bacterial pellet was resuspended in buffer (50 mM Tris pH 8, 100 mM NaCl, 2 mM ß-mercaptoethanol, antiprotease cocktail) containing 2M Urea or 0.2% (w/v) of one of the following detergents: octyl-ß-D-glucopyranoside, NP40, Triton X-100, Tween 20, N-lauroyl sarcosine, Na-deoxycholate, Sodium-dodecylsulfate or CHAPS. Suspensions were incubated overnight at room temperature on a rocking shaker. Then, tubes were centrifuged at 4000 rpm (4050 g, rotor JS-4, Beckman) for 30 min at 4°C. Supernatants were collected and pellets resuspended in PBS.

NiNTA affinity chromatography All the following steps were performed in a glass column (2.5 cm x 30 cm) operated in gravity mode. NiNTA resin as above was equilibrated with solubilisation buffer (50 mM Tris pH 8, 100 mM NaCl, 2 mM ß-mercaptoethanol, 0.2% N-lauroylsarcosine, 5 mM Imidazole and antiprotease cocktail). The supernatant from the solubilisation step was then incubated with the resin for 2h at room temperature in the glass column on an horizontal shaker (180 rpm). After incubation, the flow-through was collected and the resin was washed with solubilisation buffer containing 50 mM Imidazole. Bound proteins were eluted with 10 ml solubilisation buffer containing 100, 200 or 400 mM imidazole and each fraction was collected separately. Fractions were then resolved on a 10% SDS-PAGE and analyzed on Western blot for OPA1 if necessary.

2.2.6 Protein characterization

2.2.6.1 Protein concentration

The protein concentration in a sample was measured with the Bradford assay (BioRad) (Bradford, 1976) using BSA as a standard.

Table 2.8 – Characteristics of the primary antibodies used in this study.

Target	Isotype	Species	Dilution	Manufacturer
OPA1	monoclonal	mouse	1/1000	612607 BD Biosciences
OPA1	polyclonal	rabbit	1/1000	ABN95 Merck
His-tag	monoclonal	mouse	1/1000	2366S Cell signaling
NDPK-D	polyclonal serum	rabbit	1/1000	homemade (Milon et al., 2000)

2.2.6.2 Sodium dodecyl sulfate - polyacrylamide gel electrophoresis (SDS-PAGE)

For polyacrylamide gels, resolving gel was made up with 0.38 mM Tris-HCl pH 6.8, 0.1% SDS, 10% or 12% acrylamide / bisacrylamide 4K (37.5:1), 0.1% APS and 0.1% TEMED, and overlayed by a stacking gel (125 mM Tris-HCl pH 6.8, 0.1% SDS, 5% acrylamide/bisacrylamide 4K (37.5:1), 0.1% APS, 0.1% TEMED) with a 10 or 15 well comb inserted (minigel format). Samples mixed with a 6x Leammli buffer (Laemmli, 1970) (200 mM Tris-HCl pH 6.8, 8% (w/v) SDS, 40% glycerol, 4% (v/v) ß-mercaptoethanol, 50 mM EDTA and 0.08% (w/v) bromophenol blue), were boiled for 5 min at 95°C and loaded on the gel. The electrophoresis was performed at 30 mA/gel for 1h in 1x running buffer (25 mM Tris-HCl pH 8.2, 192 mM Glycine, 0.1% SDS). When needed, gels were stained with Rotiblue Quick (Carl Roth).

2.2.6.3 Protein transfer and immunodetection

Proteins were transferred from SDS-PAGE onto a nitrocellulose membrane for 1h at 100 V in a wet buffer system (0.192 mM Glycin, 25 mM Tris-Base, 0.01% SDS, 20% Ethanol). Transfer efficiency was then checked with Ponceau Red (staining for 1-2 min, destaining in water). The membrane was then blocked with 20 ml of blocking buffer (TBS-Tween 0.1% (v/v) + 5% (w/v) milk) for 1h at room temperature. Then the membrane was incubated with primary antibodies in blocking buffer overnight at 4°C (see Table 2.8 for specifications). Subsequently, membranes were incubated with secondary antibodies couple to horse-radish peroxidase (HRP): donkey anti-rabbit HRP-linked (NA934V from GE Healthcare, 1/3000) or horse anti-mouse HRP-linked (7076 from Cell signaling, 1/2000). Signals were revealed with Amersham™ ECL Prime™ reagent (GE Healthcare) and acquired with ImageQuant™ LAS 4000 (GE Healthcare).

2.2.6.4 Mass spectrometry

Bands in SDS-PAGE stained with Rotiblue Quick (see 2.2.6.2) and corresponding to bands immunoreactive with anti-OPA1 antibodies in parallel Western blots were precisely excised and stored at 4°C in 10% (v/v) acetic acid/water. At the proteomic

platform Prométhée, bands were destained and protein in-gel digestion was then carried out with trypsin supplemented with surfactant. Peptides were extracted twice from the gel and concentrated with a 10 µl ZipTip C18 (Millipore). MS analysis was performed on a 4800 MALDI-TOF/TOF (*Sciex*) in a positive reflectron mode with a standard method for each samples. The calibration was performed by placing 0.5 µl calibration solution (Peptide calibration Standard II, Bruker) and 0.5 µl α-cyano-4-hydroxycinnamic acid (HCCA) matrix at 10 mg/ml on a target near the sample. For each sample, 0.5 µl were spotted on a MALDI plate (Opti-TOF 384 well MALDI Plate insert) together with 0.5 µl HCCA matrix. The identification of the peptides was performed with Protein Pilot v4.0 software (Sciex) using the Mascot algorithm (Perkins et al., 1999) and the Uniprot/Swissprot databases (*uniprot-sprot-2014-02*, (Bateman et al., 2015)). The taxonomies used are Human (all entries) and *E. coli* for all samples. The Table 2.9 shows the parameters used for protein identification.

Table 2.9 – Parameters used for a Mascot search to identify proteins

Parameters for Mascot search	
Sample type	Identification
Digestion	Trypsin
Instrument	MALDI-TOF/TOF 4800
Species	Human, all entries, E.coli
Database	Swissprot
Fixed and variable modifications	Carbamidomethyl (C), Oxidation (HWM), Deaminated (KNQ)
Missed cleavage	2
Precursor tolerance	50 ppm for samples, 70 ppm for MW control
MS/MS fragment tolerance	0.2 Da for samples and 0.3 Da for MW control
Peptide charge	1+
Parameters for identification	
Number of peptides	$\geq$3
% of coverage	$\geq$20%
Score (95% confidence)	>45

2.2.6.5 GTPase assay

Function of recombinant OPA1 was analyzed by a GTP/ATPase assay. Presence of function is generally also a good measure for correct folding of a recombinant protein. The classical assay is based on the reaction of liberated inorganic phosphate (P_i) with ammonium molybdate to yield phosphomolybdate. This compound forms a complex with malachite green that can be detected at 630 nm (Leonard et al., 2005; Quan and Robinson, 2006; Boissan et al., 2014).

$$\text{Enzyme + substrate} \rightarrow \text{[ES]} \rightarrow \text{Enzyme + } P_i$$
$$P_i + (NH_4)_2MoO_4 \rightarrow H_3PMo_{12}O_{40}$$
$$H_3PMo_{12}O_{40} + HMG^{2+} \rightarrow (MG^{+})(H_2PMo_{12}O_{40}) + 2H^{+}$$

A GTP (disodium salt) stock solution at 50 mM was prepared in distilled water, controlled for nucleotide concentration by measuring the absorbance at 253 nm (ε (253nm) = 13 700 $M^{-1}.cm^{-1}$), and stored in frozen aliquots at -80°C. A detection solution (1 mM Malachite green, 10 mM ammonium molybdate in 1N HCl) was prepared by dissolving 34 mg malachite green carbinol base in 40 ml 1N HCl and 1 g ammonium molybdate tetrahydrate in 14 ml 4N HCl. Both solutions were then mixed, diluted to 100 ml with distilled water, filtered through a 0.45 µm filter and stored in the dark at 4°C. Stocks solutions of EDTA (0.5 M) and KH_2PO_4 (0.5 M) were prepared in distilled water.

In the reaction mix, 0.2 mg/ml OPA1 and 300 µM GTP in GTPase buffer (20 mM Hepes-KOH pH 7.55, 100 mM KCl, 2 mM $MgCl_2$, 1 mM DTT) were incubated at 37°C and the kinetics of P_i was followed every 30 min for a total of 3h. Each time, a 10 µl aliquot was transferred into a 96-well plate containing 10 µl 0.5 M EDTA which quenches the Mg^{2+}-dependent reaction. Finally, 135 µl malachite green stock solution was added into each well, the plate incubated for 15 min at room temperature and absorption at 630 nm measured with a plate reader spectrophotometer (Biotek EL808), (see Fig.2.2). For each experiment, a calibration curve was performed for a range of inorganic phosphate (KH_2PO_4) from 0 to 200 µM.

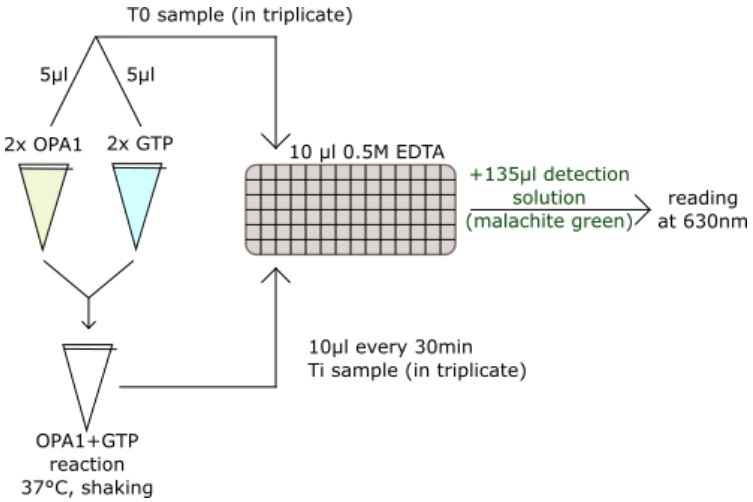

Figure 2.2 – Diagram of malachite green-based GTP/ATPase assay. Stock solution of 2x OPA1 (0.4 mg/ml) and 2x GTP (600 µM) were prepared separately in GTPase buffer. For T_0 time point, 5 µl of both OPA1 and GTP stock solutions were taken and placed into the corresponding well containing 10 µl EDTA at 0.5 M. The reaction was initiated by mixing 150 µl of both stock solutions in a new tube which was then incubated at 37°C under shaking for 3h. Time points were performed by pipetting 10 µl of the reaction mix every 30 min, in triplicates. At the end, 135 µl detection solution was added to each well and the color was allowed to develop at room temperature for 15émin before reading at 630 nm.

Table 2.10 – NDPK-D purification protocol. This table summarizes protein concentration and amount in different fractions of the Blue Sepharose and NiNTA chromatography steps. Abbreviations: FT, flow-through; W, wash.

Blue Speharose										
	Lysat	FT	W	A2	A3	A4	A5	A6	A7	
concentration (mg/ml)	22	0.7	0.56	0.52	2.9	2.34	1.21	0.87	0.67	
total mass (mg)	290	143		1.56	8.7	7.02	3.63	2.61	1.97	
NiNTA										
	Lysat	FT	W	A15	B15	B14	B13	B12	B11	B10
concentration (mg/ml)	1.24	0.06	0.23	0.28	0.83	2.23	3.24	2.36	1.12	0.29
total mass (mg)	22.26	2	9	0.28	0.83	2.23	3.24	2.36	1.12	0.29

2.3 Results

To engage into *in vitro* experiments on the interaction between NDPK-D and OPA1, we first aimed at the expression of functional forms of both human enzymes, using bacterial expression systems and affinity purification procedures.

2.3.1 Expression and purification of recombinant human NDPK-D

The mature human NDPK-D wild-type protein, lacking the first 33 amino-acids (mitochondrial targeting sequence) and known to have a NDP kinase activity (Milon et al., 2000), was recombinantly expressed in E. coli BL21-(DE3)-RIPL by induction with 0.5 mM IPTG for 3h at 37°C. The protein was purified from bacterial lysates with a two-step affinity chromatography procedure including Blue Sepharose and NiNTA matrices. The fractions eluted from Blue Sepharose with ATP were resolved on SDS-PAGE in order to identify elution peak fractions containing the purest protein (Fig.2.3 A). Fractions A2 to A7, containing NDPK-D as the major protein, were pooled and injected onto the NiNTA column. Protein bound to NiNTA was then eluted with a gradient from 0 to 200 mM imidazole. Fractions were again resolved on SDS-PAGE. Fractions B14 and B13 presented the highest purity (Fig.2.3 B). Table 2.10 summarizes the concentrations and protein amounts in the fractions of the Blue Sepharose and NiNTA steps used to purify NDPK-D. This purification process allowed production of 5.4 mg recombinant NDPK-D with a 90% purity from 400 ml bacterial culture.

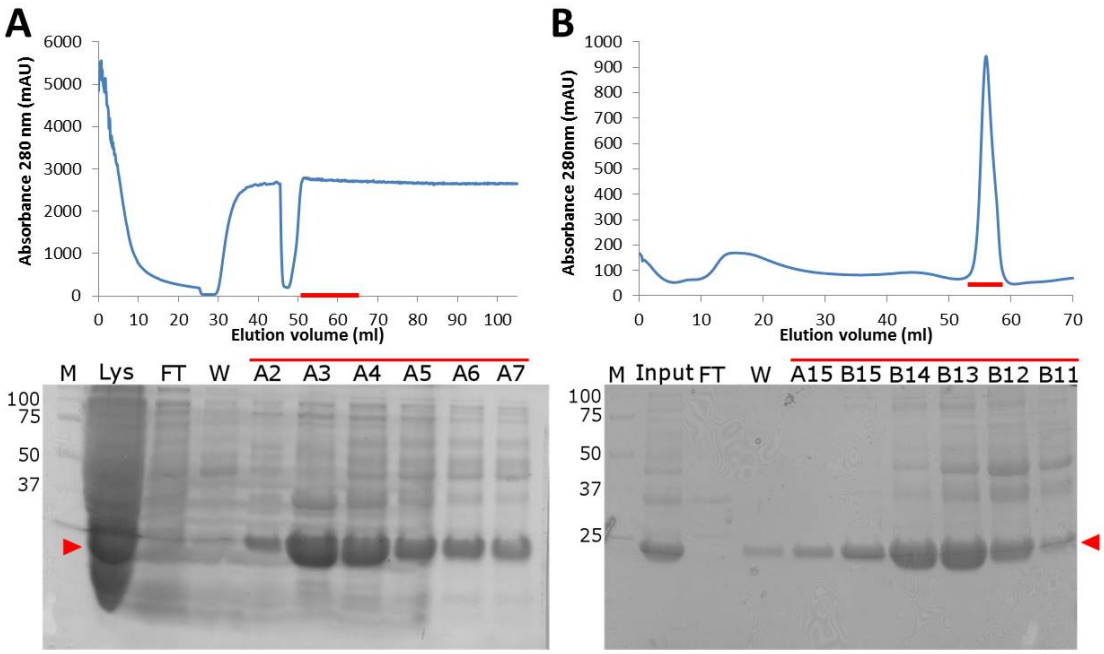

Figure 2.3 – Two step purification of NDPK-D recombinant protein. Protein elution profile (top) and Coomassie Blue-stained 12% SDS-PAGE of individual fractions (bottom) of **(A)** Blue Sepharose and **(B)** NiNTA-agarose columns. NDPK-D was expressed in E. coli.(see Materials and Methods). Abbreviations: MW, molecular weight marker; Lys, supernatant of bacterial lysis; FT, flow-through; W, wash; A2-A7, fractions eluted from Blue Sepharose; Input, pooled fractions from Blue Sepharose loaded onto NiNTA; A15-B11, fractions eluted from NiNTA. Red arrowheads indicate the band corresponding to NDPK-D, the red lines indicate the fractions pooled and injected on NiNTA (in A) and the fractions containing purified NDPK-D (in B).

2.3.2 pACE-10His-OPA1 plasmid construction

The human opa1 cDNA (O60313, UniProtKB database) from the pMSCV-OPA1 plasmid was amplified using the two primers listed in table 2.3. Size and purity of the amplified cDNA were verified on 1% agarose gels (Fig.2.4 A). The band between 2500 bp and 3000 bp corresponds to the size of the opa1 cDNA. The absence of additional bands confirmed the purity of the sample. The amplified cDNA was then purified with a final concentration of about 282 ng/µl (A_{260}=0,111). The absorbance ratios A_{260}/A_{280}=1,852 and A_{260}/A_{230}=2,825 indicated only minimal protein contamination and the absence of contamination by salt or organic compounds, respectively.

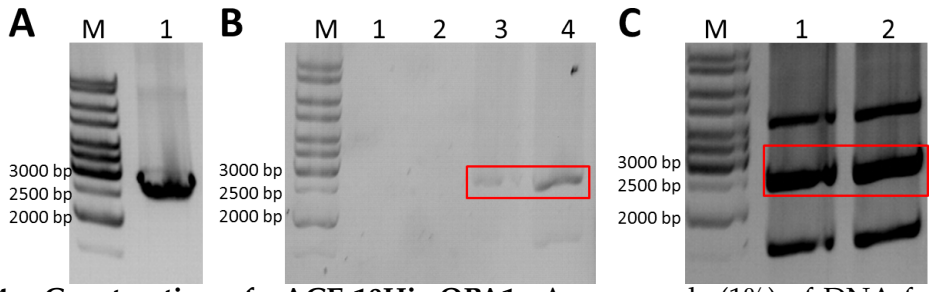

Figure 2.4 – Construction of pACE-10His-OPA1. Agarose gels (1%) of DNA fragments and DNA ladders (M in (A), (B) and (C)) visualized with BET. **(A)** Opa1 cDNA after amplification by PCR (lane 1). Note: The band between 2500 bp and 3000 bp corresponds to the size of the opa1 cDNA. **(B, C)** pACE-10Hisa2-T172A plasmid sample 1 (B) and sample 2 (C) after digestion with Nde1 and XhO1 restriction enzymes. The red rectangles show the bands corresponding to the vector backbone size. These bands were excised and used for DNA extraction.The bands above and under correspond respectively to the non-digested vector and to the inserted T172A cDNA.

Opa1 fragment and pACE-His10a2-T172A were both digested with the same restriction enzymes (Nde1 and Xho1). The opa1 fragment was directly purified, while the plasmid fragments were first separated on agarose gels (Fig 2.4 B,C) and then purified from excised bands. Final concentrations were 125 ng/µl (A_{260}=0,050) for the opa1 fragment and 35 ng/µl (sample 1) or 57.5 ng/µl (sample 2) for pACE-His10a2-T172A. Purity of opa1 fragment was high (A_{260}/A_{280} =1.786; A_{260}/A_{230} =1.064). Finally, plasmid backbone and opa1 gene were ligated to yield pACE-10His-OPA1. MACH1 bacteria were transformed with different ligation products, resulting colonies grown in suspension culture, and plasmids purified. Yield and quality of the pACE-10His-OPA1 preparations were evaluated by absorbance measurements (Table 2.11) and a restriction mapping (Fig.2.5). Digestion by EcoR1 gave the expected bands at 1900 bp and 3218 bp for clones 2.1.A, 2.1.C, 2.2.B and 2.2.C. The latter three clones were sequenced, revealing a correct sequence for clone 2.1.C, while clones 2.2.B and 2.2.C carried a deletion at position 2488. Therefore, clone 2.1.C was used as pACE-10His-OPA1 throughout this project.

Table 2.11 – pACE-10His-OPA1 ligation products. Absorbance and concentration (C) of plasmids amplified in MACH1 bacteria and purified. Analyzed ligation products are: 1.1, 2h ligation with pACE-10his sample1; 1.2, overnight ligation with pACE-10his sample1; 2.1, 2h ligation with the pACE-10his sample2; 2.2 overnight ligation with the pACE-10his sample2. Plates 2.1 and 2.2 gave three colonies labeled A, B and C.

	Plasmids							
	1.1	**1.2**	**2.1.A**	**2.1.B**	**2.1.C**	**2.2.A**	**2.2.B**	**2.2.C**
C (ng/µl)	72.5	222	60	67.5	65	95	95	102
A_{230}	0.011	0.047	0.013	0.012	0.013	0.014	0.015	0.022
A_{260}	0.028	0.092	0.024	0.027	0.025	0.038	0.037	0.041
A_{280}	0.014	0.051	0.013	0.014	0.014	0.021	0.020	0.023

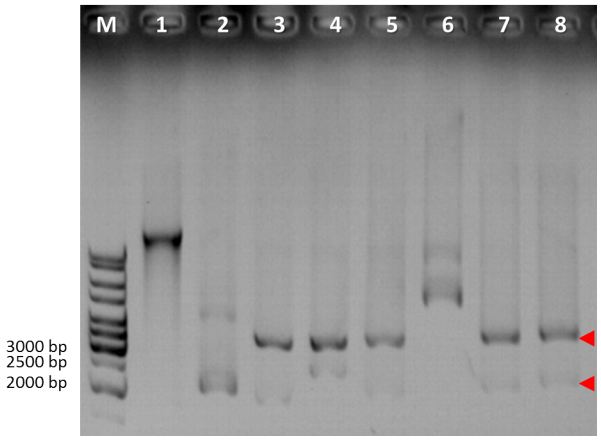

Figure 2.5 – Restriction mapping of pACE-10HisOPA1.1% agarose gel visualized by BET showing the EcoR1 digestion products of the different pACE-10His-OPA1 clones. The red arrowheads indicate the two bands characteristic of pACE-10His-OPA1 digestion by EcoR1 at 3218 bp and 1900 bp. Abbreviations: M, DNA ladder; 1, clone 1.1; 2, clone 1.2; 3 clone 2.1.A; 4, clone 2.1.B; 5, clone 2.1.C; 6, clone 2.2.A; 7, clone 2.2.B; 8, clone 2.2.C (for details and abbreviations of the different clones see Table 2.11).

2.3.3 Expression of recombinant human OPA1 protein

Recombinant human OPA1 was first produced in *E. coli* BL21Star (DE3) following induction with 0.5 mM IPTG for 4h at 37°C. Figure 2.6 shows the expression level of OPA1 by Western blot at the time of induction, after 4h and in the supernatant after lysis of bacteria. Immunoblotting with a monoclonal antibody detecting the N-terminal His-tag gave a signal below 37 kDa which was not prominent in the clarified lysate (Fig.2.6.A). Additional immunoblotting with monoclonal anti- OPA1 antibody which detects the more C-terminal GTPase domain gave a signal at 75 kDa, also found in the clarified lysate. Other bands were detected around 60 kDa, 45 kDa and 30 kDa at both T_0 and T_f, but were not detectable in the clarified lysate (Fig.2.6.B). Given the short length of all bands below the expected 100 kDa for OPA1, and the fact that no band was simultaneously detected by both antibodies, expression of human OPA1 in *E. coli* BL21Star (DE3) yielded only OPA1 fragments. These include a major N-terminal fragment (with the His-tag) and several more C-terminal fragments. The longest and only soluble C-terminal fragment has a size of about 75 kDa was used for some further studies.

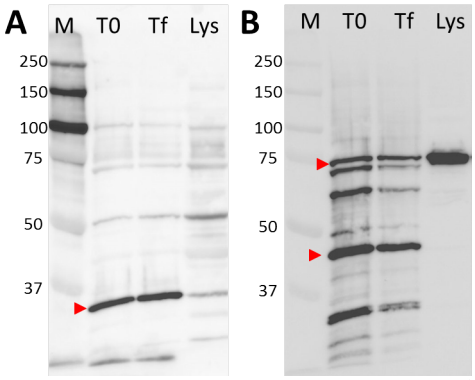

Figure 2.6 – Expression of human OPA1 recombinant in *E. coli* BL21Star (DE3). Western blot detecting (A) His tagged protein or **(B)** OPA1 (GTPase domain) using monoclonal antibodies. Samples: Bacteria just before (T_0) and after 4h IPTG induction (T_f) and directly lysed in PAGE sample buffer, or clarified final bacterial lysates (Lys). M, molecular weight marker (kDa).

Since some of the encountered problems in obtaining full-length human OPA1 could be due to rare *E. coli* codons, we used *E. coli* BL21 CodonPlus-(DE3)-RIPL under identical experimental conditions for the next experiment. Under these conditions, a band at about 100 kDa occured that is close to the calculated size of full-length OPA1 (see red arrowhead in Fig. 2.7.A). Further, band intensity increased over the four hours of IPTG induction. Both, anti-His-tag and anti-OPA1 antibodies detected the 100 kDa band in bacteria after induction (Fig.2.7.B). An overlay of Ponceau Red protein stain and OPA1 immunodetection on the same blotting membrane (Fig.2.7.C) confirmed that the 100 kDa protein band corresponds to OPA1. Taken together, this confirms that the 100 kDa protein is an OPA1 species containing N-terminus and GTPase domain, suggesting that it could indeed be a full-length version. Since this band was clearly visible on the Ponceau and Coomassie stains, the protein amount should be sufficient for analysis by mass spectrometry. This should clarify whether the band is the full-length protein or a fragment containing the His-tag and the GTPase domain, lacking the end of the protein (see 2.3.6). However, the 100 kDa band was not detectable in the final, centrifuged lysate, showing that the protein is not soluble. To work with this protein, we needed to set-up a solubilization strategy (see 2.3.6.1).

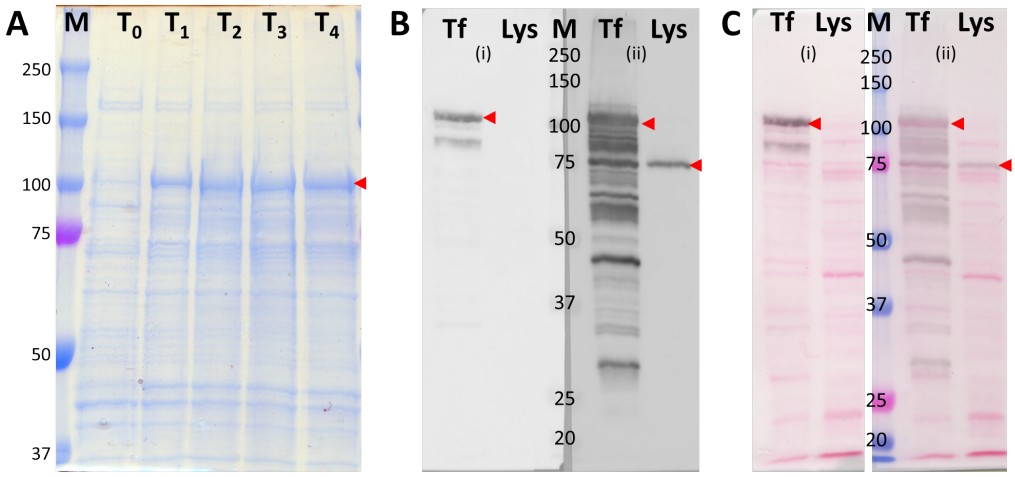

Figure 2.7 – Expression of human OPA1 recombinant in *E. coli* BL21CodonPlus-(DE3)-RIPL. (A) Coomassie-stained 10% SDS-PAGE showing the protein profile 0h, 1h, 2h, 3h and 4h after IPTG induction. Red arrowhead: band at about 100 kDa, the approximative size of OPA1 full-length. **(B)** Western blots with anti-His-tag (i) and anti-OPA1 (ii) monoclonal antibodies of bacteria 4h after IPTG induction. Red arrowheads: band at about 100 kDa detected by both antibodies, and band at 75 kDa detected by anti-OPA1 only (see Fig.2.6) **(C)** Overlay of the western blot in (B) and the corresponding Ponceau Red stained membrane. M, molecular weight marker in kDa, T_0, T_1, T_2, T_3 and T_4, time after induction, T_f is bacteria sample 4h after induction; Lys, supernatant of the clarified final bacterial lysate.

2.3.4 Purification of soluble human OPA1 fragments

Recombinant OPA1 fragment expressed in E. coli BL21(DE3) solubilized in lysis buffer was subjected to NiNTA affinity chromatography with elution by 20 mM imidazole buffer. Fractions were analyzed by Coomassie-stained SDS-PAGE and Western blot with monoclonal anti-OPA1 antibody (Fig 2.8). The immunoblots (Fig 2.8.B,C) again identify the soluble band at 75 kDa which binds to NiNTA (almost absent in the flow-through, see Fig 2.8.B) and is eluted by imidazole (red arrowheads in Fig 2.8). Since this fragment is not recognized by anti-His-tag antibodies (Fig 2.6.A), we assume that its binding to NiNTA is determined by an internal His-rich sequence. However, this OPA1 fragment is not very much enriched in the elution fractions, since under the chosen conditions many proteins bind to NiNTA and elute at 20 mM imidazole (Fig 2.8.A). However, since the elution band is visible in Coomassie-stained SDS-PAGE, the quantity of this fragment should be sufficient for mass spectrometric analysis.

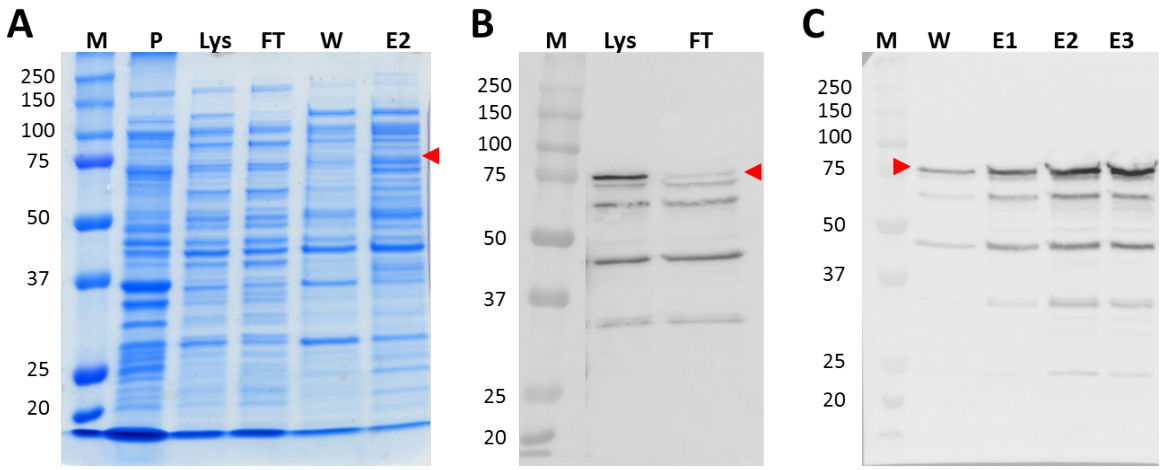

Figure 2.8 – NiNTA enrichment of recombinant human OPA1 75 kDa soluble fragment. **(A)** 10% SDS-PAGE stained with Coomassie blue of purification fractions. **(B), (C)** Western blot against OPA1 with mouse anti-OPA1 monoclonal antibody on fractions of NiNTA purification. The red arrow heads show 75 kDa fragment. M, molecular weight marker (kDa); P, pellet of bacterial lysate; Lys, supernatant of bacterial lysate; FT, flow-through of NiNTA; W, 5 mM imidazole wash; E1, E2, E3, elution fractions with 20 mM imidazole.

2.3.5 Mass spectrometric analysis of human OPA1 species

To gain more insight into the nature of the OPA1 species identified by antibodies, different bands along with a known marker enzyme as a quality control (ß-galactosidase, 116 kDa) were excised from a SDS-PAGE (Fig. 2.9), trypsin digested, and analyzed by MALDI-TOF/TOF. Only the marker band and two OPA1 bands yielded MS data that allowed unambiguous identification (Table 2.12, Fig. 2.9). The 100 kDa band corresponds to OPA1 with a coverage of 57% and a high Mascot score (2350). Moreover, the identified peptides span all along the OPA1 sequence (Fig.2.10, OPA1-1), from the N- to the C-terminus. This confirms the immunoblotting experiments and provides unambiguous evidence for a full-length version of OPA1, *i.e.* a protein containing His-tag, MTS, TM, GTPase and C-terminal domains. The 75 kDa band (Fig. 2.9) was also identified as OPA1, but the peptides only covered the C-terminal part of the OPA1 sequence (Fig.2.10, OPA1-2), as was already suggested by the immunoblotting experiments. If we consider that the most N-terminal peptide is not specific to OPA1 (occurring also in other proteins), we can calculate the molecular weight of the putative OPA1 fragment as being between 82 kDa (2nd peptide to C-terminus) and 79 kDa (2nd to last peptide), using the web tool Protparam (http://web.expasy.org/cgi-bin/protparam/protparam).

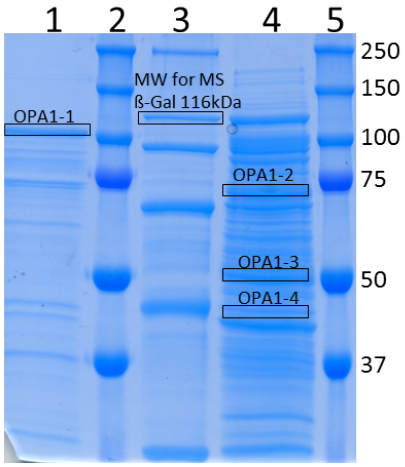

Figure 2.9 – Samples excised from Coomassie-stained SDS-PAGE analyzed by mass spectrometry. Different recombinant OPA1-containing samples were separated on 10% SDS-PAGE and stained with MS-compatible colloidal Coomassie Blue. Bands identified in parallel immunoblots were excised and processed for MS. Samples were from following OPA1 expressions: lane 1, *E. coli* BL21CodonPlus-(DE3)-RIPL after 0.5 mM induction, 4h, 37°C (see Fig.2.7); lanes 2, 3, 5, different molecular weight markers; lane 4, elution E3 of the NiNTA purification from *E. coli* BL21Star (DE3) (see Fig. 2.8). Excised bands: OPA1-1, 100 kDa band expressed in BL21CodonPlus (DE3)-RIPL; OPA1-2, soluble fragment at ~75 kDa; OPA1-3, OPA1-4, fragments at 50 and 45 kDa, respectively.

Table 2.12 – Bio-informatic analysis of mass spectrometric data. Results of a search on the Mascot server for OPA1-1 and OPA1-2 samples, and ß-galactosidase (control).

	OPA-1	**OPA1-2**	**Control**
Expected MW (Da)	114 600	75 000	116 500
Description	Dynamin-like 120kDa protein, mitochondrial		β-galactosidase
Species	Homo sapiens		E. coli
Theoretical MW (Da)	112 131	112 131	117 351
Mascot Score	2350	528	552
Nb of peptides	82	38	33
% coverage	57	29	20

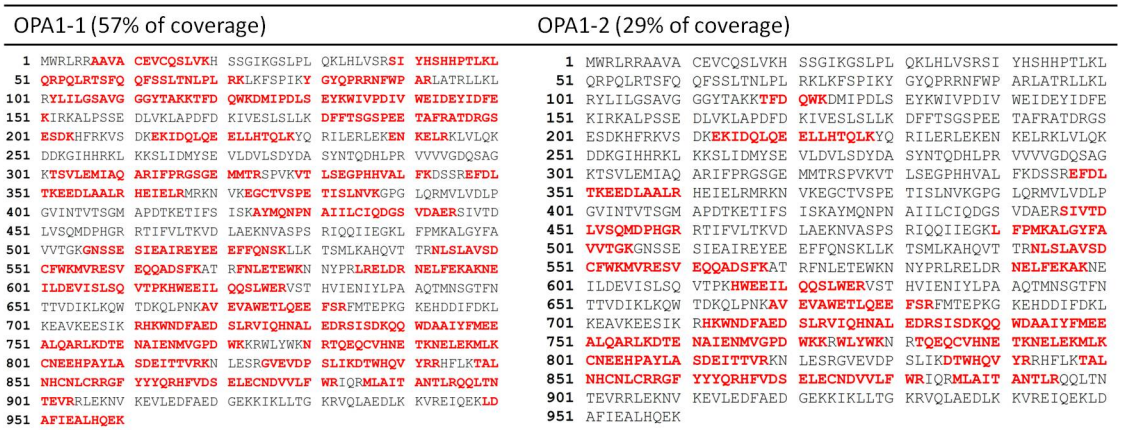

Figure 2.10 – Localization of peptides identified by mass spectrometry within the OPA1 sequence. Peptides are labeled in red within the sequence of human OPA1 (UniprotKB: O60313). OPA1-1 and OPA1-2 are the two samples identified, representing 100 kDa and 75 kDa OPA1 species.

2.3.6 Solubilization and purification of full-length human OPA1

Full-length recombinant human OPA1 could be expressed in *E. coli* BL21CodonPlus-(DE3)-RIPL, but was insoluble (cf. Fig2.7) and seemed to remain in inclusion bodies. In order to recover soluble and potentially enzymatically active full-length OPA1, different strategies were followed. First, to increase bacterial production of soluble OPA1, expression was performed at 16°C for 21h instead of 4h at 37°C. This is known to yield more soluble protein, or at least non-classical inclusion bodies more suitable to recover well-folded proteins (Jevševar et al., 2005; Singh et al., 2015). Second, a solubilization screen was set up to find mild conditions that favor proper refolding, minimize protein denaturation and preserve enzyme activity (Rudolph and Lilie, 1996; Singh et al., 2015).

For the solubilization screen, the insoluble pellet was treated with different buffers containing either 2M Urea or 0.2% detergent of ionic (N-lauroyl sarcosine, Na-deoxycholate, sodium-dodecylsulfate), non-ionic (Triton X-100, Tween 20, Nonidet P-40, octyl-ß-D-glucopyranoside) or zwitterionic (CHAPS) character (see chapter 2.2.5.7 for protocol). After centrifugation, supernatants and pellets were analyzed by SDS-PAGE and Western blotting for the presence of OPA1 in samples from expressions performed at 37°C (Fig.2.11) or at 16°C (Fig.2.12). Two major bands, corresponding to the full-length 100 kDa species and 80 kDa fragment (see red arrowheads in Figs 2.11 and 2.12) were detected by both anti-OPA1 and His-tag antibodies, indicating that they contain the N-terminus and the more C-terminal OPA1 GTPase domain. These bands were largely solubilized (~90%) by the non-denaturating detergent N-lauroylsarcosine for expression at both temperatures, in addition to the more denaturating SDS taken as a control.

This is the first time that a soluble full-length form of OPA1 has been obtained with non-denaturing detergent (Pernas and Scorrano, 2016).

Lower temperature led to higher overall yield of insoluble OPA1 species in the primary lysate, but did not yield much more solubilized full-length OPA1 relative to contaminating fragments. Expression at 37°C and solubilization with 0.2% N-lauroyl-sarcosine was retained for production of full-length OPA1.

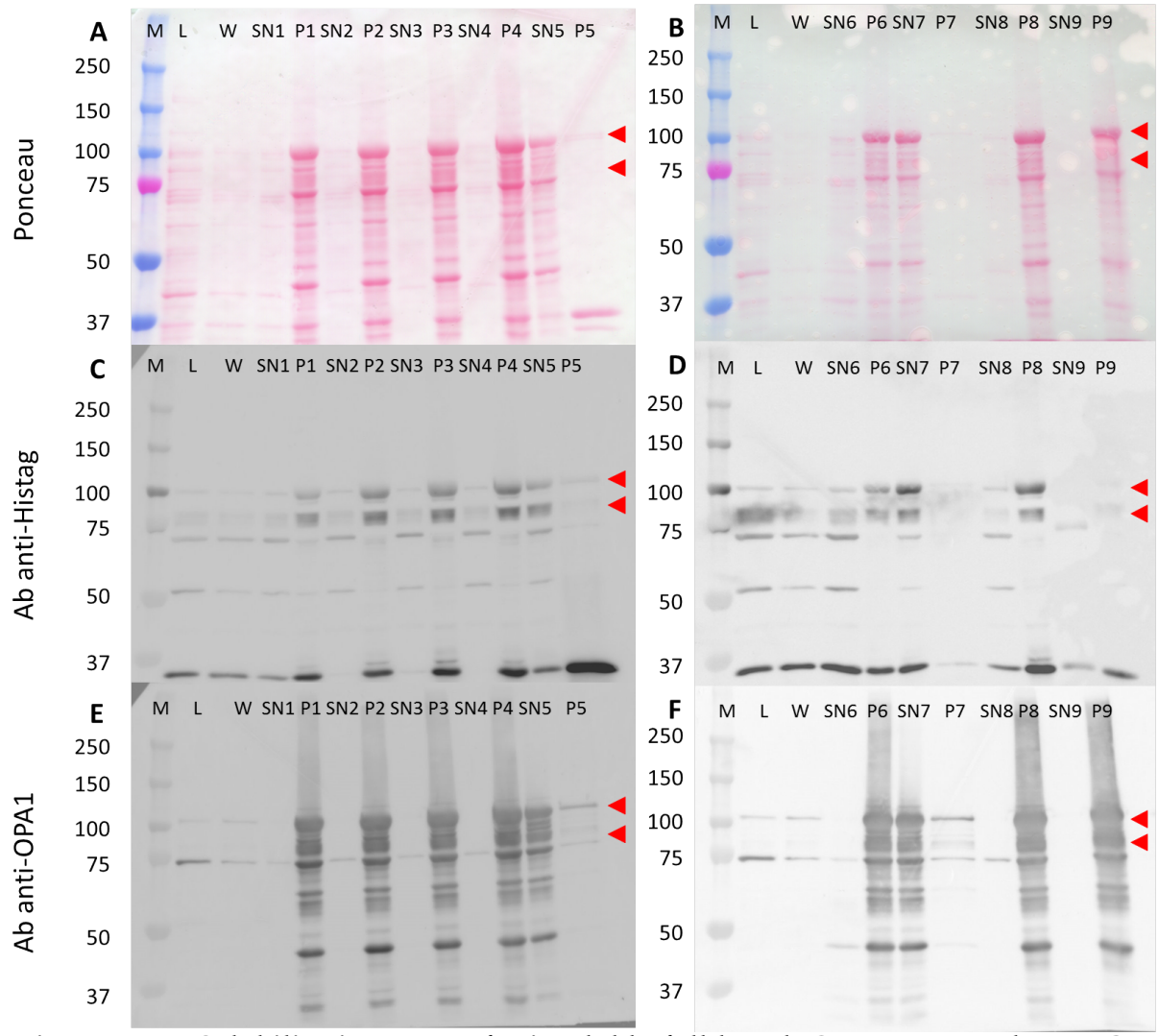

Figure 2.11 – Solubilization screen for insoluble full-length OPA1 expressed at 37°C. Samples from different solubilization conditions were separated by SDS-PAGE and blotted. **(A, B)** Ponceau Red stain of nitrocellulose membranes. **(C, D)** OPA1 immunodetection with monoclonal anti-His-tag antibody. **(E, F)**OPA1 immunodetection with monoclonal anti-OPA1 antibody (reprobing of C and D). Abbreviations: M, molecular weight marker; Lys, supernatant of bacterial lysis; W, supernatant after pellet wash with PBS; P, pellet after solubilization; SN, supernatant after solubilization; solubilization conditions: 1, 0.2% octyl-ß-D-glucopyranoside; 2, 0.2% NP 40; 3, 0.2% Triton X-100; 4, 0.2% Tween 20; 5, 0.2% N-lauroylsarcosine; 6, 0.2% Na-deoxycholate; 7, 0.2% SDS; 8, 0.2% CHAPS; 9, 2M Urea.
Note: red arrowheads indicate the full-length 100 kDa and the 80 kDa species.

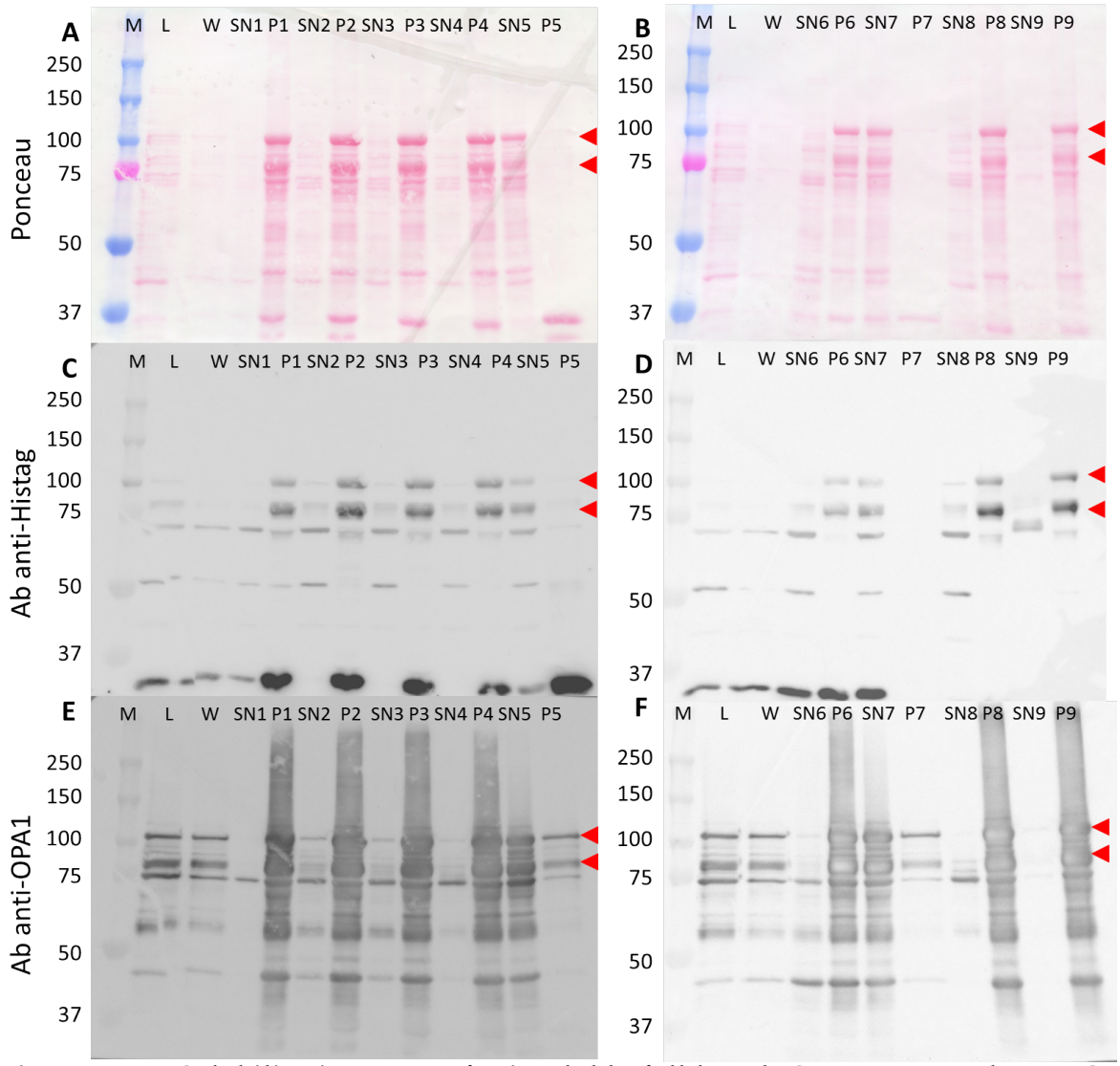

Figure 2.12 – Solubilization screen for insoluble full-length OPA1 expressed at 16°C. Samples from different solubilization conditions were separated by SDS-PAGE and blotted. **(A, B)** Ponceau Red stain of nitrocellulose membranes. **(C, D)** OPA1 immunodetection with monoclonal anti-His-tag antibody. **(E, F)**OPA1 immunodetection with monoclonal anti-OPA1 antibody (reprobing of C and D). Abbreviations: M, molecular weight marker; Lys, supernatant of bacterial lysis; W, supernatant after pellet wash with PBS; P, pellet after solubilization; SN, supernatant after solubilization; solubilization conditions: 1, 0.2% octyl-ß-D-glucopyranoside; 2, 0.2% NP 40; 3, 0.2% Triton X-100; 4, 0.2% Tween 20; 5, 0.2% N-lauroylsarcosine; 6, 0.2% Na-deoxycholate; 7, 0.2% SDS; 8, 0.2% CHAPS; 9, 2M Urea.
Note: red arrowheads indicate the full-length 100 kDa and the 80 kDa species.

For large scale production of soluble full-length OPA1, expression in *E. coli* BL21-CodonPlus-(DE3)-RIPL at 37°C and solubilization with 0.2% N-lauroylsarcosine was coupled to purification with a NiNTA affinity resin and an imidazole step gradient (Fig. 2.13). N-lauroylsarcosine could partially solubilize the 100 kDa species (see red arrowhead in Fig. 2.13), together with several contaminating bands, but only part of solubilized OPA1 was binding to the NiNTA matrix. Some major contaminating

Table 2.13 – OPA1 purification protocol. This table summarizes protein concentration and amount in different fractions of the NiNTA chromatography step. Abbreviations: Lys, supernatant of bacterial lysis; W, supernatant after pellet wash with PBS; P, pellet after solubilization with 0.2% N-lauroylsarcosine; SN, supernatant after pellet solubilization; FT, flow-through of the NiNTA purification; 50, 100, 200, 400, elution with 50, 100, 200 or 400 mM imidazole.

	NiNTA								
	Lysat	W	P	SN	FT	50	100	200	400
concentration (mg/ml)	1.78	0.5	0.9	2.37	2.18	0.43	0.49	0.34	0.07
total mass(mg)	53.4	15	189	118.5	109	6.45	4.9	3.4	0.7

smaller fragments could be eluted already at 50 mM imidazole, while others eluted together with the 100 kDa full-length OPA1 at higher imidazole concentrations. The total amount of OPA1 recovered in the 100 and 200 mM imidazole elution fraction can be estimated to be ~1 mg, considering the purity achieved (see Fig.2.13 and Tab. 2.13). Therefore, the yield of recombinant human OPA1 from 1 l of bacterial culture, again considering the purity achieved can be estimated to about 2.5 mg.

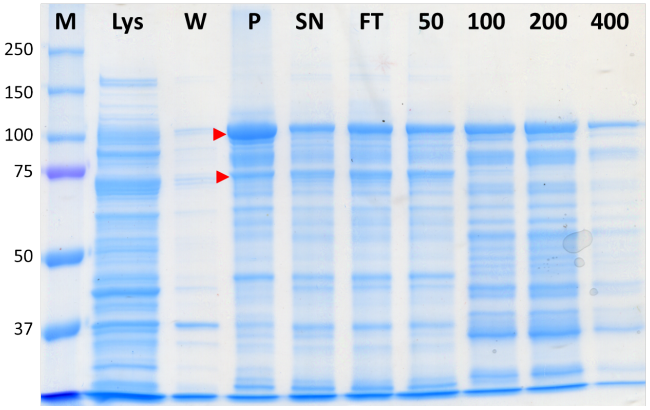

Figure 2.13 – NiNTA purification of solubilized full-length OPA1. Coomassie-stained SDS-PAGE showing full-length OPA1 expression at 37°C, solubilization with 0.2% N-lauroylsarcosine, and NiNTA purification. Abbreviations: M, molecular weight marker (kDa); Lys, supernatant of bacterial lysis; W, supernatant after pellet wash with PBS; P, pellet after solubilization with 0.2% N-lauroylsarcosine; SN, supernatant after pellet solubilization; FT, flow-through of the NiNTA purification; 50,100,200,400, elution with 50, 100, 200 or 400 mM imidazole. The red arrowheads indicate full-length OPA1 at 100 kDa and the 75 kDa fragment.

2.3.6.1 GTPase activity of human OPA1

Finally, we determined the GTPase activity of different OPA1 species using a malachite green based assay that detects the release of inorganic phosphate. Enzymatic activity is also a good quality parameter for correct protein folding, which is important in particular for proteins solubilized from inclusion bodies. First, insoluble OPA1 solubilized

by 0.2% N-lauroylsarcosine and 0.2% SDS was analyzed. In fractions from the solubilization screen containing the 100 kDa OPA1 species (see Figs.2.11 and 2.12), those that were solubilized with N-lauroylarcosine and expressed at 16°C gave the highest GTPase activity (2,7 nmole/min/mg); much less was detectable with the same detergent when expression was done at 37°C (0,7 nmole/min/mg) (Fig. 2.14). In fractions from the large-scale full-length OPA1 production (Fig. 2.15), GTPase activity was detected in the NiNTA flow-through (1,4 nmole/min/mg), containing both the 100 kDa OPA1 species and some fragments, but not in the 200 mM imidazole elution fraction, containing the full-length 100 kDa protein. Second, we determined GTPase activity of the short C-terminal soluble OPA1 fragment purified earlier (Fig.2.8), which was 2.2 nmole/min/mg (Fig.2.15). However, if this sample was mixed with the full-length OPA1 eluted at 200 mM imidazole, GTPase activity disappeared. This suggests that sample composition, in particular imidazole, interferes with the activity assay.

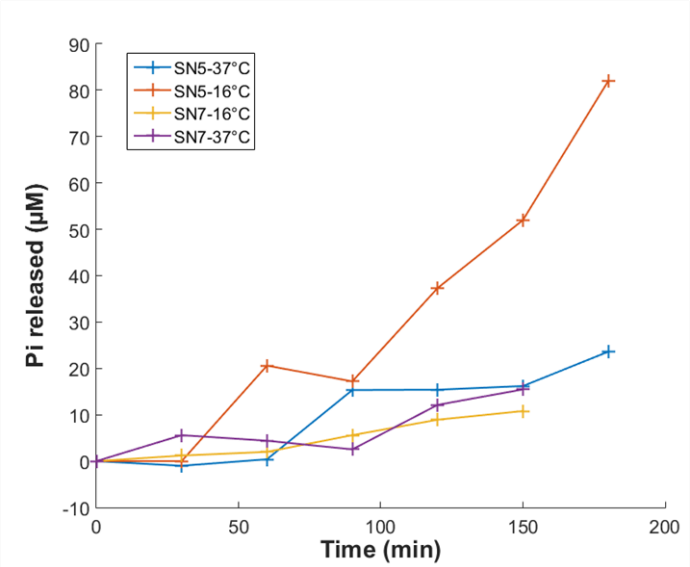

Figure 2.14 – GTPase activity of solubilized full-length OPA1. Measurement of the GTPase activity in supernatants after solubilization with 0.2% N-lauroylsarcosine (SN5) or 0.2% SDS (SN7) from OPA1 expressions at 16°C or 37°C. Enzyme assay based on malachite green in presence of 300 µM GTP and 0.2 mg/ml protein at 37°C (see Material & Methods).

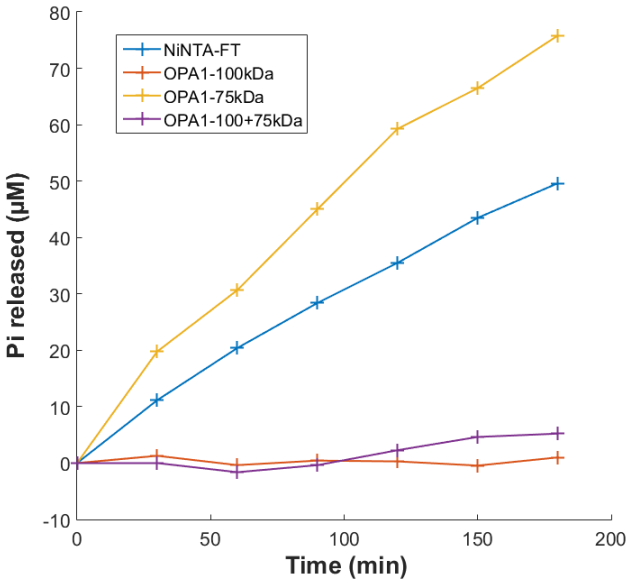

Figure 2.15 – GTPase activity of different OPA1 species and mixtures. GTPase activity was determined with *(i)* the solubilized OPA1, including the NiNTA flow-through (NiNTA-FT) and the 200 mM imidazole elution (OPA1-100kDa) containing full-length 100 kDa OPA1, *(ii)* the soluble OPA1 C-terminal 75 kDa fragment (OPA1-75kDa), and *(iii)* a 1:1 mixture of full-length 100 kDa OPA1 and 75 kDa C-terminal fragment. Enzyme assay based on malachite green in presence of 300 µM GTP and 0.2 mg/ml protein at 37°C (see Material & Methods)

2.4 Discussion

Despite intense research on OPA1 and its crucial roles for cell physiology and human health (Pernas and Scorrano, 2016), so far no high yield expression system is available to generate full-length recombinant OPA1. While the soluble short OPA1 forms that span a large part of the extramembrane domain can be expressed and recovered in a soluble, active form from different organisms, including *E. coli* (Ban et al., 2010; Liu and Chan, 2015), full-length OPA1 has been produced so far only at the µg-scale in eukaryotic cells or in vitro by different groups (e.g. (Olichon et al., 2002; Stafa et al., 2014) and some commercial providers. Here we present a first approach to high yield expression of full-length OPA1 splice variant 1 (Ban et al., 2010) in *E. coli* using a strain providing tRNAs for rare codons and a resolubilization procedure for inclusion bodies.

The human OPA1 splice variant 1 used in this study has been expressed earlier as a short variant, lacking the N-terminal part that contains a transmembrane domain (Ban et al., 2010). Our results show that bacterial expression of this OPA1 species in its full length version is limited by codon bias, *i.e.* differences between species in the frequency of occurrence of synonymous codons in coding DNA. Such codon

bias frequently affects expression levels of recombinant proteins (Rosano and Ceccarelli, 2014; Gustafsson et al., 2004; Kane, 1995). The sequence of the human opa1 gene contains many such codons that are rarely used in *E. coli*, but common in human genes. This leads to amino acid misinsertion and truncated protein affecting expression level and activity (Gustafsson et al., 2004). Analysis of the opa1 sequence (hyperlink "http://nihserver.mbi.ucla.edu/RACC/") identifies the position of many rare E. coli codons, in particular a high content of those for arginine and isoleucine, and to a lesser extend those for proline and leucine. Standard *E. coli* strains such as BL21 (DE3) Star are therefore inappropriate, and others like BL21CodonPlus-(DE3)-RIPL are necessary. The latter carries extra copies of the argU, ileY, and leuW tRNA genes, and this allowed expression of OPA1 in its full-length version. However, the protein accumulated in insoluble inclusion bodies.

A strategy to increase soluble protein production is expression at lower temperature. This can lead to the formation of non-classical inclusion bodies which allow the extraction of more native proteins (Jevševar et al., 2005) or even decrease protein aggregation in inclusion bodies (Rosano and Ceccarelli, 2014; Schein and Noteborn, 1988; Vasina and Baneyx, 1997). However, we could not observe such beneficial effects by expressing at 16°C. Alternatively, solubilization of proteins from inclusion bodies can be achieved by denaturating conditions (urea, guanidine-HCl) and refolding of proteins by dialysis, on-column or by dilution (Cabrita and Bottomley, 2004). However, this harsh approach may fail to yield properly refolded protein, can lead to aggregation of unfolded protein during refolding, and is time-consuming for screening a large number of conditions (Singh et al., 2015). Another approach uses mild, non denaturating solubilisation conditions to recover enzymatically active protein without the need of a denaturation-refolding step (Singh et al., 2015; Singh and Panda, 2005). This is possible with detergents used below their critical micelle concentration (CMC), where they interact with the protein allowing its solubilization and stabilization, without creating micelles which may denature proteins (Otzen, 2011). We could successfully solubilize full-length OPA1 with a low concentration of N-lauroylsarcosine (0.2% or 3.3 mM; CMC: 14.6 mM), along with shorter OPA1 fragments. Interestingly, low temperature had some positive effect on OPA1 protein yield after solubilization, but did not improve purity of resolubilized full-length OPA1 relative to smaller contaminating fragments.

Solubilized full-length OPA1 can be enriched by NiNTA affinity chromatography, which elimlinates certain contaminating fragments, but co-enriches other, probably His-tagged containing N-terminal fragments. To obtain higher purity, the purification process has to be improved. In addition to classical ion exchange or gel permeation chromatography, the affinity of the protein for GTP could be exploited, or an additional

C-terminal tag introduced. Moreover, the solubilization procedures may be improved. Data from the work on the short OPA1-S1 variant (Ban et al., 2010) suggest positive effects on OPA1 solubility when increasing the salt concentration up to 300 mM or adding GTP or GDP in the lysis buffer. However, higher salt concentration would also inhibit GTPase activity. It may also be appropriate to further examine the effect of lower temperature during expression, since e.g. the GTPase domain of OPA1 was well expressed even in BL21(DE3)pLysS bacteria when cultured at 27°C for only 2h after induction with low IPTG concentration (0.04 mM) (Griparic and Van Der Bliek, 2005).

GTPase activity of OPA1 was determined as a parameter of correctly refolded, native protein. This activity can be measured by radiolabeled GTP (Griparic and Van Der Bliek, 2005; Gout et al., 1993), a coupled enzymatic reaction (Ingerman and Nunnari, 2006), or as in our case with a malachite green based assay (Leonard et al., 2005), which is sensitive and allows high-throughput screening. Full-length OPA1 preparations after solubilization with N-lauroylsarcosine show GTPase activity (0,7 - 2,7 nmole/min/mg) in a range also observed with the short OPA1 forms (Samant et al., 2014), but this activity disappears after NiNTA affinity chromatography. However, GTPase activity also disappears if an active fraction is mixed with a NiNTA elution fraction, suggesting that composition of the elution buffer inhibits GTPase activity and/or the activity assay. Indeed, OPA1 is eluted from the NiNTA column at 200 mM imidazole, and imidazole concentrations higher than 40 mM are known to inhibit GTPase activity of Dnm1 and other dynamin-related proteins (Ingerman and Nunnari, 2006). Thus, the activity loss may not be due to elimination of an active fragment in the preparation, but most probably caused by buffer interference, a point that has to be addressed in a future optimization of the purification protocol. To elucidate whether the recombinant full-length OPA1 has true GTPase activity, it has to be further purified to separate it from OPA1 fragments and other contaminating GTPases, and care has to be taken for buffer effects, in particular by eliminating imidazole. However, it is still possible that full-length OPA1 is per se inactive. In case of the yeast OPA1 homologue, Mgm1, no GTPase activity was detected for the long form l-Mgm1 in its monomeric state, and this did change only marginally if the protein was inserted in cardiolipin containing liposomes (DeVay et al., 2009). In addition, the full-length OPA1 expressed here still has the mitochondrial targeting sequence which might also interfere with perfect folding of the protein (Van Wuytswinkel et al., 1995).

Instead of yielding full-length OPA1 protein, BL21 (DE3) bacteria produced only OPA1 fragments with two major forms: an insoluble N-terminal 30 kDa protein (containing the His-tag) and a soluble 75 kDa protein comprising the GTPase epitope (position 708-830) as recognized by monoclonal antibody. Most likely, they correspond to the N- and C-terminal fragments resulting from proteolytic cleavage of full-length

OPA1 in this particular bacterial strain. According to our mass spectrometry data, the soluble 75 kDa species spans from about position 213 to at least 895 (or up to the C-terminus). It is thus almost identical to the short sOPA1 forms cleaved in mitochondria by the OMA1 protease at around position 200. Despite the absence of a His-tag, this OPA1 species could be partially enriched by NiNTA affinity chromatography, and the preparation showed a relatively high GTPase activity (2,2 nmole/min/mg), close to what has been reported earlier (Samant et al., 2014).

Taken together, our study provided evidence that recombinant full-length l-OPA1 can be obtained from expression in *E. coli* in soluble and potentially active form, along with an active short fragment almost identical to the physiologically active s-OPA1. However, further attempts are necessary to improve purity of the preparations.

Chapter 3

Dual function of NDPK-D: local GTP supply and intermembrane lipid transfer activities

This work has been published as part of the following publications:

Boissan, M., Montagnac, G., Shen, Q., Griparic, L., Guitton, J., Romao, M., Sauvonnet, N., Lagache, T., Lascu, I., Raposo, G.,Desbourdes, C., Schlattner, U., Lacombe, M.L., Polo, S., van der Bliek, A.M., Roux, A., and Chavrier, P. (2014) Nucleoside diphosphate kinases fuel dynamin superfamily proteins with GTP for membrane remodeling. *Science* **344**, 1510-5.

Kagan, E., Jiang, J., Huang, Z., Tyurina, Y.Y., Desbourdes, C., Cottet-Rousselle, C., Dar, H.H., Verma, M., Tyurin, V.A., Kapralov, A.A., Cheikhi, A., Mao, G., Stolz, D., St. Croix, C.M., Watkins, S., Shen, Z., Li, Y., Greenberg, M.L., Tokarska-Schlattner, M., Boissan, M., Lacombe, M.L., Epand, R.M., Chu, C.T., Mallampalli, R., Bayir, H., and Schlattner, U. (2016) NDPK-D (NM23-H4)-mediated externalization of cardiolipin enables elimination of depolarized mitochondria by mitophagy. *Cell Death Diff.* **23**, 1140-51.

3.1 Introduction and objectives

In this chapter we address the recently proposed model of a dual function of NDPK-D in the mitochondrial intermembrane space (IMS) (Schlattner et al., 2013a) (see chapter 1.3.2 for more details). NDPK-D is a kinase which transfers phosphate from ATP to different NDPs for NTP generation. This defines the phosphotransfer mode of NDPK-D which is coupled to respiration via ANT (Tokarska-Schlattner et al., 2008) and is inhibited when NDPK-D cross-links liposomes *in vitro* or binds to mitochondrial membranes in cells (Schlattner et al., 2013a). The second function of this kinase is intermembrane lipid transfer, especially of cardiolipin (CL), from the IMM to the OMM of mitochondria, defined as lipid transfer mode in the model mentioned above.

Generation of NTPs, including mainly GTP, by NDPK-D in the mitochondrial IMS suggests the presence of a particular sink for GTP in this compartment. We hypothesized that one of these GTP consumers could be the dynamin-related mitochondrial GTPase OPA1. OPA1 is involved in IMM dynamics and structure, including mitochondrial fusion. A direct channeling of GTP from the kinase active site to the GTPase could explain why the presence of NDPK-D in the IMS is important, despite the existence of several cytosolic NDPK isoforms, whose reaction products are generally assumed to equilibrate with the IMS.

The appearance of CL at the mitochondrial surface upon a mitophagy trigger has been identified as a novel signal for mitophagy (Chu et al., 2013). Indeed, collapse of CL asymmetry between IMM and OMM by externalization of CL to the OMM leads to recognition of these mitochondria by autophagosomes, mediated by interaction of CL with autophagosomal LC3-II (Chu et al., 2013; Li et al., 2015; Kagan et al., 2014; Kagan et al., 2009). This finally leads to elimination of damaged mitochondria, an important step in mitochondrial quality control. Although Chu et al. showed that CL externalization is a mitophagic signal, the mechanism for such CL externalization remained unclear. We hypothesized that NDPK-D could play a role in this process by its lipid transfer mode, thus acting as a component of a pro-mitophagic signaling pathway.

Further, it has been shown that the lipid transfer and phosphotransfer activities of NDPK-D are dependent on the membrane binding state of the protein, and that both activities normally do not occur at the same time (Tokarska-Schlattner et al., 2008; Schlattner et al., 2013a). Thus, an important remaining question concerns the mechanism responsible for the switch between the two functions. We hypothesized that at least one element of this switch could involve the NDPK-D interaction partner OPA1.

In order to test these different hypothesis, we used two cellular models. First, we employed HeLa cells, naturally almost devoid of endogenous NDPK-D, to express

wild-type or mutated NDPK-D. Second, we used mouse lung epithelial cells (MLE), where NDPK-D can be knocked down by siRNA. This allowed *(a)* to study the channeling of GTP, *(b)* to quantify the appearance of CL at the mitochondrial surface following a mitophagic stilmuli, and *(c)* to test the relationship between NDPK-D and OPA1.

3.2 Material and methods

3.2.1 Reagents

Carbonyl cyanide m-chlorophenylhydrazone (CCCP), protease inhibitor cocktail, fetal bovine serum for MLE and HeLa cells (FBS), human serum albumin essentially fatty acid free, phosplipase A2 from porcine pancreas (PLA2) and mouse actin antibody (a3853) were purchased from Sigma (St Louis, MO, USA). Lipofectamine reagent RNAiMax and Oligofectamine were from Life Technologies. Mouse NDPK-D siRNAs were from Origene (SR404588). Zeocine (ant-zn-1p) and blasticidine (ref: 46-1120) were from Invivogen. LC-MS grade Chloroform and Methanol were from Fischer Scientific. All reagents were from Sigma unless stated otherwise.

3.2.2 Cell culture

Mouse lung epithelial cells (MLE15) MLE cells were cultivated according to the manufacturer's protocol in HITES media which is formulated as follow: Ham's F12 media (DMEM/F12, Invitrogen) supplemented with insulin (0.005 mg/ml final), transferrin (0.01 mg/ml), sodium selenite (30 nM), hydrocortisone (10 nM), Hepes (10 nM), ß-estradiol (10 nM), L-glutamine (2 mM in addition to what is in the base medium) and 10% (v/v) FBS.

T-ReX HeLa cells T-Rex HeLa cells (Invitrogen) stably transfected with the vector pcDNA™4/TO (Invitrogen) without insert (CTRL) or with an insert coding for the protein NDPK-D wild-type (WT), mutated at His151 in the catalytic site (H151N) or at Arg90 on the lipid binding site (R90D) were grown in a humidity chamber at 37°C, 95% O2 and 5% CO2, in medium formulated as follow: MEM medium (Gibco), FBS 10% (v$\check{}$) final, Glutamine (2 mM final, PAA Laboratories), Penicillin-Streptomycin 1000 U/ml final (PAA Laboratories). Hela cell lines were plated at 0.5 cells/cm² in a 2 well labtek® (Nunc) 3 days before observation with a confocal microscope.

3.2.3 NDPK-D knock-down in MLE15 cells

One day before the transfection, 0.5 - 0.75 million cells were seeded in ø10 cm dishes. The transfection was then performed according to the manufacturer's protocol (Life technologies) using medium without antibiotics (Opti® -MEM reduced serum medium). According to preliminary studies, 3 different siRNAs sequences were used: SR404588A– rGrCrArGrCrGrArArCrUrGrUrUrGrArArCrUrGrGrGrCrAGA; SR404588B– rGrGrA-rArCrGrUrCrArUrCrCrArUrGrCrUrArGrCrGrArUTC; SR404588C–rArCrCrUrArCrU-rArCrCrU rCrUrGrUrCrArArCrArArGrAAG. Nucleotides were resuspended in the provided buffer at a final concentration of 50 µM. 10 µl of each siRNAs were mixed leading to an equimolar mix of the three references at 50 µM. The day of the transfection, two solutions were prepared: the first one contained OPTI-MEM (5 ml) + siRNAs (29 µl) and the second one was made with OPTI-MEM (5 ml) + lipofectamine RNAiMax (430 µl). Then solutions were mixed together and incubated 5 min at room temperature. After incubation, 1 ml of mix was added per plate containing 9 ml culture medium without antibiotics. The day after the transfection (12-16h), the culture medium was changed by a new one containing antibiotics. CCCP treatment was performed 60h after transfection.

3.2.4 PLA_2 assay using liquid chromatography mass spectrometry

Induction of mitophagy by CCCP For MLE15 control cells, CCCP treatment was performed one day after seeding the cells and 60h after transfection for NDPK-D deficient MLE15 cells. For both group of cells, treatment duration was 3h at 20 µM final CCCP (ci=50 mM).

Crude mitochondria isolation After treatment, the medium was removed and cells were collected with 1 ml trypsin per dishes (5 min incubation at 37°C). Cells were centrifuged 5 min at 700 g, 4°C. The pellet was then washed once with 20 ml PBS and cells were pelleted 5 min at 700 g and 4°C. Then the cells were resuspended in 1 ml of MIB1 buffer (210 mM Mannitol, 70 mM sucrose, 10 mM Hepes, pH7.4, 1 mM EDTA, 0.1% BSA, protease inhibitor cocktail) and homogenized with a Potter homogenizer using 100 strockes at 1600 rpm. The homogenized cells were transferred into 2 ml eppendorf tubes and centrifuged at 700 g for 5 min, 4°C. The supernatant was collected and centrifuged at 6000 g for 5 min at 4°C. Then the pellet (containing crude mitochondria) was resuspended with 1 ml MIB2 buffer (210 mM Mannitol, 70 mM sucrose, 10 mM Hepes, pH7.4) and centrifuged at 10000 g for 10 min at 4°C. The supernatant was discarded and the pellet was kept on ice until PLA_2 treatment (not more than 30 min).

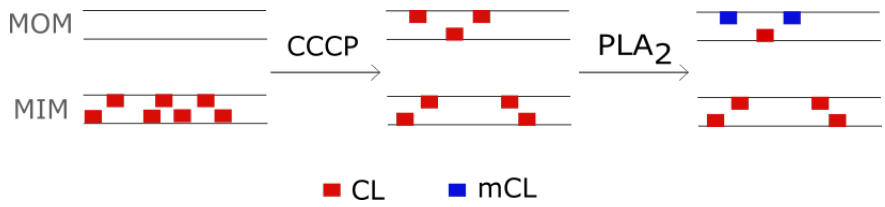

Figure 3.1 – Phospholipase A2 treatment of isolated mitochondria to quantify CL externalization. MOM: mitochondrial outer membrane, MIM: mitochondrial inner membrane, CL: cardiolipin, mCL: monolysocardiolipin, CCCP: carbonyl cyanide m-chlorophenylhydrazone, PLA_2: phospholipase A2

Phospholipase A2 treatment The phospholipase A2 enzyme is able to hydrolyze phospholipids at the second carbon group of glycerol (sn-2 position) into lysophospholipids and fatty acid. Under conditions used in this study, CL is externalized at the mitochondrial surface due to CCCP treatment. Then, PLA2 will hydrolyze CL species localized at the outer leaflet of the OMM into monolysocardiolipin (mCL) (Fig. 3.1). These species will then be then analyzed and quantified by mass spectrometry.

The crude mitochondria were resuspended with 60-100 µl MIB3 buffer (210 mM Mannitol, 70 mM sucrose, 10 mM Hepes, 100 µM $CaCl_2$), depending on the pellet size. The protein amount is determined with the Bradford protein assay (Biorad). Then, 25-45 µl of mitochondria (50-100 mg of mitochondrial proteins) depending on the yield of the isolation step were treated with PLA_2 by adding 20 mg/ml final of human serum albumin essentially fatty acid free, and PLA_2 at a final concentration of 0.0005 U/µg of mitochondrial protein (PLA2 was preliminary diluted at 0.02 U/µl in MIB2 buffer). MIB3 was added in order to obtain a mitochondrial protein concentration of 1 mg/ml in the reaction volume, which was then incubated on ice for 45 min.

Lipid extraction protocol The mitochondrial pellet fraction treated or not with PLA_2 was then diluted with 0.75% KCl solution and then lipids were extracted with chloroform:methanol (2:1) according to the Folch's procedure (Folch et al., 1957) by vortexing every 10 min for 1h, on ice. Tubes were left at -20°C overnight before extraction of the lower phase. A second extraction was then performed only with chloroform (same volume as the fist one extracted). After extraction, the lipid extract was dried under nitrogen and resuspended in 50 or 100 µl of chloroform:methanol (2:1). 10 µl were then used to determine the phosphorus concentration in the sample by a spectrophotometric method using ascorbic acid (Rouser et al., 1970).

Sample preparation for MS Samples for calibration curve were prepared with 0.1 µM of internal standard of mCL $(14:0)_3$ and increasing concentration of mCL $(18:2)_3$. To plot the calibration curve, the ratio between the peak area of the standard (mCL $(18:2)_3$) and the peak area of the internal standard (mCL$(14:0)_3$) was first calculated and plotted

against the concentration of the standard in the calibration sample. Samples for LC-MS analysis were prepared with 0.1 µM final of internal standard of mCL $(14:0)_3$. The sample volume to add in the vial was calculated in the way that the final concentration of total phosphorus was 0.2 to 0.5 mM. After drying the sample under N2, the sample was resuspended with 15 µl of mobile phase A. Each sample was run twice.

Parameters of the LC-MS device The samples were analyzed on a Dionex Ultimate™ 3000 HPLC coupled on-line to a Q-Exactive hybrid quadrupole Orbitrap mass spectrometer (ThermoFisher Scientific, San Jose, CA). The injection volume was 5 µl. The solvent system was the following: solvent A (43% Hexane / 56% Propanol / 1% H_2O + 10 mM ammonium acetate / 0.01% formic acid / 0.5% triethylamine) and solvent B (40% Hexane / 53% Propanol / 7% H_2O + 10 mM ammonium acetate / 0.01% formic acid / 0.5% triethylamine). The characteristics of liquid chromatography and mass spectrometer devices were the following: chromatography column: Normal phase, Luna silica (2) 3 µm particle size, 100 Å pore size, 2.0x150 mm (ID x length), Phenomenex; HPLC device: Dionex Ultimate 3000; mass spectrometer, on line: ThermoFischer Q Exactive-ESI-Orbitrap MS in negative mode; Capillary voltage: 3.2 kV; capillary temperature: 320°C; sheath gas flow rate: 8 units; S-lens RF: 65. Injected samples contained all class of phospholipids. The elution gradient (Table 3.1) used allows the separation of mCL species from other phospholipids.

Table 3.1 – Elution gradient used for phospholipids separation on normal phase liquid chromatography coupled on line with mass spectrometer.

Time (min)	% solvent B	Flow (µl/min)
0	10	200
15	37	200
23	65	200
25	100	200
	100	225
47	100	225
57	10	200
70	10	200

LC-MS quantification For quantification of the amount of CL available for PLA2 treatment, a ratio between the peak area of mCL species and mCL internal standard was calculated. The concentration of mCL was then calculated based on the calibration curve.

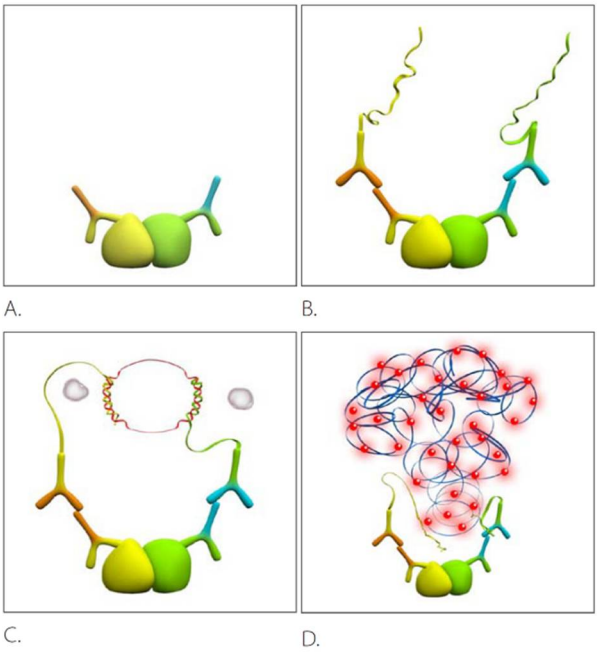

Figure 3.2 – Principle of the proximity ligation assay (PLA). A: Fixation of primary antibodies. B: Addition of secondary antibodies conjugated with oligonucleotides. C: Ligation step, hybridization if the two probes were in close proximity. D: Amplification step, rolling-circle amplification (RCA).

3.2.5 *In situ* proximity ligation assay

The *in situ* proximity ligation assay (PLA) is a tool used for protein-protein interaction studies. The targeted proteins are first labeled with a specific primary antibody (Fig 3.2.A). Then secondary antibodies tagged with oligonucleotides directed against IgG of the primary antibodies are used (Fig 3.2.B). If the targeted proteins are in close proximity (< 40 nm), the oligonucleotides of the secondary antibodies hybridize (Fig 3.2.C) and an amplification reaction will occur. With the use of fluorescently labeled nucleotides, a fluorescence signal will appear at the site of the proximity of the two proteins (Fig 3.2.D).

Staining *In situ* proximity ligation assay (PLA) was performed using a Duolink kit (Olink Bioscience, Uppsala, Sweden) as previously described (Söderberg et al., 2006). Cells grown on chamber microscopy slides were fixed with 3% paraformaldehyde-PBS solution for 10 min at 37°C, permeabilized with 0.2% Triton X-100 in PBS, blocked 1h with a Duolink blocking agent and then incubated 1h at room temperature with primary antibodies (monoclonal mouse anti-OPA1, 612607 from BD Biosciences, and rabbit polyclonal anti-NDPK-D produced and characterized as described earlier (Milon et al., 2000)). PLA probes (secondary antibodies tagged with DNA oligonucleotides) were then added. Hybridization, ligation, amplification and detection using Duolink

Detection Reagents Red (excitation 594 nm, emission 624 nm) were performed according to the manufacturer's protocol. Briefly, secondary antibodies were incubated in preheated humidity chamber for 1h at 37°C. Ligation was performed with a ligase-containing solution for 30 min at 37°C. Finally, the amplification step was performed with a polymerase-containing solution for 1h 40 min at 37°C. Nuclei were stained with Hoechst 33258. In parallel, expression of OPA1 and NDPK-D was analyzed using the same NDPK-D and OPA1 primary antibodies and standard immunofluorescence procedure (with Alexa Fluor 488- and Cy5-conjugated secondary IgGs).

Image acquisition and analysis Images were collected with a Leica TCS SP2 AOBS inverted laser scanning confocal microscope using a 63x oil immersion objective. Laser excitation was 351-364 nm for Hoechst 33258, 488 nm for Alexa 488, 543 nm for PLA and 633 nm for Cy5. Fluorescence emissions adjusted with AOBS were 480 nm for Hoechst 33258, 500-535 nm for Alexa 488, and 565-600 nm for PLA and 645-685 nm for Cy5. Acquisitions were performed on a randomly chosen field containing 15-25 cells. The background noise autofluorescence was removed by fine filter (Kernel 3×3) using Volocity software (Improvision). Image quantification was performed using Image J (Schneider et al., 2012) and Volocity softwares. The PLA signal was quantified and normalized to cell number.

3.2.6 OPA1 knock-down in HeLa cells

siRNA oligonucleotides were synthesized by Eurogentec S.A (Seraing, Belgium). The following sequences were used : OPA1: 5'-GAUCAUCUGCCACGGGUUG ; scramble: 5'-GGCUGUAGAAGCUAUAGUU according to (Boissan et al., 2014). HeLa cells ($1.5.10^6$ cells/dish) were transfected with 50 nM oligonucleotide using 3 µl oligofectamine in ø10cm dish. The experiments were performed 72h after transfection.

3.2.7 Mitotracker Red CMXRos staining

Cells were stained 72h after transfection with 250 nM Mitotracker® Red CMXRos (Invitrogen, excitation/emission: 579/599 nm) for 30 min at 37°C to label mitochondria prior treatment and haversting.

3.2.8 Annexin V binding assay using flow cytometry

The relative CL amount in the outer leaflet of the OMM was evaluated using the Annexin V binding assay (Chu et al., 2013). Isolated crude mitochondria were incubated with FITC-labeled Annexin V (Interchim) to stain for anionic phospholipids and then

subjected to flow cytometric analysis (FACSCanto, Becton-Dickinson, Pont de Claix, France) of the green FITC fluorescence. Mitochondrial analysis was performed after appropriate settings of the forward light scatter and side light scatter detectors. The FITC fluorescence from gated red fluorescent mitochondria events was determined to evaluate the binding of Annexin-V to mitochondria.

3.3 Results

3.3.1 Membrane bound NDPK-D and OPA1 are in close proximity for interaction

Following earlier data on interaction of OPA1 with NDPK-D, we further analyzed the relationship between these two proteins by a proximity ligation assay in HeLa cells stably transfected with a vector expressing either the wild-type NDPK-D (WT), the kinase inactive (H151N) or the lipid binding deficient protein (R90D). *In situ* proximity ligation assays can detect whether two proteins are in close proximity (<40 nm) and can interact. In this case, a red fluorescence becomes detectable. Representative pictures of the experiments are shown in Fig.3.3.A along with quantifications which were performed by counting the number of spots per cell (Fig. 3.3.B). Results show that both wild-type or the kinase inactive NDPK-D are in close proximity with OPA1, suggesting that the mutation in the catalytic site of NDPK-D does not affect OPA1 interaction. However, for cells expressing the lipid-binding deficient NDPK-D, the number of PLA spots significantly decreased ($p<0.01$), suggesting that NDPK-D membrane binding is necessary for efficient OPA1/NDPK-D interaction.

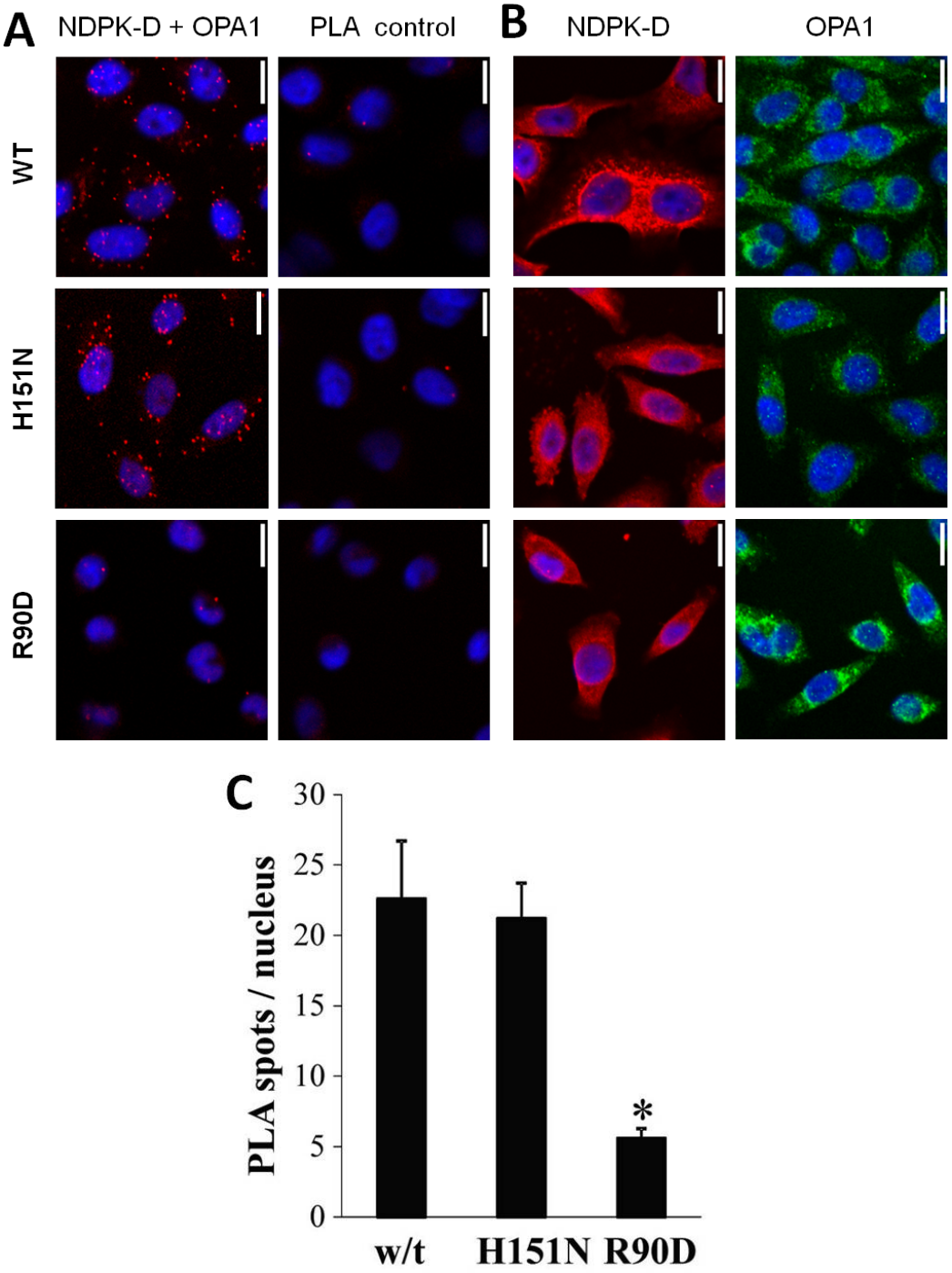

Figure 3.3 – Association of OPA1 with NDPK-D in HeLa cells. HeLa cells stably expressing NDPK-D wild-type (WT or w/t), CL-transfer-deficient mutant (R90D), or kinase-inactive mutant (H151N) were used to quantify OPA1 association with these NDPKs by proximity ligation assay (PLA). PLA signals correspond to red spots. Representative magnifications of confocal pictures are given, scale bar is 20 µm. **(A)** PLA with NDPK-D and OPA1 primary antibodies and control PLA without primary antibodies. **(B)** Control immunostainings showing expression of NDPK-D and OPA1 as detected by the same anti-NDPK-D and -OPA1 primary antibodies. **(C)** Quantification of PLA as shown in (A) from three experiments; data are given as mean ± SD (n=6), * $p<0.01$ compared to cells expressing w/t.

3.3.2 NDPK-D is necessary for cardiolipin externalization during CCCP-induced mitophagy.

Externalization of cardiolipin is a trigger for mitophagy and can recruit LC3 (Chu et al., 2013). Here we test whether NDPK-D is necessary for CL externalization during mitophagy. Mouse lung epithelial cells (MLE15) were used as a model system in addition to HeLa cells (shown in (Kagan et al., 2016)), comparing wild-type cells as a control with NDPK-D-silenced cells. Cells were then treated with CCCP to collapse the inner membrane potential and to induce mitophagy. After treatment, mitochondria were isolated, incubated with PLA_2 to hydrolyze externalized CL into mCL, the lipids extracted, and mCL species analyzed and quantified by LC-MS (Fig. 3.4).

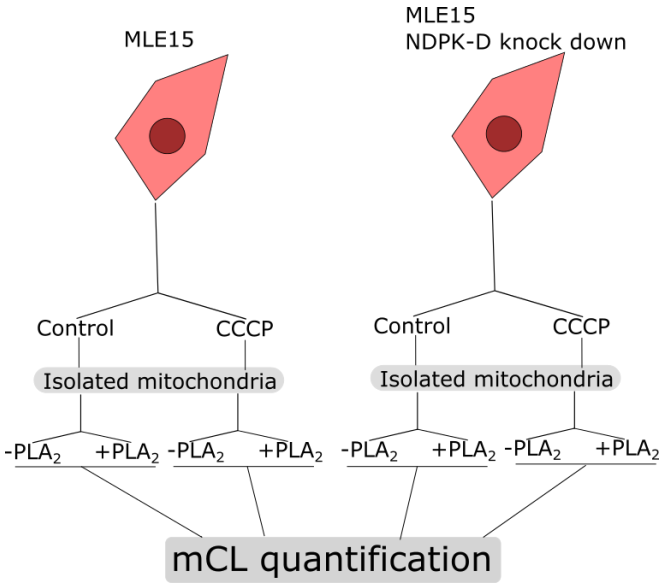

Figure 3.4 – Quantification of externalized cardiolipin by mass spectrometry in MLE cells. Flow diagram showing the experimental steps: CCCP treatment, mitochondrial isolation, PLA treatment, and mCL quantification with Annexin V.

NDPK-D in MLE cells was silenced by siRNA, leading to a knock-down of the protein by about 60% as seen in a Western blot of cell lysates analyzed for NDPK-D (Fig. 3.5.A). MLE control and silenced cells were treated or not by CCCP and analyzed by mass spectrometry for detectable species and quantity of mCL generated by PLA. CCCP-treatment did not generate new mCL species as e.g. oxidized or otherwise modified CL (Fig. 3.5.C). However, mCL increased in control cells treated with CCCP (Fig. 3.5.C), showing that more CL was available at the mitochondrial surface to serve as a substrate for PLA2 (Fig. 3.5.B). This confirmed that under our conditions CCCP-induced mitophagy indeed also leads to CL externalization as proposed earlier (Chu et al., 2013). By contrast, in the NDPK-D silenced cells, no such change in the level of

CL available for PLA_2 was observed after CCCP-treatment. This shows that NDPK-D is required during the process of CL externalization in MLE15 cells.

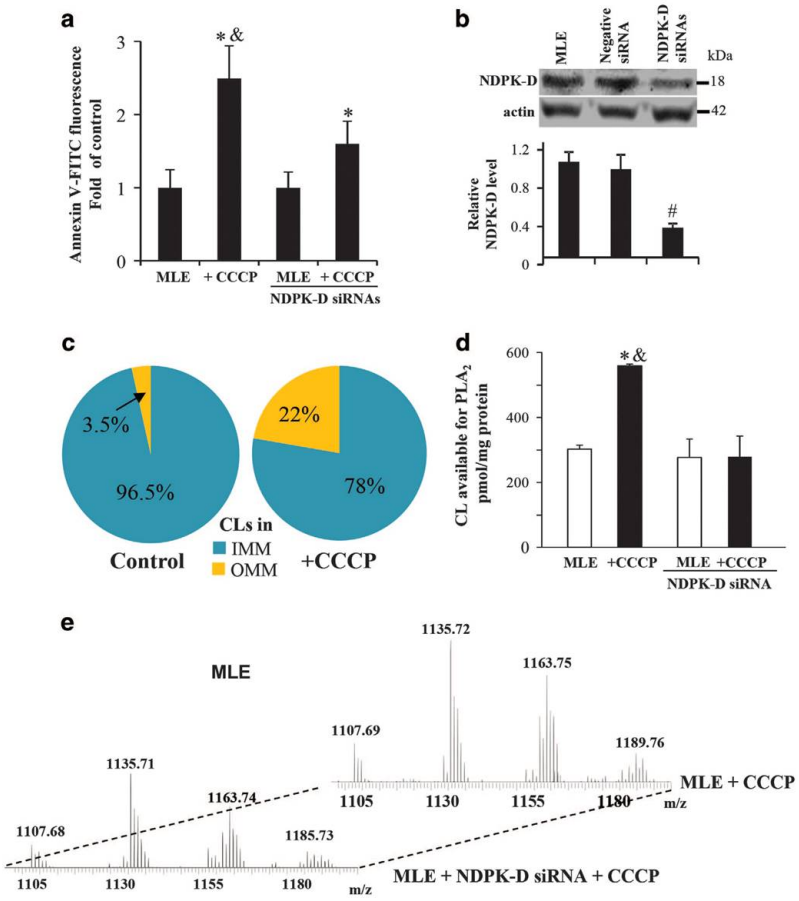

Figure 3.5 – CCCP induces externalization of cardiolipin in MLE cells. **(a)** Evaluation of CL in the outer leaflet of OMM using Annexin V-binding assay in w/t and NDPK-D RNAi MLE cells. Cells were treated with 20 µM CCCP for 3 h. Isolated mitochondria were incubated with FITC-labeled Annexin V to stain surface-exposed CL (anionic phospholipids) and then subjected to flow cytometric analysis (FACSCanto, Becton-Dickinson). **(b)** Knock-down of NDPK-D using siRNA interference in MLE cells. As controls, cells were mock transfected or transfected with non-targeted negative siRNAs. Expression of NDPK-D was evaluated by western blotting. Lower panel shows the relative NDPK-D expression calculated based on densitometry (n=3). **(c)** LC-MS analysis-based relative contents of CL in OMM and IMM in control and CCCP-treated MLE cells are presented. **(d)** Evaluation of CL in the outer leaflet of OMM in w/t and NDPK-D knocked down MLE cells using PLA_2 treatment with subsequent assay of mono-lyso-CL by LC-MS analysis. **(e)** Representative MS spectra of mono-lyso CL from MLE cells with normal expression of endogenous NDPK-D or after treatment with NDPK-D siRNAs. # $P<0.05$ versus cells transfected with non-targeting negative siRNAs. * $P<0.05$ versus control cells without CCCP treatment. & $P<0.05$ versus MLE cells transfected with NDPK-D siRNAs under the same condition (20 µM CCCP/3 h).

3.3.3 OPA1 affects NDPK-D-mediated cardiolipin externalization

The final question that we addressed was how pro-mitophagic triggers like CCCP, or pro-apoptotic triggers like rotenone used earlier (Schlattner et al., 2013a), can induce CL transfer by NDPK-D. In other words, how NDPK-D can switch from the phosphotransfer to the lipid transfer mode. Since we showed that NDPK-D phosphotransfer involves OPA1/NDPK-D interaction (3.3.1 and (Schlattner et al., 2013a)) and OPA1 acts as some sort of sensor of mitophagy (MacVicar and Langer, 2016), this GTPase could be also involved in initiating NDPK-D lipid transfer. OPA1 is structurally altered early during mitophagy by proteolytic cleavage from long into short variants, and this event could also play a role in switching between the two modes of NDPK-D action: phosphotransfer and lipid transfer.

As a first test of this hypothesis, we analyzed the effect of a partial OPA1 knock-down on CCCP-induced CL externalization. HeLa cells expressing NDPK-D wild-type (WT) or lipid binding-deficient mutant (R90D) were transiently transfected with OPA1 siRNA. Partial silencing of OPA1 was chosen, since full silencing would directly induce mitophagy. CL content at the mitochondrial surface was assessed by Annexin V staining, which in mitochondria is specific for CL due to the lack of PE (Horvath and Daum, 2013). Together with Mitrotracker staining, this allowed quantification of CL at the mitochondrial surface per mitochondria (Fig.3.6). Figure 3.6 shows the samples analyzed by flow-cytometry for control and OPA1 knock-down cells in both Hela WT and R90D.

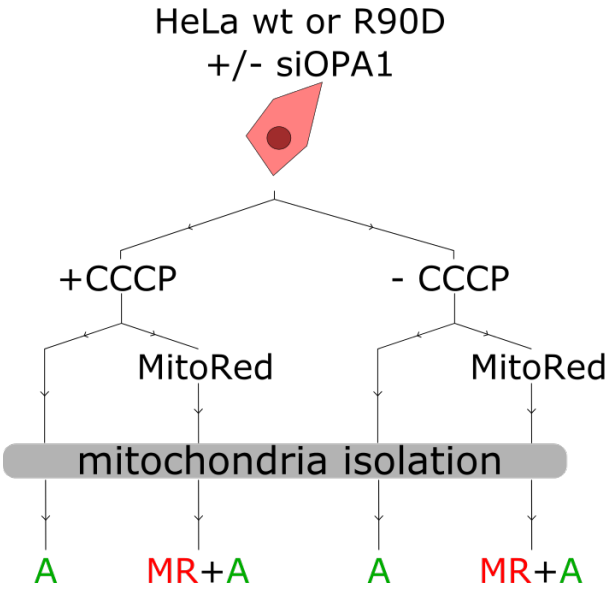

Figure 3.6 – Quantification of externalized cardiolipin by annexin V staining in HeLa cells. Labeling and detection of Annexin V (A) and Mitotracker Red (MR or MitoRed).

Western blots for OPA1 in extracts of WT and R90D HeLa cells revealed a total of five different OPA1 bands that could be assigned according to Duvezin-Caubet et al.

(Duvezin-Caubet et al., 2007). Under control conditions, there were three major bands, representing 95 kDa and 90 kDa long variants, and a 80 kDa short variant (Fig. 3.7.A), while under mitophagy conditions further short variants at 75 kDa and above 80 kDa occurred (Fig. 3.7.B). Interestingly, already expression of R90D mutant instead of WT NDPK-D changed the OPA1 pattern, with the 95 kDa long variant strongly decreasing in favor of the 90 kDa long variant (Fig. 3.7.A).

Partial OPA1 silencing led to an about 60% decrease that affected all OPA1 species to similar extend (Fig. 3.7.A). When cells were then treated with 20 µM CCCP for 3h, a condition known to induce mitophagy (Kagan et al., 2016), both large OPA1 species at 90 and 95 kDa disappeared, as already reported earlier (Griparic et al., 2007). In contrast, short OPA1 variants became prominent, in particular the 75 kDa and 80 kDa species in WT, but only the 75 kDa species in R90D expressing cells (Fig. 3.7.B).

We then quantified how much CL is externalized in HeLa mitochondria under the different conditions, using Annexin V staining of isolated mitochondria. In Hela cells expressing wild-type NDPK-D, addition of CCCP induced the externalization of CL under both OPA1 control and silenced conditions as expected, correlating with the disappearance of long OPA1 variants (Fig. 3.7.C). This was not the case with the R90D mutant, which is constitutively CL-binding and -transfer incompetent. If one now compares the CL on the mitochondrial surface between the transfer-competent NDPK-D WT HeLa cells and the transfer incompetent R90D mutant HeLa cells, the difference was 1.38-fold with scrambled siRNA, and 1.65-fold with OPA1 siRNA. In other words, partial silencing of OPA1 increased the capacity of CL transfer of WT NDPK-D as compared to R90D, supporting a negative effect of OPA1 on NDPK-D-supported CL transfer.

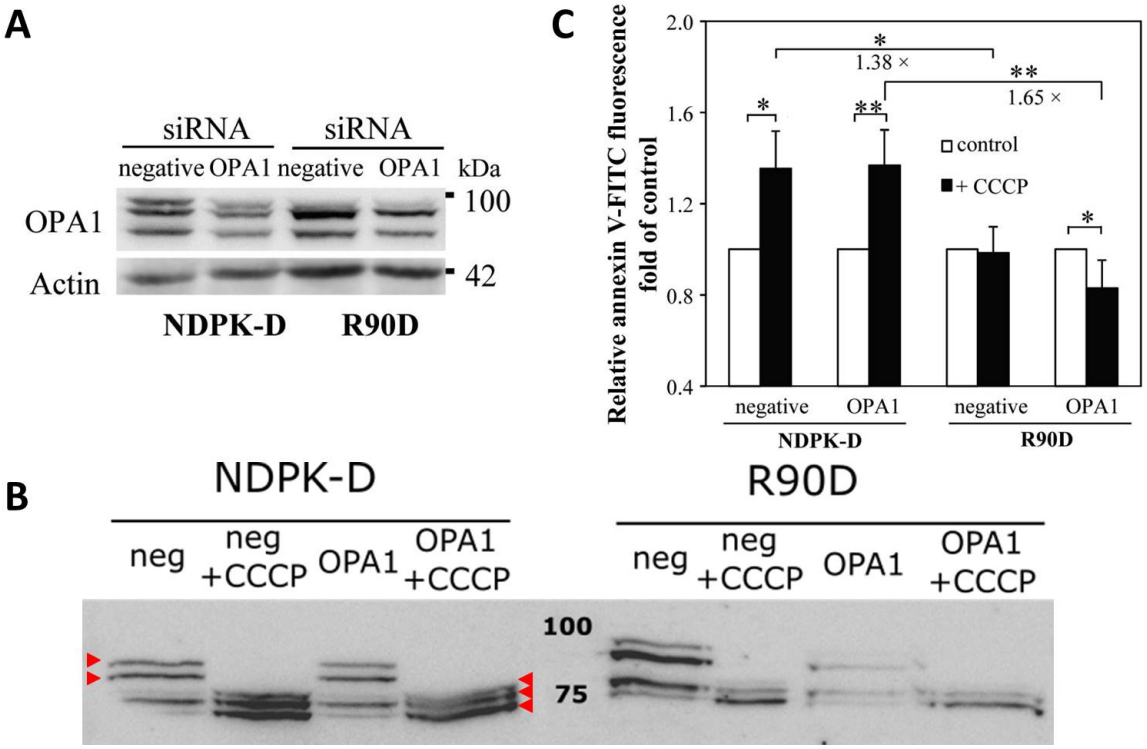

Figure 3.7 – Effect of partial OPA1 silencing on CL externalization. (A,B) Representative immunoblots of partial OPA1 silencing in HeLa cells expressing WT NDPK-D and R90D mutant using siRNA. HeLa cells stably transfected with WT NDPK-D or R90D mutant were transfected with negative or siRNA against OPA1. Red arrowheads indicate the five bands corresponding to OPA1 isoforms. **(C)** Surface assessable CL was quantified by an Annexin V binding assay. MitoTracker-positive particles of appropriate size were analyzed for FITC fluorescence by FACS. Data are means ± SD (n=3-4); * $p < 0.05$; ** $p < 0.01$. negative or neg., scrambled siRNA; OPA1, OPA1 siRNA. Note: Numbers in (C) indicate the fold-difference between CCCP-treated R90D- and WT NDPK-D-expressing cells, either on a control (1.38-fold) or partial OPA1 silenced background (1.65-fold).

3.4 Discussion

Data obtained here advance our understanding of the dual function of NDPK-D in phosphotransfer or lipid transfer. We show that:*(i)* NDPK-D interacts with OPA1 as a condition for direct fueling of OPA1 with GTP, shown in detail in the full project (Boissan et al., 2014); *(ii)* NDPK-D is necessary for CL externalization to the mitochondrial surface during the mitophagy induced by collapsing the mitochondrial membrane potential; this is shown here for MLE cells, but occurs similarly in HeLa cells (Kagan et al., 2016), and that *(iii)* OPA1 might repress NDPK-D CL-transfer activity, possibly by the direct interaction of NDPK-D with OPA1, in particular the long variants.

First, wild-type or kinase inactive NDPK-D show a close proximity between NDPK-D and OPA1, allowing an interaction between these proteins. However, when NDPK-D is unable to bind to the mitochondrial membrane, NDPK-D and OPA1 are not able to

interact any more, suggesting that CL interaction of NDPK-D (and possibly also OPA1) is necessary for complex formation. Such complexes are probably necessary to allow the direct GTP fueling of OPA1. Indeed, CL-containing liposomes were used to show in vitro that NDPK-D increases GTP consumption rate of OPA1 in presence of physiological nucleotide concentrations (1 mM ATP, 100 µM GTP, 10 µM GDP) (Boissan et al., 2014). Other results on the cytosolic isoforms of NDPK, published by our collaborators (Boissan et al., 2014) (see Appendix A), show that also cytosolic NDPK-A/B interact with dynamin-1/2 to favor dynamin-mediated membrane fission at the clathrin-coated pits and to enhance dynamin GTPase activity. Alltogether, the general principle seems to be that NDPKs provide GTP to dynamins directly within NDPK/dynamin complexes. In case of NDPK-D, GTP directly provided to OPA1 is regenerated through consumption of mitochondrial ATP. Indeed, the cellular concentration of GTP is 10 times lower than the one of ATP (Traut, 1994), while the Km of the dynamin GTPase activity is comparable to ATPases. Thus, through the conversion of the most abundant nucleotide, ATP, into the lesser abundant GTP, NDPK-D increases a local pool of GTP for its interaction partner OPA1. Similar local supply of ATP has recently been shown for vesicle-bound glycolytic enzymes to drive vesicle transport along axons in neuronal cells (Zala et al., 2013; Hinckelmann et al., 2016).

Secondly, we show that NDPK-D is essential for CL externalization during CCCP-induced mitophagy. We show this here in mouse lung epithelial cells, and it was shown at the same time for HeLa cells (Kagan et al., 2016). Importantly, these conclusions were reached by two independent methods using isolated, intact mitochondria (Kagan et al., 2016): a mass spectrometric approach quantifying PLA-accessible CL at the mitochondrial surface and an Annexin V staining assay to quantify the amount of CL at the mitochondrial surface (see Fig. 2a in (Kagan et al., 2016); Appendix B). Moreover, no oxidized CL is detected in our conditions, indicating that CL has not been oxidized by cytochrome C as it occurs during apoptosis (Kagan et al., 2009; Kagan et al., 2014). Non-oxidized CL can be recognized by LC3-II which mediates autophagosomes formation and thus leads to mitochondrial autophagy (Kagan et al., 2009; Kagan et al., 2014). It has to be noted that CL species identified at the mitochondrial surface after CCCP treatment are the same as the one identified in the mitochondrial outer membrane in healthy mitochondria. This shows that CL is redistributed at the mitochondrial surface during mitophagy without altering its molecular structure. Such CL redistribution is in agreement with the model of a rotary wheel behavior of NDPK-D to externalize CL (Schlattner et al., 2013a). In addition to our data, the importance of NDPK-D for mitophagy is supported by several other evidences reported by Kagan et al. (Kagan et al., 2016) for CCCP-challenged cells: *(i)* NDPK-D knock-down in MLE cells reduces the co-localization of mitochondria and lysozomes (see Fig. 1 and suppl

Fig. 2, Appendix B); *(ii)* expression of the lipid binding-deficient NDPK-D in HeLa cells precludes autophagy and degradation of mitochondrial marker proteins (see Appendix B-Fig. 4); *(iii)* knock-down of NDPK-D in MLE cells inhibits degradation of mitochondrial marker proteins (MnSOD, TIM23, Cyt C) (see Appendix B-suppl. Fig. 3), and a similar phenotype occurs in case of CL synthase knock-down in the same cells (suppl. Fig. 1, Appendix B); *(iv)* HeLa cells without additional NDPK-D expression (see Fig. 5, Appendix B) or siNDPK-D treated MLE cells (suppl. Fig. 4, Appendix B) both show reduced mitochondrial fragmentation less decreased mitochondrial volume as compared to NDPK-D expressing control cells. Alltogether, these data confirm the key role of NDPK-D in CL externalization and mitophagy. Our data thus largely confirm the model proposed earlier (Schlattner et al., 2013a). In particular under conditions of CCCP exposure, leading to a collapse of the IMM potential, NDPK-D is necessary for CL externalization and full induction of mitophagy.

Finally, a remaining question is how NDPK-D switches to the lipid transfer function during CCCP-induced mitophagy. Our current hypothesis would involve the GTPase OPA1, a mitochondrial fusion protein (Belenguer and Pellegrini, 2013; Anand et al., 2014), and its interaction with NDPK-D. Indeed, as one of the first events after a pro-mitophagic trigger has occurred, the long OPA1 isoforms anchored in the IMM are cleaved into short isoforms (Belenguer and Pellegrini, 2013). This short isoform is even proposed to act as a pro-fission factor (Anand et al., 2014; Wai and Langer, 2016), thus increasing the mitochondrial fragmentation which is observed during mitophagy (Baker et al., 2014; Kubli and Gustafsson, 2012). If we assume that IMM-anchored, long OPA1 isoforms are necessary for NDPK-D interaction and GTP fueling, their cleavage into short isoforms could release NDPK-D from its complexes with OPA1, allowing it to engage into simultaneous binding to IMM and OMM (Tokarska-Schlattner et al., 2008) and intermembrane CL transfer. This model is consistent with all published data, and supported by the partial knock-down of OPA1, which slightly increases CL transfer, suggesting that (long) OPA1 has a negative effect on CL transfer mediated by NDPK-D. Further experiments will be necessary to fully reveal the complex relationship between NDPK-D and OPA1. Recombinant proteins whose development is discussed in another chapter (Chapter 2) will be very useful for these approaches.

Chapter 4

Disruption of NDP kinase activity or cardiolipin interaction of NDPK-D (NM23-H4, NME4) in HeLa cells: mitochondrial impairment, altered cellular proteome, and metastasis-like phenotype

FRM consortium on NDPK-D/NM24-H4
Université Pierre et Marie Curie, University Paris 06, and Saint-Antoine Research Center, INSERM UMR-S 938, Paris, France
University Grenoble Alpes - UJF, Laboratory of Fundamental and Applied Bioenergetics, SFR Environmental and Systems Biology (BEeSy), and INSERM U1055, Grenoble, France.

This work is a manuscript in preparation. C.D. was involved in the characterization of the mitochondrial phenotype of NDPK-D mutations in HeLa cells.

Abstract

NDPK-A (NM23-H1, NME1) has been the first metastasis suppressor established. However, few is known in this respect about other members of this multi-protein family, in particular the mitochondrial isoform NDPK-D (NM23-H4, NME4) which is mainly localized in the mitochondrial intermembrane space. As we showed earlier, NDPK-D provides GTP to the mitochondrial GTPase OPA1, stimulates respiration, binds to cardiolipin and promotes its inter-membrane transfer to the mitochondrial surface. Here we deleted either its NDP kinase activity (H151N mutant) or its cardiolipin interaction (R90D mutant) and expressed these mutants or WT protein in HeLa cells that are almost devoid of endogenous NDPK-D. Both mutations independently led to a similar cellular phenotype, characterized by inhibited cell-cell contact, growth of individualized cells, and increased migratory and invasive potential, the typical properties of a metastatic phenotype. This morphotypic switch was associated in both mutant clones with an altered cellular proteomic profile, including several metastasis-related proteins, the cell-cell contact protein N-cadherin, and mitochondrial proteins, as well as structural and functional changes of the mitochondrial network. These data suggest that NDPK-D has a role reminiscent to the metastasis suppression well known for NDPK-A. Loss of function leads to primary alterations in mitochondria that probably elicit an unknown mitochondria-nuclear communication responsible for pro-metastatic reprogramming of the cellular proteome.

4.1 Introduction and objectives

Carcinomas, the most prevalent malignancies in humans, arise from normal epithelium tissues in a multistep progression from benign precursor lesions. Metastasis, the final step in malignancy, is the cause of death for 90% of cancer patients. Molecular mechanisms underlying metastasis have to be elucidated for accurate detection and treatment (Chaffer and Weinberg, 2011). During metastatic disease, complex pathways involving the tumor cell and the microenvironment mediate tumor invasion at the primary site, survival and arrest in the bloodstream, extravasation, and colonization at a secondary site. The breakdown of epithelial intercellular adhesion and the acquisition of an invasive program allowing epithelial cancer cells to breach the basement membrane and to invade stromal type I fibrillar collagen, referred to as epithelial-mesenchymal transition (EMT), are considered crucial events in malignancy yet poorly understood. During EMT, epithelial cells lose some of their epithelial characteristics, including cell adhesion and cell polarity; cytoskeletal rearrangement occurs that ultimately leads to an increased motility and an invasive phenotype.

The first metastasis suppressor gene discovered, NM23-H1/NME1 (Steeg et al., 1988) encodes the nucleoside diphosphate kinase A (NDPK-A), which catalyzes synthesis of nucleoside triphosphates including GTP from corresponding nucleoside diphosphates and ATP. In human, ten isoforms of the NM23/NME/NDPK family have been identified (reviewed in (Boissan et al., 2009)), among those the specific mitochondrial isoform NM23-H4 (NME4/NDPK-D) (Milon et al., 1997). If NM23-H1 has a well-known anti-metastatic activity, the contribution of the other isoforms, such as NM23-H2, -H3 or -H4 are much less documented in this respect.

NME4/NM23-H4, further called NDPK-D, is a mitochondrial enzyme, principally localized in the intermembrane space, which binds to the mitochondrial inner membrane (MIM) through anionic phospholipids, mainly cardiolipin (Milon et al., 2000; Tokarska-Schlattner et al., 2008). The enzyme acts as a lipid-dependent mitochondrial switch with dual function (1) in phosphotransfer serving, in particular, for local GTP supply to the mitochondrial dynamin Optic Atrophy 1 (OPA1), a driver of mitochondrial fusion (Boissan et al., 2014; Schlattner et al., 2013a) and (2) in cardiolipin transfer from the inner to the outer membrane, where it serves as pro-mitophagic or pro-apoptotic signal (Kagan et al., 2016; Schlattner et al., 2013a).

Here we analyzed whether the described NDPK-D functions also affect the cellular growth phenotype. HeLa TRexTM cells, which naturally express very low levels of NDPK-D, were stably transfected with pcDNA4/TO vectors, either empty or designed to express NDPK-D wild type (WT) or mutant proteins. Single point mutations were chosen to suppress either the catalytic NDPK activity of the enzyme (H151N) or

its ability to bind cardiolipin (R90D), which is essential for its function in cardiolipin intermembrane transfer. Strikingly, both mutations led to similar alterations in the cell phenotype, linked to altered mitochondrial structure and function, reprogramming of protein expression, and a morphotypic switch with a pro-metastatic phenotype.

4.2 Material and methods

Materials T-Rex™ HeLa cells and the pcDNA4/TO vector were obtained from Invitrogen (ThermoFischer Scientific). Recombinant expression and purification of NDPK-D, as well as generation of anti-human NDPK-D polyclonal antibodies in rabbits are described elsewhere (Milon et al., 2000).

Cell culture and preparation of cellular extracts T-Rex™ HeLa cells stably transfected with the vector pcDNA4/TO (Invitrogen) without insert (control) or with an insert coding for the NDPK-D WT or NDPK-D mutated at His151 in the catalytic site (H151N) or at Arg90 at the cardiolipin binding site (R90D) were grown in MEM medium in a humidity chamber at 37°C, 95% O2 and 5% CO2 as previously described (Tokarska-Schlattner et al., 2008). Construction of pcDNA4/TO vectors to stably express NDPK-D wild type (WT) or R90D mutants T-Rex™ HeLa cells is also described elsewhere (Tokarska-Schlattner et al., 2008). The H151N mutant was obtained by site mutagenesis of the WT sequence in the pcDNA4/TO vector by using Genecust (Dudelange, Luxembourg). Clones overexpress comparable levels of proteins already without specific induction. Maximal expression levels of both NDPK-D proteins can be achieved by incubation with 1 µg/ml tetracycline for 24 h. Cells grown in 3.5 cm diameter Petri dishes or in 6 well plates were rinsed twice with ice-cold PBS, and lysed in 50 µl RIPA/well containing anti-proteases (Calbiochem, cocktail set III), anti-phosphatases (Sigma, cocktail n°2) and 1 mM EDTA, or ready made protease inhibitor mix (Complete® Merck, 1 tablet per 50 ml of buffer). The lysate was either used immediately (immunoblots), or sonicated for additional 5 sec at 50% power and centrifuged at 10 000 g for 20 min at 4°C and the supernatant kept (for citrate synthase activity measurements). Lysate was stored by freezing in liquid nitrogen and storage at -20°C until use. The protein concentration was determined by a BCA protein assay (Pierce) using BSA as standard.

Immunoblot analysis Proteins from cell extracts were electrophoretically separated on 10 or 12.5% SDS polyacrylamide gels and transferred onto Immobilon P membranes (0.1 µm, Millipore) for 2 h at 22 V in 10 mM CAPS buffer, pH 11, 10% methanol for

NDPK-D and Mn-SOD, as described in (Milon et al., 2000) or onto nitrocellulose membranes for 90 min at 50 V in 0.025 M Tris-base, 0.192 M glycine, 20% methanol, and 0.02% SDS for the other proteins. The transfer and blotting procedures are described elsewhere (Tokarska-Schlattner et al., 2008). The primary antibodies were (with dilution): polyclonal anti-NDPK-D (1/7500; (Milon et al., 2000)), monoclonal anti-Mn-SOD (1/2000; Bender Medsystems GmbH, Vienna, Austria)). The peroxidase-coupled secondary antibodies were (with dilution): anti-rabbit IgG (1/10,000) or anti-mouse IgG antibodies (1/2000). The blots were revealed using the Amersham Biosciences ECL PlusTM immunoblotting detection system from GE Healthcare.

NDPK activity NDPK enzyme activity of Nm23-H4 was determined with a photometric coupled enzyme assay, as described previously (Milon et al., 2000), using kinase buffer (50 mM Tris- HCl, pH 7.4, 50 mM KCl, 5 mM $MgCl_2$, 1 mg/ml BSA, and 100 µM Ap5A to inhibit endogenous adenylate kinase). Briefly, 0.2 mM ATP and 0.2 mM TDP were used as substrates (all substrates from Roche Applied Science), and ADP production was coupled with pyruvate kinase (Sigma) and lactate dehydrogenase (Roche Applied Science) to NADH oxidation.

Citrate synthase activity (CS) CS activity was measured in the cell lysate in presence of 150 mM Tris pH 8, 150 µM 5',5'-ditiobis(2-nitrobenzoic acid) (DTNB), 300 µM acetylcoenzyme A and 500 µM oxaloacetate (adapted from (Li et al., 2014)). The reduction of DTNB by CS was followed at 412 nm on a Specord 210 spectrophotometer for 5 min at 37°C, after the addition of oxaloacetate. The CS activity was measured in triplicate at different protein concentrations (25, 40 and 50 µg of cellular protein per cuvette) for each HeLa mutant. The activity of citrate synthase was then expressed in nkat/mg of total protein.

Cell dispersion, aggregation and invasion assays Cellular spatial distribution was characterized and quantified using algorithmic programs of cellular sociology based on the use of three previously described geometrical models, namely Voronoï's partition, Delaunay' graph and minimum spanning tree (MST) as described (Nawrocki Raby et al., 2001). The aggregation assay was performed as reported (Boterberg et al., 2000) by seeding cells on top of a gelified agar medium. Aggregate formation was scored after 24 h incubation at 37°C. Native type I collagen and Matrigel invasion assays were performed as described earlier (Fritah et al., 2008; De Wever et al., 2010).

Fluorescence microscopy and immunocytochemistry For cellular staining of mitochondria and NDPK-D, cells cultivated on microscope glass slides were fixed in 3.7%

paraformaldehyde, permeabilized in PBS containing 0.5% Triton, blocked in PBS containing 3% BSA, and incubated with anti-NDPK-D affinity-purified primary antibody (dilution 1:500; (Milon et al., 2000)) and the anti-rabbit Alexa-Fluor 488-conjugated secondary antibody. Slides were mounted with Fluoromount-G (Electron Microscopy Sciences, Hatfield, PA) and examined with a Leica HC microscope. For an alternative mitochondrial staining, cells were treated similarly and incubated with anti-mouse Mn-SOD primary antibody (dilution 1:150) and with donkey anti-mouse IgG secondary antibody, Alexa Fluor 488-conjugate (dilution 1:150; Thermo Scientific).

2D-DIGE proteomic analysis *Sample preparation for 2D-electrophoresis.* Cells were grown in 6 cm diameter Petri dishes close to confluence (106 cells), washed in cold PBS, harvested with a rubber policeman and pelleted by centrifugation at 800 g for 5 min. Pellets, dried by aspiration, were frozen in liquid nitrogen and stored at -80°C until use. Pellets were lysed and homogenized 20 min on ice in 100 µl of UTCD buffer (8 M urea, 2 M thiourea, 4% CHAPS and 50 mM Dithiothreitol). The samples were treated with 1% Nuclease mix (GE Healthcare) to remove all traces of nucleic acids. The lysates were centrifuged at 20,000 g and 4°C for 1 h. The supernatants were collected and proteins were precipitated with a 2-D Clean-Up Kit (GE Healthcare) following the manufacturer's instructions. The pellets were solubilized in 100 µl of UTC buffer (UTCD buffer without DTT) and the protein concentration determined using Quick-Start Bradford Dye Reagent (Bio-Rad).

Two-dimensional differential in-gel electrophoresis (2D-DIGE). Three independent samples of two independent clones for each condition (control HeLa-Trex cells transfected with empty vector (V1A, B, C; V2B, C, D); cells overexpressing the wild-type NDPK-D (H1A, B, C; H2A, C, D), the catalytically inactive (N1A, B, D; N2A, B, C) and the cardiolipin binding deficient enzyme (R1A, B, C; R2A, B, D) were analyzed by 2D-DIGE. 50 µg of proteins of each sample were labeled with Cy3 or Cy5 CyDy™ DIGE Fluor minimal dyes (GE Healthcare) following the manufacturer's instructions. The internal standard (IS = Std) was prepared by mixing equal amounts of each sample and labeled with Cy2. 50 µg of labeled samples (Cy3 or Cy5) and internal standard (Cy2) were mixed in twelve different combinations as follows: H1A-Cy3/V1A-Cy5/IS-Cy2, H2A-Cy3/V2B-Cy5/IS-Cy2, N2A-Cy3/H2C-Cy5/IS-Cy2, H1B-Cy3/N1A-Cy5/IS-Cy2, R1A-Cy3/H2D-Cy5/IS-Cy2, R2A-Cy3/H1C-Cy5/IS-Cy2, N1B-Cy3/V1B-Cy5/IS-Cy2, V2C-Cy3/N1D-Cy5/IS-Cy2, R1B-Cy3/N2B-Cy5/IS-Cy2, N2C-Cy3/R2B-Cy5/IS-Cy2, V1C-Cy3/R1C-Cy5/IS-Cy2 and V2D-Cy3/R2D-Cy5/IS-Cy2. Each of the twelve mixes (150 µg) was analyzed by 2D-DIGE as previously described with minor modifications (Prévilon et al., 2013). Protein separation was performed by isoelectrofocusing on 18 cm pH 3–11NL Immobiline™ Drystrips (IPG strips, GE Healthcare) in the first dimension and

SDS-PAGE on twelve different 8 to 18% acrylamide gels in the second dimension. Cy2, Cy3, and Cy5 components of each gel were individually imaged as described previously (Prévilon et al., 2013).

Statistical analysis. Image analysis, relative quantification of spot intensity, statistical evaluation using the Student's t-test p-value and PCA (principal component analysis) were carried out with DeCyder 7.0 software (GE Healthcare). Normalization across all gels was performed using the internal standard. A spot was considered as differentially represented between two sample groups if the following conditions were fulfilled: protein abundance fold change above +1.3 or below -1.3, Student's t-test p-value below 0.05.

Modeling with ingenuity pathway analysis. Functional analyses were generated through the use of QIAGEN's Ingenuity Pathway Analysis (IPA® QIAGEN Redwood City, www.qiagen.com/ingenuity).

Protein identification by Mass Spectrometry (MS) and database searching. For MS identification of proteins of interest, two distinct semipreparative 2D-gels were prepared using 400 µg of H and 400 µg of a mix of R and N respectively to rehydrate the IPG strips. After electrophoresis, 2D-gels were fixed and stained in 1 µM RUBPS as described in Pieri et al. (Pieri et al., 2016). Gels were scanned using a Typhoon 9400 Trio Variable Mode Imager (GE Healthcare) at 488/520 nm, 100 µm resolution. Spots of interest were excised using the Ettan spot picker (GE Healthcare). In-gel digestion was carried out with trypsin, according to a published procedure with minor adjustments (Shevchenko and Shevchenko, 2001) and using for all steps a Freedom EVO 100 digester/spotter robot (Tecan, Switzerland): sample was destained twice with a mixture of 100 mM ammonium bicarbonate (ABC) and 50% (v/v) acetonitrile (ACN) for 45 min at 22°C and then dehydrated using 100% ACN for 15 min, before being reduced with 25 mM ABC containing 10 mM DTT for 1 h at 56°C and alkylated with 55 mM iodoacetamide in 25 mM ABC for 30 min in the dark at 22°C. Gel pieces were washed twice with 25 mM ABC and dehydrated (twice, 15 min) and dried (10 min) with 100% ACN. Gel cubes were incubated with sequencing grade modified trypsin (Promega, USA; 12.5 ng/µl in 40 mM ABC with 10% ACN, pH 8.0) overnight at 40°C. After digestion, peptides were washed with 25 mM ABC, dehydrated with 100% ACN and extracted twice with a mixture of 5% formic acid (FA)-50% ACN. Extracts were dried using a vacuum centrifuge Concentrator plus (Eppendorf). For MS and MS/MS ORBITRAP, analyses were performed using an Ultimate 3000 Rapid Separation Liquid Chromatographic (RSLC) system (Thermo Fisher Scientific) online with a hybrid LTQ-Orbitrap-Velos mass spectrometer (Thermo Fisher Scientific). Briefly, peptides were dissolved in 4 µl of 10% ACN–0.1% TFA (Trifuoro acetic acid). Then peptides were loaded and washed on a C18 reverse phase precolumn (3 µm particle size, 100 Å pore

size, 150 µm i.d., 0.5 cm length). The loading buffer contained 98% H2O, 2% ACN and 0.1% TFA. Peptides were then separated on a C18 reverse phase resin (2 µm particle size, 100 Å pore size, 75 µm i.d., 15 cm length) with a 16 minutes gradient from 100% A (0.1% FA and 100% H2O) to 50% B (80% ACN, 0.085% FA and 20% H2O). The Linear Trap Quadrupole Orbitrap mass spectrometer acquired data throughout the elution process and operated in a data dependent scheme with full MS scans acquired with the Orbitrap, followed by up to 20 LTQ MS/MS CID spectra on the most abundant ions detected in the MS scan. Mass spectrometer settings were: full MS (AGC: 1 × 106, resolution: 6 × 104, m/z range 400–2000, maximum ion injection time: 500 ms) and MS/MS (AGC: 5 × 103, maximum injection time: 20 ms, minimum signal threshold: 500, isolation width: 2 Da, dynamic exclusion time setting: 30 s). The fragmentation was permitted for precursors with a charge state of 2, 3, 4 and above. For the spectral processing, the software used to generate .mgf files was Proteome discoverer v1.4.0.288. The threshold of Signal to Noise for extraction values is 3. Database searches were carried out using Mascot version 2.4 (Matrix Science, London, UK) on "homo sapiens" proteins (20,345 sequences) from the SwissProt databank containing 542,503 sequences (192,888,369 residues) (February 2014). The search parameters were as follows: carbamidomethylation as a variable modification for cysteins, and oxidation as a variable modification for methionines. Up to 1 missed tryptic cleavage was tolerated, and mass accuracy tolerance levels of 10 ppm for precursors and 0.45 Da for fragments were used for all tryptic mass searches. Positive identification was based on a Mascot score above the significance level (i.e. b5%).

Mitotracker labeling MitoTracker® Green FM (Invitrogen, M-7514) was solubilized in DMSO to obtain a 5 mM stock solution. For mitochondrial network analysis in live cells, Hela cell lines were plated at 0.5 cells/cm² in a two-well Labtek® (Nunc) three days before observation with a confocal microscope. Mitochondria were labeled with 100 nM MitoTracker Green for 20 min at 37°C in a humidity chamber (95% O2 and 5% CO2). Images were acquired with a confocal laser-scanning microscope Leica TCS SP2 AOBS (Leica, Heidelberg, Germany) equipped with a 63x oil immersion objective (HCX PL APO 63.0 x 1.40), a perfusion chamber (POC chamber, LaCon, Erbach, Germany) and an incubation system (O2-CO2-°C, PeCon, Erbach, Germany). Laser excitation was 488 nm for MitoTracker Green and the fluorescence emissions adjusted with the confocal was 500-550 nm. The confocal pinhole was set to 1 Airy and kept constant during the whole experiments as all the other parameters. Experiments were performed on a randomly chosen field containing 8-12 cells. Images were encoded in a 512x512 pixels (8-bit) format with the Leica acquisition software.

For mitochondrial mass determination, cells were harvested and 2.10^5 cells were

labeled with 100 nM MitoTracker® for 20 min at 37°C. Then cells were subjected to flow cytometric analysis (FACS Fortessa SORP1P, Becton-Dickinson, Le Pont de Claix, France) of the green fluorescence of MitoTracker Green (detection at 575 ± 13 nm). The intensity of the green fluorescence was measured after appropriate set-up of the forward scatter and side scatter detectors on 10,000 to 20,000 events. Data were acquired and processed using BD FACSDiva software v6.1.3.

As an estimate for the membrane potential of MIM, about 10^6 cells per sample were incubated for 30 min at 37°C with 50 nM TMRM, a membrane potential sensitive dye, and 100 nM Mitotracker Green. They were then centrifuged at 700 g for 4 min at 4°C, the pellet was resuspended in 1 ml PBS and then TMRM fluorescence gated by Mitotracker signal was analyzed by FACS. Cells were then incubated with 1 µl 50 mM CCCP for another 5 min at room temperature to entirely depolarize the mitochondria, and again analyzed by FACS. About 20,000-50,000 events gated on Mitotracker fluorescence were measured, and differences in samples before and after addition of CCCP calculated as readout for mitochondrial membrane potential

Quantitative analysis of the mitochondrial network Mitochondria in fixed cells immunostained for mitochondrial Mn superoxide dismutase (MnSOD), or in live cells stained with Mitotracker Green (see above) were subjected to image analysis. Image J software (Schindelin et al., 2015) was used to extract foreground and segment mitochondria using an adaptive threshold ("top-hat filtering"). In the resulting binary image, regions of interest (ROI) were selected in peripheral regions of cells, where individual mitochondrial elements can be more easily detected as compared to the mitochondrial clusters close to the nucleus. Morphometric analysis of each ROI was done with Volocity v.4.0.1 software. This directly yielded parameters like average length, area, and perimeter of the detected elements, as well as further derived parameters such as the elongation factor (calculated as (mean_perimeter^2)/(4 π mean_area)).

4.3 Results

4.3.1 HeLa cells are a convenient model system to study the effect of NDPK-D variants

Control HeLa clones present a very low amount of NDPK-D, at the detection limit of immunoblots, while clones expressing WT or mutant enzymes exhibit a single band at the size of mature enzyme (Fig. 4.1). NDP kinase activity measured in mitochondria purified from vector control and H151N mutant clones was barely detectable, while it was high within the same order of magnitude in WT and R90D mutant clones (Fig. 4.1).

This also indicates that the overexpressed NDPK-Ds were correctly imported and processed in mitochondria.

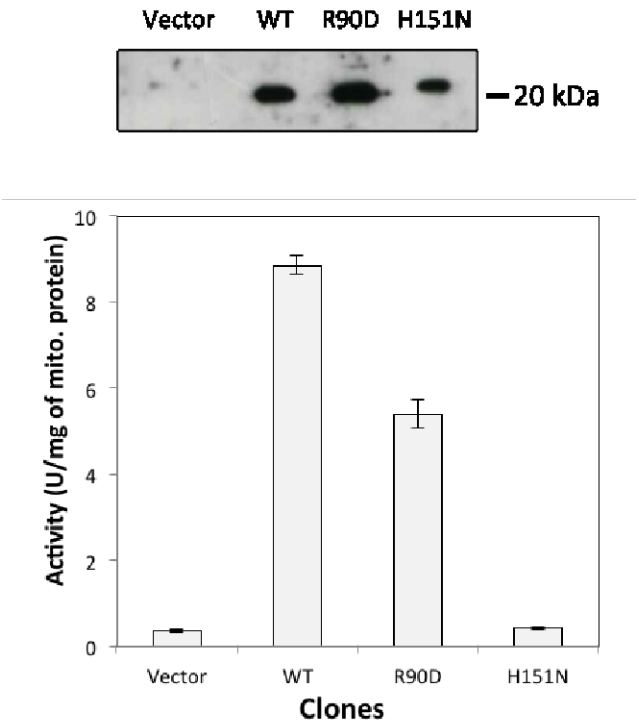

Figure 4.1 – NDPK-D protein levels and NDP kinase activity of the four different HeLa clones. HeLa cells were stably transfected with empty pcDNA4TO (vector) or constructs for expression of NDPK-D WT or mutants R90D (CL binding deficient) or H151N (kinase dead). (Top) Representative immunoblot probed with poly¬clonal anti-NDPK-D antibodies (Milon et al., 2000). (Bottom) NDP kinase activity in purified HeLa mitochondria. Values are the mean ± SD (n=3).

4.3.2 NDPK-D mutations induce a morphotypic switch linked to reduced N-cadherin expression

We first investigated growth pattern and cell morphology of the four HeLa clones and observed two distinct and very different cellular phenotypes (Fig. 4.2.A). While controls or NDPK-D WT expressing cells were organized as epithelioid clusters, cells expressing either of the two NDPK-D mutants, R90D or H151N, grew as randomly dispersed single cells, exhibiting no or very few cell-cell contacts. This latter phenotype was most pronounced in the H151N mutant (Fig. 4.2.A).

The acquisition of a scattered cellular growth phenotype is often associated with alterations in intercellular adhesion. We therefore investigated the impact of NDPK-D mutations on the cell-cell adhesion properties of HeLa cells (Fig. 4.2.B). In a slow aggregation assay, where cells are grown on soft agar, control and NDPK-D WT expressing clones formed compact islands, whereas again both mutant clones did not.

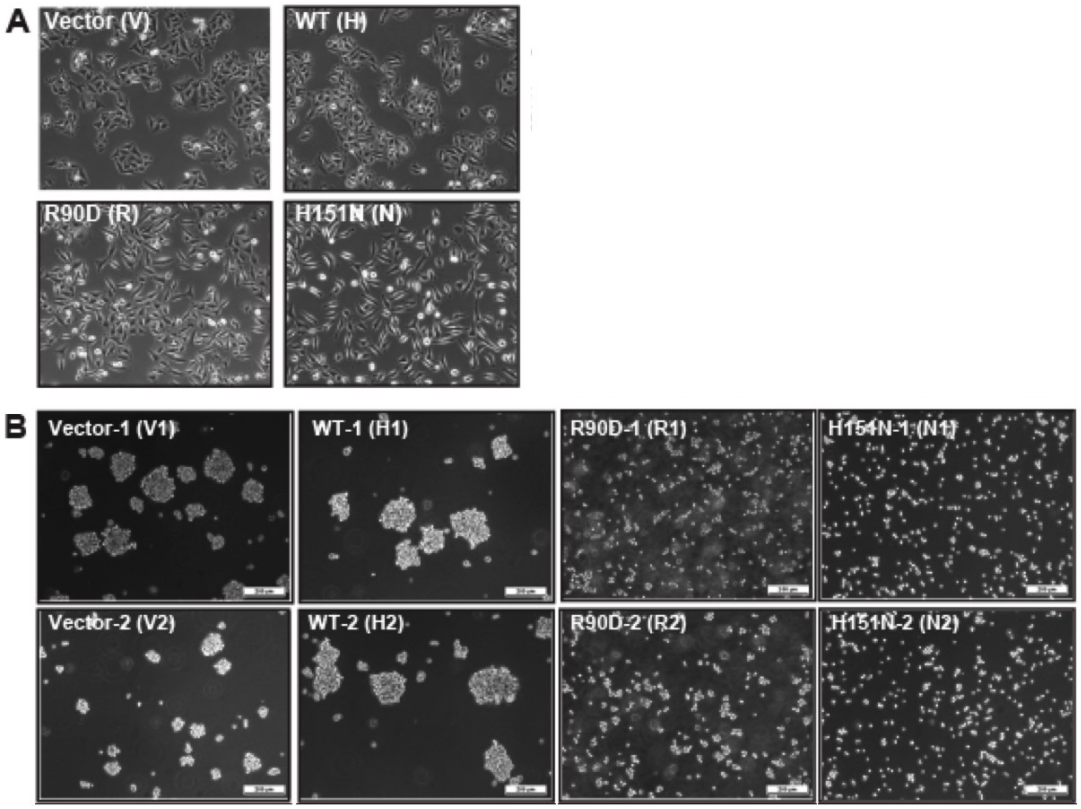

Figure 4.2 – Morphology and aggregation of the four different HeLa clones. **(A)** Morphology assessed by phase-contrast microscopy. Scale bar x µm . **(B)** Slow aggregation assay was performed by seeding the HeLa clones on top of a gelified agar medium. Aggregate formation was scored under an inverted microscope at x10 magnification after 24h incubation at 37°C. Scale bar x µm . Abbreviations for HeLa clones based on their expression vector: empty vector (V), WT NDPK-D (H), CL binding deficient R90D NDPK-D (R) or kinase dead H151N NDPK-D(N). Note that both mutations of NDPK-D induce a clear morphotypic switch.

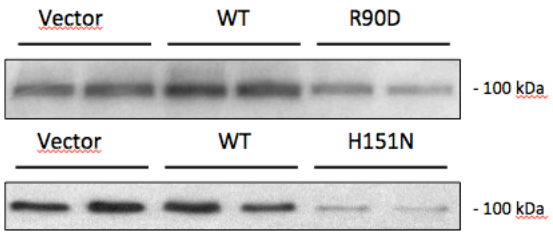

Figure 4.3 – Protein expression level of N-cadherin in the four different HeLa clones. Representative immunoblots of HeLa cell extracts (as in Fig. 4.1), run in duplicate.

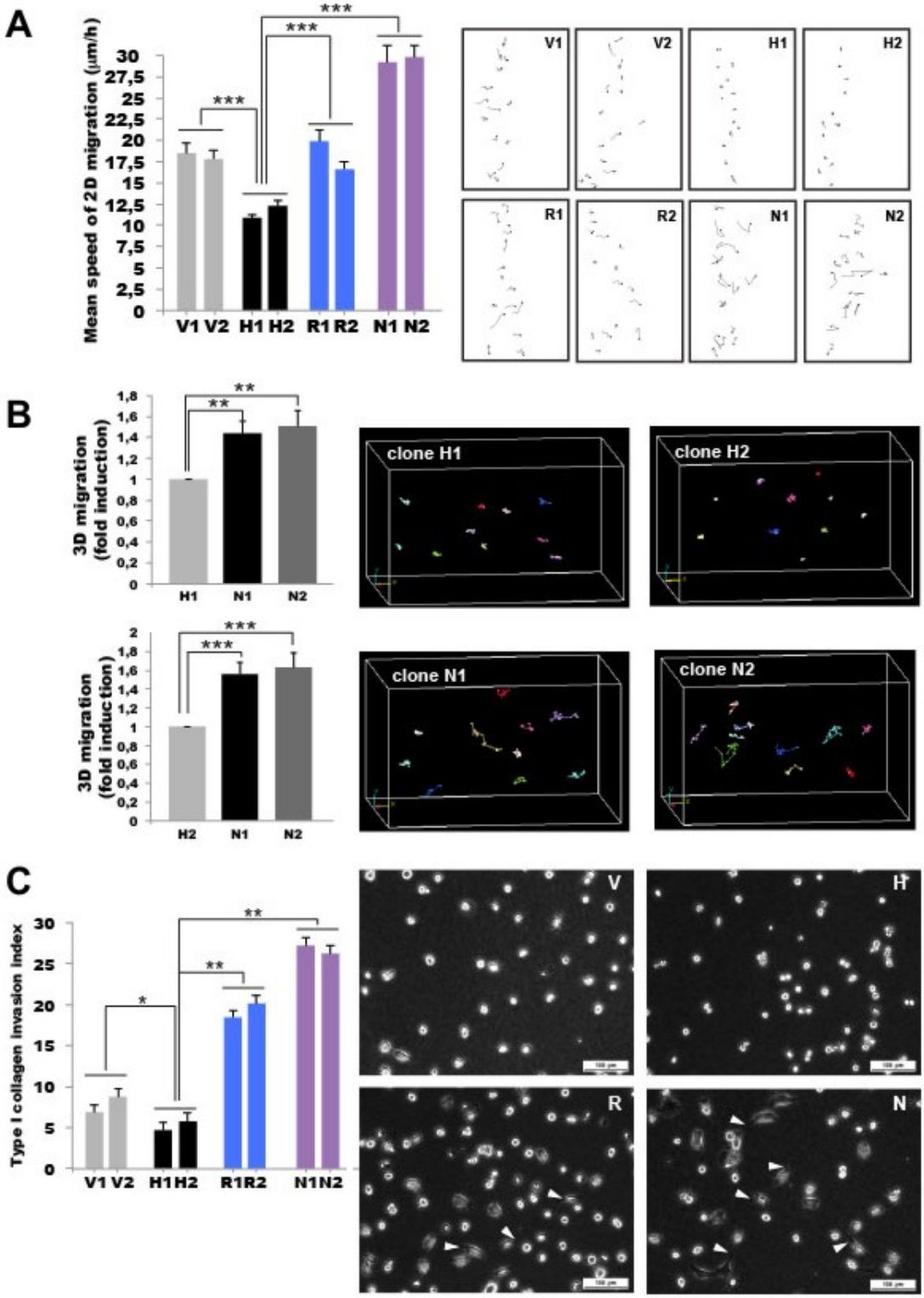

Figure 4.4 – Migration and invasion assays with the HeLa clones. (A) 2D migration assay. Migration speed (left) and trajectories (right) of the four different HeLa clones V, H, R and N. The migration trajectories of cells were computed from images recorded every 15 minutes for 1 hour. **(B)** 3D migration assay. Migration speed (left) and trajectories along the x-y-z plane (right) of the HeLa clones H and N. **(C)** Collagen invasion assay. Invasion index (left) and the morphological aspect of cells in type I collagen (right; arrowheads point to membrane protrusions) are shown for the four different HeLa clones V, H, R and N. For abbr. see Fig.2. Note that mutations of NDPK-D result in the invasion of HeLa cells into native type I collagen gel. Data show mean ± SEM (n=?). Note that also differences between individual V, H, R and N clones, without pooling, is highly significant.

We thus analyzed expression of the cell-cell adhesion protein N-cadherin in the four HeLa clones (Fig. 4.3). Cells expressing mutant NDPK-D exhibited a marked decrease in the level of N-cadherin as compared to control and WT NDPK-D expressing cells, again more pronounced for the catalytically inactive H151N mutant, consistent with the observed cellular phenotype. Taken together, we observed a morphotypic switch in the mutant NDPK-D expressing clones, with a marked loss of cell-cell aggregation and cell-cell contact.

4.3.3 NDPK-D mutations increase cell migration and invasive potential

To further examine consequences of altered cell morphology and cell-cell adhesion induced by NDPK-D mutants, we applied different migration assays (Fig. 4.4). In the 2D assay (Fig. 4.4.A), trajectories of controls and WT NDPK-D expressing clones were restricted and random, while a strikingly directional migration was observed with mutant expressing clones. In addition, the 2D migration speed was significantly increased in mutant expressing clones as compared to controls and WT NDPK-D expressing clones (clone V1: 18.5 ± 1.12 µm/h; clone V2: 17.8 ± 1 µm/h; clone H1: 10.9 ± 0.4 µm/h; clone H2: 12.3 ± 0.64 µm/h; clone R1: 19.9 ± 1.38 µm/h; clone R2: 16.6 ± 0.9 µm/h; clone N1: 29.2 ± 2.05 µm/h; clone N2: 29.8 ± 1.38 µm/h). Similarly, the 3D migration assay (Fig. 4.4.B) revealed higher migration speed along the x-y-z planes for the two mutant expressing clones as compared to the WT NDPK-D expressing clone (fold-change normalized to H1 - N1: 1.44 ± 0.12, N2: 1.51 ± 0.15; fold-change normalized to H2 - N1: 1.56 ± 0.13, N2: 1.63 ± 0.16).

Because the capacity to breach extracellular matrix barriers is critical for metastasis, we assessed whether expression of NDPK-D mutation affects the ability of HeLa cells to invade a three-dimensional matrix of native type I collagen during 24 hours (Fig. 4C). Expression of both NDPK-D mutants strongly increased invasion through type I collagen as compared to WT NDPK-D; the latter was even lower as compared to the control (invasion index (%): clone V1: 6.88 ± 0.94, clone V2: 8.75 ± 0.90; clone H1: 4.68 ± 0.94, clone H2: 5.78 ± 0.9; clone R1: 18.44 ± 1, clone R2: 20.15 ± 0.94, clone N1: 27.2 ± 0.95, clone N2: 26.5 ± 1). When seeded on native type I collagen, mutant NDPK-D formed numerous cellular protrusions (arrow heads), which invaded the collagen layer, while controls and WT enzyme expressing cells presented only few of these (Fig. 4.4.C). The invasive phenotype of mutant NDPK-D expression was further confirmed by a 14-day

invasion assay (Suppl. Fig. 4.11). Here, sections of the collagen layer were examined two-weeks after seeding the HeLa clones expressing WT or catalytically inactive enzyme. While the former remained on the surface, the latter deeply penetrated into the collagen layer.

4.3.4 The cellular proteome reveals changes in metastasis-related and mitochondrial proteins

The morphotypic switch and the pro-invasive phenotype observed for Hela cells expressing NDPK-D mutants are striking features, considering that they are triggered by a single point mutation in a mitochondrial protein. This implies communication between molecular NDPK-D structure/function and cellular behavior in respect to cell-cell contact, motility and invasive potential. Since this should be mediated by changes in the cellular proteome, we next performed a comparative 2D-DIGE proteomic study. For each of the four experimental groups corresponding to HeLa cells transfected with empty vector or vector expressing WT, H151N or R90D NDPK-D, two independent clones were analyzed in triplicate. To identify significant changes within the differential expression pattern, multiple group-to-group comparisons were performed using the DeCyder biological variation analysis module (Fig. 4.5).

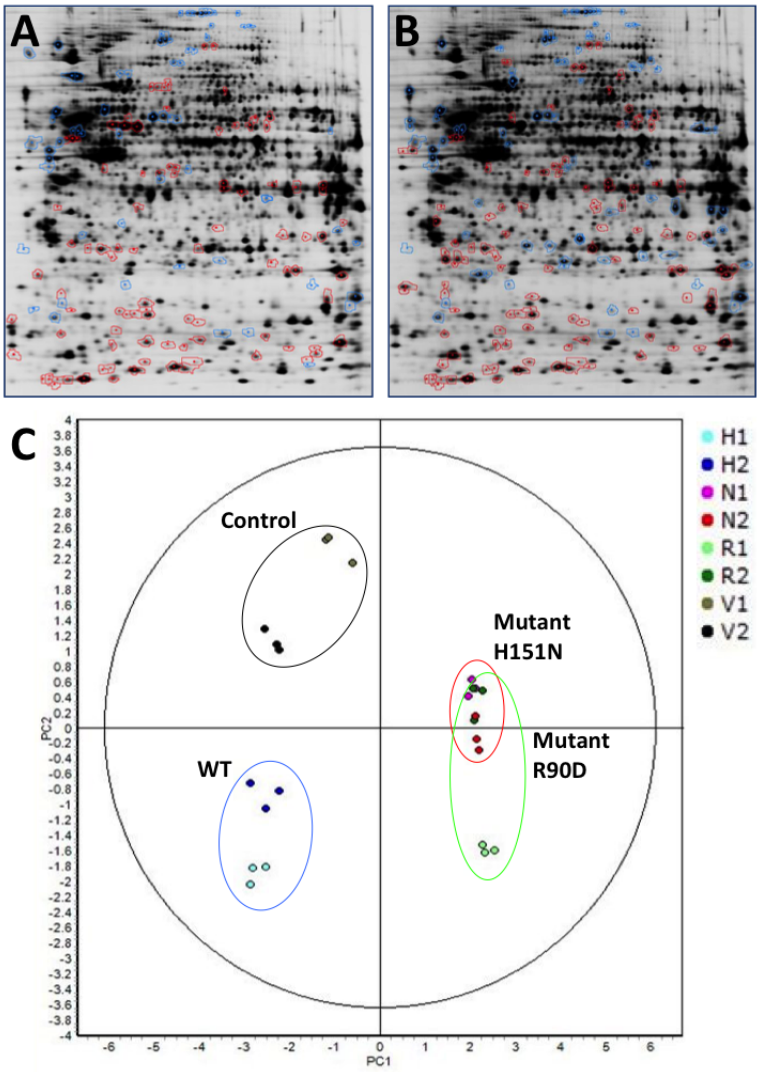

Figure 4.5 – 2D-DIGE proteomic analysis of the four different HeLa clones. (A,B) Two exemplary 2D gels showing identified differentially expressed protein spots, upregulated (circled in red) or down-regulated (circled in blue) relative to WT. **(A)** H151N mutant vs. WT: 157 spots differentially expressed, of which 94 spots upregulated and 63 spots down-regulated. **(B)** R90D mutant vs WT, 198 spots differentially expressed, of which 111 up-regulated and 87 downregulated. **(C)** Principal component analysis, performed from the protein spots and matched. The score plot shows experimental maps. For details see material and methods.

A total of 219 differentially expressed protein spots were identified by mass spectrometry, corresponding to 157 different proteins. Importantly, most changes in protein abundance relative to WT NDPK-D expressing cells occurred in the same sense for both mutants, the kinase-dead H151N (Fig. 4.5A) and the cardiolipin-binding deficient R90D (Fig. 4.5.B). To compare the protein expression pattern more quantitatively, principle component analysis was performed on the entire set of detected protein spots. Clearly, all samples of the two mutant NDPK-D HeLa cells segregated from samples of WT NDPK-D Hela cells, while the control samples were different from both of the

former groups (Fig. 4.5.C; each group circled). The two clones analyzed for each of the four experimental groups segregated also, but remained very close, showing the good reproducibility of the analysis. In summary, these proteomic profiles recapitulate the similarities seen for the morphological and invasive phenotypes. They suggest that both NDPK-D mutations trigger similar pathways to acquire these phenotypes, possibly acting via a change in the cellular protein expression and/or degradation program.

Analysis of differentially expressed and functionally related groups of proteins with Ingenuity Path Designer software (Qiagen) identified more than twenty proteins involved in metastasis. They all show a change in expression level between WT and mutant NDPK-D expressing clones (Fig. 4.6). Of the overexpressed proteins, fifteen were found in both mutant clones, the kinase dead H151N and the cardiolipin binding deficient R90D; only one was unique to H151N (AKR1C3) and one to R90D (TPT1). Of the downregulated proteins, again six are found in both mutant clones, and only one was unique to R90D (ROAA). The strongest overexpression was found for γ-synuclein (SNCG), whose levels increased 8- and 11-fold in H151N and R90D mutant clones, respectively. This gene was reported to be associated with tumor progression and to play a role in microtubule regulation (Kumar et al., 2015; Zhang et al., 2011). Fascin (FSCN1 gene), an actin-bundling protein, which is almost 3-fold overexpressed in both mutants, is also highly related to metastasis (Huang et al., 2016; Kulasingam and Diamandis, 2013). The S100 proteins, S100A4 and S100A11, which are calcium-binding proteins, are about 5- and 2-fold overexpressed, respectively, in both mutants. Expression of S100A4 is particularly associated with metastasis in several tumor types (for reviews see (Bresnick et al., 2015; Lukanidin and Sleeman, 2012)). Also other S100 proteins, including S100A6, S100A8, S100A13, and S100A16, were overexpressed in the mutants, although not assigned by the software to the metastasis pathway. However, deregulated expression of several members of the S100 family occurs in most cancers, and typically involves up-regulation. Another highly overexpressed protein was ISG15 (8-fold in H151N versus WT), recently reported to promote invasion (Hermann et al., 2016).

Finally, immunoblotting analysis of several proteins identified by 2D-DIGE confirmed their overexpression in mutant NDPK-D expressing clones, including Fascin, γ-synuclein, ISG15 and S100A4 (Fig. 4.7). Altogether, the coordinated deregulation of multiple proteins involved in metastasis, similar in both NDPK-D mutant-expressing clones, provides a molecular rationale for a role of NDPK-D in the metastatic process.

Ingenuity pathway analysis identified as most strongly affected functional groups in addition to Cellular Growth and Proliferation also Mitochondrial Dysfunction and Oxidative Stress. Indeed, among proteins differentially expressed in mutant H151N and R90D clones, were many mitochondrial proteins (fold-changes are given as H151N

vs. WT and R90D vs. WT respectively). A marked change was downregulation of several core subunits of ATP synthase: alpha (ATPA: -1.5, -1.7), beta (ATPB: -2.0, -1.9) and d (ATP5H: -1.3, -1.6). Few changes were detected in the respiratory chain, all concerning complex I. These changes concern a downregulation of the core subunit NADH-ubiquinone oxidoreductase 75 kDa (NDUS1, -1.7, -1.6) in the matrix-facing dehydrogenase module of the peripheral arm, and upregulation of the accessory subunit NADH dehydrogenase 1 alpha subcomplex subunit 8 (NDUFA8, +1.7, +1.7), which faces the intermembrane space and is essential for complex I assembly (Fiedorczuk et al., 2016; Stroud et al., 2016).

Interestingly, there was also downregulation of two other mitochondrial proteins that could potentially compensate for NDPK-D functions: adenylate kinase 3, a GTP: AMP phosphotransferase (KAD3: -1.6, -1.4) able to generate GTP from GDP and ADP, and MICOS complex subunit MIC60 (IMMT: -1.8, -1.7). The latter complex can bridge inner and outer mitochondrial membrane, similar to NDPK-D, and may also function in lipid transfer (Aaltonen et al., 2016; Schlattner et al., 2014; Tatsuta et al., 2014). Finally, within the family of voltage-dependent anion channels (VDACs) controlling among others outer mitochondrial membrane permeability, an isoform switch occurred, with upregulated isoform 3 (VDAC3: +2.4, +1.3) and downregulated isoforms 1 (VDAC1: -1.4, -1.5) and isoform 2 (VDAC2: -1.4, -1.6). Based on these data, and the phenotype of NDPK-D mutant expression described herein, we hypothesized *(i)* that there should be a primary effect of NDPK-D mutations on mitochondrial structure and/or function, and *(ii)* that this effect should be similar for both mutants.

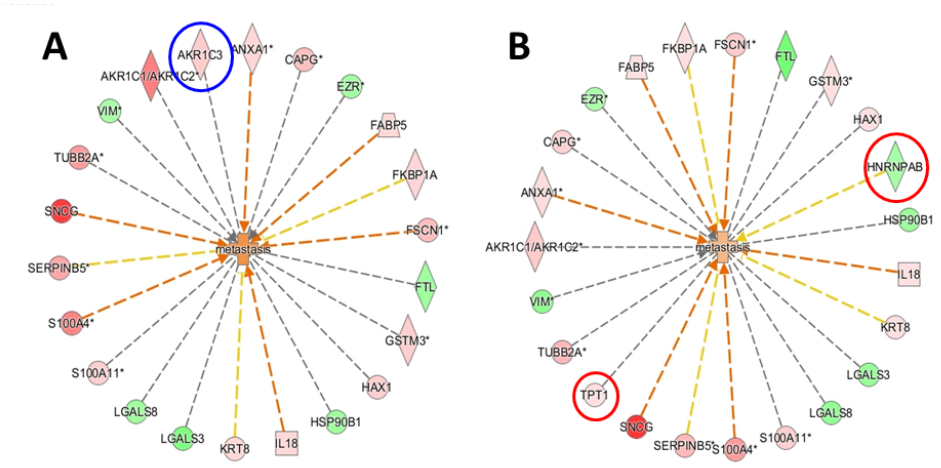

Figure 4.6 – Metastasis-related proteins differentially regulated in NDPK-D mutant HeLa clones. Proteins were identified by the Path Designer software (Qiagen). **(A)** Comparison H151N vs. WT includes 22 differently expressed proteins (16 up- and 6 down-regulated). **(B)** Comparison R90D vs. WT includes 23 differently expressed proteins (16 up- and 7 down-regulated), of which 21 are common with those in (A). Color code for proteins: up-regulation in pink, down-regulation in green. The protein circled in blue is unique to the H151N vs. WT comparison; proteins circled in red are unique to the R90D vs. WT comparison.

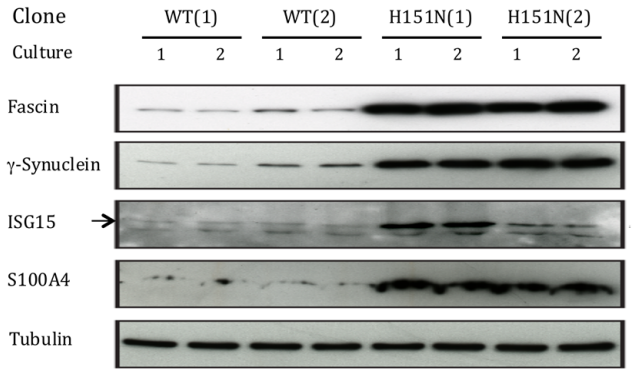

Figure 4.7 – Immunoblot of proteins identified by proteomics as overexpressed in H151N vs. WT. Control of protein levels of four proteins (Fascin, γ -synuclein, ISG15 and S100A4) that were found overexpressed in two independently isolated clones expressing the H151N mutant as compared to WT NDPK-D. Protein extracts of two different cultures were tested for each protein. Tubulin is given as a loading control. The arrow indicates the correct ISG15 band.

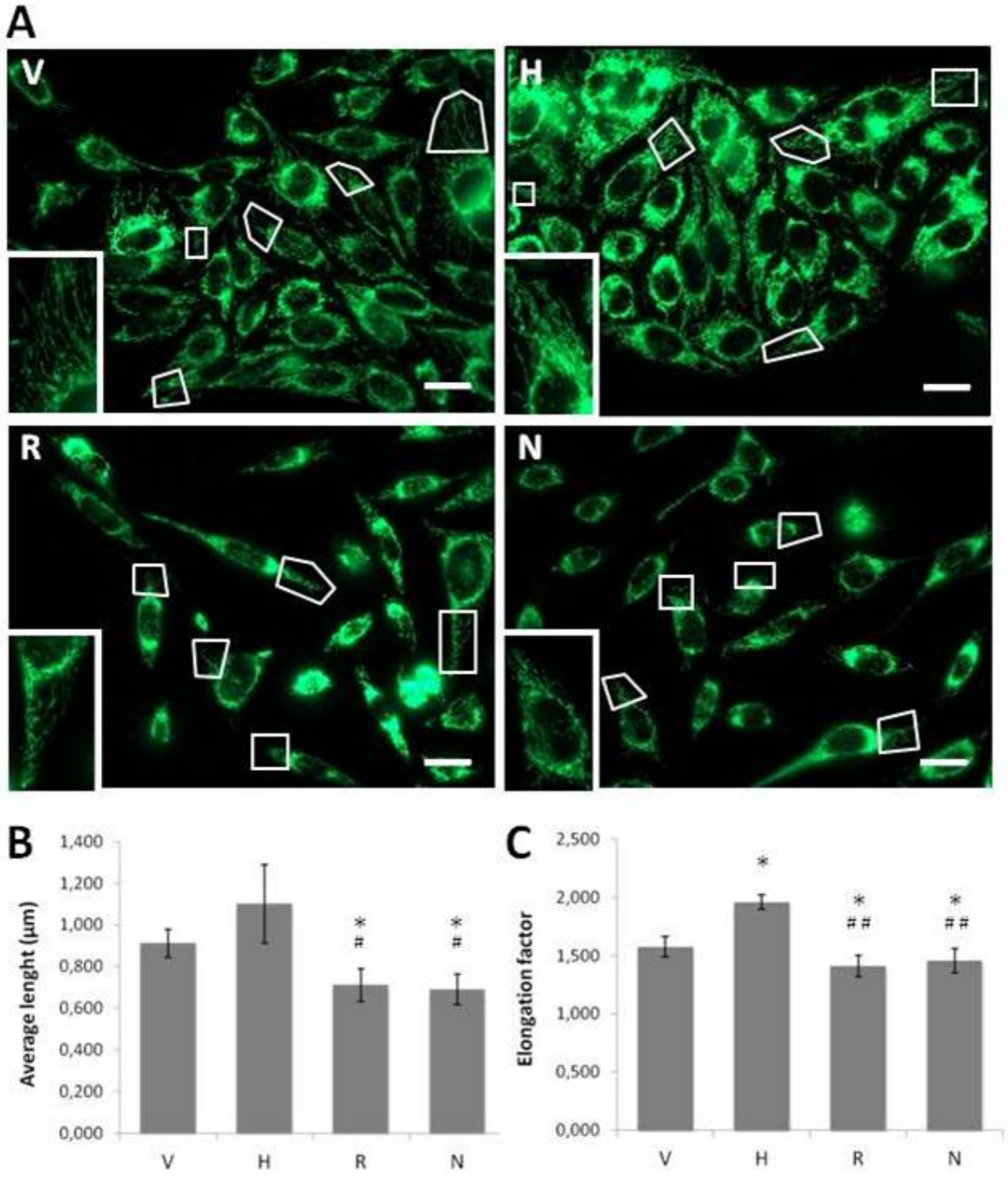

Figure 4.8 – Mitochondrial network and average filament length in immunostained cells of the four different HeLa clones. HeLa cells stably transfected with empty vector (V), or vector expressing NDPK-D WT (H), cardiolipin-binding deficient R90D (R) or the kinase-dead H151N mutant (N). **(A)** Immunostaining of mitochondria with MnSOD. The representative confocal images show the region of interests used for the quantification below and a representative, magnified detail. Scale bar is 20 µm. **(B)** Average length of the mitochondrial filaments in the regions of interest analyzed. **(C)** Elongation factor of the mitochondtrial filaments in the regions of interest analyzed. All data are mean ± SEM (n=5). *p<0.05 relative to V; # p<0.05 relative to H; ## p<0.01 relative to H.

4.3.5 NDPK-D mutations fragment the mitochondrial network

We first studied the effect of NDPK-D mutations on the mitochondrial network of HeLa cells, either fixed and immunostained for the mitochondrial protein Mn superoxide dismutase (MnSOD; Fig. 4.8), or live HeLa cells stained with MitoTracker Green (Suppl. Fig. 4.12). Immunostained cells, giving the more contrasted images, were used for quantifying size and form of mitochondrial filaments (Fig. 4.8.B,C). Average length (Fig. 4.8.B) and elongation factor (Fig. 4.8.C) of the filaments were significantly lower in mutant NDPK-D expressing HeLa cells as compared to controls or WT expressing cells. There were no such significant differences between the two mutant NDPK-D expressing clones for any parameter. However, the WT NDPK-D expressing clone had a higher elongation factor as compared to controls. Thus, high levels of wild-type NDPK-D led to an even more pronounced filamentous mitochondrial network, while expression of NDPK-D mutants led to mitochondrial fragmentation. These effects are most probably directly related to the role of NDPK-D in fueling the GTPase OPA1, a key player in mitochondrial fusion (see discussion).

4.3.6 NDPK-D mutations lead to a loss of mitochondrial mass

To assess the mitochondrial mass in each HeLa cell line, we determined the activity of citrate synthase (CS), an established quantitative and linear readout for the mitochondrial mass of a cell (Fig. 4.9.A). CS activity was down to 65-75% in mutant NDPK-D expressing clones, while it was increased by about 20% in WT NDPK-D expressing cells, always as compared to controls. CS activity was also higher in the H151N relative to the R90D mutant cells. MitoTracker Green (MT) staining of live cells was used as a second, independent assay for mitochondrial mass (Fig. 4.9.B). This dye passively diffuses across mitochondrial membranes, reacts with available protein cysteine thiols, and thus provides a potential-independent live stain for total mitochondrial mass. MitoTracker fluorescence entirely confirmed the significantly decreased mitochondrial mass in mutant NDPK-D expressing clones as compared to both controls and WT expression. However, no significant difference was observed between WT excpression and controls with this method, possibly due to known limitations of the Mitotracker staining, which depends on the total inner membrane surface (Cottet-Rousselle et al., 2011), a parameter potentially differing between the HeLa clones.

In conclusion, expression of NDPK-D mutants not only led to mitochondrial fragmentation (see Fig. 4.8), but also to reduced mitochondrial biogenesis and/or increased elimination of mitochondria, while overexpression of WT NDPK-D favors mitochondrial fusion and slightly increases mitochondrial mass.

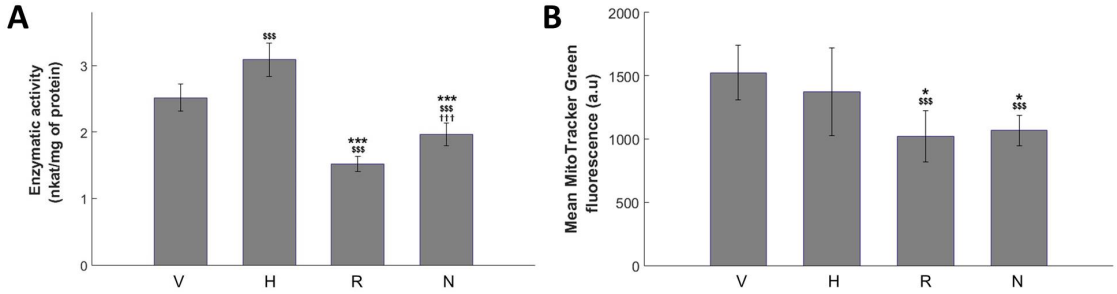

Figure 4.9 – Mitochondrial mass of the four different HeLa clones. HeLa cells stably transfected with empty vector (V), or vector expressing wild-type NDPK-D (H), lipid binding defficient R90D mutant (R) or the kinase-inactive H151N mutant (N). **(A)** Enzyme activity of citrate synthase in cellular extracts. **(B)** MitoTracker Green fluorescence of live cells measured by FACS. The data shown are mean ± SD (n=7-9 in A, n=6-10 in B). $$$ $p<0.005$ relative to V; *** $p<0.005$ relative to H; ††† $p<0.005$ relative to R.

4.3.7 NDPK-D mutations increase the mitochondrial membrane potential

The average membrane potential per mitochondria was determined by TMRM fluorescence and normalization to mitochondrial mass as determined by CS activity (Fig. 4.10). Significant differences were observed when comparing pooled data of controls and WT NDPK-D expressing clones versus both mutant NDPK-D expressing clones. The mitochondrial membrane potential was significantly higher in the latter group as compared to the former. Thus, expression of mutant NDPK-D increases the mitochondrial membrane potential. This hyperpolarization may be due to a decreased use of the electrochemical gradient for respiration, since *(i)* inactive (H151N mutant) or mislocated kinase (R90D mutant) would reduce ADP supply to ATP synthase (Tokarska-Schlattner et al., 2008) and *(ii)* ATPase expression itself is reduced in mutant cells as seen in the proteomic analysis (see discussion).

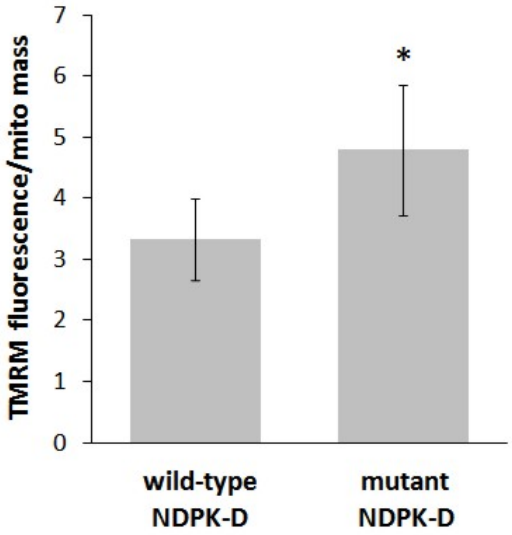

Figure 4.10 – Mitochondrial membrane potential determined by TMRM fluorescence. HeLa cells expressing wild-type NDPK-D (V: endogenous low levels, H: high levels) or expressing mutant NDPK-D (R: lipid binding deficient R90D mutant, N: kinase-inactive H151N mutant) were labeled with 50 nM TMRM. Fluorescence intensity of the dye was measured by FACS, and values normalized to average mitochondrial mass per cell as determined by CS activity. The diagram shows means ± SD (n=6), * $p<0.05$ relative to wild-type NDPK-D expressing HeLa.

4.4 Discussion

Metastasis is a most lethal process in cancer. Over the past 25 years, over a dozen of metastasis-suppressor genes has been described that specifically inhibit metastasis formation without necessarily affecting primary growth (Shoushtari et al., 2011). Metastasis-suppressors are involved in diverse molecular processes in multiple tumor types, mostly acting via altered cell signaling, including NDPK-A (NM23-H1) and possibly also NDPK-B (NM23-H2). In the present study, we identify NDPK-D, a mitochondrial protein, as a novel metastasis suppressor. NDPK-D mutations invalidating either the catalytic NDP kinase activity of the enzyme (H151N) or its ability to bind cardiolipin to MIM (R90D) both induced a strong metastatic phenotype in HeLa cells. This morphotypic switch was accompanied by profound changes in the cellular proteome and mitochondrial structure and function. Our data suggest a communication between mitochondria, cytosol and nuclear genes for a pro-metastatic reprogramming of cellular protein expression.

The pro-metastatic phenotype of cells expressing NDPK-D mutants was apparent by pronounced cellular scattering, loss of intercellular adhesion, increased 2D and 3D cell migration, and 3D invasion through type I collagen. By contrast, expressing WT NDPK-D, at least for some parameters, showed a mild anti-metastatic phenotype as compared to control cells expressing the empty vector control. The NDPK mutant

phenotype is reminiscent to the silencing effect of the cytosolic anti-metastatic isoform NDPK-A (Boissan et al., 2010). We hypothesize that downstream effectors of NDPK-D function as a barrier against epithelial–mesenchymal transition (EMT) i.e. as a barrier against the in situ transition to invasive carcinoma. Of particular note, protein levels of NDPK-A and NDPK-B remained unchanged in the NDPK-D mutant cells (data not shown), an observation which reinforces *per se* the specific anti-metastatic activity of WT NDPK-D.

Only few data are available on NDPK-D/NME-4 expression in human cancers, in contrast to the abundant literature on the metastatic suppressor NME1. Most of them show overexpression of NME4 mRNA in several types of tumors as compared to uninvolved tissue (Seifert et al., 2005; Xu et al., 2010), and in case of gastric cancer this was predictive for patient survival (Xu et al., 2010). Other studies report a lower NME4 expression correlating with aggressiveness. In hepatocarcinoma derived cell lines, NME4 expression was lower in cell lines with high metastatic potential (Qin et al., 2007). In sporadic breast cancers, loss of heterozygosity or allelic imbalance, associated with nodal metastases, was observed in the NME4 gene region (Patocs et al., 2007). Further, deletion of NME4 gene region was observed in testicular germ cell tumors of adolescent and young adult men (Skotheim et al., 2006). In oral cancer, miR-196 was highly overexpressed in cancer tissue and correlated with lymph node metastasis. Functionally, this onco-miR promoted cell migration, invasion and lymph node metastasis without affecting cell growth through inhibition of NME4 expression (Lu et al., 2014). Certainly, further targeted studies are required to confirm a metastasis suppressor role of NDPK-D in human cancer.

Molecular mechanisms underlying the morphotypic switch were studied with different approaches. They all revealed very similar changes in both mutant NDPK-D expressing HeLa clones relative to control and WT NDPK-D expression, often more pronounced for the kinase dead H151N, entirely consistent with the cellular phenotype. In many cases, expressing WT NDPK-D led to a rather opposite phenotype relative to control. Targeted proteomics showed a reduction of N-cadherin in mutant cells, which could explain the loss of cell-cell contacts (Nguyen and Mege, 2016). Importantly, comparative non-biased proteomics of the four different HeLa clones revealed more than 150 proteins that were differently expressed between the WT and the two mutant clones. Once again, the two mutant clones were very similar, sharing the large majority of observed changes in protein abundance. A major group of 23 altered proteins was related to metastasis, suggesting that NDPK-D mutation triggered a pro-metastatic reprogramming of the cellular proteome.

The non-biased proteomics also revealed a second group of proteins differentially expressed in both mutants, namely those related to mitochondrial dysfunction. This

suggests a primary effect of both NDPK-D mutations on their immediate mitochondrial environment, potentially affecting mitochondrial structure and/or function. Indeed, mutant cells showed a more fragmented mitochondrial network, a loss in mitochondrial mass per cell, and a reduced membrane potential at MIM. These results reflect a major impact of invalidating NDPK-D functions on mitochondria and support a close coupling between mitochondria, proteome and cellular phenotype.

How exactly the two totally different NDPK-D mutants exert their very similar effects is an intriguing question. However, recent work in our groups sheds some light on this issue (Boissan et al., 2014; Kagan et al., 2016; Schlattner et al., 2013a). There is only one known consequence that both mutations have in common: their failure to supply GTP and ADP, the main products of the NDPK-D reaction in mitochondria, to their functional interaction partners at MIM, the OPA1 GTPase and the ATP/ADP translocator (ANT). This occurs either simply because the mutant is catalytically dead (H151N) or in a more sophisticated way because of mislocalization (R90D). In the latter case, the lack of cardiolipin interaction impedes complex formation or close association of NDPK-D with OPA1 and ANT (Kagan et al., 2016; Schlattner et al., 2013a). These alterations would interrupt the direct GTP fueling of OPA1 (Boissan et al., 2014), leading to reduced MIM fusion rates, mitochondrial fragmentation, and eventually also mitochondrial elimination. Further, reduced ADP supply to ANT and finally the ATP synthase would reduce ATP synthesis rate and the use of the MIM electrochemical gradient, resulting in the observed hyperpolarization at MIM. Reduced levels ATP synthase detected in the proteomic screen would reinforce the latter process.

Thus, failure of NDPK-D mutants to supply GTP and ADP to its partners may be sufficient to explain the entire mitochondrial phenotype. However, how these changes then translate into similar, yet undefined, messages to the cytosol and the nucleus, with downstream pro-metastatic effects, remains to be investigated.

Acknowledgements

This work was supported by the Fondation pour la Recherche Médicale (FRM; number DPM20121125557), a CMIRA Explo'ra doc fellowship (to C.D. and U.S.) of the Region Rhone Alpes, and the Groupement des Entreprises Françaises contre le Cancer (GEFLUC) to M.B.

4.5 Supplementary material

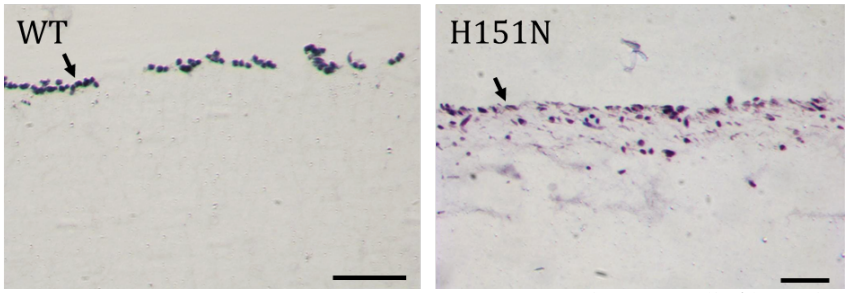

Figure 4.11 – 14-days invasion assay of HeLa clones. Clones H (left) and N (right) are shown (for abbr. see Fig. 4.2). Cells were seeded on the surface of collagen type I indicated by an arrow. Representative haematoxylin/eosin stained cross-sections of the collagen gel after a 14-day culture period are shown (scale bars, 100 µm).

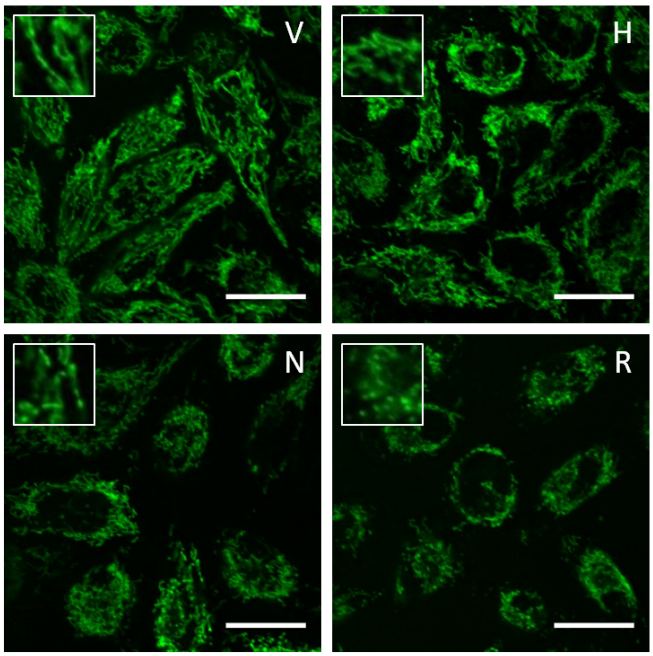

Figure 4.12 – Mitochondrial network arrangement in live-stained HeLa cells. HeLa cells stably transfected with empty vector (V), or vector expressing NDPK-D WT (H), cardiolipin-binding defficient R90D (R) or the kinase-dead H151N mutant (N). HeLa cells are labeled with 100 nM Mitotracker Green. Representative confocal images are given together with a magnified detail. The scale bar is 20 µm.

Chapter 5

General discussion and perspectives

NDPK-D as a multifunctional protein

Mitochondria are organelles involved in a plethora of cellular functions. They ensure bioenergetics functionality such as ATP production or ß-oxidation of fatty acids, but also regulate several cellular signaling pathways such as calcium signaling or apoptosis. To afford these functions, mitochondria contain around thousand proteins which have evolved to sustain the increasing complexity of function and regulation in eukaryotic cells. The increasing demand for additional mitochondrial functions may be one of the reasons why more and more proteins have acquired distinct multiple activities. These particular proteins, also called "moonlighting proteins" (Jeffery, 1999; Jeffery, 2003), are coded by the same gene and have two or more completely different functions. A protein is considered as moonlighting when it has different functions depending e.g. on cellular localization, cell type, oligomeric state or cellular concentration of a ligand, substrate, cofactor or product (Jeffery, 1999).

The best known example may be cytochrome C, which functions in the mitochondrial respiratory chain, but once released into the cytosol is also the key signaling molecule for apoptosis (Liu et al., 1996; Kroemer et al., 1998). Also other such pro-apoptotic proteins have another function in mitochondria, e.g. apoptosis inducing factor (AIF) (for review see (Kaufmann and Hengartner, 2001)). Several enzyme of the Krebs cycle have multiple functions, often also linked to multiple localization. Some of them localize to the cytosol like fumarase, isocitrate dehydrogenase and aconitase. The latter has a key function in cellular iron homeostasis (Sriram et al., 2005; Huberts and van der Klei, 2010). These Krebs cycle enzymes, including in addition components of the pyruvate dehydrogenase, also localize to the nucleus where they are involved in epigenetic remodeling via histone acetylation (Nagaraj et al., 2017). Other proteins seem to translocate from mitochondria to the nucleus where they may again have a similar or different function (for review see (Monaghan and Whitmarsh, 2015)).

Here we have studied NDPK-D as yet another mitochondrial protein, and provide novel evidence that it can be considered as a true moonlighting protein. Indeed, this

protein, located at the mitochondrial intermembrane space, exhibits two different functions. Its primary, long-known function is to regenerate NTP through the consumption of the most available ATP. The second one is to bind and transfer anionic phospholipids, especially CL, from the inner to the outer mitochondrial membrane (Schlattner et al., 2013a). Both functions depend on each other: in vitro evidence suggests that lipid transfer activity of the protein is low when the protein active in phosphotransfer and vice versa (Schlattner et al., 2013a). The aim of this work was to gain a more detailed understanding of the model of NDPK-D dual function proposed earlier (Schlattner et al., 2013a), using cellular and in vitro models. Our approach discovered a much more specific NDPK-D functions in phosphotransfer, in partnership with the GTPase OPA1 (Chapter 3), and in CL transfer, identifying it as part of a pro-mitophagic lipid signaling pathway (Chapter 3). We further discovered that mutations interfering with correct NDPK-D localization and phosphotransfer trigger a pro-metastatic phenotype, a link that merits further studies (Chapter 4). We finally attempted to study the interaction of NDPK-D with OPA1, which may play a role for both phospho- and lipid transfer functions, by establishing an in vitro system with recombinant protein.

Phosphotransfer: NDPK-D is a GTP channeling enzyme

Metabolite channeling refers to direct supply of metabolites or metabolic intermediates from one enzyme to the second enzyme within a sequential chain reaction without its dilution or diffusion into the surrounding environment (Ovadi and Srere, 2000; Schlattner et al., 2013b). The two enzymes need to be in close proximity, e.g. either directly interacting or being part of a same complex (Srere, 1987). This presents several advantages like: local supply of substrate which drives the enzymatic reactions and increases reaction rates; no dilution of the substrate in the surrounding environment, which decreases the substrate consumption through other metabolic reactions and thus the competition between reactions. In mitochondria, metabolite channeling occurs between enzymes of the Krebs cycle or electron transport chain but also within the mitochondrial intermembrane space with the mitochondrial creatine kinase (Schlattner et al., 2013b) which channels ADP and phosphocreatine to mitochondrial matrix and cytosol, respectively, through interaction with ANT and VDAC.

The situation for NDPK-D is quite similar as it fuels the mitochondrial dynamin OPA1 with GTP (Boissan et al., 2014). Our current hypothesis is that within NDPK-D/OPA1 complexes, NDPK-D directly provides GTP to the active site of OPA1. This activity of fueling requires very close proximity or direct interaction between the two proteins, as already shown through the proximity ligation assay (cf chapter 3) and immunoprecipitation (Schlattner et al., 2013a), and is maintained by the kinase function

of NDPK-D whereby the protein uses mitochondrial ATP and GDP for local GTP production (Schlattner et al., 2013a; Boissan et al., 2014). As GTP is less abundant than ATP (Traut, 1994), but GTPases and ATPases have similar Km, enzymes using GTP may be prone to operate at sub-optimal GTP concentrations. Within NDPK-D/OPA1 complexes, permanent supply of mitochondrial ATP and removal of GTP by OPA1 drives the reversible NDP kinase reaction towards the production of GTP, and diminishes the risk of GTP consumption through other metabolic pathways.

So far, NDPK-D and OPA1 are not known to be extensively engaged in protein/protein interactions. Indeed, NDPK-D is found associated with ANT thus allowing stimulation of respiration (Tokarska-Schlattner et al., 2008). OPA1 is known to interact with Bnip3, a BH3-only protein from the Bcl2 family to promote mitochondrial fragmentation and apoptosis (Landes et al., 2010).

The NDPK-D/OPA1 interaction and thus the GTP channeling seems to be dependent on the NDPK-D membrane bound state. Indeed, when NDPK-D is unable to bind to CL (R90D mutation), the protein is not in close proximity with OPA1 and an interaction between both proteins and most likely the resulting channeling cannot occur.

Lipid transfer: NDPK-D is part of a lipid signaling pathway

We further discovered that the lipid transfer ability of NDPK-D allows externalization of the mitochondrial anionic phospholipid cardiolipin to the mitochondrial surface, and that this is part of a signaling pathway in mitochondrial quality control. Indeed, we show that upon a collapse of the mitochondrial membrane potential, NDPK-D is necessary for CL externalization, which then serves as a signal for recognition of these damaged mitochondria by autophagosomes. The latter has been shown earlier to occur through LC3-II interaction with CL externalized to the mitochondrial surface (Kagan et al., 2016). Induction of such cardiolipin transfer mediated by NDPK-D might be mediated, at least in part, through the NDPK-D/OPA1 interaction (Kagan et al., 2016).

The externalization of CL can be compared to another phospholipid: phosphatidylserine (PS). PS is composed of two acyl chain linked by a serine and is mostly located in the cell membrane. This phospholipid, like CL, serves as a signal during apoptosis (Segawa and Nagata, 2015). Indeed, under normal conditions, PS is located in the cell membrane facing the cytosol, but when the cell enters in apoptosis, PS is flipped towards the extracellular surface of the cell via scramblase. This "externalization" of PS acts as a signal for macrophages to engulf the cell (Segawa and Nagata, 2015). Unlike PS, CL externalization needs 3 steps (Kagan et al., 2014). First, the transfer from the inner leaflet to the outer leaflet of IMM. Second, the transfer from IMM to inner leaflet of OMM. And finally, the transfer from the inner leaflet to the outer leaflet of OMM. NDPK-D is supposed to participate in the second step whereby CL is transfered from

IMM to OMM. This involves its high affinity for CL, its capability to cross-link mitochondrial membranes, thus creating contact sites where CL can be transferred more easily, and finally its capacity to transfer CL between membranes as shown with liposomes in vitro (Schlattner et al., 2013a; Tokarska-Schlattner et al., 2008; Epand et al., 2007).

As mentioned before, CL externalization at the mitochondrial surface is a signal for autophagosomes recognition in mitophagy (Chu et al., 2013). However, this CL externalization plays also a role in apoptosis (Kagan et al., 2014; Kagan et al., 2009). The difference lies on the oxidative state of the externalized cardiolipin. Indeed, high amounts of CL are found in cristae in which Cyt C is retained. Kagan et al. (Kagan et al., 2005) showed that Cyt C has a peroxidase activity when bound to CL, thus leading to formation of oxidized CL. Such oxidized CL favors Cyt C detachment from the IMM and, after transfer to the OMM, permeabilizisation of OMM by recuiting pore-forming proapoptotic proteins. This finally leads to Cyt C release from mitochondria into the cytosol and induction of apoptosis.

An uncoupler such as CCCP and the following collapse of IMM potential may also activate other pro-mitophagic pathways such as the Pink/Parkin pathway (Soubannier et al., 2012). Based on data from Kagan et al. (Kagan et al., 2016), there could be an interplay between the NDPK-D-CL pathway and the Pink/Parkin pathway, since CL may facilitate Parkin accumulation in mitochondria during mitophagy.

Interfering with NDPK-D functions causes a pro-metastatic phenotype

Cytosolic NDPK proteins (NDPK-A and B) are known to have anti-metastatic properties (Lacombe et al., 2000; Boissan et al., 2009; Boissan and Lacombe, 2012) as they are highly expressed in tumors compared to normal tissus. NDPK-A expression is reduced in highly metastatic melanoma cell lines, and was identified as the first metastasis suppressor gene (Steeg et al., 1988). Therefore, we examined whether this is also the case for NDPK-D. We could show that NDPK-D point mutations invalidating either phosphotransfer or cardiolipin interaction of NDPK-D induce a metastatic phenotype at the cellular level. This phenotype includes loss of cell-cell contact, higher migratory and invasive potential, and overexpression of several metastasis-related proteins. In addition, these mutations induce changes at the mitochondrial level, such as decreasing mitochondrial mass and network structure, but also in the mitochondrial membrane potential. This suggests that initial changes occur in mitochondria, followed by a tight communication between mitochondria, cytosol and nucleus to alter protein expression and to induce the pro-metastatic phenotype. In addition, there is a common point to these two point mutation which can explain the similar phenotype observed in HeLa cells. Indeed, H151N mutation leads to an enzymatically inactive protein enabled to

produce GTP for OPA1 and ADP for ANT. The R90D mutation leads to a lack of CL binding capacity, NDPK-D is not in close proximity with its partners OPA1 and ANT for metabolite channeling (see above). A decrease in GTP supply to OPA1 would lead to decreased fusion rate of IMM and mitochondrial fragmentation. A decrease in ADP supply to ANT would lead to a decrease in ATP regeneration, thus potentially decreasing the use of the electrochemical gradient.

Such communication between mitochondria and the nucleus is currently object of intense research, since it is important to synchronize expression of mtDNA encoded and nuclear encoded proteins, in particular those that are part of the same respiratory complexes and which have defined subunit stoichiometry. In fact, only a dozen of mitochondrial proteins are encoded by mtDNA, all others are expressed in the cytosol from nuclear transcripts (Quirós et al., 2016; Wasilewski et al., 2017). Therefore, a tight regulation of the expression level of mitochondrial proteins is performed via a complex communication between mitochondria and nucleus. Indeed, the regulation of mitochondrial activity is performed by anterograde and retrograde communications between nucleus and mitochondria. This allows the mitochondria to adapt to the cellular environment (Quirós et al., 2016). Mitochondria can also modulate the level of metabolites such as ATP, acetyl-CoA, NAD^+ or reactive oxygen species (ROS) to adjust the nuclear function (Quirós et al., 2016).

Recombinant NDPK-D and OPA1 will allow detailed study of their interplay

In order to further test and improve the model on NDPK-D dual function by *in vitro* experiments, we intended to express and purify the necessary recombinant proteins, NDPK-D and OPA1. This will allow to study interactions and functional domains of the proteins at a molecular level.

We were able to obtain recombinant full-length OPA1 expressed in *E. coli*. Some preliminary co-immunoprecipitation experiments were performed with recombinant OPA1 and NDPK-D proteins to investigate the NDPK-D/OPA1 interaction (data not shown). These experiments indicate a possible direct effect of cardiolipin on this interaction. However, these results need to be confirmed with a purified antibody. In addition, the effect of lipids on GTPase activity was studied with non-purified OPA1 fragments, indicating that CL increases this GTPase activity (data not shown). However, one cannot exclude that other GTPases or ATPases in the used fractions might be involved in this effect, since the malachite green based assay used only detects the hydrolysis product inorganic free phosphate. Improvements in the expression and purification processes of full-length OPA1 are thus necessary *(i)* to proof the feasibility

of recombinant production of full-length OPA1, and *(ii)* to confirm the mentioned preliminary experiments. This will improve our understanding of the CL-bound NDPK-D/OPA1 complex and its role in the dual function of NDPK-D.

Perspectives: NDPK-D functions at the molecular and cellular level

Our results allowed us to extend our model in many respect. We can hypothesize that in the complex of NDPK-D and OPA1, the kinase fuels OPA1 with GTP and channels ADP via ANT into the mitochondrial matrix to stimulate respiration and ATP regeneration. This allows mitochondria to fuse and maintain mitochondrial dynamics as well as to maintain the required bioenergetic activity. When mitochondria enter in mitophagy, the NDPK-D/OPA1 complex collapses, possibly because OPA1 is processed into its short isoform. NDPK-D would then be able to cross-link IMM and OMM and to transfer CL to the mitochondrial surface, where it serves as a signal for recognition by autophagosomes.

There is still quite some work to do at different levels for a complete understanding of NDPK-D function and regulation. At the molecular level, we need to better understand what is the pathway of CL transfer via NDPK-D and how the switch between lipid and phosphotransfer mode is regulated. Deeper investigations into the NDPK-D/OPA1 interaction are necessary, e.g. which amino acids are involved, how the interaction is regulated, or what is the role of lipids in this interaction. This can be performed with the recombinant proteins by co-immunoprecipitation, surface plasmon resonance or even isothermal titration calorimetry. In case of direct interaction between proteins, we can imagine to obtain a structure of the complex which might help for molecular modeling to better understand the CL transfer pathway.

At the cellular level, we need to improve our understanding on the communication between mitochondria and nucleus, especially how NDPK-D is involved in the regulation of this type of communication. In addition, we need to study whether there is any cross-talk between other mitophagic triggers and NDPK-D-mediated CL transfer.

Finally, we have now the possibility to work with NDPK-D KO mice. We will first need to confirm the results obtained at the molecular and cellular levels (CL externalization experiments, co-localization of NDPK-D and OPA1). A study of the phenotype of these mice and a focus on the liver where NDPK-D is highly expressed, will help to understand NDPK-D function at the organ and organism level.

Chapter 6

Discussion générale et perspectives

NDPK-D comme protéine multifonctionnelle

Les mitochondries sont des organites impliqués dans de nombreuses fonctions cellulaires. Elles assurent des fonctions bioénergétiques telles que la production d'ATP ou la ß-oxydation des acides gras. Elles régulent également plusieurs voies de signalisation cellulaires comme la signalisation calcique ou l'apoptose. Afin de réaliser ces fonctions, les mitochondries sont composées de milliers de protéines qui ont évolué pour maintenir la complexité croissante des fonctions et de la régulation dans les cellules eucaryotes. La demande croissante pour de nouvelles fonctions mitochondriales est peut-être la raison pour laquelle de plus en plus de protéines ont acquis des fonctions distinctes et multiples. Ces protéines un peu spéciales, aussi appelées « moonlighting proteins » (Jeffery, 1999; Jeffery, 2003), sont codées par un seul et même gène et présentent au moins deux fonctions complètement différentes. Une protéine est dite « moonlighting » lorsque sa fonction diffèrent suivant : la localisation cellulaire, le type cellulaire dans lequel elle est exprimée, l'état oligomérique dans lequel elle se trouve (monomère, dimère…) ou encore suivant la concentration en ligand, substrat, cofacteur ou produit dans la cellule (Jeffery, 1999).

L'exemple le plus connu de « moonlighting proteins » est certainement le cytochrome C qui intervient dans la chaîne respiratoire mitochondriale. Cependant, lorsqu'il est libéré dans le cytosol, il joue le rôle de molécule clée dans la signalisation de l'apoptose (Liu et al., 1996; Kroemer et al., 1998). De même, d'autres protéines pro-apoptotiques ont une autre fonction dans les mitochondries comme l'apoptosis inducing factor (AIF) (pour revues voir (Kaufmann and Hengartner, 2001)). Plusieurs enzymes du cycle Krebs ont différentes fonctions, souvent associées à une localisation multiple. Certaines d'entre elles se localisent au niveau du cytosol comme la fumarase, l'isocitrate déshydrogénase et l'aconitase. Cette dernière a une fonction clée dans l'homéostasie du fer (Sriram et al., 2005; Huberts and van der Klei, 2010). Ces enzymes du cycle de Krebs, ainsi que des composants de la pyruvate déshydrogénase, se situent également dans le noyau où elles sont impliquées dans un remodelage épigénétique via

l'acétylation des histones (Nagaraj et al., 2017). D'autres protéines semblent se transposer des mitochondries au noyau où elles peuvent encore une fois avoir une fonction similaire ou différente (pour complément, voir (Monaghan and Whitmarsh, 2015)).

Ici, nous avons étudié NDPK-D, une autre protéine mitochondriale, et fournissons des preuves nouvelles qu'elle peut être considérée comme une véritable "moonlighting protein". En effet, cette protéine, située dans l'espace inter-membranaire mitochondrial, présente deux fonctions différentes. Sa principale fonction, connue depuis longtemps, est de régénérer le NTP grâce à la consommation de l'ATP. La seconde est de lier et de transférer des phospholipides anioniques, en particulier la cardiolipine (CL), de la membrane interne à la membrane externe des mitochondries (Schlattner et al., 2013a). Les deux fonctions dépendent l'une de l'autre: les preuves *in vitro* suggèrent que l'activité de transfert de lipides de la protéine est faible lorsque la protéine est dans le mode phosphotransfert et vice versa (Schlattner et al., 2013a). Le but de ce travail était d'obtenir une compréhension plus détaillée du modèle de double fonction de NDPK-D proposé précédemment (Schlattner et al., 2013a), en utilisant des modèles cellulaires et *in vitro*. Notre approche a révélé des fonctions de NDPK-D beaucoup plus spécifiques dans le mode phosphotransfert, en partenariat avec la GTPase OPA1 (chapitre 3) et dans le transfert de CL, l'identifiant comme faisant partie d'une voie de signalisation lipidique pro-mitophagique (chapitre 3). Nous avons également découvert que les mutations entravant la bonne localisation de NDPK-D et le phosphotransfert déclenchent un phénotype pro-métastatique, un lien qui nécessite d'autres études plus approfondies (chapitre 4). Finalement, nous avons tenté d'étudier l'interaction entre NDPK-D et OPA1, qui peut jouer un rôle aussi bien au niveau du transfert de phosphate que du transfert de lipides, en établissant un système *in vitro* avec des protéines recombinantes.

Phosphotransfert: NDPK-D est une enzyme du channeling du GTP

Le channeling des métabolites se réfère à l'apport direct de métabolites ou d'intermédiaires métaboliques d'une enzyme à une autre enzyme dans une réaction en chaîne, sans sa dilution ou sa diffusion dans le milieu environnant (Ovadi and Srere, 2000; Schlattner et al., 2013b). Les deux enzymes doivent être très proches l'une de l'autre, par exemple soit en interagissant directement ou en faisant partie d'un même complexe (Srere, 1987). Cela présente plusieurs avantages comme: l'apport local de substrat qui oriente les réactions enzymatiques et augmente le taux de réaction; pas de dilution du substrat dans le milieu environnant, ce qui diminue la consommation du substrat par d'autres réactions métaboliques et donc la concurrence entre les réactions. Dans les mitochondries, le channeling des métabolites a lieu entre les enzymes du cycle de Krebs ou de la chaîne respiratoire, mais aussi au sein de l'espace intermembranaire mitochondrial

avec la créatine kinase mitochondriale (Schlattner et al., 2013b) qui canalise l'ADP et la phosphocréatine vers la matrice et le cytosol respectivement, par interaction avec ANT et VDAC.

La situation pour NDPK-D est assez similaire car elle fournit le GTP nécesaire à la dynamine mitochondriale OPA1 (Boissan et al., 2014). Notre hypothèse actuelle est que, au sein du complexe NDPK-D/OPA1, NDPK-D fournit directement le GTP au site actif de OPA1. Cette activité de ravitaillement nécessite une proximité étroite ou une interaction directe entre les deux protéines, comme cela a déjà été démontré par "proximity ligation assay (PLA)" (cf chapitre 3) et immunoprécipitation (Schlattner et al., 2013a), et est maintenue par la fonction kinase de NDPK-D à travers laquelle la protéine utilise l'ATP et le GDP mitochondrial pour produire localement le GTP (Schlattner et al., 2013a; Boissan et al., 2014). Comme le GTP est moins abondant que l'ATP (Traut, 1994), et que les GTPases et les ATPases ont un Km similaire, les enzymes utilisant le GTP peuvent donc fonctionner à des concentrations de GTP sous-optimales. Dans les complexes NDPK-D/OPA1, l'apport permanent d'ATP mitochondrial et l'élimination du GTP par OPA1 entraînent la réaction réversible de la NDP kinase vers la production de GTP, diminuant le risque de consommation de GTP à travers d'autres voies métaboliques.

Jusqu'à présent, NDPK-D et OPA1 ne sont pas connues pour être largement impliqués dans d'autres interactions protéines/protéines. En effet, NDPK-D est trouvée associée à ANT, ce qui permet de stimuler la respiration (Tokarska-Schlattner et al., 2008). OPA1 est connue pour interagir avec Bnip3, une protéine BH3 de la famille Bcl2 qui favorise la fragmentation mitochondriale et l'apoptose (Landes et al., 2010).

L'interaction NDPK-D/OPA1 et donc le channeling de GTP semble dépendre de l'état de liaison à la membrane de NDPK-D. En effet, lorsque NDPK-D est incapable de se lier à CL (mutation R90D), la protéine n'est pas très proche de OPA1, une interaction entre les deux protéines et probablement le channeling ne peuvent donc pas se produire.

Transfert de lipides: NDPK-D est un élément d'une voie de signalisation lipidique
Nous avons également découvert que la capacité de transfert de lipides de NDPK-D permet l'externalisation de phospholipides anioniques mitochondriaux, la cardiolipine, à la surface des mitochondries et que cela fait partie d'une voie de signalisation dans le contrôle qualité des mitochondries. En effet, nous montrons qu'après un effondrement du potentiel de membrane mitochondrial, NDPK-D est nécessaire à l'externalisation de CL, qui sert alors de signal pour la reconnaissance par les autophagosomes de ces mitochondries endommagées. Celà a été montré précédemment

par l'intermédiaire de l'interaction entre LC3-II et CL externalisée à la surface des mitochondries (Kagan et al., 2016). L'induction d'un tel transfert de cardiolipine via NDPK-D pourrait se faire, au moins en partie, à travers l'interaction NDPK-D/OPA1 (Kagan et al., 2016).

L'externalisation de CL peut être comparée à un autre phospholipide: la phosphatidylsérine (PS). Composée de deux chaînes acyle reliées par une sérine, PS est principalement située dans la membrane cellulaire. Ce phospholipide, comme CL, sert de signal pendant l'apoptose (Segawa and Nagata, 2015). En effet, dans des conditions normales, PS est située dans la membrane cellulaire tournée vers le cytosol, mais lorsque la cellule entre en apoptose, PS est renversée vers la surface extracellulaire de la cellule par des scramblases. Cette "externalisation" de PS agit comme un signal pour que les macrophages évacuent la cellule (Segawa and Nagata, 2015). Contrairement à PS, l'externalisation de CL se fait en 3 étapes (Kagan et al., 2014). Tout d'abord, le transfert du feuillet interne vers le feuillet externe de la membrane interne des mitochondries. Deuxièmement, le transfert de la membrane interne mitochondriale vers le feuillet interne de la membrane externe des mitochondries. Et enfin, le transfert du feuillet interne vers le feuillet externe de la membrane externe des mitochondries. NDPK-D est censée participer à la deuxième étape pendant laquelle CL est transférée de la membrane interne vers la membrane externe des mitochondries. Cela fait appel à sa grande affinité pour CL, à sa capacité à réticuler les membranes mitochondriales, créant ainsi des sites de contact où CL peut être transférée plus facilement et enfin à sa capacité à transférer CL entre les membranes comme montré *in vitro* avec des liposomes (Schlattner et al., 2013a; Tokarska-Schlattner et al., 2008; Epand et al., 2007).

Comme mentionné précédemment, l'externalisation de CL à la surface mitochondriale est un signal de reconnaissance pour les autophagosomes, dans la mitophagie (Chu et al., 2013). Cependant, cette externalisation de CL joue également un rôle dans l'apoptose (Kagan et al., 2014; Kagan et al., 2009). La différence réside dans l'état d'oxydation de la cardiolipine externalisée. En effet, de grandes quantités de CL se trouvent au niveau des crêtes mitochondriales où le Cyt C est retenu. Kagan et al. (Kagan et al., 2005) ont montré que Cyt C a une activité peroxydase lorsqu'il est lié à CL, conduisant ainsi à la formation de CL oxydée. Ceci favorise ainsi le détachement de Cyt C de la membrane interne mitochondriale et, après transfert à la membrane mitochondriale externe , la perméabilisation de la membrane mitochondriale externe en recrutant des protéines pro-apoptotiques formant des pores. Cela conduit finalement à la libération de Cyt C des mitochondries dans le cytosol et à l'induction de l'apoptose.

Un découplant tel que le CCCP (carbonylcyanure m-chlorophénylhydrazone) et

l'effondrement du potentiel de membrane mitochondriale qui s'ensuit peuvent également activer d'autres voies pro-mitophagiques telles que la voie Pink/Parkin (Soubannier et al., 2012). D'après les données de Kagan et al. (Kagan et al., 2016), il pourrait y avoir une interaction entre la voie NDPK-D-CL et la voie Pink/Parkin, car CL peut faciliter l'accumulation de Parkin dans les mitochondries pendant la mitophagie.

Interférer sur les fonctions de NDPK-D induit un phénotype pro-métastatique

Les protéines NDPK cytosoliques (NDPK-A et B) sont connues pour avoir des propriétés anti-métastatiques (Lacombe et al., 2000; Boissan et al., 2009; Boissan and Lacombe, 2012) car elles sont fortement exprimées dans les tumeurs par rapport aux tissus normaux. L'expression de NDPK-A est réduite dans les lignées cellulaires de mélanome hautement métastatique et a été identifiée comme le premier gène suppresseur de métastase (Steeg et al., 1988). Par conséquent, nous avons examiné si cela est également le cas pour NDPK-D. Nous avons pu montrer que les mutations localisées de NDPK-D invalidant l'activité phosphotransfert ou l'interaction avec la cardiolipine induisent un phénotype métastatique au niveau cellulaire. Ce phénotype comprend la perte de contact cellule-cellule, une élévation du potentiel migratoire et invasif et une surexpression de plusieurs protéines liées aux métastases. De plus, ces mutations induisent des changements au niveau mitochondrial, comme une diminution de la masse mitochondriale et une désorganisation du réseau mitochondrial, mais aussi au niveau du potentiel de membrane mitochondriale. Cela suggère que les changements initiaux se produisent dans les mitochondries, suivient d'une communication étroite entre mitochondries, cytosol et noyau pour modifier l'expression des protéines et induire le phénotype pro-métastatique. En outre, il existe un point commun à ces deux mutations qui peut expliquer la similitude du phénotype observé dans les cellules HeLa. En effet, la mutation H151N conduit à une protéine enzymatiquement inactive incapable de produire du GTP pour OPA1 et de l'ADP pour ANT. La mutation R90D, quant à elle, entraîne un déficit dans la capacité de liaison à CL, NDPK-D n'est pas proche de ses partenaires OPA1 et ANT pour le channeling des métabolites (voir ci-dessus). Une diminution dans l'approvisionnement de OPA1 en GTP entraînerait une diminution du taux de fusion de la membrane mitochondriale interne et donc la fragmentation des mitochondres. Une diminution dans l'approvisionnement de l'ANT en ADP entraînerait une diminution de la régénération de l'ATP, ce qui réduirait certainement l'utilisation du gradient électrochimique.

Une telle communication entre les mitochondries et le noyau fait actuellement l'objet d'une recherche intense car il est important de synchroniser l'expression des protéines codées par l'ADN mitochondrial et par le noyau, en particulier celles qui font partie des

mêmes complexes respiratoires et qui ont une stœchiométrie bien définie de leurs sous-unités. En fait, seulement une douzaine de protéines mitochondriales sont codées par l'ADN mitochondrial, toutes les autres sont exprimées dans le cytosol à partir de transcriptions nucléaires (Quirós et al., 2016; Wasilewski et al., 2017). Par conséquent, une régulation étroite du niveau d'expression des protéines mitochondriales est réalisée par une communication complexe entre les mitochondries et le noyau. En effet, la régulation de l'activité mitochondriale est réalisée par des communications antérogrades et rétrogrades entre le noyau et les mitochondries. Cela permet aux mitochondries de s'adapter à l'environnement cellulaire (Quirós et al., 2016). Les mitochondries peuvent également moduler le niveau des métabolites tels que l'ATP, l'acétyl-CoA, le NAD^+ ou les espèces réactives de l'oxygène (ROS) pour ajuster la fonction nucléaire (Quirós et al., 2016).

NDPK-D et OPA1 recombinantes vont permettre une etude détaillée de leur interaction

Afin de tester et améliorer le modèle sur la double fonction de NDPK-D par des expériences *in vitro*, nous avons essayé d'exprimer et de purifier les protéines recombinantes nécessaires, NDPK-D et OPA1. Cela permettra d'étudier les interactions et les domaines fonctionnels des protéines au niveau moléculaire.

Nous avons pu obtenir OPA1 complète de façon recombinante exprimée dans *E. coli*. Certaines expériences préliminaires de co-immunoprécipitation ont été réalisées avec les protéines recombinantes OPA1 et NDPK-D pour étudier l'interaction NDPK-D/OPA1 (données non présentées). Ces expériences indiquent un possible effet direct de la cardiolipine sur cette interaction. Cependant, ces résultats doivent être confirmés avec un anticorps purifié. En outre, l'effet des lipides sur l'activité GTPase a été étudié avec des fragments d'OPA1 non purifiés, ceux-ci indiquent que CL augmente l'activité GTPase de OPA1 (données non présentées). Cependant, on ne peut pas exclure que d'autres GTPases ou ATPases présentes dans les fractions utilisées puissent être impliquées dans cet effet, puisque le dosage utilisé, à base de vert de Malachite, détecte uniquement le produit issu de l'hydrolyse, le phosphate inorganique. Des améliorations dans les processus d'expression et de purification de l'OPA1 sont donc nécessaires *(i)* pour prouver la faisabilité de la production recombinante d'OPA1 complète et *(ii)* pour confirmer les expériences préliminaires mentionnées. Cela améliorera notre compréhension du complexe NDPK-D/OPA1 lié à CL et de son rôle dans la double fonction de NDPK-D.

Perspectives: les fonctions de NDPK-D aux niveaux moléculaires et cellulaires
Nos résultats nous ont permis d'étendre notre modèle à bien des égards. Nous pouvons émettre l'hypothèse que, dans le complexe NDPK-D/OPA1, la kinase alimente OPA1 en GTP et channel ADP via ANT dans la matrice mitochondriale pour stimuler la respiration et la régénération d'ATP. Cela permet aux mitochondries de fusionner et de maintenir la dynamique mitochondriale ainsi que de maintenir l'activité bioénergétique requise. Lorsque les mitochondries entrent en mitophagie, le complexe NDPK-D/OPA1 se désassemble, peut être parce que OPA1 est transformée en son isoforme courte. NDPK-D pourrait ensuite réticuler les membranes mitochondriales interne et externe et transférer CL à la surface mitochondriale où elle sert de signal pour la reconnaissance par les autophagosomes des mitochondries endommagées.

Il reste encore beaucoup à faire à différents niveaux pour une compréhension complète de la fonction et de la régulation de NDPK-D. Au niveau moléculaire, nous devons mieux comprendre qu'elle est la voie du transfert de CL par NDPK-D et comment le changement de mode de fonctionnement (transfert lipidique à phosphotransfert) est régulé. Des recherches plus approfondies sur l'interaction NDPK-D/OPA1 sont nécessaires, par exemple : quels acides aminés sont impliqués, comment l'interaction est régulée ou quel est le rôle des lipides dans cette interaction. Ceci peut être réalisé avec les protéines recombinantes par co-immunoprécipitation, résonance plasmonique de surface (SPR, Biacore) ou même titration calorimétrique isotherme (ITC). En cas d'interaction directe entre les protéines, nous pouvons imaginer obtenir une structure du complexe qui pourrait aider à la modélisation moléculaire pour mieux comprendre la voie de transfert de CL.

Au niveau cellulaire, nous devons améliorer notre compréhension de la communication entre les mitochondries et le noyau, en particulier la façon dont NDPK-D est impliquée dans la régulation de ce type de communication. En outre, nous devons étudier s'il existe des discussions croisées entre d'autres déclencheurs mitophagiques et le transfert de CL médié par NDPK-D.

Enfin, nous avons maintenant la possibilité de travailler avec des souris NDPK-D KO. Nous devrons tout d'abord confirmer les résultats obtenus aux niveaux moléculaires et cellulaires (expériences d'externalisation de CL, co-localisation de NDPK-D et OPA1). Une étude du phénotype de ces souris et un accent sur le foie où NDPK-D est fortement exprimée, aideront à comprendre la fonction de NDPK-D au niveau des organes et des organismes.

Appendix A

Nucleoside diphosphate kinases fuel dynamin superfamily proteins with GTP for membrane remodeling.

Boissan, M., Montagnac, G., Shen, Q., Griparic, L., Guitton, J., Romao, M., Sauvonnet, N., Lagache, T., Lascu, I., Raposo, G.,Desbourdes, C., Schlattner, U., Lacombe, M.L., Polo, S., van der Bliek, A.M., Roux, A., and Chavrier, P. (2014) *Science* **344**, 1510-5.

Abstract

Dynamin superfamily molecular motors use guanosine triphosphate (GTP) as a source of energy for membrane-remodeling events. We found that knockdown of nucleoside diphosphate kinases (NDPKs) NM23-H1/H2, which produce GTP through adenosine triphosphate (ATP)-driven conversion of guanosine diphosphate (GDP), inhibited dynamin-mediated endocytosis. NM23-H1/H2 localized at clathrin-coated pits and interacted with the proline-rich domain of dynamin. In vitro, NM23-H1/H2 were recruited to dynamin-induced tubules, stimulated GTP-loading on dynamin, and triggered fission in the presence of ATP and GDP. NM23-H4, a mitochondria-specific NDPK, colocalized with mitochondrial dynamin-like OPA1 involved in mitochondria inner membrane fusion and increased GTP-loading on OPA1. Like OPA1 loss of function, silencing of NM23-H4 but not NM23-H1/H2 resulted in mitochondrial fragmentation, reflecting fusion defects. Thus, NDPKs interact with and provide GTP to dynamins, allowing these motor proteins to work with high thermodynamic efficiency.

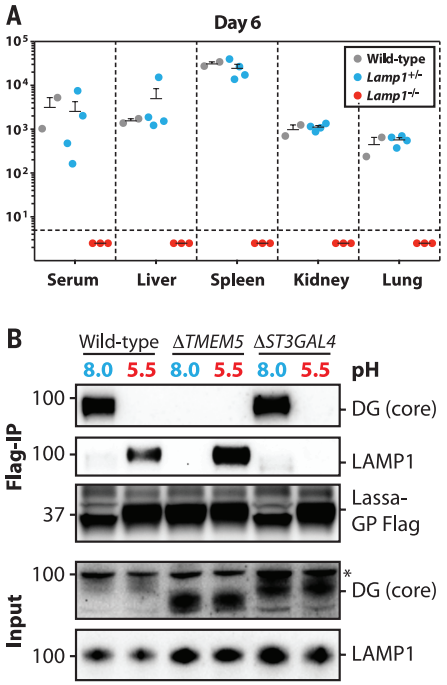

Fig. 4. *Lamp1* knockout mice are resistant to wild-type Lassa virus, and the receptors require distinct glycosyltransferases. (**A**) Lassa virus propagation in *Lamp1*$^{+/+}$, *Lamp1*$^{+/-}$, and *Lamp*$^{-/-}$ mice. Mice were injected intraperitoneally with wild-type Lassa virus, and viral titers (*y* axis, plaque-forming units/mL) were determined after 6 days in the indicated tissues. The horizontal line marks the detection limit. (**B**) Flag-tagged Lassa-GP was immobilized on beads and incubated with cell lysates from wild-type, *TMEM5*-, or *ST3GAL4*-deficient cells at the indicated pH. The glycosyltransferase TMEM5 is needed to generate an epitope on α-DG that is recognized by Lassa-GP (*4*). Bound proteins were subjected to immunoblot analysis. Asterisk indicates nonspecific background band.

virus (*23*) that requires low pH (*24*). Our findings rationalize these observations and emphasize the emergence of intracellular receptors for virus entry.

REFERENCES AND NOTES

1. S. Kunz *et al.*, *J. Virol.* **79**, 14282–14296 (2005).
2. W. Cao *et al.*, *Science* **282**, 2079–2081 (1998).
3. I. S. Lukashevich, R. F. Maryankova, F. M. Fidarov, *Acta Virol.* **27**, 282–285 (1983).
4. L. T. Jae *et al.*, *Science* **340**, 479–483 (2013).
5. F. Saito *et al.*, *FEBS Lett.* **579**, 2359–2363 (2005).
6. Materials and methods are available as supplementary materials on *Science* Online.
7. W. Zhu, J. Li, G. Liang, *Biomed. Environ. Sci.* **24**, 81–87 (2011).
8. N. Andrejewski *et al.*, *J. Biol. Chem.* **274**, 12692–12701 (1999).
9. J. Rohrer, A. Schweizer, D. Russell, S. Kornfeld, *J. Cell Biol.* **132**, 565–576 (1996).
10. T. Nishi, M. Forgac, *Nat. Rev. Mol. Cell Biol.* **3**, 94–103 (2002).
11. J. E. Carette *et al.*, *Nature* **477**, 340–343 (2011).
12. C. Di Simone, M. J. Buchmeier, *Virology* **209**, 3–9 (1995).
13. J. York, D. Dai, S. M. Amberg, J. H. Nunberg, *J. Virol.* **82**, 10932–10939 (2008).
14. J. H. Nunberg, J. York, *Viruses* **4**, 83–101 (2012).
15. E. J. Bowman, A. Siebers, K. Altendorf, *Proc. Natl. Acad. Sci. U.S.A.* **85**, 7972–7976 (1988).
16. M. Heffernan, S. Yousefi, J. W. Dennis, *Cancer Res.* **49**, 6077–6084 (1989).
17. S. R. Carlsson, P. O. Lycksell, M. Fukuda, *Arch. Biochem. Biophys.* **304**, 65–73 (1993).
18. W. C. Wang, R. D. Cummings, *J. Biol. Chem.* **263**, 4576–4585 (1988).
19. A. Ibricevic *et al.*, *J. Virol.* **80**, 7469–7480 (2006).
20. M. de Graaf, R. A. Fouchier, *EMBO J.* **33**, 823–841 (2014).
21. K. Shinya *et al.*, *Nature* **440**, 435–436 (2006).
22. W. H. Haas *et al.*, *Clin. Infect. Dis.* **36**, 1254–1258 (2003).
23. P. Y. Lozach, J. Huotari, A. Helenius, *Curr. Opin. Virol.* **1**, 35–43 (2011).
24. F. L. Cosset *et al.*, *J. Virol.* **83**, 3228–3237 (2009).

ACKNOWLEDGMENTS

We thank T. Sixma, A. Perrakis, E. von Castelmur, D. Lefeber, and members of the Brummelkamp group for discussion; M. Rusch for mouse breeding; S. Kunz for a plasmid encoding Lassa-GP; E. Ollmann-Saphire for an Fc-fusion vector; R. Schoepp for GP1 antibodies; and M. Verheije for DF1 cells. This work was supported by CGC.nl, Nederlandse Organisatie voor Wetenschappelijk Onderzoek Vidi grant 91711316, and European Research Council (ERC) Starting Grant (ERC-2012-StG 309634) to T.R.B.; Deutsche Forschungsgemeinschaft (DFG SPP1580 and GRK1459) to P.S.; and NIH grants AI081842 and AI109740 to S.P.W. J.M.D was supported by the Defense Threat Reduction Agency (CB3947). The HAP1 cells that were used are distributed under a materials transfer agreement. Opinions, interpretations, conclusions, and recommendations are those of the author and are not necessarily endorsed by the U.S. Army. T.R.B. is a cofounder and shareholder of Haplogen GmbH, a company involved in haploid genetics. Sequencing data are accessible at www.ncbi.nlm.nih.gov/sra (accession SRP041566).

SUPPLEMENTARY MATERIALS

www.sciencemag.org/content/344/6191/1506/suppl/DC1
Materials and Methods
Figs. S1 to S22
Tables S1 to S4
References (*25*–*44*)

20 February 2014; accepted 30 May 2014
10.1126/science.1252480

MEMBRANE TRAFFICKING

Nucleoside diphosphate kinases fuel dynamin superfamily proteins with GTP for membrane remodeling

Mathieu Boissan,[1,2,3,4]* Guillaume Montagnac,[1,2]† Qinfang Shen,[5] Lorena Griparic,[5] Jérôme Guitton,[6,7] Maryse Romao,[1,8] Nathalie Sauvonnet,[9] Thibault Lagache,[10] Ioan Lascu,[11] Graça Raposo,[1,8] Céline Desbourdes,[12,13] Uwe Schlattner,[12,13] Marie-Lise Lacombe,[3,4] Simona Polo,[14,15] Alexander M. van der Bliek,[5] Aurélien Roux,[16] Philippe Chavrier[1,2]*

Dynamin superfamily molecular motors use guanosine triphosphate (GTP) as a source of energy for membrane-remodeling events. We found that knockdown of nucleoside diphosphate kinases (NDPKs) NM23-H1/H2, which produce GTP through adenosine triphosphate (ATP)–driven conversion of guanosine diphosphate (GDP), inhibited dynamin-mediated endocytosis. NM23-H1/H2 localized at clathrin-coated pits and interacted with the proline-rich domain of dynamin. In vitro, NM23-H1/H2 were recruited to dynamin-induced tubules, stimulated GTP-loading on dynamin, and triggered fission in the presence of ATP and GDP. NM23-H4, a mitochondria-specific NDPK, colocalized with mitochondrial dynamin-like OPA1 involved in mitochondria inner membrane fusion and increased GTP-loading on OPA1. Like OPA1 loss of function, silencing of NM23-H4 but not NM23-H1/H2 resulted in mitochondrial fragmentation, reflecting fusion defects. Thus, NDPKs interact with and provide GTP to dynamins, allowing these motor proteins to work with high thermodynamic efficiency.

The 100-kD dynamin guanosine triphosphatase (GTPase) promotes uptake of cell-surface receptors both by clathrin-dependent and -independent pathways (*1*, *2*). Dynamin polymerizes into helix around the neck of endocytic pits and induces guanosine triphosphate (GTP) hydrolysis–driven membrane fission (*3*–*7*). Typical of molecular motors, dynamin has a low affinity for GTP and a high basal GTP-hydrolysis rate, which can be further stimulated by dynamin polymerization (*8*, *9*). This maximizes chemical energy gain and kinetics of hydrolysis, respectively, which in vivo depend on high concentration ratios of adenosine triphosphate/adenosine diphosphate (ATP/ADP) or GTP/guanosine diphosphate (GDP). The cellular concentrations of GTP and GDP are at least a factor of 10 lower than those of ATP and ADP, and GTP/GDP ratios could thus decrease much more rapidly at elevated workload, both of which make GTP not an ideal substrate for high-turnover, energy-dependent enzymes. Paradoxically, dynamin GTPases are among the most powerful molecular motors described (*7*).

Studies in *Drosophila* identified a genetic interaction between dynamin and *Awd* (*10*–*12*). Awd belongs to the family of nucleoside diphosphate kinases (NDPKs), which catalyze synthesis of nucleoside triphosphates, including GTP, from corresponding nucleoside diphosphates and ATP (*13*). The most abundant human NDPKs are the highly related cytosolic proteins NM23-H1 and -H2. NM23-H4, another NDPK-family member, localizes exclusively at the mitochondrial inner membrane (*14*, *15*). Mitochondrial

[1]Institut Curie, Research Center, Paris, France. [2]Membrane and Cytoskeleton Dynamics, CNRS UMR 144, Paris, France. [3]Université Pierre et Marie Curie, University Paris 06, Paris, France. [4]Saint-Antoine Research Center, INSERM UMR-S 938, Paris, France. [5]Department of Biological Chemistry, David Geffen School of Medicine at University of California, Los Angeles, Los Angeles, CA, USA. [6]Hospices Civils de Lyon, Pierre Bénite, France. [7]Université de Lyon, Lyon, France. [8]Structure and Membrane Compartments, CNRS UMR 144, Paris, France. [9]Institut Pasteur, Unité de Biologie des Interactions Cellulaires, Paris, France. [10]Quantitative Image Analysis Unit, Institut Pasteur, Paris, France. [11]Institut de Biochimie et Génétique Cellulaires-CNRS, Université Bordeaux 2, Bordeaux, France. [12]Université Grenoble Alpes, Laboratory of Fundamental and Applied Bioenergetics, Grenoble, France. [13]Inserm, U1055, Grenoble, France. [14]IFOM, Fondazione Istituto FIRC di Oncologia Molecolare, Milan, Italy. [15]Dipartimento di Scienze della Salute, Universita' degli Studi di Milano, Milan, Italy. [16]Biochemistry Department, University of Geneva, & Swiss National Center for Competence in Research Program Chemical Biology, Geneva, Switzerland.
***Corresponding author. E-mail: mathieu.boissan@inserm.fr (M.B.); philippe.chavrier@curie.fr (P.C.)** †Present address: Institut Gustave Roussy, Inserm U1009, Villejuif, France

membrane dynamics require dynamin-related GTPases (*16*). We hypothesized that NDPKs could influence the function of dynamin family members in membrane-remodeling events through spatially controlled GTP production and availability.

Knockdown of NM23-H1 and -H2 (fig. S1, A to E) reduced clathrin-dependent endocytosis of the transferrin (Tf) and epidermal growth factor (EGF) receptors (Fig. 1, A and B, and fig. S2, A to E) and clathrin-independent dynamin-dependent endocytosis of interleukin-2 receptor β subunit (Fig. 1C). The endocytic defect of EGF receptor was partially rescued by expression of wild-type, small interfering RNA (siRNA)–resistant NM23-H1, but not by kinase-dead NM23-$H1^{H118N}$ mutant (Fig. 1D). Thus, the function of Awd/NM23 in dynamin-mediated endocytosis is conserved from *Drosophila* to mammalian cells [(*10*) and this study].

Like in dynamin-null cells (*17*), NM23-H1/H2 depletion increased the density of clathrin-coated pits (CCPs) at the plasma membrane (Fig. 2, A and B, and fig. S3, A and B). Silencing of NM23-H1/H2 led to the accumulation of deeply invaginated CCPs, in contrast to control cells, where CCPs were rarely detected at the plasma membrane (Fig. 2, C to F). Scoring for Tf-positive CCPs and vesicles in the vicinity of the plasma membrane revealed an approximately threefold augmentation in the absence of NM23 (Fig. 2G), similar to the phenotype reported in dynamin-null cells (*17*), suggesting a role for NM23-H1/H2 in dynamin-mediated membrane fission at CCPs.

We examined the intracellular distribution of NM23-H1/H2 and confirmed that both isoforms were predominantly cytosolic, although a low but reproducible association of both isoforms with membranes was found (fig. S4, A and B). Total internal reflection fluorescence

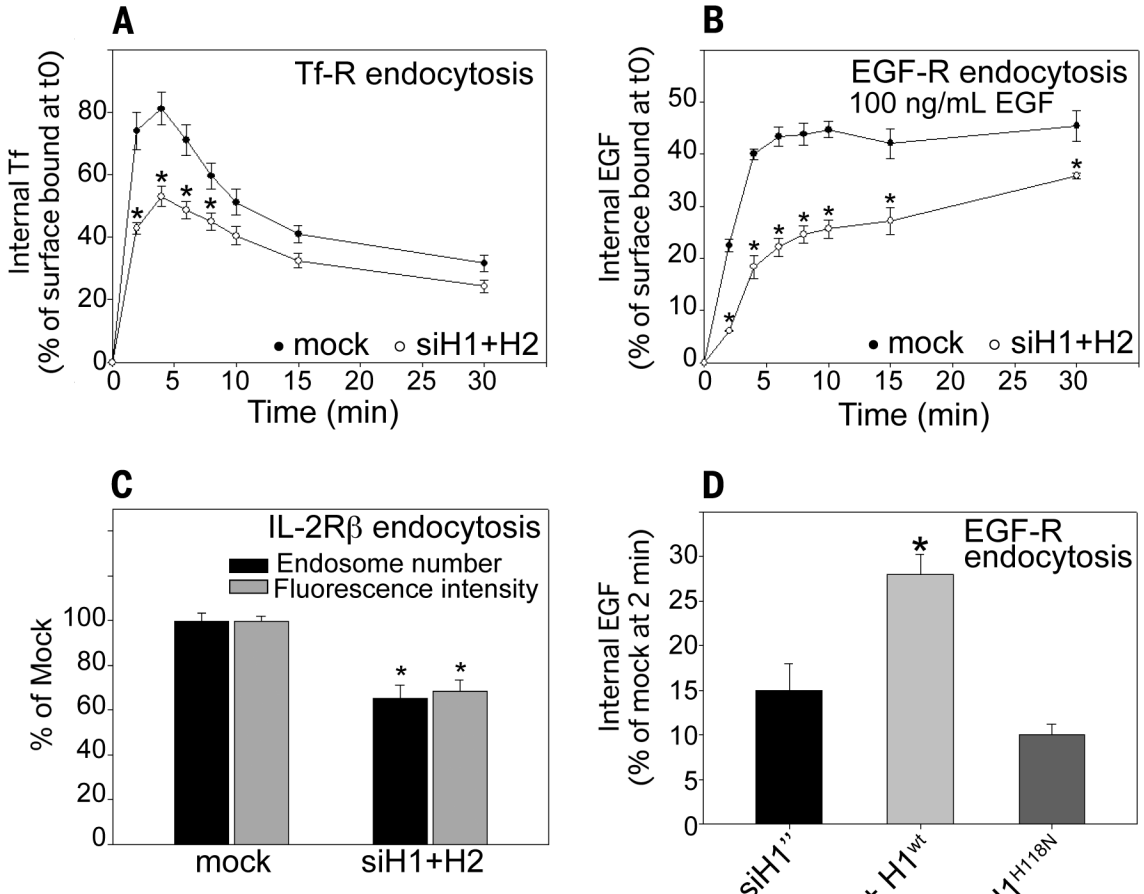

Fig. 1. Nucleoside diphosphate kinases NM23-H1/H2 are required for efficient dynamin-mediated endocytosis. (**A**) HeLa cells were mock-treated or treated with a pair of siRNAs to simultaneously knock down NM23-H1 and NM23-H2 and assessed for endocytosis of Alexa488-Tf. Data are expressed as percentage of internal Tf compared with surface-bound Tf at time 0 ± SEM from four independent experiments. **P* < 0.05 compared with mock-treated cells. (**B**) HeLa cells, either mock-treated or treated with NM23-H1/H2 siRNAs, were assessed for endocytosis of Alexa488-EGF (100 ng/ml). Data are expressed as percentage of internal EGF compared with surface-bound EGF at time 0 ± SEM from four independent experiments. **P* < 0.05 compared with mock-treated cells. (**C**) Hep2 cells stably expressing the interleukin-2 receptor β subunit (IL-2Rβ) were mock-treated or treated with siRNA for NM23-H1/H2 and incubated in the presence of Cy3-coupled antibody to IL-2Rβ for 5 min at 37°C. Data are expressed as average intracellular fluorescence intensity normalized to the intensity of mock-treated cells ± SEM and endosome number normalized to endosome number in mock-treated cells ± SEM. 100 cells were analyzed from three independent experiments. **P* < 0.05 compared with mock-treated cells. (**D**) HeLa cells mock-treated or treated with NM23-H1 siRNA were transfected with siRNA-resistant wild-type ($H1^{wt}$) or kinase-dead NM23-H1 ($H1^{H118N}$). EGF endocytosis after 2 min at 37°C was assessed as in (B). **P* < 0.05 compared with siH1''-treated cells.

(TIRF) microscopy analysis of cells labeled with antibody to NM23-H2 revealed the colocalization of NM23-H2 with AP-2 (α-adaptin) and dynamin-2 at CCPs (fig. S5, A to D), which was confirmed by means of proximity ligation assay (PLA), which showed a close proximity of NM23-H1/H2 with α-adaptin and dynamin-2 at CCPs (Fig. 2, H and I, and figs. S6 and S7). Furthermore, NM23-H1/H2 coimmunoprecipitated with dynamin-1 (Fig. 3A) and with dynamin-2 (Fig. 3B), and purified full-length recombinant NM23-H2 and dynamin-2 interacted directly in vitro (Fig. 3C). We investigated the contribution of the C-terminal proline-rich domain (PRD) of dynamin-2 to this interaction because this domain binds to several dynamin regulators and effectors (*18*). The dynamin-2 PRD domain fused to glutathione *S*-transferase (GST) pulled-down NM23-H1 and -H2, indicating that dynamin-2 physically interacts with both NM23-H1/H2 isoforms through its PRD (Fig. 3D). Thus, NM23-H1/H2 interact with endocytic dynamins at CCPs.

Next, we explored the role of NM23 NDPK activity in dynamin function. Whereas silencing of both NM23-H1 and -H2 isoforms caused a ~80% decrease of NDPK activity (fig. S8A), overall intracellular GTP levels were not affected by NM23 knockdown (fig. S8B) [nor were other nucleoside triphosphate levels affected (fig. S8C)]. Thus, decreased endocytic rate and increased CCP accumulation of NM23-depleted cells were not a consequence of a reduced bulk intracellular GTP concentration, but rather support a role of NM23-dynamin complexes in which NM23 generates GTP in the vicinity of dynamins to avoid a local drop in GTP/GDP ratio. Indeed, in the absence of added GTP and in the presence of NM23 substrates GDP (1 mM) and ATP (1 mM), catalytically active recombinant NM23-H1 and -H2 proteins triggered GTPase activity of dynamin-1 and -2 (Fig. 3E), whereas kinase-dead NM23-H1^{H118N} mutant did not (Fig. 3E). In the presence of nucleotide concentrations close to cellular levels—100 μM GTP, 10 μM GDP, and 1 mM ATP—NM23-H1 and -H2 were still able to enhance dynamin-1's GTPase activity by 30 to 35%, indicating that NM23 could stimulate dynamin activity further in the presence of physiological GTP level (Fig. 3F). This reflects the capacity of H1/H2 to directly provide GTP to dynamins within NM23/dynamin complexes.

Next, we monitored the capacity of NM23 to promote dynamin-mediated membrane fission in vitro. Classical dynamins can tubulate membrane sheets in the absence of GTP and then fragment the tubules depending on GTP hydrolysis (*6*). Dynamin-induced tubular networks remained stable in the presence of 1 mM ATP and 1 mM GDP and in the absence of NM23 (Fig. 3G and movie S1), and tubules were not altered by NM23-H1 or -H2 in the absence of nucleotides (Fig. 3G and movies S2 and S3, time 0). In contrast, in the presence of NM23, addition of 1 mM ATP and 1 mM GDP induced breakage and collapse of the tubule network (Fig. 3G and movies S2 and S3), with a fission density of 1 event per 8.3-μm tube length (n = 20 tubes). Most of the fission events occurred during the first 60 s after addition of ATP and GDP (fig. S9A). Immunogold electron microscopy (EM) on liposomes incubated in the presence of purified NM23-H2 and dynamin-1 revealed that NM23-H2 decorated the length of the membrane tubules (Fig. 3, H and I). In addition, EM of negatively stained preparations of membrane tubules confirmed the association of NM23-H2 to the surface of dynamin-1–coated tubules

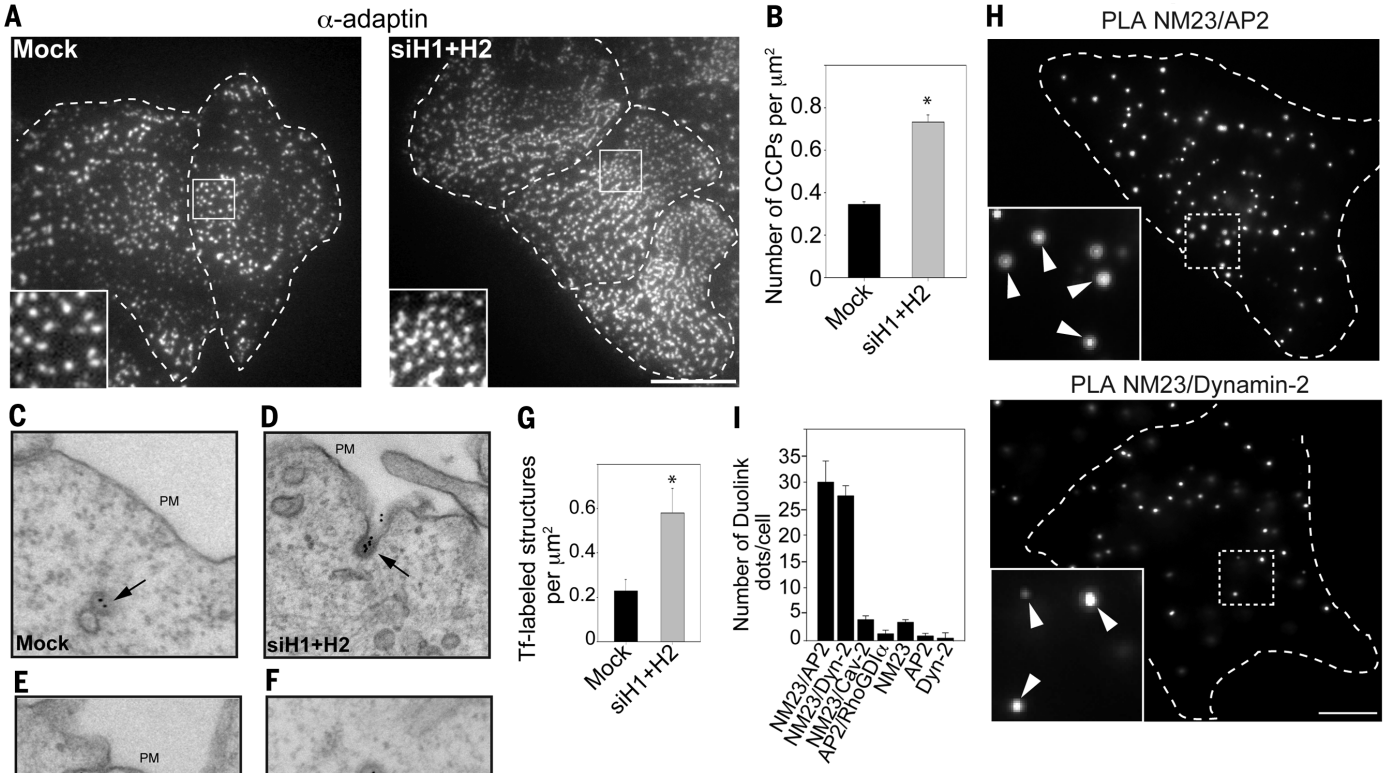

Fig. 2. Accumulation and tubulation of clathrin-coated pits in the absence of NM23-H1/H2. (**A** and **B**) AP-2 staining (α-adaptin) reveals higher CCP density in HeLa cells knocked down for NM23-H1/H2. Scale bar, 5 μm. Graph in (B) represents the mean CCP number/μm² ± SEM (n = 10 cells for each condition). *P < 0.05 compared with mock-treated cells. (**C** to **F**) HeLa cells mock-treated (C) or silenced for NM23-H1/H2 [(D) to (F)] were allowed to internalize Tf-Biotin for 4 min at 37°C and analyzed with electron microscopy by means of immunogold labeling with anti-Biotin antibodies and protein-A gold conjugates. Scale bar, 200 nm. (**G**) Number of Tf-positive structures (CCPs and vesicles)/μm² in a 1.9 μm-wide region, including the plasma membrane. *P < 0.05 compared with mock-treated cells. (**H**) PLA signal using combination of NM23 and AP-2 (α-adaptin) antibodies (top), or dynamin-2 antibodies (bottom). (Insets) Higher magnification of boxed regions. Scale bar, 5 μm. (**I**) Quantification of PLA dots per cell using different antibody pairs as indicated (mean ± SEM, n = 30 cells/condition from three independent experiments).

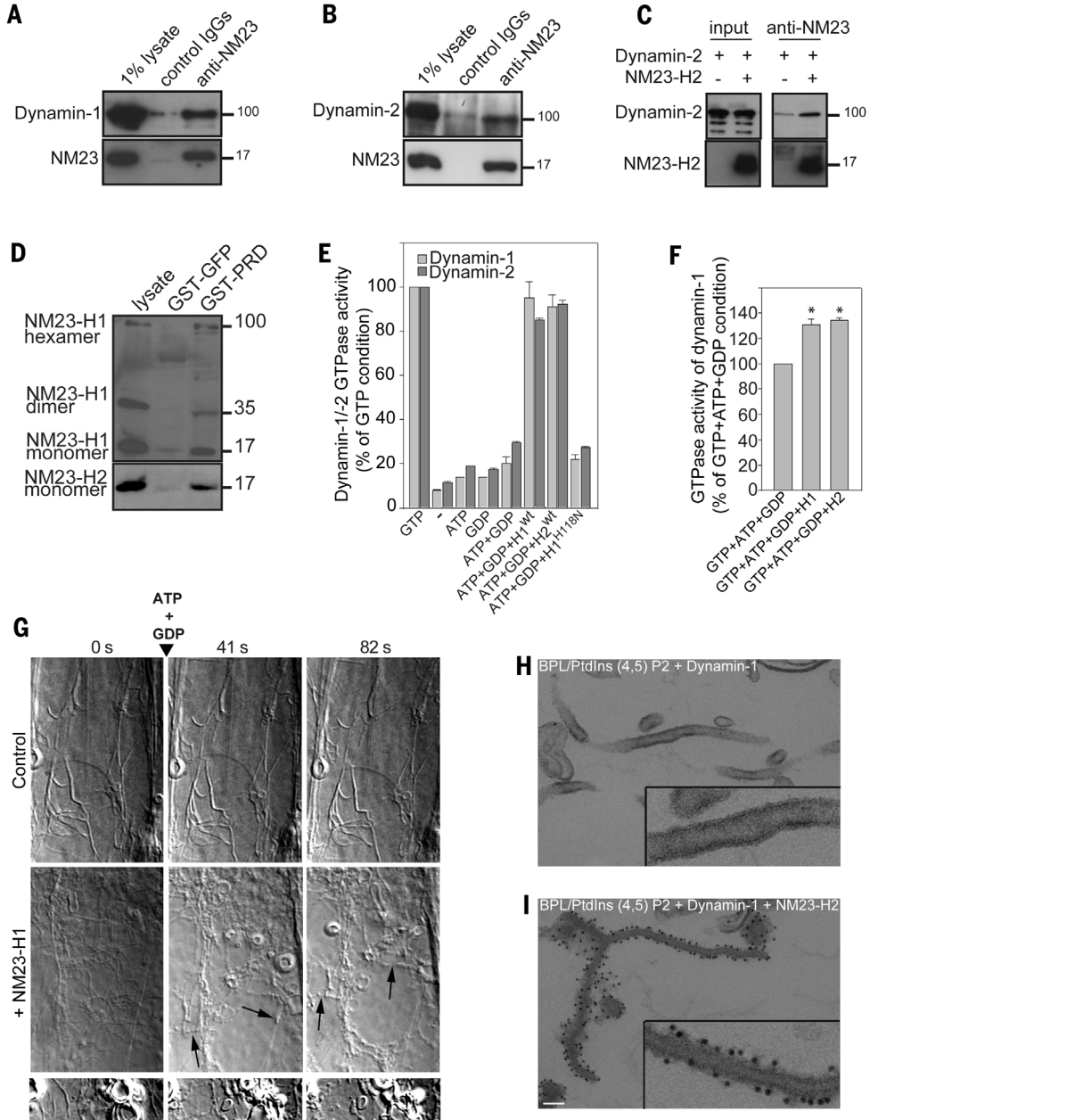

Fig. 3. NM23-H1/H2 promotes dynamin-mediated membrane fission by local GTP regeneration. (**A** and **B**) Lysates of (A) mouse brain or (B) HeLa cells immunoprecipitated with pan–NM23-H1/H2 antibodies and bound proteins analyzed with antibodies to dynamin-1 (A) and -dynamin-2 (B). One percent of total lysate was loaded as a control (input). (**C**) Purified recombinant human NM23-H2 and dynamin-2 were mixed and immunoprecipitated by using antibodies to NM23. Bound proteins were detected with dynamin-2 and NM23 antibodies as indicated. (**D**) Pull-down assays of NM23-H1/H2 from HeLa cell lysates with dynamin-2 GST-PRD or GST-GFP constructs. Bound proteins were detected with specific antibodies to NM23-H1 and -H2. Monomers and denaturation-resistant dimers and hexamers of NM23-H1 interact with dynamin-2 PRD domain. (**E**) GTPase activity of purified human dynamin-1 and -2 measured in the presence of 95% brain polar lipids (BPL)/5% PtdIns(4,5)P_2 liposomes, recombinant purified wild-type or catalytically dead (H118N) NM23-H1/H2 and nucleotides (1 mM) as indicated. Results are expressed as percentage of controls (1 mM GTP) from triplicate samples from four independent experiments. (**F**) GTPase activity of human dynamin-1 measured as in (E) in the absence or in the presence of NM23-H1 or -H2 and in the presence of physiological nucleotide concentrations (1 mM ATP, 100 μM GTP, and 10 μM GDP). Results are expressed as percent of control condition (ATP+GTP+GDP) from triplicate samples from two independent experiments. *$P < 0.05$ compared with control condition. (**G**) Selected frames from time-lapse sequences showing the effect of purified human NM23-H1/H2 on dynamin-induced membrane tubules after addition of 1 mM ATP and 1 mM GDP. Rat brain dynamin induces tubule formation from the 95% BPL/5% PtdIns (4,5) P_2 liposomes (time 0). Arrows point to tubule fission events in the presence of NM23-H1 or -H2. Representative frames from four independent experiments are shown. (**H** and **I**) Electron micrographs of liposomes incubated (H) with human dynamin-1 alone, which induced tubulation or (I) together with NM23-H2 and stained for NM23 by means of immunogold-labeling. (Insets) Higher magnification. Scale bar, 100 nm.

(fig. S9B). Thus, NM23 bound to membrane-associated dynamin affects dynamin function in membrane fission.

Given the efficiency of NM23-driven GTP supply to dynamins, we explored whether in another compartment, the mitochondria, mitochondrial NM23-H4 isoform was capable of supporting dynamin-related GTPase OPA1. In contrast to the typical tubular morphology of mitochondria in HeLa cells transfected with MitoDsRed, cells silenced for NM23-H4 showed abnormally fragmented and swollen mitochondria (Fig. 4, A and B). Depletion of NM23-H4 phenocopied the loss of OPA1 on mitochondrial morphology, whereas knockdown of NM23-H1/H2 did not alter mitochondrial morphology (Fig. 4, A and B). EM confirmed the severity of mitochondria alterations in NM23-H4–depleted cells (Fig. 4C), which is reminiscent of mitochondrial fusion defects as a result of OPA1 loss of function (*19*). Furthermore, immunofluorescence staining and PLA documented the colocalization and close proximity of NM23-H4 and OPA1 in mitochondria (Fig. 4D and fig. S10), which is in agreement with their reported interaction (*20*). To directly show the involvement of NM23-H4 in GTP fueling to OPA1, we determined the GTP hydrolysis rate of OPA1 reflecting GTP loading. Recombinant NM23-H4 triggered OPA1's GTPase activity in the presence of liposomes, mimicking the composition of the mitochondrial inner membrane (Fig. 4E). GTP loading on OPA1 was further increased by ~30% by NM23-H4 in the presence of native mitochondrial GTP concentration (Fig. 4F), which is similar to that observed for NM23-H1/H2 on classical dynamins (Fig. 3F).

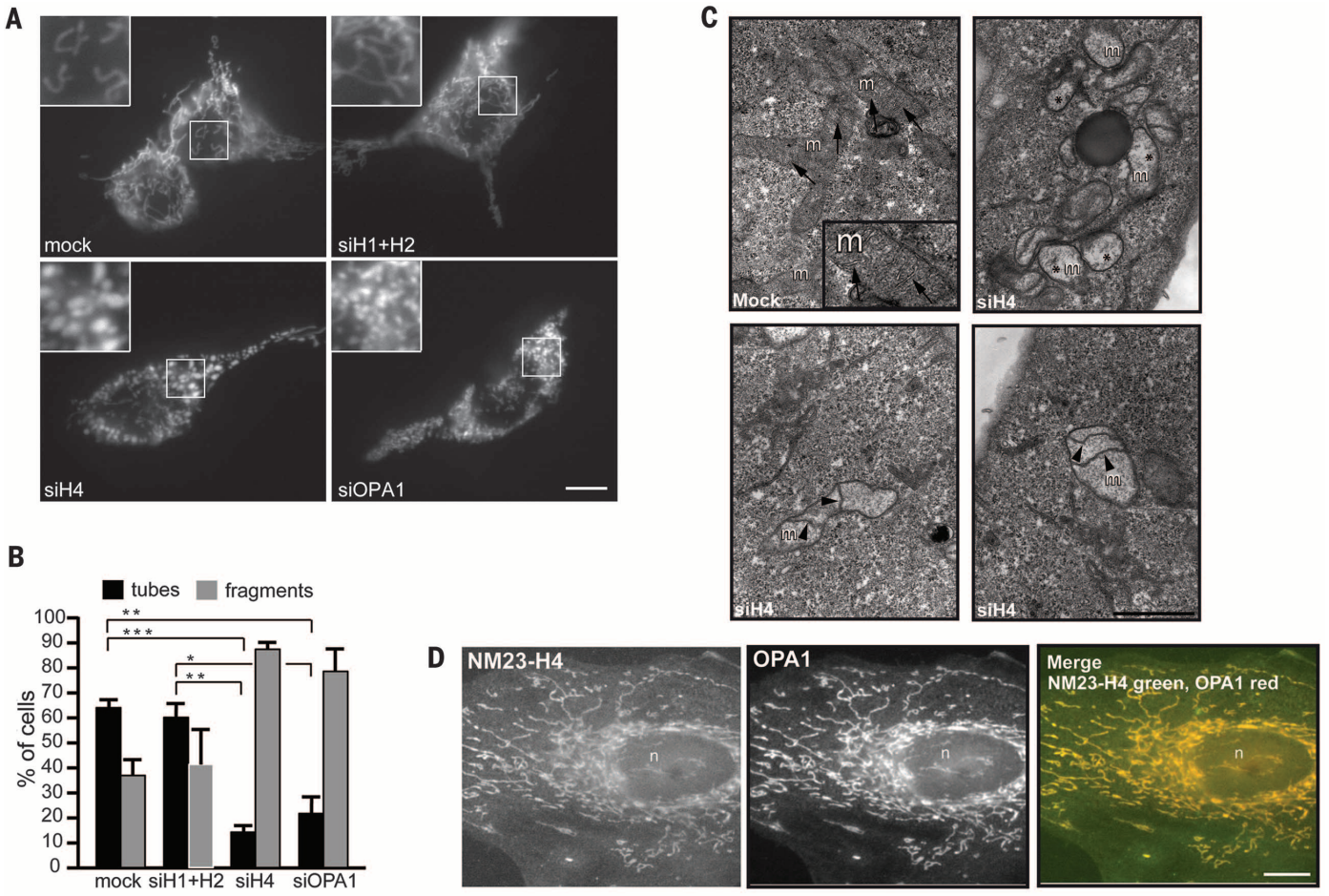

Fig. 4. Mitochondrial NM23-H4 controls mitochondria membrane dynamics through dynamin-related GTPase OPA1. (**A**) HeLa cells transfected with mitochondrial marker mitoDsRED were treated with siRNAs targeting NM23-H1/H2, NM23-H4, or OPA1. Scale bar, 10 μm. (**B**) Percentage of cells with tubular or fragmented mitochondrial morphology in different cell populations as in (A). Mean and SEM are shown for three independent experiments (>100 cells per experiment). ***$P < 0.001$; **$P < 0.01$; *$P < 0.05$. (**C**) EM of HeLa cells silenced for NM23-H4, showing alterations of mitochondrial morphology as compared with that in mock-treated cells. Arrows point to mitochondrial cristae in mock-treated cells. Asterisks indicate mitochondria with loss of cristae and electron-lucent matrix in cells knocked down for NM23-H4. Arrowheads point to internal septae, which appear to divide the inner membrane compartment in H4-KD cells. Scale bar, 1 μm. (**D**) Colocalization of NM23-H4 and OPA1 in mitochondria in HeLa cells. Scale bar, 10 μm. (**E**) GTPase activity of purified recombinant human OPA1 measured in the presence of 25% cardiolipin-enriched liposomes and purified NM23-H4 as in Fig. 3E. Results are expressed as percentage of control condition (1 mM GTP) from three independent experiments. *$P < 0.05$ compared with the ATP+GDP condition. (**F**) GTPase activity of human OPA1 in the presence of cardiolipin-enriched liposomes and NM23-H4 measured in the presence of physiological mitochondrial nucleotide concentration (1 mM ATP, 100 μM GTP, and 10 μM GDP). Results are expressed as percent of control (ATP+GTP+GDP) from duplicate samples from two independent experiments. *$P < 0.05$ compared with the control condition.

We have shown that members of the NM23/NDPK family interact directly and specifically with members of the dynamin superfamily and thus are positioned to maintain high local GTP concentrations and promote dynamin-dependent membrane remodeling. The role of NM23 is well supported by their high NDPK turnover number [k_{cat} 600 s^{-1} per active site (*21*)]. Furthermore, the localization of the NM23-H3 isoform at the mitochondrial outer membrane (fig. S11), where dynamin Drp1 is recruited to mediate mitochondrial fission, suggests that NM23-H3 could assist Drp1 in this process. These findings identify a general mechanism by which different NDPKs maintain high GTP concentration to high-turnover GTPase dynamins for efficient work in different membrane compartments.

REFERENCES AND NOTES

1. S. M. Ferguson, P. De Camilli, *Nat. Rev. Mol. Cell Biol.* **13**, 75–88 (2012).
2. S. L. Schmid, V. A. Frolov, *Annu. Rev. Cell Dev. Biol.* **27**, 79–105 (2011).
3. J. E. Hinshaw, S. L. Schmid, *Nature* **374**, 190–192 (1995).
4. K. Takei, P. S. McPherson, S. L. Schmid, P. De Camilli, *Nature* **374**, 186–190 (1995).
5. S. M. Sweitzer, J. E. Hinshaw, *Cell* **93**, 1021–1029 (1998).
6. A. Roux, K. Uyhazi, A. Frost, P. De Camilli, *Nature* **441**, 528–531 (2006).
7. S. Morlot *et al.*, *Cell* **151**, 619–629 (2012).
8. D. D. Binns *et al.*, *Biochemistry* **39**, 7188–7196 (2000).
9. B. Marks *et al.*, *Nature* **410**, 231–235 (2001).
10. K. S. Krishnan *et al.*, *Neuron* **30**, 197–210 (2001).
11. V. Dammai, B. Adryan, K. R. Lavenburg, T. Hsu, *Genes Dev.* **17**, 2812–2824 (2003).
12. G. Nallamothu, J. A. Woolworth, V. Dammai, T. Hsu, *Mol. Cell. Biol.* **28**, 1964–1973 (2008).
13. M. Boissan *et al.*, *Mol. Cell. Biochem.* **329**, 51–62 (2009).
14. L. Milon *et al.*, *J. Biol. Chem.* **275**, 14264–14272 (2000).
15. M. Tokarska-Schlattner *et al.*, *J. Biol. Chem.* **283**, 26198–26207 (2008).
16. A. M. van der Bliek, Q. Shen, S. Kawajiri, *Cold Spring Harb. Perspect. Biol.* **5**, a011072 (2013).
17. S. M. Ferguson *et al.*, *Dev. Cell* **17**, 811–822 (2009).
18. G. J. Praefcke, H. T. McMahon, *Nat. Rev. Mol. Cell Biol.* **5**, 133–147 (2004).
19. L. Griparic, N. N. van der Wel, I. J. Orozco, P. J. Peters, A. M. van der Bliek, *J. Biol. Chem.* **279**, 18792–18798 (2004).
20. U. Schlattner *et al.*, *J. Biol. Chem.* **288**, 111–121 (2013).
21. I. Lascu *et al.*, *J. Biol. Chem.* **272**, 15599–15602 (1997).

ACKNOWLEDGMENTS

We thank P. De Camilli, E. Smythe, and J. Bertoglio for reagents; S. L. Schmid and M. Mettlen for discussion; the Nikon Imaging Center@Institut Curie & Centre National de la Recherche Scientifique (CNRS) for image acquisition; and I. Hurbain for EM quantification. This work was supported by Institut Curie, CNRS, Fondation ARC pour la Recherche sur le Cancer, Groupement des Entreprises Françaises contre le Cancer, Fondation pour la Recherche Médicale, the Human Frontier Science Program, the Swiss National Fund for Research Grant, and the European Research Council.

SUPPLEMENTARY MATERIALS

www.sciencemag.org/content/344/6191/1510/suppl/DC1
Materials and Methods
Supplementary Text
Figs. S1 to S11
References (*22*–*33*)
Movies S1 to S3

24 March 2014; accepted 5 June 2014
10.1126/science.1253768

SENSORY BIOLOGY

Flower discrimination by pollinators in a dynamic chemical environment

Jeffrey A. Riffell,[1]* Eli Shlizerman,[2] Elischa Sanders,[1] Leif Abrell,[3] Billie Medina,[1] Armin J. Hinterwirth,[1] J. Nathan Kutz[2]

Pollinators use their sense of smell to locate flowers from long distances, but little is known about how they are able to discriminate their target odor from a mélange of other natural and anthropogenic odors. Here, we measured the plume from *Datura wrightii* flowers, a nectar resource for *Manduca sexta* moths, and show that the scent was dynamic and rapidly embedded among background odors. The moth's ability to track the odor was dependent on the background and odor frequency. By influencing the balance of excitation and inhibition in the antennal lobe, background odors altered the neuronal representation of the target odor and the ability of the moth to track the plume. These results show that the mix of odors present in the environment influences the pollinator's olfactory ability.

The olfactory environment is complex and rich, filled with natural, biogenically emitted volatile compounds (volatiles) and closely related volatiles from anthropogenic sources, such as those from combustion engines (*1*–*4*). Insects must successfully discriminate and locate biologically important scents, such as those emitted by food, mates, or hosts, from within this complex mixture (*5*–*8*). How does the insect olfactory system accomplish this task? Our understanding of these effects has been hampered by an inability to measure natural scents at time scales experienced by insects in nature and to link this information with an understanding of how the brain discriminates olfactory stimuli from the background odor landscape.

In the southwest USA, the *Manduca sexta* (hereafter, *Manduca*) moth navigates to, and pollinates, *Datura wrightii* flowers that are separated by hundreds of meters (*9*–*11*). *D. wrightii* (hereafter, *Datura*) often grow in dense stands of creosote bush (*Larrea tridentata*), which emit a high-intensity odor (>100 mg/h) that includes some of the same aromatic volatiles (e.g., benzaldehyde) as the scent of *Datura* (*9*, *12*).

A proton transfer–reaction mass spectrometer, which enables simultaneous measurement of multiple volatiles at subsecond time scales, allowed us to measure the scent plume from *Datura* flowers and characterize its dynamics (Fig. 1A). Measurement of ions from oxygenated aromatics (ARs, e.g., benzaldehyde) and monoterpenes (MOs, linalool and geraniol) showed that the floral plume increased in frequency and decreased in intermittency with increasing distance from the flower (Fig. 1, A to C). The ratio of volatiles in the plume also changed as the background volatiles from neighboring vegetation, including creosote bush plants, became intermixed with the plume (Fig. 1, D and E).

To determine how the changing frequency of the target odor influenced the moth's ability to locate the flower, we used a wind tunnel and a computer-controlled odor-stimulus system to test the moths' response to the *Datura* mixture at different frequencies (1 to 20 Hz) and embedded in different backgrounds [figs. S1 and S2; table S1; see supplementary materials (SM) for details]. Compared with the responses to a mineral oil (no-odor) control, moths exhibited the strongest response to odor pulses of 1 Hz (Fig. 2A_1) (2 × 2 χ^2 test, $P < 0.001$). However, frequencies higher than 1 to 2 Hz resulted in behavior similar to that displayed in response to the no-odor controls (Fig. 2, A_2 and B) (2 × 2 χ^2 test, $P > 0.33$).

We next tested the moths' ability to track the flower-odor plume at a frequency of 1 Hz among a background of different odors, ranging from volatiles that do not occur in the *Datura* mixture [nonoverlapping, ethyl sorbate] to those that do: for instance, (i) volatiles that occur in the flower odor and thereby change the constituent ratio (e.g., benzaldehyde) and (ii) the complex odor background of creosote bush (*L. tridentata*) that also shares volatiles with *Datura*. The volatile background significantly modified the moth's odor-tracking ability (Fig. 2, C and D). For example, when exposed to the *Datura* plume with a background of ethyl sorbate [a volatile that is not in the *Datura* floral odor and chemically dissimilar to constituents of the *Datura* mixture (*10*)], moths navigated to and located the odor source (Fig. 2, C_1 and D) (2 × 2 χ^2 test, $P < 0.001$). By contrast, when challenged with the *Datura* plume in a background of benzaldehyde (a volatile in creosote bush and *Datura* scents), the moth's ability to correctly navigate to the odor significantly decreased (Fig. 2C_2) (2 × 2 χ^2 test relative to *Datura* mixture, $P < 0.01$; χ^2 test relative to no odor control, $P = 0.44$). Similar results occurred

[1]Department of Biology, University of Washington, Seattle, WA 98195–1800, USA. [2]Department of Applied Mathematics, University of Washington, Seattle, WA 98195–3925, USA. [3]Department of Chemistry and Biochemistry and Department of Soil, Water, and Environmental Science, University of Arizona, AZ 85721–0077, USA
*Corresponding author. E-mail: jriffell@u.washington.edu

Appendix B

NDPK-D (NM23-H4)-mediated externalization of cardiolipin enables elimination of depolarized mitochondria by mitophagy.

Kagan, E., Jiang, J., Huang, Z., Tyurina, Y.Y., Desbourdes, C., Cottet-Rousselle, C., Dar, H.H., Verma, M., Tyurin, V.A., Kapralov, A.A., Cheikhi, A., Mao, G., Stolz, D., St. Croix, C.M., Watkins, S., Shen, Z., Li, Y., Greenberg, M.L., Tokarska-Schlattner, M., Boissan, M., Lacombe, M.L., Epand, R.M., Chu, C.T., Mallampalli, R., Bayir, H., and Schlattner, U. (2016) *Cell Death Diff.* **23**, 1140-51.

Abstract

Mitophagy is critical for cell homeostasis. Externalization of the inner mitochondrial membrane phospholipid, cardiolipin (CL), to the surface of the outer mitochondrial membrane (OMM) was identified as a mitophageal signal recognized by the microtubule-associated protein 1 light chain 3. However, the CL-translocating machinery remains unknown. Here we demonstrate that a hexameric intermembrane space protein, NDPK-D (or NM23-H4), binds CL and facilitates its redistribution to the OMM. We found that mitophagy induced by a protonophoric uncoupler, carbonyl cyanide m-chlorophenylhydrazone (CCCP), caused externalization of CL to the surface of mitochondria in murine lung epithelial MLE-12 cells and human cervical adenocarcinoma HeLa cells. RNAi knockdown of endogenous NDPK-D decreased CCCP-induced CL externalization and mitochondrial degradation. A R90D NDPK-D mutant that does not bind CL was inactive in promoting mitophagy. Similarly, rotenone and 6-hydroxydopamine triggered mitophagy in SH-SY5Y cells was also suppressed by knocking down of NDPK-D. In situ proximity ligation assay (PLA) showed that mitophagy-inducing CL-transfer activity of NDPK-D is closely associated with the dynamin-like GTPase OPA1, implicating fission-fusion dynamics in mitophagy regulation.

Cell Death and Differentiation (2016), 1–12

www.nature.com/cdd

NDPK-D (NM23-H4)-mediated externalization of cardiolipin enables elimination of depolarized mitochondria by mitophagy

VE Kagan*,[1], J Jiang[1], Z Huang[1], YY Tyurina[1], C Desbourdes[2,3], C Cottet-Rousselle[2,3], HH Dar[1], M Verma[4], VA Tyurin[1], AA Kapralov[1], A Cheikhi[1], G Mao[1], D Stolz[5], CM St. Croix[5], S Watkins[5], Z Shen[6], Y Li[6], ML Greenberg[6], M Tokarska-Schlattner[2,3], M Boissan[7,8], M-L Lacombe[7], RM Epand[9], CT Chu[4], RK Mallampalli[10,11], H Bayır*,[12] and U Schlattner*,[2,3]

Mitophagy is critical for cell homeostasis. Externalization of the inner mitochondrial membrane phospholipid, cardiolipin (CL), to the surface of the outer mitochondrial membrane (OMM) was identified as a mitophageal signal recognized by the microtubule-associated protein 1 light chain 3. However, the CL-translocating machinery remains unknown. Here we demonstrate that a hexameric intermembrane space protein, NDPK-D (or NM23-H4), binds CL and facilitates its redistribution to the OMM. We found that mitophagy induced by a protonophoric uncoupler, carbonyl cyanide *m*-chlorophenylhydrazone (CCCP), caused externalization of CL to the surface of mitochondria in murine lung epithelial MLE-12 cells and human cervical adenocarcinoma HeLa cells. RNAi knockdown of endogenous NDPK-D decreased CCCP-induced CL externalization and mitochondrial degradation. A R90D NDPK-D mutant that does not bind CL was inactive in promoting mitophagy. Similarly, rotenone and 6-hydroxydopamine triggered mitophagy in SH-SY5Y cells was also suppressed by knocking down of NDPK-D. *In situ* proximity ligation assay (PLA) showed that mitophagy-inducing CL-transfer activity of NDPK-D is closely associated with the dynamin-like GTPase OPA1, implicating fission–fusion dynamics in mitophagy regulation.
Cell Death and Differentiation advance online publication, 8 January 2016; doi:10.1038/cdd.2015.160

Appreciation of the central role of the mitochondrion as a hub controlling multiple intra- and extra-cellular metabolic responses, as well as cellular life or death decisions, has raised great interest in the processes involved in their maintenance and quality control.[1,2] The homeostatic health of mitochondria is preserved owing to coordinated functions of several control mechanisms, including proteolysis of misfolded proteins, proteasomal degradation of aberrant proteins on their surface, dynamic repair processes of fission and fusion, formation and budding off of specialized mitochondrial particles, and autophagic degradation of the entire organelle in lysosomes (mitophagy).[3] In the latter process, identification of the signals distinguishing 'fit' from dysfunctional mitochondria is particularly important, and several essential molecular interactions are beginning to emerge.[3,4] Pink1-Parkin-mediated ubiquitination of the outer mitochondrial membrane (OMM) proteins and their indirect interactions with the autophagy protein MAP1-light chain 3/Atg8 (LC3) via LC3-interacting region (LIR) domain adaptor proteins have been proposed as one of the potentially essential mitophageal signaling pathways.[5]

Recently, we reported that a mitochondria-unique anionic phospholipid, cardiolipin (CL), undergoes redistribution and externalization to the surface of mitsochondria injured by a variety of insults in several types of cells.[6] The externalized CL is recognized by LC3, thus triggering the elimination of

[1]Department of Environmental and Occupational Health, Center for Free Radical and Antioxidant Health, University of Pittsburgh, Pittsburgh, PA, USA; [2]University Grenoble Alpes—UJF, Laboratory of Fundamental and Applied Bioenergetics (LBFA), and SFR Environmental and Systems Biology (BEeSy), U1055, Grenoble, France; [3]Inserm, U1055, Grenoble, France; [4]Department of Pathology, University of Pittsburgh, Pittsburgh, PA, USA; [5]Department of Cell Biology and Physiology, University of Pittsburgh, Pittsburgh, PA, USA; [6]Department of Biological Sciences, Wayne State University, Detroit, MI, USA; [7]Sorbonne Universités, UPMC Univ Paris 06, Saint-Antoine Research Center, INSERM UMR-S 938, Paris, France; [8]AP-HP, Service de Biochimie et Hormonologie, Hôpital Tenon, Paris, France; [9]Department of Biochemistry and Biomedical Sciences, McMaster University, Hamilton, Ontario, Canada; [10]Department of Medicine, Acute Lung Injury Center of Excellence, University of Pittsburgh, Pittsburgh, PA, USA; [11]Medical Specialty Service Line, Veterans Affairs Pittsburgh Healthcare System, Pittsburgh, PA, USA and [12]Department of Critical Care Medicine, University of Pittsburgh, Pittsburgh, PA, USA

*Corresponding author: VE Kagan, Department of Environmental and Occupational Health, Center for Free Radical and Antioxidant Health, University of Pittsburgh, Bridgeside Point, 100 Technology Drive, Suite 350, Pittsburgh, PA 15219, USA. Tel: 412 624 9474; Fax: 412 624 9361; E-mail: Kagan@pitt.edu

or H Bayır, Department of Critical Care Medicine, University of Pittsburgh, 3434 Fifth Ave, Pittsburgh, PA 15260, USA. Tel: 412 692 5164; Fax: 412 324 0943; E-mail: hub22@pitt.edu

or U Schlattner, University Grenoble Alpes—UJF, Laboratory of Fundamental and Applied Bioenergetics (LBFA), and SFR Environmental and Systems Biology (BEeSy), U1055; BP 53, Grenoble cedex 9, F-38041, France. Tel: +33 476 51 46 71; Fax: +33 476 51 42 18; E-mail: uwe.schlattner@ujf-grenoble.fr

Abbreviations: ATG, autophagy-related gene-related; CCCP, carbonyl cyanide *m*-chlorophenylhydrazone; CL, cardiolipin; CLS, cardiolipin synthase; cyt c, cytochrome c; IMM, inner mitochondrial membrane; LC-MS, liquid chromatography–mass spectrometry; LC3, microtubule-associated protein 1A/1B-light chain 3; LIR, LC3-interacting region; mFAP, mitochondrial-targeted fluorogen-activating protein; MLE, mouse lung epithelial; NDPK-D, nucleoside diphosphate kinase D; 6-OHDA, 6-hydroxydopamine; OMM, outer mitochondrial membrane; OPA1, optic atrophy 1; ROT, rotenone; PG, phosphatidylglycerol; PLA, proximity ligation assay; PLA_2, phospholipase A_2; PMI, p62-mediated mitophagy inducer

Received 05.5.15; revised 11.10.15; accepted 19.11.15; Edited by M Piacentini

damaged mitochondria. However, the protein machinery responsible for CL externalization remained enigmatic. As the majority of CL, synthesized by cardiolipin synthase 1 (CLS-1), are normally confined to the inner leaflet of the inner mitochondrial membrane (IMM), three translocations are required for CL exposure on the mitochondrial outer surface. Our previous work demonstrated that an intermembrane space hexameric protein, NDPK-D (also called NM23-H4 and encoded by the *NME4* gene), can bind CL and facilitate its redistribution to the OMM.[7,8] Here, we tested the hypothesis that NDPK-D regulates the elimination of mitochondria via autophagy, thus acting as a mechanism of mitochondrial quality control.

Results

To explore the role of NDPK-D in mitophagy-associated CL redistribution we assessed the amounts of CLs externalized to the surface of mitochondria in response to a standard model of carbonyl cyanide *m*-chlorophenylhydrazone (CCCP) – induced mitophagy in two different cell lines – MLE (mouse lung epithelial), and HeLa – in which we manipulated the content of the wild-type (w/t) NDPK-D or mutated protein.[9]

Depolarization of mitochondria by the protonophoric uncoupler, CCCP (Figure 1a), activated autophagy in MLE cells, resulting in dose- and time-dependent conversion of LC3-I into LC-3-II (Figure 1b). The activation of the autophagic machinery was accompanied by the appearance of mitochondria in the lysosomal compartment, as detected by the co-localization of mitochondrial-targeted fluorogen-activating protein (mFAP) with LysoTracker Red-labeled lysosomes (Figure 1c). Further evidence for mitophagic clearance of depolarized mitochondria was obtained by western blotting of three mitochondrial marker proteins (Supplementary Figure 1a). The OMM protein TOM40, the IMM protein TIM23, and the matrix protein MnSOD showed decreased levels after treatment with CCCP (Supplementary Figure 1a).

To evaluate the role of CL in CCCP-induced clearance of damaged mitochondria, we knocked down CLS-1, the enzyme catalyzing the final stage of CL biosynthesis from phosphatidylglycerol precursors.[10] RNAi against CLS-1 caused a >2.5-fold decrease in the content of the CLS-1 in MLE cells (Supplementary Figure 1b) associated with a previously demonstrated robust decrease of CL levels.[11] This led to marked inhibition of CCCP-induced mitophagy as assessed by the loss of mitochondrial proteins (Supplementary Figure 1).

Most importantly, CCCP caused NDPK-D-dependent externalization of CL to the mitochondrial surface. We used two independent methods to detect and quantify the appearance of CL on the mitochondrial surface. In the first approach, we took advantage of the well-known lack of phosphatidylserine in mitochondria[12] and used Annexin V-FITC to monitor the content of accessible CL on the surface.[6] Mitochondria from MLE cells treated with CCCP responded with a ~ 2.5-fold increase in the fluorescence of Annexin V-FITC (Figure 2a). Notably, this response was dependent upon NDPK-D, as it was much reduced in MLE cells treated with NDPK-D RNAi (Figure 2a and b).

To more directly characterize CL externalization, we performed liquid chromatography–mass spectrometry (LC-MS) characterization of CL in the OMM and IMM isolated from mitochondria of control cells and cells exposed to CCCP (Figure 2c). The content of CL in the OMM was increased almost sixfold in response to CCCP without any significant changes in the CL molecular speciation (Table 1). To estimate the amounts of CL exposed on the outer leaflet of OMM, we performed LC-MS analysis of mono-lyso-CLs generated by phospholipase A_2 (PLA_2) treatment of control and CCCP-depolarized mitochondria (Figure 2d and e). CCCP exposure increased the content of mono-lyso-CLs after PLA_2 treatment by almost twofold (~3 mol% *versus* ~1.5 mol%) (300 *versus* 575 pmol/mg protein, $P<0.05$, Figure 2d). Analysis of LC-MS spectra did not reveal the appearance of new molecular species of mono-lyso-CL after the exposure to CCCP. This is consistent with redistribution of existing CL species caused by CCCP (Table 1). Of note, no oxidized CL species were detectable in CCCP-treated MLE cells. The quantity of detectable mono-lyso-CL at the mitochondrial surface was dependent on NDPK-D expression. Knockdown of NDPK-D in MLE cells prevented changes in the level of mono-lyso-CLs after the CCCP exposure (Figure 2d).

Transmission electron microscopy revealed the appearance in CCCP-treated cells of autophagic structures with condensed, partially degraded mitochondria (Supplementary Figure 2). In contrast, in cells with knocked down NDPK-D, the autophagic structures induced by CCCP were devoid of mitochondria.

The delivery of mitochondria into the lysosomal compartment (Figure 1c), combined with the TEM appearance of autophagic structures at different stages of degradation (Supplementary Figure 2), indicated that autophagic maturation was intact. Notably, knocking down of NDPK-D blocked CCCP-induced co-localization of mitochondria with lysosomes (Figure 1c) and degradation of mitochondrial marker proteins (Supplementary Figure 3). To further directly assess for completion of mitophagy, we studied the loss of mitochondria content. By using mFAP, we observed the CCCP-induced loss of mitochondrial volume and increased mitochondrial fragmentation (as assessed by increased sphericity of small mitochondrial fragments) in MLE cells (Supplementary Figure 4). Both of these effects were attenuated by knocking down of NDPK-D.

Combined, these data obtained with MLE cells provide strong evidence that NDPK-D was essential for the translocation of CL to the surface of depolarized mitochondria and for their mitophagic clearance.

To examine whether this pathway of NDPK-D-driven CL externalization and mitophagy of damaged mitochondria could be observed in other cell types, we chose to study Parkin-expressing HeLa cells, one of the most commonly used cell type for the study of depolarization-induced mitophagy.[4,13] HeLa cells constitutively express negligible levels of NDPK-D,[14] which allowed us to introduce either w/t or mutant protein. The R90D mutant is unable to translocate lipids between donor and acceptor bilayer vesicles in general,[15] and it is unable to bind CL and therefore to mediate the translocation of CL from IMM to OMM.[7] We found that w/t but not R90D NDPK-D facilitated CCCP-induced translocation of CL from the IMM to the mitochondrial surface in Parkin-HeLa cells. This was estimated by using either the Annexin V-FITC externalization

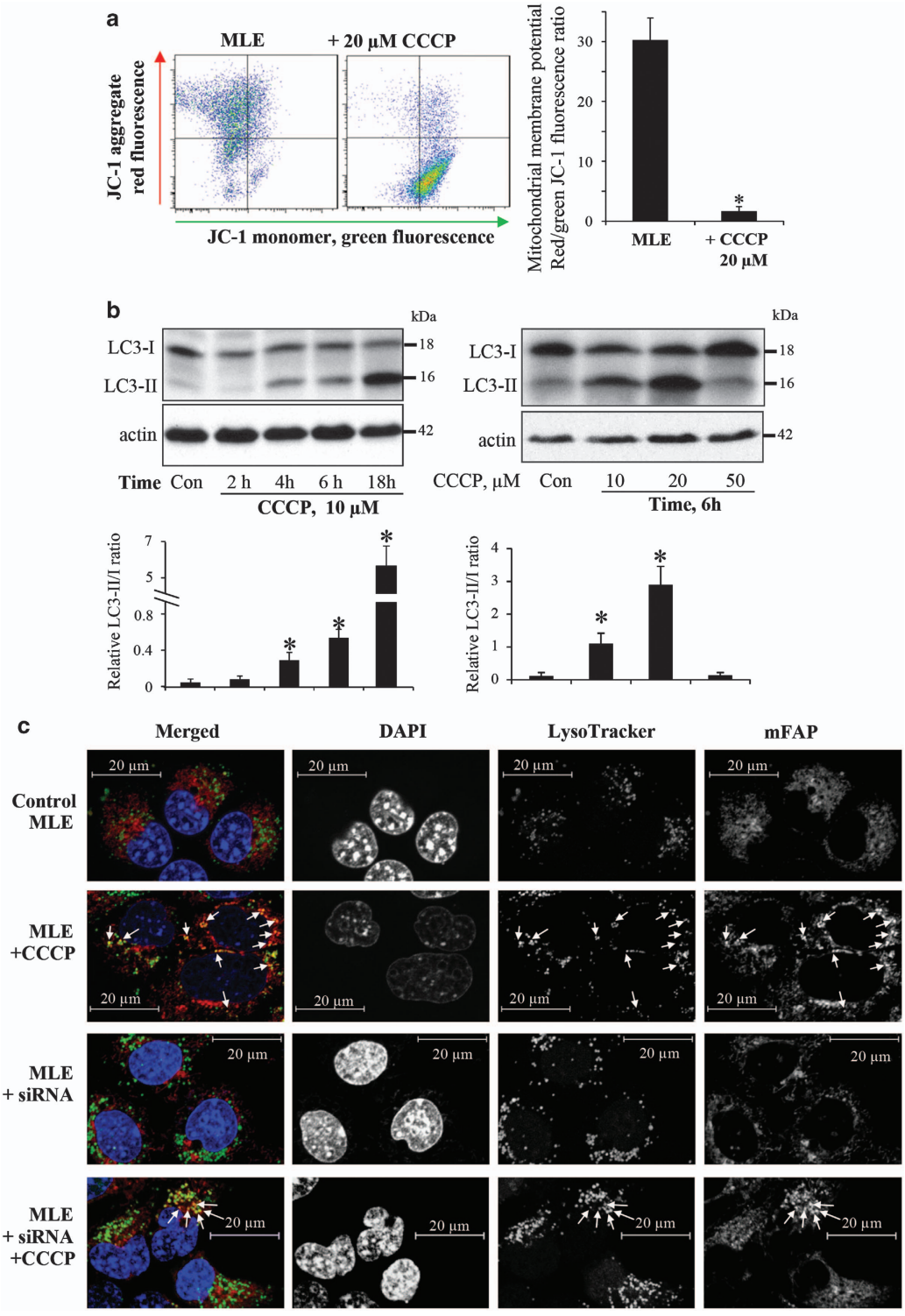

Figure 1 Characterization of CCCP-induced damage of mitochondria and mitophagy in mouse lung epithelial cells. (**a**) Membrane potential in CCCP-treated MLE cells (20 μM/30 min) determined by JC-1 using flow cytometry ($n=3$). (**b**) Dose- and time-dependent CCCP-induced conversion of LC3-I to LC3-II using western blot analysis. Cells were treated with 10 μM CCCP for indicated time (2, 4, 6, and 18 h, left panel), or cells were treated with different concentrations (10, 20, and 50 μM, right panel) of CCCP for 6 h. The histograms under the blots show the LC3-I/II ratio calculated based on densitometry ($n=3$). (**c**) Representative immunofluorescence imaging of mitochondria (mFAP) and lysosomes (LysoTracker Red) showing co-localization (arrows), scale bar is 20 μm. *$P<0.05$ *versus* control cells without CCCP treatment

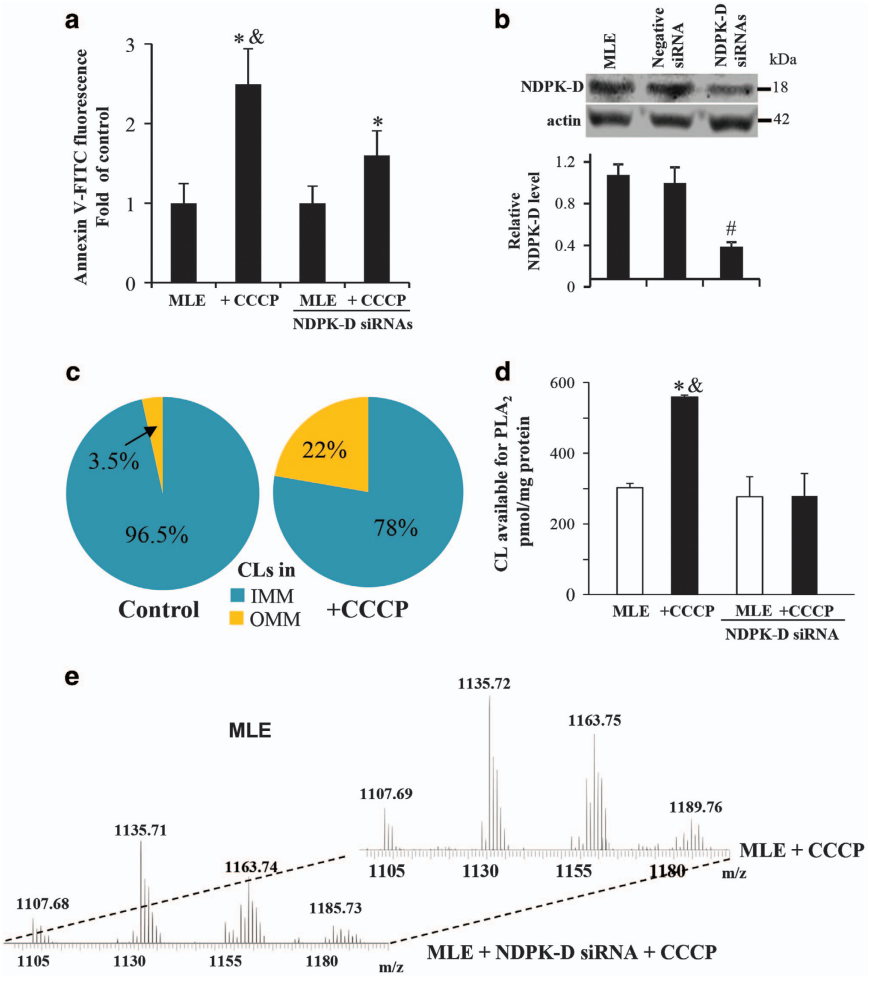

Figure 2 CCCP induces externalization of cardiolipin in MLE cells. (**a**) Evaluation of CL in the outer leaflet of OMM using Annexin V-binding assay in w/t and NDPK-D RNAi MLE cells. Cells were treated with 20 μM CCCP for 1 h. Isolated mitochondria were incubated with FITC-labeled Annexin V to stain surface-exposed CL (anionic phospholipids) and then subjected to flow cytometric analysis (FACSCanto, Becton-Dickinson). (**b**) Knockdown of NDPK-D using siRNA interference in MLE cells. As controls, cells were mock transfected or transfected with non-targeted negative siRNAs. Expression of NDPK-D was evaluated by western blotting. Lower panel shows the relative NDPK-D expression calculated based on densitometry ($n=3$). (**c**) LC-MS analysis-based relative contents of CL in OMM and IMM in control and CCCP-treated MLE cells are presented. (**d**) Evaluation of CL in the outer leaflet of OMM in w/t and NDPK-D knocked down MLE cells using PLA_2 treatment with subsequent assay of mono-lyso-CL by LC-MS analysis. (**e**) Representative MS spectra of mono-lyso CL from MLE cells with normal expression of endogenous NDPK-D or after treatment with NDPK-D siRNAs. $^{*}P<0.05$ *versus* control cells without CCCP treatment. $^{\#}P<0.05$ *versus* cells transfected with non-targeting negative siRNAs. $^{\&}P<0.05$ *versus* MLE cells transfected with NDPK-D siRNAs under the same condition (20 μM CCCP/1 h)

assay (Figure 3a) or LC-MS-based quantitation of mono-lyso-CLs generated by hydrolysis of molecular species of CL accessible to externally added PLA_2 (Figure 3b). In both cases, robust externalization of CL on depolarized mitochondria was detected in cells transfected with w/t NDPK-D, but not with the R90D mutant. In agreement with the important role of NDPK-D in translocating and externalizing CL as a mitophageal signal, the effectiveness of mitochondrial elimination – as documented by the loss of the mitochondrial marker proteins by western blotting (Figure 4) – the loss of mitochondrial volume, and increased mitochondrial fragmentation assessed using mFAP-infected cells (Figure 5 and Supplementary Figure 6) required w/t NDPK-D. The mitochondrial network is filamentous in HeLa cells expressing w/t NDPK-D. After treatment with CCCP, the mitochondrial filamentous network was disrupted. In addition, the LC3 labeling, mainly as puncta, was significantly increased as compared with control cells without CCCP treatment. Several yellow spots – indicative of LC3 and mitochondria co-localization – were also noticeable. By sharp contrast, only a slight increase in LC3 labeling was observed in HeLa cells expressing R90D mutant (Supplementary Figure 7).

To evaluate if NDPK-D could regulate the Parkin translocation to mitochondrial compartment after mitochondrial damage, we performed experiments in which we examined the effects of NDPK-D and its R90D mutant on Parkin translocation in CCCP-treated HeLa cells. Parkin-expressing cells were transiently transfected with vectors expressing w/t NDPK-D or R90D mutant. Studies of the time course showed that Parkin translocation was much faster in w/t NDPK-D transfected cells than in R90D transfected cells (Supplementary Figure 8a). In a different cell line, SH-SY5Y

cells, assessments of translocated Parkin using fluorescence imaging of the protein demonstrated that the percentage of w/t SH-SY5Y cells with translocated Parkin after CCCP treatment was significantly decreased in cells transfected with siRNA against NDPK-D (Supplementary Figure 8b).

Although most studies of mitophagy mechanisms have used CCCP, it has become clear that mitophagy can also be induced by stimuli causing lesser degrees of depolarization (such as rotenone, ROT) or even in the absence of depolarization (PMI, P62-mediated mitophagy inducer).[16] We thus examined other pharmacological inducers (ROT and 6-hydroxy-dopamine, 6-OHDA) of mitophagy that do not cause severe depolarization. We found that knocking down of NDPK-D using siRNAs significantly attenuated ROT and 6-OHDA-induced mitophagy in SH-SY5Y cells (Supplementary Figure 9). A robust mitophagy triggered by ROT treatment of w/t SH-SY5Y cells was less apparent in the NDPK-D-deficient cells (compare merged images in rows 3 and 4, Supplementary Figure 9a). Similarly, a greater level of mitophagy was observed in w/t SH-SY5Y cells *versus* NDPK-D-deficient cells upon treatment with 6-OHDA (compare merged images in rows 5 and 6, Supplementary Figure 8a). Quantitative analysis of the images clearly demonstrated weakening of the mitophageal responses to either ROT or 6-OHDA in NDPK-depleted cells as compared with w/t SH-SY5Y cells (Supplementary Figure 9b). In line with these imaging results, western blot analysis revealed less robust degradation of IMM marker proteins (ATP5a, UQCRC2, and COX-IV) in w/t SH-SY5Y cells depleted for NDPK-D (Supplementary Figure 9c).

To further diversify the spectrum of stimulants and type of cells undergoing mitophageal responses, we employed *Saccharomyces cerevisae* yeast cells in which mitophagy can be triggered by switching the cells from synthetic complete (SC) medium to synthetic medium containing a non-fermentable carbon source and depleted of essential nutrients.[17] To detect mitophagy, we used an isocitrate dehydrogenase (Idh1)-GFP processing assay.[18] Wild-type cells and cells deleted for yeast nucleoside diphosphate kinase Ndk1/Ynk1 (*ndk1Δ*) also localizing to mitochondria were pre-cultured in SC medium and then transferred to synthetic lactate medium to induce mitophagy.[19] During mitophagy, mitochondria, along with Idh1-GFP, are delivered into the vacuole for degradation. Idh1 is proteolytically removed or degraded, whereas the GFP moiety is relatively stable and accumulates in the vacuole. After 6–7 h, cells were harvested and analyzed for release of free GFP, indicative of mitophagy.[18–24] The free GFP band was apparent beginning at 6 h after induction of mitophagy in w/t cells, and was markedly decreased in *ndk1Δ* cells, indicating the impaired

Table 1 Molecular species of CL in the outer mitochondrial membrane

(M-H)$^-$ m/z	Identified acyl chains	Molecular species
1344	C16:1/C16:1/C16:1/C16:1	64:4
1346	C16:1/C16:1/C16:1/C16:0	64:3
1346	C16:1/C16:1/C14:0/C18:1	64:3
1370	C16:1/C16:1/C16:1/C18:2	66:5
1372	C16:1/C16:1/C16:0/C18:2	66:4
1372	C16:1/C16:1/C16:1/C18:1	66:4
1374	C16:1/C16:1/C16:0/C18:1	66:3
1376	C16:1/C16:0/C16:0/C18:1	66:2
1386	C16:1/C17:1/C16:1/C18:1	67:4
1396	C16:1/C18:2/C16:1/C18:2	68:6
1398	C16:1/C16:1/C18:1/C18:2	68:5
1400	C16:1/C18:1/C16:1/C18:1	68:4
1402	C16:1/C18:1/C16:0/C18:1	68:3
1404	C16:0/C18:1/C16:0/C18:1	68:2
1404	C16:0/C16:0/C18:1/C18:1	68:2
1414	C16:1/C18:1/C17:1/C18:1	69:4
1424	C16:1/C18:1/C18:2/C18:2	70:6
1426	C16:1/C18:1/C18:1/C18:2	70:5
1428	C16:1/C18:1/C18:1/C18:1	70:4
1430	C16:0/C18:1/C18:1/C18:1	70:3
1432	C16:0/C18:1/C18:1/C18:0	70:2
1448	C18:2/C18:2/C18:2/C18:2	72:8
1450	C18:2/C18:2/C18:1/C18:2	72:7
1452	C18:1/C18:2/C18:1/C18:2	72:6
1454	C18:1/C18:2/C18:1/C18:1	72:5
1456	C18:1/C18:1/C18:1/C18:1	72:4

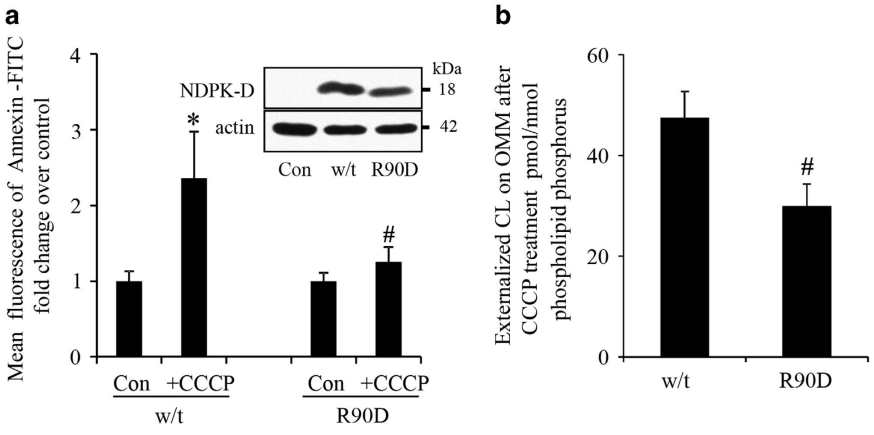

Figure 3 Characterization of CCCP-induced cardiolipin externalization in HeLa cells transfected with wild-type or R90D mutant of NDPK-D. (**a**) HeLa cells were transiently transfected with vectors expressing w/t or R90D NDPK-D for 48 h followed by treatment with 20 μM CCCP for 4 h. Crude mitochondria were isolated for determination of CL externalization using Annexin V-binding ($n=3$). Insert: representative western blots of NDPK-D expression in HeLa cells. (**b**) LC-MS-based relative amounts of CL in OMM and IMM in HeLa cells expressing w/t NDPK-D and R90D mutant. Data are means $\pm$ S.D., $n=3$. *$P<0.05$ compared with cells without CCCP treatment, $^{\#}P<0.05$ compared with cells expressing w/t NDPK-D under the same conditions (20 μM CCCP/4 h)

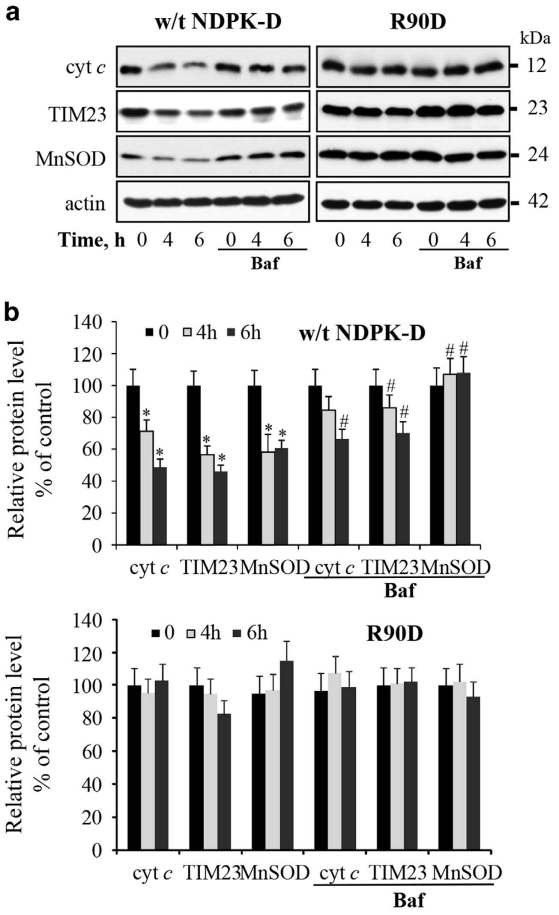

Figure 4 Characterization of CCCP-induced mitophagy in HeLa cells. After treatment of cells with 20 μM CCCP for the indicated times, CCCP-induced degradation of mitochondrial marker proteins (cyt *c*, Tim23, and MnSOD) were determined by western blotting (**a**). Autophagy inhibitor, bafilomycin A1 (baf), was added to cells 2 h prior to harvesting. The panel (**b**) shows the densitometry analysis. Data are means $\pm$ S.D. ($n=3$). $^{*}P<0.05$ compared with 0 h, $^{\#}P<0.05$ compared with 4 h and 6 h CCCP without bafilomycin A1 treatment

mitophagy in the latter (Supplementary Figure 10). These findings suggest that Ndk1/Ynk1 is an important contributor to the elimination of mitochondria induced by starvation of yeast cells.

It is not known so far how NDPK-D adapts to its different functions. We recently showed that the dynamin-like GTPase OPA1 forms complexes with NDPK-D, both proteins bound to the CL-rich IMM, and that in this topology OPA1 is directly fueled with GTP by the kinase.[16] Earlier, we observed that NDPK-D that cross-links IMM and OMM, a topology that is able to support CL transfer, is kinase inactive,[7] suggesting that this is an uncomplexed form of the kinase. Thus, formation of OPA1/NDPK-D complexes may interfere with CL translocation. In a PLA (Figure 6a and c) only HeLa cells expressing CL-binding and principally CL-transfer competent NDPK-D proteins, i.e., w/t or the kinase-inactive H151N mutant, were found associated with OPA1, but not the CL-binding and CL-transfer-deficient R90D mutant. We then partially silenced OPA1 by siRNA to study its consequences on CCCP-induced CL transfer in NDPK-D w/t and R90D mutant HeLa cell by the Annexin V-FITC externalization assay (Figure 6d and e). OPA1 was silenced only partially (to ~60%) to observe mild phenotypes, as stronger OPA1 knockdown would itself induce mitophagy and apoptosis, independent of CCCP.[25–27] The data confirm that expression of w/t NDPK-D increases CCCP-induced CL externalization. This increase occurred under both conditions, control and OPA1 silenced, but was more statistically significant ($P<0.01$ *versus* 0.05) in OPA1-silenced cells. Such an increase was not observed in cells expressing the R90D mutant; rather, OPA1 silencing led to a decrease in externalized CL. A significant effect of partial OPA1 silencing was observed when comparing between the CCCP-treated cells expressing NDPK-D w/t or R90D mutant. In this comparison, CL externalization is more increased in the OPA1-silenced background (1.65 ± 0.24 fold) as compared with the control background (1.38 ± 0.01 fold), and this was statistically significant ($P<0.01$).

Discussion

This work demonstrates, for the first time, that NDPK-D (NM23-H4) is essential for the externalization of CL, having a key mechanistic role in regulating the appearance of this 'eat-me' signal on the mitochondrial surface thus labeling depolarized organelles destined for mitophagy.

The highly asymmetric distribution of CL between the IMM and OMM in normal, uninjured mitochondria whereby 96.5 mol % of it is confined to the IMM, creates a gradient poised to respond to changes in organelle homeostasis. Based on LC-MS assessments, this asymmetry is disturbed during depolarization, resulting in a robust CL enrichment of the OMM that is dependent upon the ability of NDPK-D to mediate its redistribution from IMM to OMM. Although the OMM content of CL is approximately doubled, this still represents only a small fraction of total cellular CL. These quantitative assessments point to the high sensitivity of the autophagic machinery to externalized CLs. The surprisingly small percentage of CL translocated between the IMM and mitochondrial surface should be considered in the context of the available pool of 'free' CLs as compared with its total abundance in the IMM. Indeed, over the last decade, extensive studies have identified multiple proteins engaged in functionally meaningful interactions with CLs. Many IMM proteins have CL-binding domains, thus limiting free exchange and redistribution of the phospholipid to the OMM.[28–36] In some of these proteins, CL molecules are buried 'deeply' within multimeric protein complexes (like in electron-transporting respirasomes[35,36]), whereas in the others the affinity and accessibility of CL for translocations seem to be less restricted (e.g., TIM40[37]). Although the exact amounts of CL in the two pools – free *versus* bound – have not been established, it is likely that in normally functioning mitochondria, the majority of the IMM CLs is not readily mobilized. This is compatible with the high sensitivity of mitophagy to decreased CLS-1 expression and the lowered total CL levels in mitochondria. The observed redistribution of CLs in depolarized mitochondria suggests that this balance is changed favoring interactions of CL with NDPK-D, resulting in translocation to the OMM. This NDPK-D-driven mechanism is engaged in CL externalization and execution of mitophagy in neuronal cells mitochondria damaged by ROT or 6-OHDA.[6]

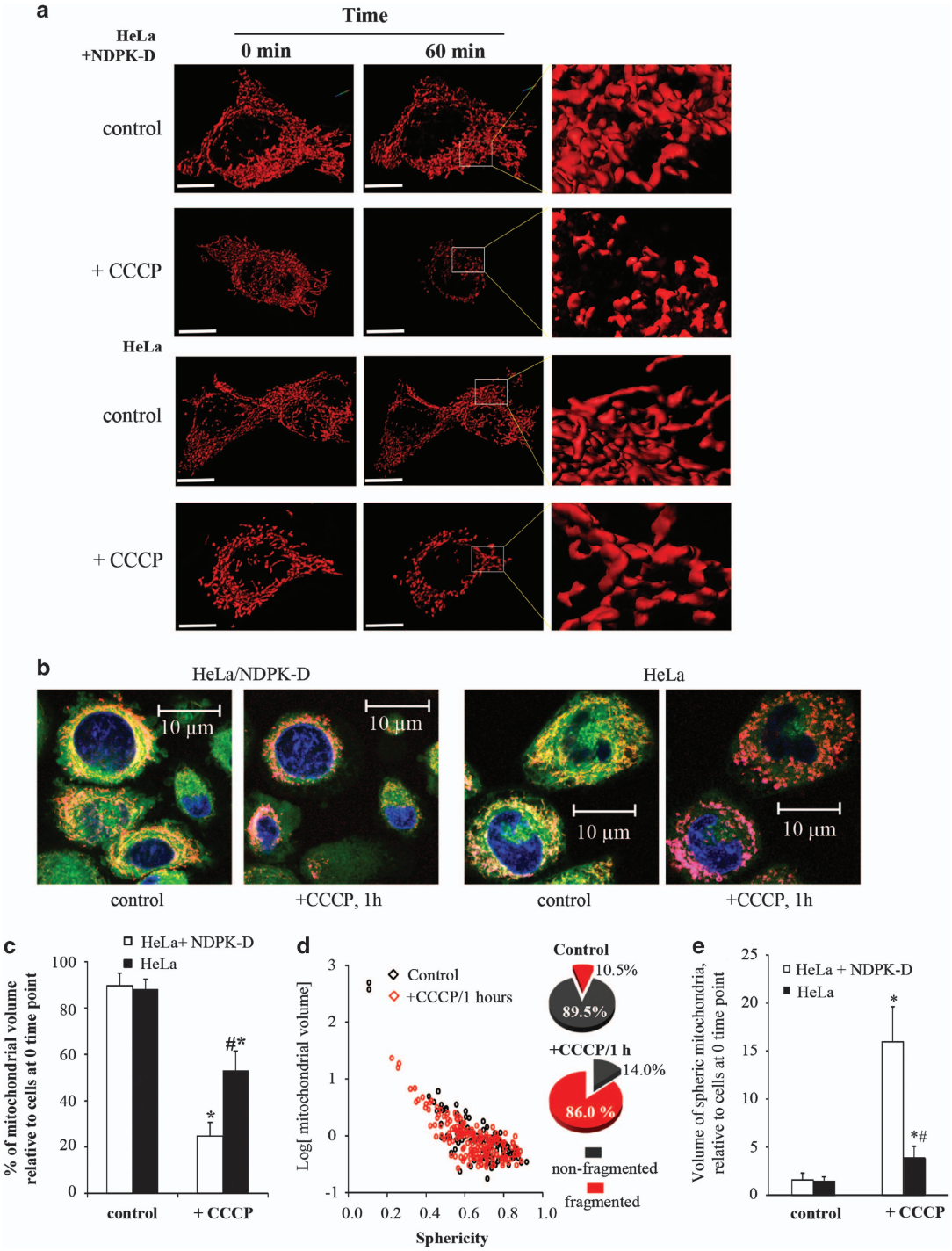

Figure 5 CCCP-induced mitochondrial volume change and fragmentation in NDPK-D-manipulated HeLa cells. (**a**) Representative images of 3D surface reconstructions using Imaris 8 software. Control HeLa cells or cells transfected with NPDK-D were infected with adenovirus expressing mCerulean/FAP. After addition of CCCP, control or NDPK-D-expressing cells were subjected to multi-position time-lapse imaging for 60 min with 5-min intervals, with a collection of z-stacks for each position, using a Nikon T1 microscope. Images were deconvolved using the 3D Landwebser deconvolution capabilities of Nikon Elements and imported into Imaris software. Mitochondrial volume, surface area, and sphericity were calculated using Imaris software. Scale bar is 20 μm. (**b**) Representative high-resolution confocal imaging of mitochondria in CCCP-treated control HeLa cells or cells transfected with w/t NDPK-D. (**c**) Wild-type NDPK-D facilitated CCCP-induced mitochondrial volume loss in Parkin-HeLa cells. The relative mitochondrial volume in HeLa cells after 1 h incubation with CCCP was calculated as the percentage of initial mitochondrial volume at the first time point ($n=6$–8 images). (**d**) Mitochondrial fragmentation in HeLa cells was assessed using sphericity parameter for small mitochondrial fragments (with an arbitrary threshold of sphericity <0.4) to differentiate the fragmented mitochondria and plotted against log (mitochondrial volume). Dot plots shown are representative of NDPK-D-expressing HeLa cells before and after (1 h) addition of CCCP. The inserted pie plots show the percentage of fragmented and non-fragmented mitochondrial volume. (**e**) The ratio of the volume of spheric (fragmented) mitochondria *versus* non-fragmented mitochondria in HeLa cells was calculated and compared with the ratio at the initial time point ($n=6$–8). $^{*,\#}P<0.05$ *versus* HeLa cells without CCCP treatment, or HeLa cells with NDPK-D under the same condition (20 μM CCCP/1 h), respectively ($n=6$–8)

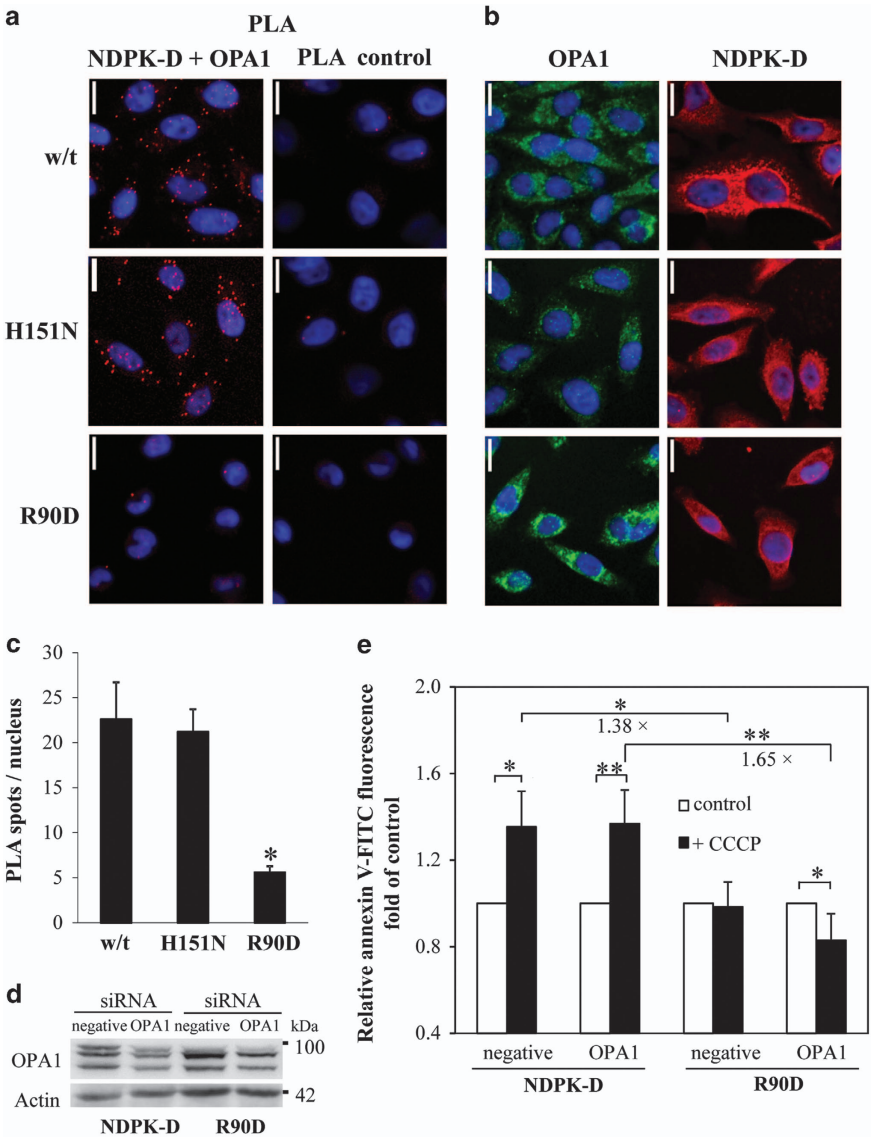

Figure 6 Association of OPA1 with NDPK-D in HeLa cells. (**a**–**c**) OPA1/NDPK-D interaction evidence by proximity ligation assay (PLA) in HeLa cells stably expressing w/t NDPK-D, kinase-inactive H151N mutant (H151N), or CL-transfer-deficient R90D mutant (R90D). Representative magnifications of confocal pictures are given, scale bar is 16 μm. (**a**) Left panel: PLA with NDPK-D and OPA1 primary antibodies; right panel: control PLA without primary antibodies. (**b**) Control immunofluorescence studies showing expression of NDPK-D (right panel) and OPA1 (left panel) as detected by the same NDPK-D and OPA1 primary antibodies. (**c**) Quantification of PLA as shown in **a** from three experiments, two quantifications each ($n=6$), $^*P<0.01$ *versus* HeLa cells expressing w/t NDPK-D. (**d**, **e**) Effect of partial OPA1 silencing on CL externalization. Representative immunoblot of partial OPA1 silencing in HeLa cells expressing w/t NDPK-D and R90D mutant using siRNA. HeLa cells permanently transfected with w/t NDPK-D or R90D mutant were transfected with negative or siRNA against OPA1. (**e**) Surface assessable CL was quantified by an Annexin V-binding assay. MitoTracker-positive particles of appropriate size were analyzed for FITC fluorescence by FACS. Data are means ± S.D. ($n=3$–4); $^*P<0.05$; $^{**}P<0.01$. Numbers indicate the fold-difference between CCCP-treated R90D- and w/t NDPK-D-expressing cells, either on a control (1.38-fold) or partial OPA1-silenced background (1.65-fold).

NDPK-D-dependent CL externalization is also accountable for the pro-mitophageal stimulation by protonophoric uncouplers such as CCCP, leading to the complete depolarization of mitochondria in pulmonary epithelial cells and cervical carcinoma cells. Interestingly, we found that yeast Ndk1/Ynk1 acts as an important contributor to the elimination of mitochondria induced by starvation of yeast cells. Notably, *S. cerevisiae* Ndk1/Ynk1 is highly homologous to other eukaryotic NDPKs, including *Homo sapiens.* It also forms a homo-hexamer and a fraction of it is localized to the mitochondrial intermembrane space.[38,39] Genetic studies demonstrated the suppressed mitophagy in CLS null mutant deficient in CL synthesis (Shen and Greenberg, unpublished). Combined with our results on impaired mitophagy in *ndk1Δ* mutant, these data are compatible with the CL-dependent mitophagy in *S. cerevisiae*.

The mechanisms of the NDPK-D-driven CL translocation process are not fully deciphered. According to one of the proposed models, the hexameric NDPK-D complex acts as a rotary nano-device, whereby the binding of negatively charged phosphate groups of CL with the positively charged R90-contaning domain triggers structural re-arrangements

that places the nano-machine in motion.[7] The very low levels of CL in the OMM are conducive for the dissociation of the complex and release of CL. Indeed, CL-induced conformational changes of NDPK-D, which result in the suppression of its kinase activity and facilitation of its lipid transfer activity, have been reported.[7] Although this hypothetical mechanism may serve as a plausible explanation for the transfer of CL between the outer monolayer of the IMM and the inner leaflet of the OMM, two additional steps – translocation within the IMM and OMM – are required for the appearance of CL on the mitochondrial surface. Although we previously reported that knockdown of phospholipid scramblase 3 inhibits mitophagy, it is currently unclear whether this enzyme may act at the IMM, the OMM, or both.[6]

Within the time frame of the current experiments, we did not detect CL oxidation during exposure of MLE or HeLa cells to CCCP. As CL translocation in some contexts may be associated with the interactions of CL with the intermembrane hemoprotein cytochrome c – known to yield a complex with peroxidase activity[40] – one may wonder why the oxidation of CL does not take place. It should be noted that the formation of the peroxidase complex is a pre-requisite for CL oxidation, which is dependent on the presence and availability of oxidizing equivalents such as H_2O_2. Given that oxidized CL can be released from mitochondria to participate in apoptosome formation,[40] we speculate that CL oxidation status may modulate the decision between cytoprotective mitophagy and stimulation of mitochondrial death pathways.

Given that NDPK-D has two major functions, phosphorylating nucleoside diphosphates and facilitating externalization of CL, its regulation, particularly in the context of switching from the kinase to the translocase activity of the protein complex, deserves further studies. *In vitro*, the kinase complex shows intermembrane lipid transfer activity as soon as it can simultaneously bind to two membranes containing some CL.[15] However, NDPK-D interacts not only with CL,[14] but also with OPA1,[7] a dynamin-like GTPase. OPA1, beyond its classical role in inner membrane fusion,[41,42] is also directly implicated in mitochondrial quality control via its stress-regulated proteolytic cleavage via OMA1.[25,26,43] In functional mitochondria, OPA1/NDPK-D interaction helps to fuel OPA1 with GTP,[44] but this topology has to be different from the one where NDPK-D is cross-linking the two mitochondrial membranes, which is kinase inactive.[7] Thus, OPA1/NDPK-D complex formation may have a role in determining NDPK-D function, and two pieces of evidence in HeLa cells support this idea. First, only CL-transfer competent NDPK-D proteins also show OPA1 association, not the R90D mutant. Second, more CL is transferred in an OPA1-reduced background as compared with a control background when comparing NDPK-D w/t with R90D after CCCP treatment. This suggests a negative effect of OPA1 on NDPK-D-facilitated CL transfer. Lower OPA1 levels, by reducing OPA1/NDPK-D complexes, could liberate non-complexed NDPK-D that would engage into the well-documented cross-linking of IMM and OMM as required for CL transfer. However, exact delineation of the role of OPA1 for NDPK-D functions will require further molecular analysis of the OPA1/NDPK-D interaction.

Among several quality-control mechanisms in yeast and mammalian cells, mitophagy has recently attracted much attention.[45] Most mitophagy studies in mammalian cells have focused on the use of depolarizing agents in triggering the Parkin/Pink1-mediated pathway.[46] Increasing evidence, however, supports the notion that mitophagy can also occur independently of Parkin/Pink1.[47–51] The initial report showing that selective mitophagy occurs in PINK1-deficient neuroblastoma cells[51] was followed by studies showing that Parkin may be recruited through PINK1-independent mechanisms both *in vitro* and *in vivo*.[52,53] Pathways independent of both PINK1 and Parkin have also emerged, often involving mitophagy stimuli that cause lesser degrees of or no mitochondrial depolarization.[6,16] Several mitophagy adaptor proteins (NIX, BNIP3, and FUNDC1) are upregulated or post-translationally modified during developmental or hypoxia-induced mitophagy to directly interact with LC3 via a LIR to recruit autophagosomes.[54] AMBRA1, an autophagy-related gene-related protein, has been also shown to bind directly with LC3 via its LIR and to induce LC3-dependent, but Parkin and p62-independent mitophagy.[55] Likewise, externalized CL is capable of directly binding LC3 during mitophagy.[6] In addition, Parkin-independent mitophagy can be triggered by PMI, which upregulates p62 transcriptionally to facilitate p62-LC3 interactions. As p62 is one of the ubiquitin-binding LIR domain adaptors, this suggests the possibility of additional ubiquitin ligases that can label mitochondria for degradation.[16] Indeed, mitochondrial ubiquitination and mitophagy are still observed in Parkin knockout cells.[56] Overall, it is clear that multiple specific molecular pathways exist for targeting damaged or unneeded mitochondria for selective clearance by autophagy. A given stimulus, such as CCCP, can trigger more than one pathway to include the canonical Pink1/Parkin pathway, a vesicular lysosomal-targeting pathway,[57] and the NDPK-D-dependent CL externalization pathway described here. Based on the comparison of the data on the effects of NDPK-D on CL translocation with those illustrating the role of NDPK-D in Parkin translocation, we suggest that these processes may be related to each other. Our results are compatible with the interpretation that CL may facilitate the accumulation of Parkin in mitochondria during mitophagy. Moreover, LC3 itself interacts with multiple mitochondrial surface molecules, either directly as in the case of CL, FUNDC1 or AMBRA, or with various ubiquitinated substrates through LIR adaptors, to affect mitophagy.

In conclusion, we have found that NDPK-D has an important role in the early stages of mitophagy as induced by CCCP as well as by PINK1-Parkin-independent stimuli such as rotenone and 6-OHDA. Given its dual function of producing nucleoside triphosphates and facilitating CL transfer, as well as its close association with Opa1, NDPK-D is capable of functioning as a key integration site to determine appropriate fission–fusion or mitophagy responses. Overall, the current data – along with the previously established role of CL as a recognition signal for mitophagy of damaged mitochondria[6] – identify NDPK-D as an important contributor to the quality control of mitochondrial health.

Materials and Methods

Reagents. CCCP, ROT, 6-OHDA, protease inhibitor cocktail, fetal bovine serum (FBS), and mouse or rabbit actin antibodies were purchased from Sigma (St. Louis, MO, USA). Lipofectamine 2000, Lipofectamine reagent RNAiMax,

CellTracker Green CMFDA, LysoTracker Red DND-99, and MitroTracker Red CMXRos were from Life Technologies (Grand Island, NY, USA). Annexin V-FITC was purchased from Biovision (Milpitas, CA, USA). Mouse NDPK-D siRNAs were from Origene (SR404588, Rockville, MD, USA). Human OPA1 siRNAs were from Eurogentec S.A. (Seraing, Belgium). Mouse anti-cyt *c*, anti-Tim23, and anti-MnSOD antibodies were from BD sciences (San Jose, CA, USA). Mouse-anti-LC3 (5F10) was from Nanotools (Teningen, Germany), and mouse anti-OPA1 antibody from BD Biosciences (Le Pont De Claix, France). The rabbit polyclonal antibody against NDPK-D was obtained as previously described.[14] All other reagents were from Sigma unless stated otherwise.

Cell culture. The murine lung epithelial cell line MLE-12 and human cervical adenocarcinoma cell line HeLa were purchased from American Type Culture Collection (ATCC, Manassas, VA, USA). MLE-12 cells were cultured at 37 °C and 5% CO_2 in DMEM/F-12 medium (ATCC) supplemented with 0.005 mg/ml insulin, 0.01 mg/ml transferrin, 30 nM sodium selenite, 10 nM hydrocortisone, 10 nM beta-estradiol, 2 mM L-glutamine, 10 mM HEPES, and 10% FBS. HeLa cells were maintained in DMEM (Life Technologies) supplemented with 10% FBS.

Transfection. The pcDNA4/TO vectors expressing w/t NDPK-D and R90D mutant were prepared as previously described.[14] HeLa cells were transiently transfected using Lipofectamine 2000 according to the manufacturer's instructions. At 48 h after transfection, cells were collected for further experiments. For knocking down the expression of NDPK-D in MLE cells, cells were transfected with 50 nM (final) siRNAs using RNAiMax. For partial silencing OPA, HeLa cells permanently transfected with w/t NDPK-D or R90D mutant were transfected with 50 nM siRNA against OPA1 using lipofectamine, and experiments were performed 72 h after transfection. As controls, cells were mock transfected or transfected with scrambled negative siRNAs. For measurements of mitochondria volume and fragmentation, MLE cells or HeLa were infected with adenovirus expressing mCerulean/FAP with COX-IV and COX-VIII mitochondrial targeting sequences, respectively.

Fluorescence microscopy. For co-localization assay of mitochondria and lysosomes, cells were grown on Matteck Dishes and transiently transfected with Mito-GFP (Clontech, Mountain View, CA, USA). Forty-eight hours after transfection, cells were treated with 20 μM CCCP for the indicated times. Cells were stained with 200 nM LysoTracker Red 30 min prior to the end point according to the manufacturer's instructions. Images were visualized and captured using a Nikon TI inverted microscope in either widefield or with and A1 scan head (Nikon Inc., Melville, NY, USA).

For determination of mitochondrial volume/fragmentation changes, cells were first infected with adenoviral vector expressing mitochondria directed mCerulean/mFAP prior to treatment. Cells were then incubated with 5 nM malachite green to reveal the transgene prior to imaging (thereby defining the mitochondria[58]) and mounted in a Tokai Hit environmental stage (Tokyo, Japan) in a Nikon TI inverted microscope equipped with a sweptfield confocal head. Three dimensional stacks were collected using a 1.49 NA oil objective with excitation/emission wavelength of 640/700 nm with a Z-space separation of 0.2 micron (20 Z-positions); each stack takes 1 s to collect. Image stacks are collected every 5 min for 60 min. Subsequent to collection images were deconvolved using the 3D Landweber deconvolution capabilities of Nikon Elements. Deconvolved images were imported into Imaris (Bitplane Company, Zurich, Switzerland) and the mitochondrial volume, surface area, and sphericity (defined as the ratio of the surface area of the given object to the surface area of a sphere with the same volume as the given object) were calculated. Imaging conditions included control cells and cells after addition of 20 μM CCCP.

Quantitation of CL levels in mitochondria OMM and IMM. The IMM and OMM fractions were obtained by incubating mitochondria with digitonin.[59] After centrifugation, the pellet and supernatant were collected as IMM and OMM fractions, respectively. The purities of the membrane fractions were examined by western blot analysis of COX-IV and TOM40, and by assaying of marker enzymes. Lipids from OMM and IMM were extracted using the Folch procedure.[60] Lipid phosphorus was determined by a micro-method.[61] CL was analyzed by LC/MS with a Dionex Ultimate 3000 HPLC (using a normal phase column, Luna Silica(2) 100A, 3 μM, 150 × 1 mm, (Phenomenex, Torrance CA, USA) coupled on-line to a linear ion trap LXQ mass spectrometer (ThermoFisher Scientific, San Jose, CA, USA) as previously described.[6] Separation of CL was performed usng gradient solvent A (hexane:propanol:water, 47:57:1, v/v) and solvent B (hexane:propanol:water, 47:57:10, v/v) each containing 5 mM ammonium acetate and 0.01M formic acid. The column was eluted at a flow rate of 0.05 mlmin as follows: 0–3 min, linear gradient, 14.5–37% solvent B; 3–12.5 min, isocratic at 37% solvent B; 12.5–20 min, linear gradient, 37–100% solvent B; 20–45 min, isocratic at 100% solvent B; 45–60 min, isocratic at 14.5% solvent B. The ESI probe was operated at a voltage of 3–5 kV in the negative ion mode. Capillary temperature was maintained at 150 °C. MS/MS analysis was employed to determine the fatty-acid composition of CL species. Tetra-myristoyl-CL (Avanti polar lipids, Alabaster, AL, USA) was used as internal standard.

Assessment of CL externalized to the mitochondrial surface. To assess CL externalized on the outer leaflet of the OMM, mitochondria were treated with PLA_2 from porcine pancreas (0.7 U/mg protein) (Sigma-Aldrich) in mitochondria isolation buffer (210 mM mannitol, 70 mM sucrose, and 5 mM HEPES, pH 7.4) containing 2 mM $CaCl_2$ and 100 μM DTPA for 45 min at 4 °C. To prevent mitochondria damage by CL hydrolysis products, essential-fatty-acid-free human serum albumin (20 mg/ml) was added to the incubation medium. At the end of incubation, lipids were extracted using the Folch procedure.[60] Mono-lyso-CL formed in PLA_2-driven reaction was analyzed by LC/MS using a Dionex Ultimate 3000 HPLC coupled on-line to a Q-Exactive hybrid quadrupole-orbitrap mass spectrometer (ThermoFisher Scientific) as previously described.[62] Mono-lyso-CLs were separated on a normal phase column (Silica Luna 3 μm, 100 A, 150 × 2 mm, Phenomenex) with flow rate 0.2 ml/min using gradient solvents containing 5 mM CH_3COONH_4 (A – *n*-hexane:2-propanol:water, 43:57:1 (v/v/v) and B – *n*-hexane:2-propanol:water, 43:57:10 (v/v/v). Mono-lyso-CL (tri-myristoyl-lyso-CL) was prepared from tetra-myristoyl-CL (Avanti polar lipids) by PLA_2 hydrolysis and used as internal standard.

Annexin V-binding assay using flow cytometry. The relative CL amount on the surface of the outer leaflet of the OMM was also evaluated using the newly developed Annexin V-binding assay.[6] Cells were stained with 250 nM Mitotracker Red CMXRos (Life Technologies) for 30 min at 37 °C to label mitochondria prior to harvesting. Isolated crude mitochondria were incubated with FITC-labeled Annexin V (Biovision) to stain for anionic phospholipids and then subjected to flow cytometric analysis (FACSCanto, BD, Rutherford, NJ or FACS Fortessa SORP1P, BD, Le Pont de Claix, France) of the green FITC fluorescence. Mitochondrial analysis was performed after appropriate settings of the forward light scatter and side light scatter detectors. The FITC fluorescence from gated red fluorescent mitochondria events was determined to evaluate the binding of Annexin V to mitochondria. Data presented are the relative FITC fluorescence intensity compared with that of mitochondria isolated from non-treated cells.

Western blotting. The harvested cells were lysed on ice for 10 min using RIPA buffer (20 mM Tris-HCl, pH 7.5, 150 mM NaCl, 1 mM EDTA, 1% Nonidet P-40, 1% sodium deoxycholate) supplemented with protease inhibitors (Sigma), the lysates were then centrifuged at 5000 × *g* for 5 min. The resulting supernatants (30 μg protein) were resolved on 12% SDS-PAGE, and transferred to a nitrocellulose membrane. Immuno-blotting was performed as per the antibody manufacturer's details.

***In situ* proximity ligation assay.** *In situ* PLA was performed using a Duolink kit (Olink Bioscience, Uppsala, Sweden) as previously described.[63] Cells grown on chamber microscopy slides were fixed with 3% cold paraformaldehyde, permeabilized with 0.2% Triton X-100 in PBS, blocked with a Duolink blocking agent and then incubated with primary antibodies (mouse anti-OPA1, BD Biosciences and rabbit anti NDPK-D produced and characterized as described earlier[9]). PLA probes (secondary antibodies tagged with DNA oligonucleotides) were then added. Hybridization, ligation, amplification, and detection using Duolink Detection Reagents Red (excitation 594 nm, emission 624 nm) were realized according to the manufacturer's protocol. In brief, secondary antibodies were incubated in preheated humidity chamber for 1 h at 37 °C. Ligation was performed with a ligase-containing solution for 30 min at 37 °C. Finally, amplification step was performed with a polymerase-containing solution for 1 h 40 min at 37 °C. Nuclei were stained with Hoechst 33258. In parallel, expression of OPA1 and NDPK-D was analyzed using the same NDPK-D and OPA1 primary antibodies and standard immuno-fluorescence procedure (with Alexa Fluor 488- and Cy5-conjugated secondary IgGs). Images were collected with a Leica TCS SP2 AOBS inverted laser scanning confocal microscope using a × 63 oil immersion objective. Laser excitation was 351–364 nm for Hoechst 33258, 488 nm for Alexa 488, 543 nm for PLA, and 633 nm for Cy5. Fluorescence emissions adjusted with AOBS were 480 nm for Hoechst 33258, 500–535 nm for Alexa488, and 565–600 nm for PLA and 645–685

for Cy5. Experiments were performed on a randomly chosen field containing 15–25 cells. The background noise autofluorescence was removed by fine filter (Kernel 3×3) using Volocity software (Perkin Elmer, Waltham, MA, USA). Image quantification was performed using ImageJ (NIH images) and Volocity software. The PLA signal was quantified and normalized to cell number.

Statistical analysis. All data presented in the study are means $\pm$ S.D. Data were analyzed using student's *t*-test and analysis of variance. For all analyses, a two-sided *P*-value < 0.05 was considered to be statistically significant. Statistical analysis was performed using STATA version 13 (STATA Corp., College Station, TX, USA).

Conflict of Interest

The authors declare no conflict of interest.

Acknowledgements. This study was supported in part by the National Institutes of Health P01HL114453, U19AI068021, NS076511, NS061817, ES020693, NS065789, AG026389, HL117880, National Institute of Occupational Safety and Health OH008282, Human Frontier Science Program HFSP-RGP0013/2014, and the Barth Syndrome Foundation of Canada and United States. This work was also supported by the Fondation pour la Recherche Médicale (FRM; DPM20121125557), a CMIRA Explo'ra doc fellowship of the Region Rhone Alpes, GEFLUC and the Natural Sciences and Engineering Council of Canada, grant 9848.

1. Kroemer G, Reed JC. Mitochondrial control of cell death. *Nat Med* 2000; **6**: 513–519.
2. Tait SW, Green DR. Mitochondria and cell signalling. *J Cell Sci* 2012; **125**(Pt 4): 807–815.
3. Ni HM, Williams JA, Ding WX. Mitochondrial dynamics and mitochondrial quality control. *Redox Biol* 2014; **4C**: 6–13.
4. Youle RJ, Narendra DP. Mechanisms of mitophagy. *Nat Rev Mol Cell Biol* 2011; **12**: 9–14.
5. Ding WX, Ni HM, Li M, Liao Y, Chen X, Stolz DB *et al.* Nix is critical to two distinct phases of mitophagy, reactive oxygen species-mediated autophagy induction and Parkin-ubiquitin-p62-mediated mitochondrial priming. *J Biol Chem* 2010; **285**: 27879–27890.
6. Chu CT, Ji J, Dagda RK, Jiang JF, Tyurina YY, Kapralov AA *et al.* Cardiolipin externalization to the outer mitochondrial membrane acts as an elimination signal for mitophagy in neuronal cells. *Nat Cell Biol* 2013; **15**: 1197–1205.
7. Schlattner U, Tokarska-Schlattner M, Ramirez S, Tyurina YY, Amoscato AA, Mohammadyani D *et al.* Dual function of mitochondrial Nm23-H4 protein in phosphotransfer and intermembrane lipid transfer: a cardiolipin-dependent switch. *J Biol Chem* 2013; **288**: 111–121.
8. Schlattner U, Tokarska-Schlattner M, Epand RM, Boissan M, Lacombe ML, Klein-Seetharaman J *et al.* Mitochondrial NM23-H4/NDPK-D: a bifunctional nanoswitch for bioenergetics and lipid signaling. *Naunyn Schmiedebergs Arch Pharmacol* 2015; **388**: 271–278.
9. Milon L, Meyer P, Chiadmi M, Munier A, Johansson M, Karlsson A *et al.* The human nm23-H4 gene product is a mitochondrial nucleoside diphosphate kinase. *J Biol Chem* 2000; **275**: 14264–14272.
10. Schlame M, Rua D, Greenberg ML. The biosynthesis and functional role of cardiolipin. *Prog Lipid Res* 2000; **39**: 257–288.
11. Huang Z, Jiang J, Tyurin VA, Zhao Q, Mnuskin A, Ren J *et al.* Cardiolipin deficiency leads to decreased cardiolipin peroxidation and increased resistance of cells to apoptosis. *Free Radic Biol Med* 2008; **44**: 1935–1944.
12. Sire O, Mangeney M, Montagne J, Bereziat G, Nordmann J. Changes of fatty acid composition of phospholipids and lipid structural order in rat liver mitochondrial membrane subsequent to galactosamine intoxication. Effect of clofibrate. *Biochim Biophys Acta* 1986; **860**: 75–83.
13. Matsuda N, Sato S, Shiba K, Okatsu K, Saisho K, Gautier CA *et al.* PINK1 stabilized by mitochondrial depolarization recruits Parkin to damaged mitochondria and activates latent Parkin for mitophagy. *J Cell Biol* 2010; **189**: 211–221.
14. Tokarska-Schlattner M, Boissan M, Munier A, Borot C, Mailleau C, Speer O *et al.* The nucleoside diphosphate kinase D (NM23-H4) binds the inner mitochondrial membrane with high affinity to cardiolipin and couples nucleotide transfer with respiration. *J Biol Chem* 2008; **283**: 26198–26207.
15. Epand RF, Schlattner U, Wallimann T, Lacombe ML, Epand RM. Novel lipid transfer property of two mitochondrial proteins that bridge the inner and outer membranes. *Biophys J* 2007; **92**: 126–137.
16. East DA, Fagiani F, Crosby J, Georgakopoulos ND, Bertrand H, Schaap M *et al.* PMI: a DeltaPsim independent pharmacological regulator of mitophagy. *Chem Biol* 2014; **21**: 1585–1596.
17. Kanki T, Klionsky DJ, Okamoto K. Mitochondria autophagy in yeast. *Antioxid Redox Signal* 2011; **14**: 1989–2001.
18. Kanki T, Klionsky DJ. Mitophagy in yeast occurs through a selective mechanism. *J Biol Chem* 2008; **283**: 32386–32393.
19. Wu X, Tu BP. Selective regulation of autophagy by the Iml1-Npr2-Npr3 complex in the absence of nitrogen starvation. *Mol Biol Cell* 2011; **22**: 4124–4133.
20. Kanki T, Kang D, Klionsky DJ. Monitoring mitophagy in yeast: the Om45-GFP processing assay. *Autophagy* 2009; **5**: 1186–1189.
21. Kanki T, Wang K, Cao Y, Baba M, Klionsky DJ. Atg32 is a mitochondrial protein that confers selectivity during mitophagy. *Dev Cell* 2009; **17**: 98–109.
22. Kanki T, Wang K, Klionsky DJ. A genomic screen for yeast mutants defective in mitophagy. *Autophagy* 2010; **6**: 278–280.
23. Mao K, Wang K, Zhao M, Xu T, Klionsky DJ. Two MAPK-signaling pathways are required for mitophagy in Saccharomyces cerevisiae. *J Cell Biol* 2011; **193**: 755–767.
24. Okamoto K, Kondo-Okamoto N, Ohsumi Y. Mitochondria-anchored receptor Atg32 mediates degradation of mitochondria via selective autophagy. *Dev Cell* 2009; **17**: 87–97.
25. Head B, Griparic L, Amiri M, Gandre-Babbe S, van der Bliek AM. Inducible proteolytic inactivation of OPA1 mediated by the OMA1 protease in mammalian cells. *J Cell Biol* 2009; **187**: 959–966.
26. MacVicar TD, Lane JD. Impaired OMA1-dependent cleavage of OPA1 and reduced DRP1 fission activity combine to prevent mitophagy in cells that are dependent on oxidative phosphorylation. *J Cell Sci* 2014; **127**(Pt 10): 2313–2325.
27. Olichon A, Baricault L, Gas N, Guillou E, Valette A, Belenguer P *et al.* Loss of OPA1 perturbates the mitochondrial inner membrane structure and integrity, leading to cytochrome c release and apoptosis. *J Biol Chem* 2003; **278**: 7743–7746.
28. Fry M, Green DE. Cardiolipin requirement for electron transfer in complex I and III of the mitochondrial respiratory chain. *J Biol Chem* 1981; **256**: 1874–1880.
29. Vik SB, Georgevich G, Capaldi RA. Diphosphatidylglycerol is required for optimal activity of beef heart cytochrome c oxidase. *Proc Natl Acad Sci USA* 1981; **78**: 1456–1460.
30. Pember SO, Powell GL, Lambeth JD. Cytochrome P-450scc-phospholipid interactions. Evidence for a cardiolipin binding site and thermodynamics of enzyme interactions with cardiolipin, cholesterol, and adrenodoxin. *J Biol Chem* 1983; **258**: 3198–3206.
31. Beyer K, Klingenberg M. ADP/ATP carrier protein from beef heart mitochondria has high amounts of tightly bound cardiolipin, as revealed by 31P nuclear magnetic resonance. *Biochemistry* 1985; **24**: 3821–3826.
32. Kadenbach B, Mende P, Kolbe HV, Stipani I, Palmieri F. The mitochondrial phosphate carrier has an essential requirement for cardiolipin. *FEBS Lett* 1982; **139**: 109–112.
33. Noel H, Pande SV. An essential requirement of cardiolipin for mitochondrial carnitine acylcarnitine translocase activity. Lipid requirement of carnitine acylcarnitine translocase. *Eur J Biochem* 1986; **155**: 99–102.
34. Paradies G, Ruggiero FM. Effect of hyperthyroidism on the transport of pyruvate in rat-heart mitochondria. *Biochim Biophys Acta* 1988; **935**: 79–86.
35. Bazan S, Mileykovskaya E, Mallampalli VK, Heacock P, Sparagna GC, Dowhan W. Cardiolipin-dependent reconstitution of respiratory supercomplexes from purified Saccharomyces cerevisiae complexes III and IV. *J Biol Chem* 2013; **288**: 401–411.
36. Arnarez C, Mazat JP, Elezgaray J, Marrink SJ, Periole X. Evidence for cardiolipin binding sites on the membrane-exposed surface of the cytochrome bc1. *J Am Chem Soc* 2013; **135**: 3112–3120.
37. Chacinska A, Pfannschmidt S, Wiedemann N, Kozjak V, Sanjuan Szklarz LK, Schulze-Specking A *et al.* Essential role of Mia40 in import and assembly of mitochondrial intermembrane space proteins. *EMBO J* 2004; **23**: 3735–3746.
38. Amutha B, Pain D. Nucleoside diphosphate kinase of *Saccharomyces cerevisiae*, Ynk1p: localization to the mitochondrial intermembrane space. *Biochem J* 2003; **370**(Pt 3): 805–815.
39. Wang H, Bao R, Jiang C, Yang Z, Zhou CZ, Chen Y. Structure of Ynk1 from the yeast *Saccharomyces cerevisiae*. *Acta Crystallogr Sect F Struct Biol Crystal Commun* 2008; **64**(Pt 7): 572–576.
40. Kagan VE, Tyurin VA, Jiang J, Tyurina YY, Ritov VB, Amoscato AA *et al.* Cytochrome c acts as a cardiolipin oxygenase required for release of proapoptotic factors. *Nat Chem Biol* 2005; **1**: 223–232.
41. Alavi MV, Fuhrmann N. Dominant optic atrophy, OPA1, and mitochondrial quality control: understanding mitochondrial network dynamics. *Mol Neurodegener* 2013; **8**: 32.
42. Belenguer P, Pellegrini L. The dynamin GTPase OPA1: more than mitochondria? *Biochim Biophys Acta* 2013; **1833**: 176–183.
43. Baker MJ, Lampe PA, Stojanovski D, Korwitz A, Anand R, Tatsuta T *et al.* Stress-induced OMA1 activation and autocatalytic turnover regulate OPA1-dependent mitochondrial dynamics. *EMBO J* 2014; **33**: 578–593.
44. Boissan M, Montagnac G, Shen Q, Griparic L, Guitton J, Romao M *et al.* Membrane trafficking. Nucleoside diphosphate kinases fuel dynamin superfamily proteins with GTP for membrane remodeling. *Science* 2014; **344**: 1510–1515.
45. Ashrafi G, Schwarz TL. The pathways of mitophagy for quality control and clearance of mitochondria. *Cell Death Differ* 2013; **20**: 31–42.
46. Narendra D, Tanaka A, Suen DF, Youle RJ. Parkin is recruited selectively to impaired mitochondria and promotes their autophagy. *J Cell Biol* 2008; **183**: 795–803.
47. Sandoval H, Thiagarajan P, Dasgupta SK, Schumacher A, Prchal JT, Chen M *et al.* Essential role for Nix in autophagic maturation of erythroid cells. *Nature* 2008; **454**: 232–235.
48. Bellot G, Garcia-Medina R, Gounon P, Chiche J, Roux D, Pouyssegur J *et al.* Hypoxia-induced autophagy is mediated through hypoxia-inducible factor induction of BNIP3 and BNIP3L via their BH3 domains. *Mol Cell Biol* 2009; **29**: 2570–2581.

49. Liu L, Feng D, Chen G, Chen M, Zheng Q, Song P *et al.* Mitochondrial outer-membrane protein FUNDC1 mediates hypoxia-induced mitophagy in mammalian cells. *Nat Cell Biol* 2012; **14**: 177–185.
50. Allen GF, Toth R, James J, Ganley IG. Loss of iron triggers PINK1/Parkin-independent mitophagy. *EMBO Rep* 2013; **14**: 1127–1135.
51. Dagda RK, Cherra SJ 3rd, Kulich SM, Tandon A, Park D, Chu CT. Loss of PINK1 function promotes mitophagy through effects on oxidative stress and mitochondrial fission. *J Biol Chem* 2009; **284**: 13843–13855.
52. Han JY, Kang MJ, Kim KH, Han PL, Kim HS, Ha JY *et al.* Nitric oxide induction of Parkin translocation in PTEN-induced putative kinase 1 (PINK1) deficiency: functional role of neuronal nitric oxide synthase during mitophagy. *J Biol Chem* 2015; **290**: 10325–10335.
53. Kubli DA, Cortez MQ, Moyzis AG, Najor RH, Lee Y, Gustafsson AB. PINK1 is dispensable for mitochondrial recruitment of parkin and activation of mitophagy in cardiac myocytes. *PloS One* 2015; **10**: e0130707.
54. Green DR, Levine B. To be or not to be? How selective autophagy and cell death govern cell fate. *Cell* 2014; **157**: 65–75.
55. Strappazzon F, Nazio F, Corrado M, Cianfanelli V, Romagnoli A, Fimia GM *et al.* AMBRA1 is able to induce mitophagy via LC3 binding, regardless of PARKIN and p62/SQSTM1. *Cell Death Differ* 2015; **22**: 517.
56. Kageyama Y, Hoshijima M, Seo K, Bedja D, Sysa-Shah P, Andrabi SA *et al.* Parkin-independent mitophagy requires Drp1 and maintains the integrity of mammalian heart and brain. *EMBO J* 2014; **33**: 2798–2813.
57. Soubannier V, McLelland GL, Zunino R, Braschi E, Rippstein P, Fon EA *et al.* A vesicular transport pathway shuttles cargo from mitochondria to lysosomes. *Curr Biol* 2012; **22**: 135–141.
58. Szent-Gyorgyi C, Schmidt BF, Creeger Y, Fisher GW, Zakel KL, Adler S *et al.* Fluorogen-activating single-chain antibodies for imaging cell surface proteins. *Nat Biotechnol* 2008; **26**: 235–240.
59. Montamat EE, Blanco A. Subcellular distribution of the lactate dehydrogenase isozyme specific for testis and sperm. *Exp Cell Res* 1976; **103**: 241–245.
60. Folch J, Lees M, Sloane Stanley GH. A simple method for the isolation and purification of total lipides from animal tissues. *J Biol Chem* 1957; **226**: 497–509.
61. Chalvardjian A, Rudnicki E. Determination of lipid phosphorus in the nanomolar range. *Anal Biochem* 1970; **36**: 225–226.
62. Tyurina YY, Poloyac SM, Tyurin VA, Kapralov AA, Jiang J, Anthonymuthu TS *et al.* A mitochondrial pathway for biosynthesis of lipid mediators. *Nat Chem* 2014; **6**: 542–552.
63. Soderberg O, Gullberg M, Jarvius M, Ridderstrale K, Leuchowius KJ, Jarvius J *et al.* Direct observation of individual endogenous protein complexes in situ by proximity ligation. *Nat Methods* 2006; **3**: 995–1000.

Supplementary Information accompanies this paper on Cell Death and Differentiation website (http://www.nature.com/cdd)

SUPPLEMENTAL INFORMATION

NDPK-D (NM23-H4)-Mediated Externalization of Cardiolipin Enables Elimination of Depolarized Mitochondria by Mitophagy

Valerian E. Kagan [a*], Jianfei Jiang [a], Zhentai Huang [a], Yulia Y. Tyurina [a],
Céline Desbourdes [b,c], Cécile Cottet-Rousselle [b,c], Haider Dar [a], Manish Verma [d], Vladimir A.Tyurin [a],
Alexandr A. Kapralov [a], Amin Cheikhi [a], Gaowei Mao [a],
Donna Stolz [e], Claudette M. St. Croix [e], Simon Watkins [e], Zheni Shen [f], Yiran Li [f],
Miriam L. Greenberg [f], Malgorzata Tokarska-Schlattner [b,c], Mathieu Boissan [g],
Marie-Lise Lacombe [b], Richard M. Epand [h], Charleen T. Chu [d],
Rama Mallampalli [i], Hülya Bayır [j*], Uwe Schlattner [b,c *]

[a] Center for Free Radical and Antioxidant Health, Departments of Environmental Health,
[d] Pathology, [e] Cell Biology and Physiology, [i] Medicine, [j] Critical Care Medicine, University of Pittsburgh, Pittsburgh, PA 15260.

[b] University Grenoble Alpes - UJF, Laboratory of Fundamental and Applied Bioenergetics (LBFA), and SFR Environmental and Systems Biology (BEeSy),

[c] Inserm, U1055, Grenoble, France.

[f] Department of Biological Sciences, Wayne State University, Detroit, MI 48202

[g] Institut Curie, Research Center, Paris, France. Membrane and Cytoskeleton Dynamics, CNRS UMR 144, Paris, France. Université Pierre et Marie Curie, University Paris 06, Paris, France. Saint-Antoine Research Center, INSERM UMR-S 938, Paris, France

[h] Department of Biochemistry and Biomedical Sciences, McMaster University , Hamilton, Ontario L8S 4K1, Canada

*Correspondence should be addressed to V.E.K. (Kagan@pitt.edu),
H.B. (hub22@pitt.edu) or U.S (uwe.schlattner@ujf-grenoble.fr).

Experimental procedures

Yeast strains and growth media

The wild type and *ndk1*Δ yeast *S. cerevisiae* strains used in this study were obtained as previously described[1, 2]. Synthetic complete (SC) media contained all the essential components of Difco yeast nitrogen base, standard concentrations of amino acids and vitamins, ammonium sulfate (0.5%), and glucose (2%). Synthetic lactate (SL) medium contained vitamin free yeast nitrogen base without amino acids (0.17%), ammonium sulfate (0.5%), and lactate (2%) [3].

Cell culture

SH-SY5Y cells were purchased from ATCC (Manassas, VA, USA). Cells were maintained in a humidified incubator with 5% CO2 at 37°C in antibiotic-free Dulbecco's modified Eagle's medium supplemented with 10% heat-inactivated fetal calf serum (BioWhittaker, Walkersville, MD, USA), 2 mM glutamine (BioWhittaker) and 10 mM HEPES (BioWhittaker).

Reagent

Rabbit anti-Tom40 antibody was from Santa Cruz Biotechnology (Dallas, Texas). Rabbit anti-mouse CLS antibody was a customized antibody by Life Technologies (Grand Island, NY). Mouse anti-cytochrome *c*, anti-Tim23 and anti-MnSOD antibodies were from BD sciences (San Jose, CA). Mitoprofile OXPHOS antibody cocktail was obtained from Abcam (Cambridge, MA). Anti-GFP antibody was from Clontech (Mountain View, CA). CLS-1 siRNA (s29307 and s29308) and Lipofectamine reagent RNAiMax were from Life Technologies.

Transmission electron microscopy (TEM)

Following treatment, cells grown in 6-well tissue culture dishes were rinsed with PBS, fixed in 2.5% glutaraldehyde overnight at 4°C. Specimens were analyzed and documented with a JEOL JEM-1011 (JEOL, Tokyo, Japan) transmission electron microscope.

siRNA Transfection

For knocking down expression of CLS-1 in MLE cells or NDPK-D in SH-SY5Y cells, cells were transfected with 50 nM (final) siRNAs against CLS-1 or NPDK-D using RNAiMax 9. As controls, cells were mock transfected or transfected with scrambled negative siRNAs.

Fluorescence Microscopy

For immuofluorescence staining of MnSOD (green) and LC3 (red) in HeLa cells transfected vectors expressing wild type NDPK-D or R90D mutant, cells were incubated with 50 μM CCCP for 2 hour. Cells were then fixed with paraformaldehyde and permeabilized using Triton X-100. Cells were stained with anti-MnSOD and anti-LC3 antibodies with fluorescence conjugated second antibodies. Images were obtained from a single focal section (scale bars 20 mm). Fluorescence was examined by confocal microscopy using a Leica TCS SP2 microscope (Leica Microsystems, GmbH).

Mitophagy was quantitatively assessed through co-localization of immunostained TOM20 with GFP-LC3 in SH-SY5Y cells. SH-SY5Y cells were co-transfected with GFP-LC3 and scrambled negative siRNA (negative) or siRNA targeting NDPK-D (si-NDPK-D) two days prior to treatment with rotenone (ROT, 1 μM, 6 h) or 6-hydroxydopamine (6-OHDA, 100 μM, 6 h). For percentage of GFP-LC3 puncta with mitochondrial co-localization, cells were stained with anti-TOM20 followed by fluorescence conjugated secondary antibody. Images were obtained with a Nikon A1 confocal microscope at 60× magnification. Two dimension projections were created from z-stacks (12 μm thick sections with 0.25 μm thick slices) using Nikon Elements software. Percent mitophagy was quantified using the “mitophagy” plugin in

Image J [4, 5]. For percentage of cells showing Parkin translocation to mitochondria, SH-SY5Y cells were co-transfected with hemagglutinin (HA) tagged Parkin and either scrambled negative siRNA (negative) or siRNA targeting NDPK-D (si-NDPK-D) two days prior to treatment with CCCP (5 μM, 6 h). After treatment, cells were fixed, immunostained with mouse anti-HA for Parkin and rabbit anti-TOM20, followed by appropriate fluorescence conjugated second antibodies. Images from 4 random fields containing ~50 cells/ field were acquired using an IX71 Olympus fluorescence microscope at a 40× magnification and a DP70 microscope digital camera. Percent translocation was quantified by: (number of cells showing mitochondrial Parkin translocation/ total number of cells counted) ×100%.

Detection of mitophagy in yeast

To monitor mitophagy in yeast, the gene encoding the mitochondrial matrix protein Idh1 was tagged with GFP and inserted into the *IDH1* locus of wild type and *ndk1*Δ strains as previously described [1, 2]. Wild type *IDH1*-GFP and *ndk1Δ-IDH1*-GFP cells were cultured at 30°C in SC medium to the mid-log phase, harvested, washed with SL medium and re-suspended in 5 ml SL medium at a starting A550 of 0.5 and incubated for 6-7 hours to induce mitophagy. Cells were then harvested, and extracts were prepared as previously described [1]. Free GFP released during mitophagy was detected by Western blot as previously described [1].

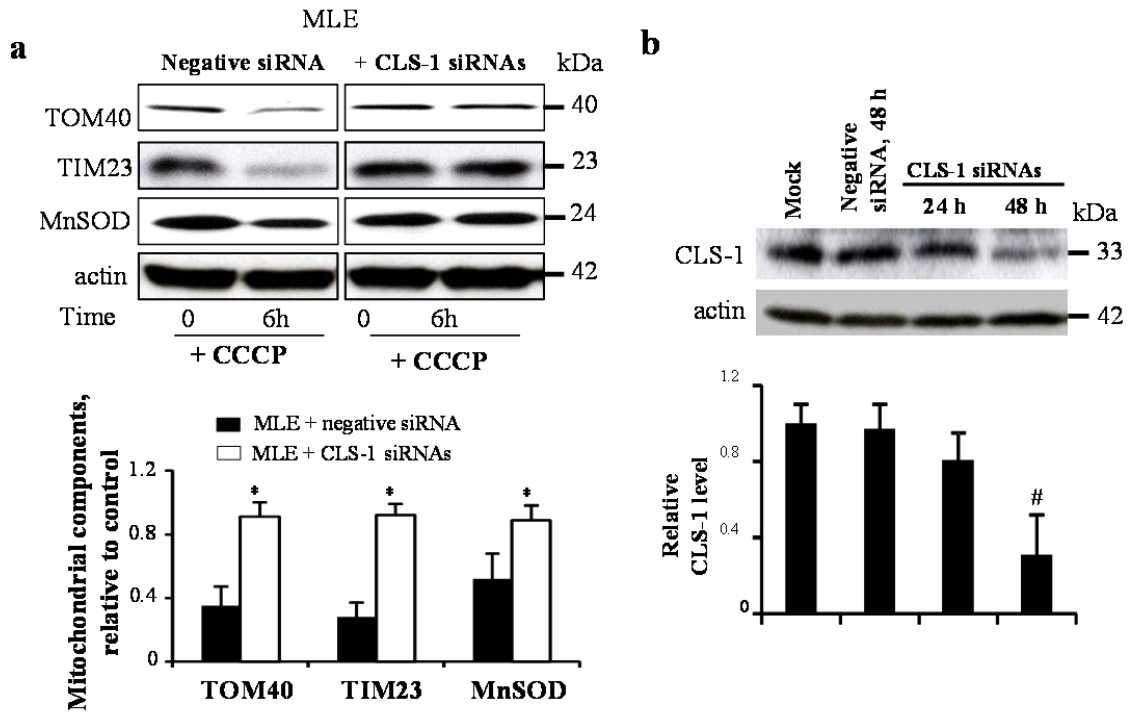

Supplemental figure 1. Knock-down of CLS-1 attenuates CCCP-induced mitochondrial protein degradation. (a) Assessment of characteristic proteins of OMM (Tim23), OMM (Tom40) and matrix (MnSOD) in CCCP-treated MLE cells. Control or CL deficient MLE cells were treated with 20 μM CCCP for 6 hours. The levels of mitochondrial proteins were determined by Western blot analysis using antibodies against Tom40, Tim23, and MnSOD. The relative levels of mitochondrial proteins in CCCP-treated cells were calculated by densitometry, normalized to actin, and expressed as percentage of the respective values in control cells without CCCP treatment (n=3). (b) Knock-down of CLS-1 using siRNA in MLE cells. Cells were transfected with CLS-1 siRNA using RNAiMax. Mock transfected cells or cells transfected with non-targeted negative control siRNAs were used as controls. At 48 hours post transfection, cells were harvested for Western blot analysis. The relative CLS-1 levels were quantified by average densitometry values normalized to actin as above (n=3). $*p < 0.05$ *vs* MLE cells transfected negative siRNAs under the CCCP exposure, $^{\#}p < 0.05$ *vs* MLE cells transfected with non-targeting negative siRNAs.

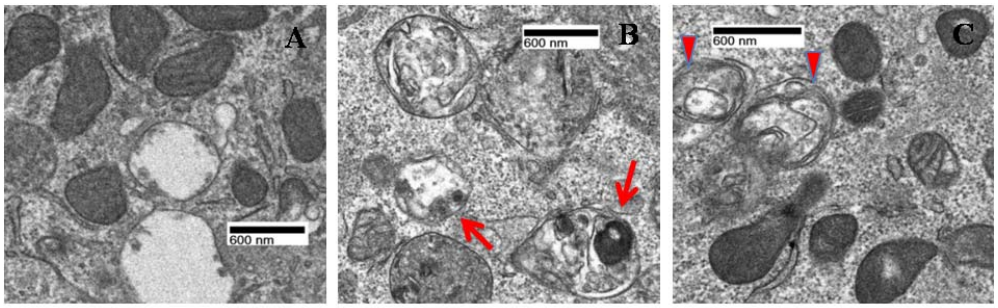

Supplemental figure 2. Transmission electron microscopy (TEM) demonstrates attenuated CCCP-induced mitophagy in MLE cells with knocked-down NDPK-D. Cells were treated with 20 μM CCCP for 4 hours. Cells were then fixed in glutaraldehyde and analyzed with a JEOL JEM-1011 transmission electron microscope. Arrows indicate autophagic structures containing mitochondrial fragments. Arrowheads indicate autophagosomes lacking obvious mitochondria-derived structures.

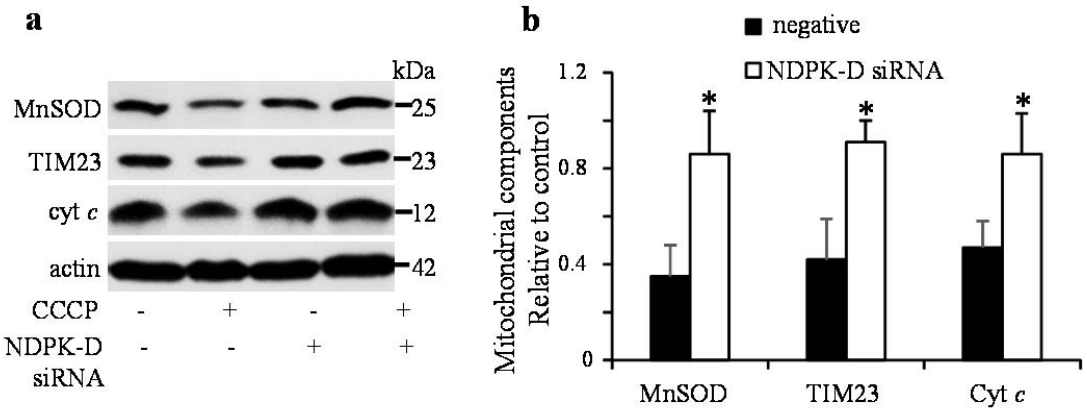

Supplemental figure 3. Effect of NDPK-D knocking down on CCCP-induced degradation of mitochondrial marker proteins (cyt *c*, Tim23 and MnSOD) in MLE cells. MLE cells were transiently transfected with siRNAs against NDPK-D for 48 hours. Wild type MLE and NDPK-D deficient MLE cells were then treated with 20 μM CCCP for 4 hours. (a) The levels of mitochondrial proteins were determined by Western blot analysis using antibodies against MnSOD, TIM23, and cytochrome *c*. (b) The relative levels of mitochondrial proteins in CCCP-treated cells were calculated by densitometry, normalized to actin, and expressed as percentage of the respective values in control cells without CCCP treatment (n=3). *$p < 0.05$ *vs* MLE cells transfected negative siRNAs under the CCCP exposure.

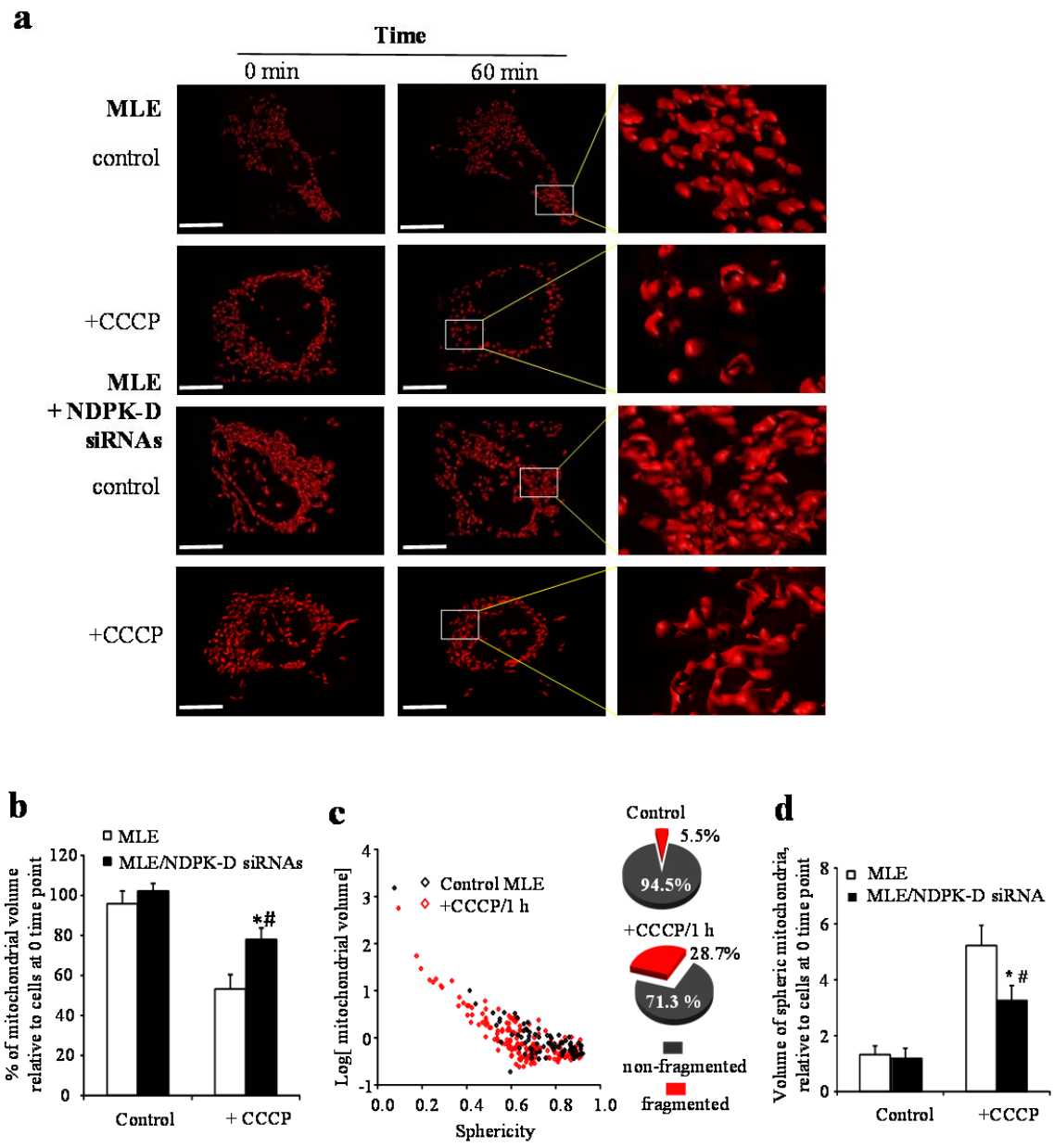

Supplemental figure 4. CCCP-induced mitochondrial volume change and fragmentation in NDPK-D manipulated MLE cells. (a) Knock-down of NDPK-D in MLE-12 cells attenuates CCCP-induced loss of volume and increased fragmentation of mitochondria. Presented are representative images of 3D surface reconstructions of mitochondria using Imaris 8 software. After addition of CCCP, MLE cells or cells transfected with siRNAs against NDPK-D were subjected to multi-position time lapse imaging for 60 min with 5 min intervals. The scale bar is 20 µm. (b) Assessment of mitochondrial volume changes in CCCP-treated (1 h) MLE-12 cells. The relative mitochondrial volume was calculated as the percentage of initial mitochondrial volume at the first time point (n=6-8 images). (c) Mitochondrial fragmentation in CCCP-treated MLE-12 cells was assessed using sphericity parameter for small mitochondrial fragments (with an arbitrary threshold of sphericity <0.4) to differentiate the fragmented mitochondria and plotted

against log (mitochondrial volume). Dot plots shown are representative of MLE cells before and after (1h) addition of CCCP. The inserted pie plots show the percentage of fragmented and non-fragmented mitochondrial volume. (d) The ratio of the volume of spheric (fragmented) mitochondria vs non-fragmented mitochondria was calculated and compared to the ratio at the initial time point (n=6-8). * #$p < 0.05$ vs cells without CCCP treatment, or MLE cells without NDPK-D knock-down under the same condition, respectively (n=6-8).

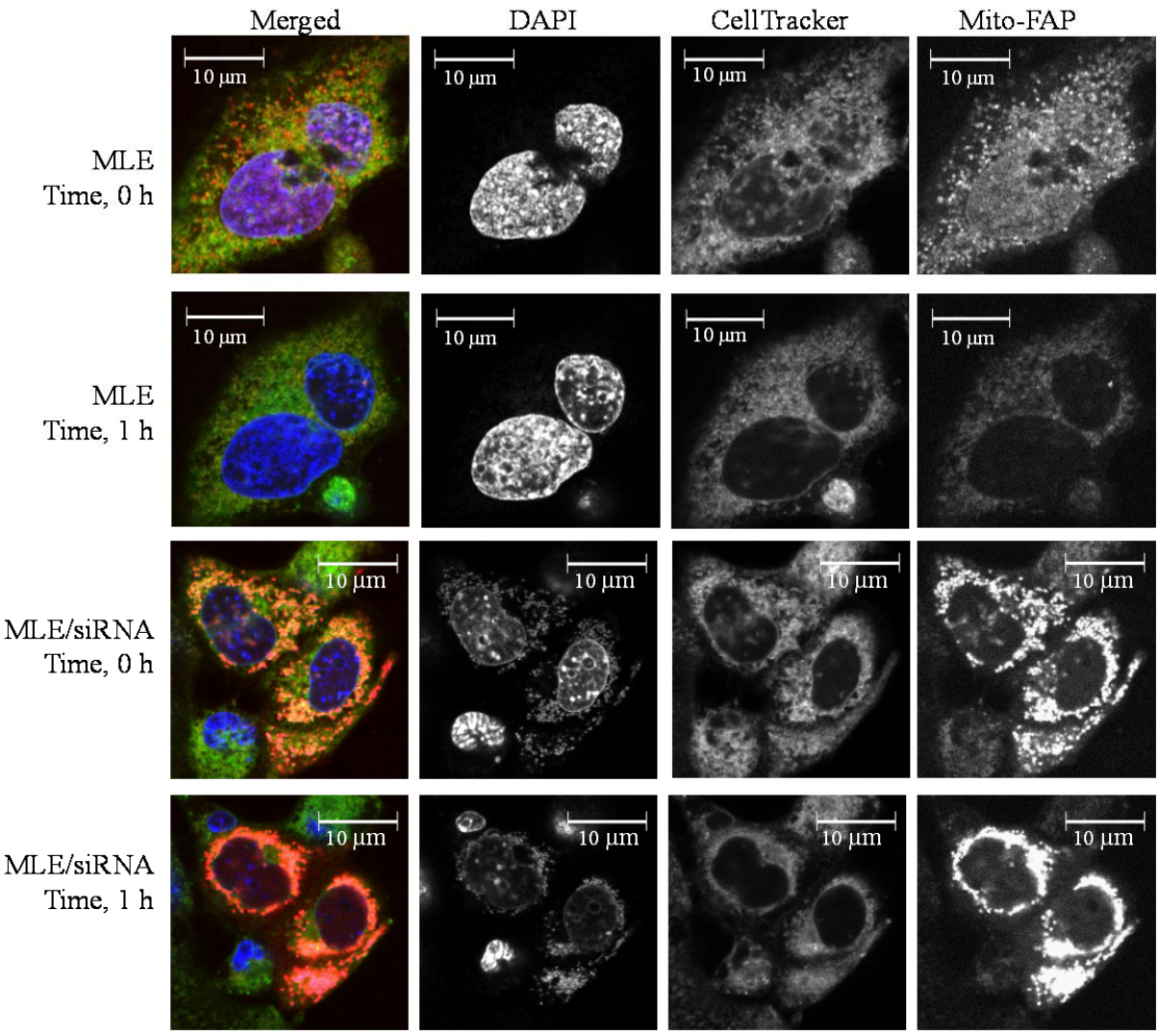

Supplemental figure 5. Effect of NDPK-D manipulation on CCCP induced mitophagy in MLE cells as evidenced by fluorescence imaging. Representative fluorescent images of mitochondria in CCCP-treated MLE cells and cells transfected with siRNAs against NDPK-D were shown. MLE cells were transiently transfected with siRNAs against NDPK-D for 48 h. To label mitochondria, cells were infected with adenoviral vector expressing mitochondria-directed mCerulean/mFAP. Cells were labeled with CellTracker and DAPI, and then imaged using a confocal microscope prior to the CCCP (20 μM) treatment and 1 hour after the CCCP treatment.

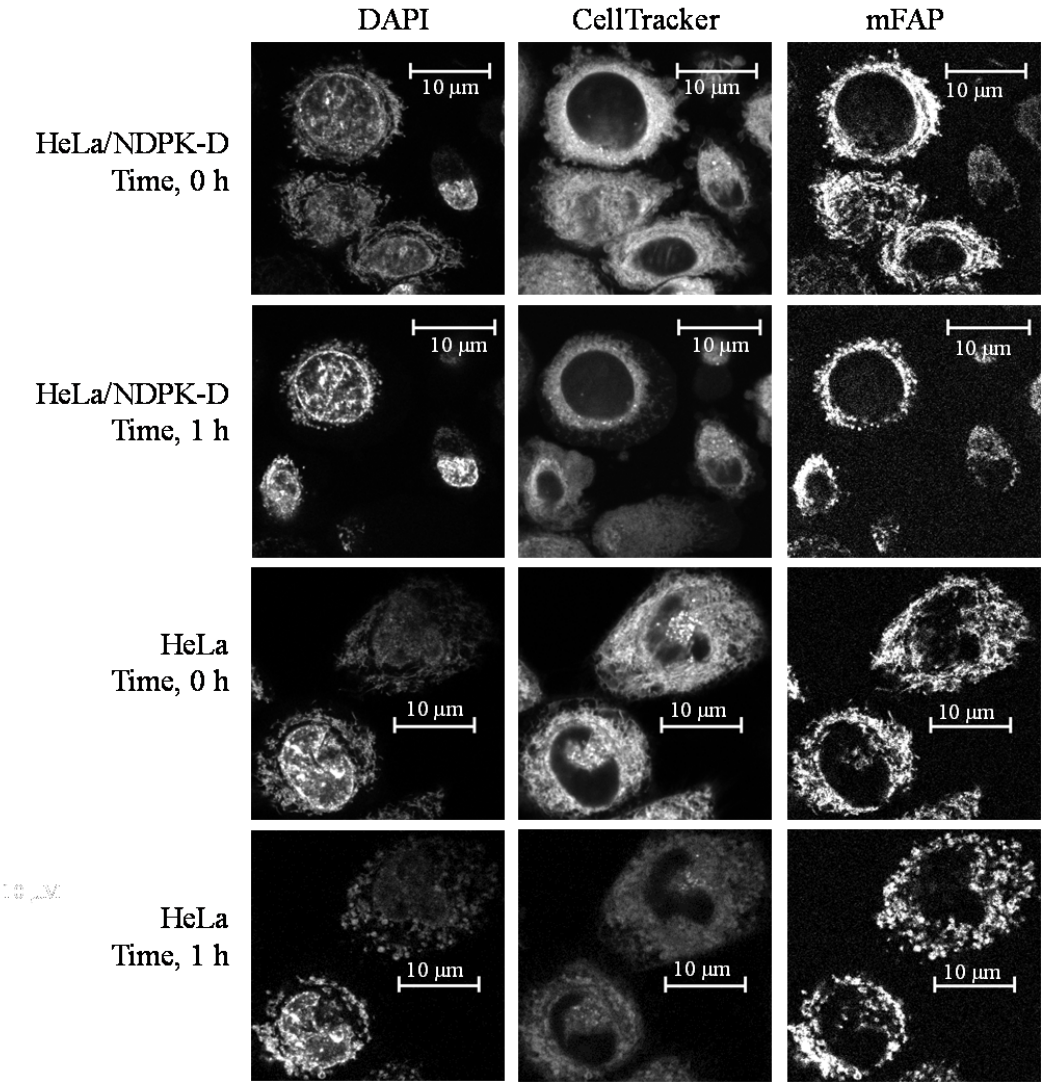

Supplemental figure 6. **Effect of NDPK-D manipulation on CCCP induced mitophagy in HeLa cells as evidenced by fluorescence imaging.** Representative fluorescent images of mitochondria in CCCP-treated HeLa cells or cells transfected with wild type NDPK-D were shown. HeLa cells were transiently transfected with vectors expressing wild type NDPK-D for 48 h. To label mitochondria, cells were infected with adenoviral vector expressing mitochondria-directed mCerulean/mFAP. Cells were labeled with CellTracker and DAPI, and then imaged using a confocal microscope prior to the CCCP (20 μM) treatment and 1 hour after the CCCP treatment. See merged images in Figure 5 in the manuscript.

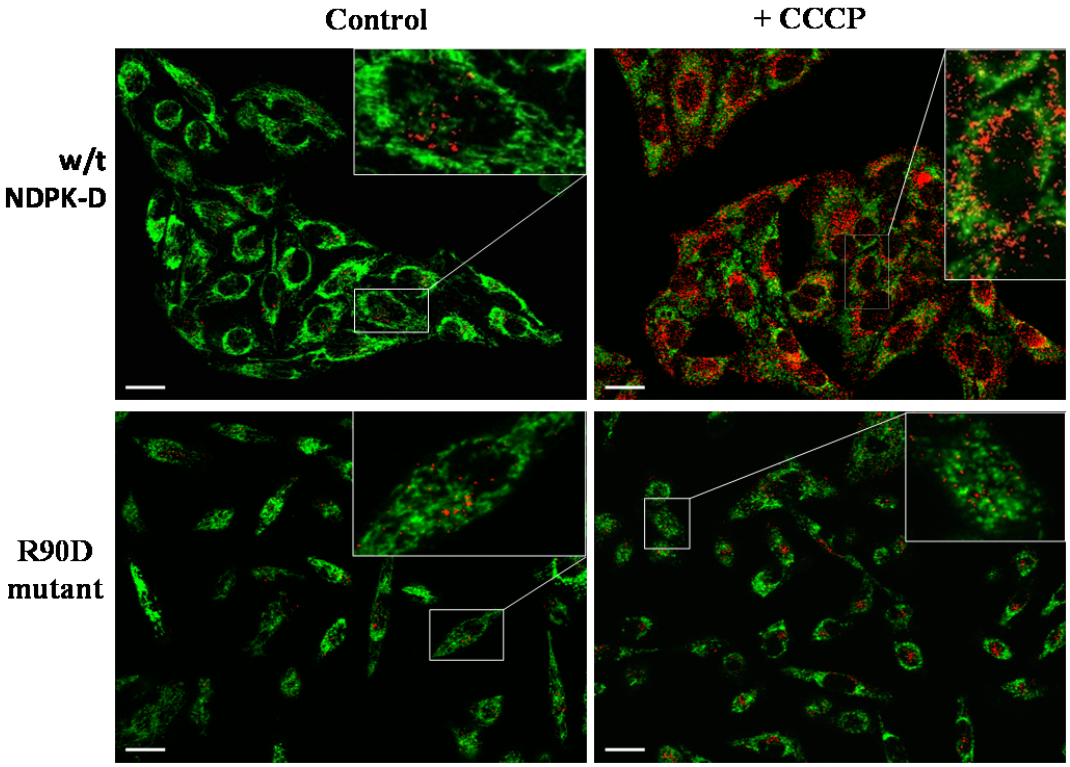

Supplemental figure 7. Immuofluorescence staining of MnSOD (green) and LC3 (red) in HeLa cells transfected vectors expressing wild type NDPK-D (upper panels) or R90D mutant (lower panels). Cells were incubated with 50 µM CCCP for 2 hour. Images were obtained from a single focal section (scale bars 20 µm). Fluorescence was examined by confocal microscopy using a Leica TCS SP2 microscope (Leica Microsystems, GmbH).

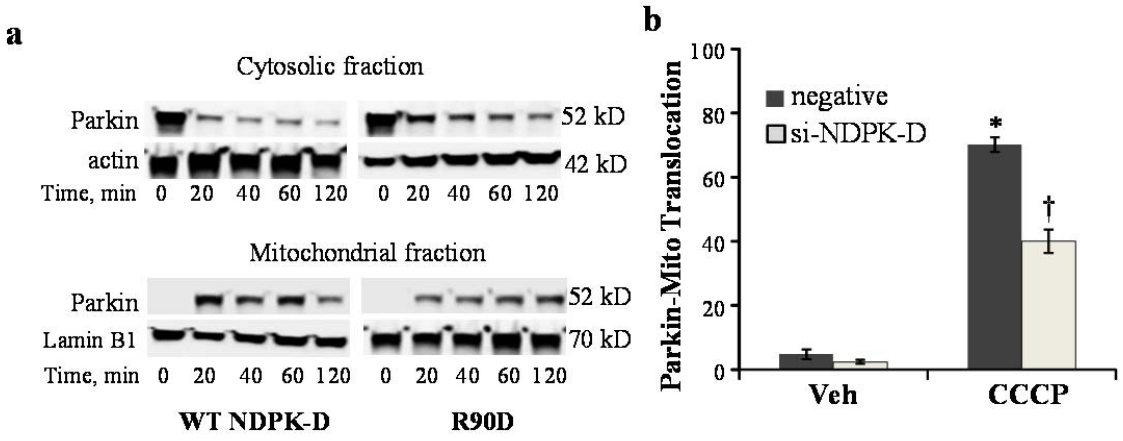

Supplemental figure 8. Effect of NPDK-D on translocation of Parkin from cytosol to mitochondria following mitochondria damage. (a) Parkin expressing HeLa were transiently transfected with vectors expressing wild type NDPK-D or R90D mutant. After 48 hours post-transfection incubation, cells were treated with 20 μM CCCP for indicated time. At the end of treatment, cells were harvested and lyzed in buffer containing 0.05% digitonin (10 min on ice). The samples were centrifuged at 5,000 × g, 4ºC for 10 min, and the supernatants were collected as cytosolic fraction. The resulting mitochondrial fractions were further lyzed with RIPA buffer. Amount of Parkin in cytosolic and mitochondrial fractions was evaluated using western blotting. (b) SH-SY5Y cells were treated with scrambled negative siRNA (negative) or siRNA targeting NDPK-D (si-NDPK-D) two days prior to treatment with CCCP (5 μM, 6 h). Control cells were treated with vehicle (Veh) alone. The percent of cells showing Parkin translocation to mitochondria was quantified (n = 200 cells/condition across 2 independent experiments). * $p < 0.01$ *vs*. Veh/negative; † $p < 0.01$ *vs*. CCCP/negative.

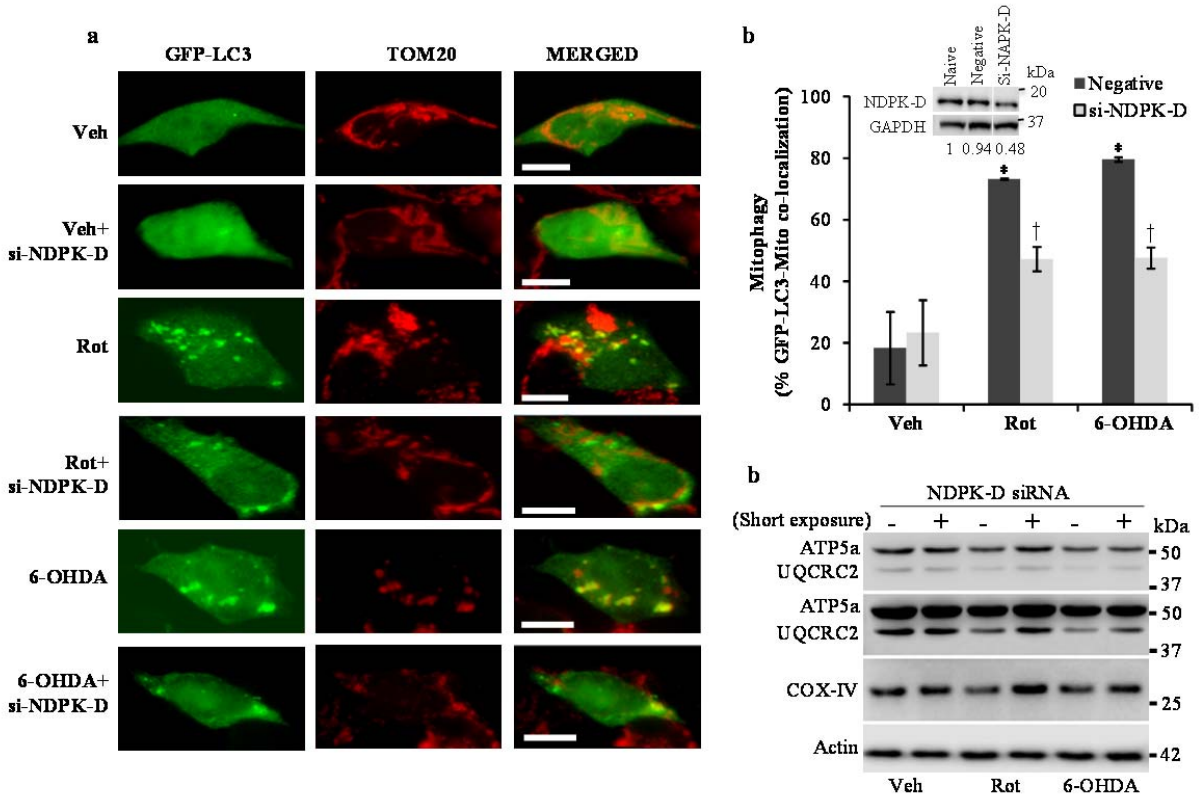

Supplemental figure 9. Effect of NDPK-D knocking-down on rotenone (ROT) and 6-hydroxy-dopamine (6-OHDA)-induced mitophagy in SH-SY5Y cells. SH-SY5Y cells were co-transfected with GFP-LC3 and scrambled negative siRNA (negative) or siRNA targeting NDPK-D (si-NDPK-D) two days prior to treatment with ROT (1 µM, 6 h) or 6-OHDA (100 µM, 6 h). Control cells were treated with vehicle (Veh) alone. Mitophagy was assessed through co-localization of immunostained TOM20 with GFP-LC3 (a, Scale bar, 20 µm), and quantified (b) as the % of GFP-LC3 puncta with mitochondrial co-localization (n=200 cells/condition across 2 independent experiments). * $p < 0.05$ *vs.* Veh/negative; † $p < 0.05$ *vs.* CCCP/negative. Protein lysates (40 µg) from an independent set of experiments were separated on 4-12% TGS gels for western blot analysis (c) of mitochondrial inner membrane proteins (ATP5a, UQCRC2, and COX-IV).

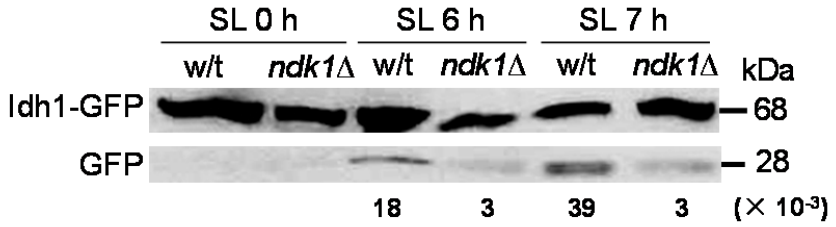

Supplemental figure 10. Decreased mitophagy in *ndk1Δ* cells grow in synthetic lactate medium. Wild type (w/t) and *ndk1Δ* cells expressing the GFP-tagged *IDH1* gene were pre-cultured in synthetic complete medium to the mid-log phase at 30˚C and shifted to synthetic lactate medium for 6-7 hours. Aliquots were collected, and extracts were then prepared as described in *Materials and Methods*. Samples (25 μg) were analyzed by SDS-PAGE and Western blot. Immunoblotting was done with anti-GFP antibody (Clontech, Mountain View, CA), and the positions of full-length Idh1-GFP and free GFP are indicated. The Image presented is representative of three independent experiments. Numbers under the GFP bands show the density ratios for GFP to Idh1-GFP in each lane. Note that the free GFP band was apparent beginning at 6 hours after induction of mitophagy, and was markedly decreased in *ndk1Δ* cells relative to the w/t cells.

References

1. Kanki T, Kang D, Klionsky DJ. Monitoring mitophagy in yeast: The Om45-GFP processing assay. *Autophagy* 2009; **5**(8)**:** 1186-1189.

2. Kanki T, Klionsky DJ. Mitophagy in Yeast Occurs through a Selective Mechanism. *The Journal of Biological Chemistry* 2008; **283**(47)**:** 32386-32393.

3. Wu X, Tu BP. Selective regulation of autophagy by the Iml1-Npr2-Npr3 complex in the absence of nitrogen starvation. *Molecular biology of the cell* 2011; **22**(21)**:** 4124-33.

4. Dagda RK, Zhu J, Kulich SM, Chu CT. Mitochondrially localized ERK2 regulates mitophagy and autophagic cell stress: implications for Parkinson's disease. *Autophagy* 2008; **4**(6)**:** 770-82.

5. Zhu J, Dagda RK, Chu CT. Monitoring mitophagy in neuronal cell cultures. *Methods in molecular biology* 2011; **793:** 325-39.

Bibliography

Aaltonen, M. J., Friedman, J. R., Osman, C., Salin, B., di Rago, J.-P., Nunnari, J., Langer, T., and Tatsuta, T. (2016). MICOS and phospholipid transfer by Ups2-Mdm35 organize membrane lipid synthesis in mitochondria. *The Journal of Cell Biology*, 213(5):525–534.

Alberts, B., Johnson, A., Lewis, J., Raff, M., Roberts, K., and Walter, P. (2002). The Mitochondrion. In *Molecular Biology of the Cell*. Garland Science, New York.

Anand, R., Wai, T., Baker, M. J., Kladt, N., Schauss, A. C., Rugarli, E., and Langer, T. (2014). The i-AAA protease YME1L and OMA1 cleave OPA1 to balance mitochondrial fusion and fission. *The Journal of Cell Biology*, 204(6):919–929.

Baker, M. J., Lampe, P. A., Stojanovski, D., Korwitz, A., Anand, R., Tatsuta, T., and Langer, T. (2014). Stress-induced OMA1 activation and autocatalytic turnover regulate OPA1-dependent mitochondrial dynamics. *EMBO Journal*, 33(6):578–593.

Ban, T., Heymann, J. A. W., Song, Z., Hinshaw, J. E., and Chan, D. C. (2010). OPA1 disease alleles causing dominant optic atrophy have defects in cardiolipin-stimulated GTP hydrolysis and membrane tubulation. *Human Molecular Genetics*, 19(11):2113–2122.

Bateman, A., Martin, M. J., O'Donovan, C., Magrane, M., Apweiler, R., Alpi, E., Antunes, R., Arganiska, J., Bely, B., Bingley, M., Bonilla, C., Britto, R., Bursteinas, B., Chavali, G., Cibrian-Uhalte, E., Da Silva, A., De Giorgi, M., Dogan, T., Fazzini, F., Gane, P., Castro, L. G., Garmiri, P., Hatton-Ellis, E., Hieta, R., Huntley, R., Legge, D., Liu, W., Luo, J., Macdougall, A., Mutowo, P., Nightingale, A., Orchard, S., Pichler, K., Poggioli, D., Pundir, S., Pureza, L., Qi, G., Rosanoff, S., Saidi, R., Sawford, T., Shypitsyna, A., Turner, E., Volynkin, V., Wardell, T., Watkins, X., Zellner, H., Cowley, A., Figueira, L., Li, W., McWilliam, H., Lopez, R., Xenarios, I., Bougueleret, L., Bridge, A., Poux, S., Redaschi, N., Aimo, L., Argoud-Puy, G., Auchincloss, A., Axelsen, K., Bansal, P., Baratin, D., Blatter, M. C., Boeckmann, B., Bolleman, J., Boutet, E., Breuza, L., Casal-Casas, C., De Castro, E., Coudert, E., Cuche, B., Doche, M., Dornevil, D., Duvaud, S., Estreicher, A., Famiglietti, L., Feuermann, M., Gasteiger, E., Gehant, S., Gerritsen, V., Gos, A., Gruaz-Gumowski, N., Hinz, U., Hulo, C., Jungo, F., Keller, G., Lara, V., Lemercier, P., Lieberherr, D., Lombardot, T., Martin, X., Masson, P., Morgat, A., Neto, T., Nouspikel, N., Paesano, S., Pedruzzi, I., Pilbout, S., Pozzato, M., Pruess,

M., Rivoire, C., Roechert, B., Schneider, M., Sigrist, C., Sonesson, K., Staehli, S., Stutz, A., Sundaram, S., Tognolli, M., Verbregue, L., Veuthey, A. L., Wu, C. H., Arighi, C. N., Arminski, L., Chen, C., Chen, Y., Garavelli, J. S., Huang, H., Laiho, K., McGarvey, P., Natale, D. A., Suzek, B. E., Vinayaka, C. R., Wang, Q., Wang, Y., Yeh, L. S., Yerramalla, M. S., and Zhang, J. (2015). UniProt: A hub for protein information. *Nucleic Acids Research*, 43(D1):D204–D212.

Belenguer, P. and Pellegrini, L. (2013). The dynamin GTPase OPA1: More than mitochondria? *Biochimica et Biophysica Acta (BBA) - Molecular Cell Research*, 1833(1):176–183.

Boissan, M., Dabernat, S., Peuchant, E., Schlattner, U., Lascu, I., and Lacombe, M. L. (2009). The mammalian Nm23/NDPK family: From metastasis control to cilia movement. *Molecular and Cellular Biochemistry*, 329(1-2):51–62.

Boissan, M., De Wever, O., Lizarraga, F., Wendum, D., Poincloux, R., Chignard, N., Desbois-Mouthon, C., Dufour, S., Nawrocki-Raby, B., Birembaut, P., Bracke, M., Chavrier, P., Gespach, C., and Lacombe, M.-L. (2010). Implication of metastasis suppressor NM23-H1 in maintaining adherens junctions and limiting the invasive potential of human cancer cells. *Cancer Research*, 70(19):7710–7722.

Boissan, M. and Lacombe, M. L. (2012). [NM23, an example of a metastasis suppressor gene]. *Bull Cancer*, 99(4):431–440.

Boissan, M., Montagnac, G., Shen, Q., Griparic, L., Guitton, J., Romao, M., Sauvonnet, N., Lagache, T., Lascu, I., Raposo, G., Desbourdes, C., Schlattner, U., Lacombe, M.-L., Polo, S., van der Bliek, A. M., Roux, A., and Chavrier, P. (2014). Membrane trafficking. Nucleoside diphosphate kinases fuel dynamin superfamily proteins with GTP for membrane remodeling. *Science*, 344(6191):1510–5.

Boterberg, T., Vennekens, K. M., Thienpont, M., Mareel, M. M., and Bracke, M. E. (2000). Internalization of the E-cadherin/catenin complex and scattering of human mammary carcinoma cells MCF-7/AZ after treatment with conditioned medium from human skin squamous carcinoma cells COLO 16. *Cell Adhesion and Communication*, 7(4):299–310.

Bradford, M. M. (1976). Rapid and Sensitive Method for Quantitation of Microgram Quantities of Protein Utilizing Principle of Protein-Dye Binding. *Analytical Biochemistry*, 72(1-2):248–254.

Bresnick, A. R., Weber, D. J., and Zimmer, D. B. (2015). S100 proteins in cancer. *Nature Reviews Cancer*, 15(2):96–109.

Cabrita, L. D. and Bottomley, S. P. (2004). Protein expression and refolding - A practical guide to getting the most out of inclusion bodies. *Biotechnology Annual Review*, 10:31–50.

Chaffer, C. L. and Weinberg, R. A. (2011). A perspective on cancer cell metastasis. *Science*, 331(6024):1559–1564.

Chan, D. C. (2006). Mitochondrial Fusion and Fission in Mammals. *Annual Review of Cell and Developmental Biology*, 22(1):79–99.

Chen, H., Chomyn, A., and Chan, D. C. (2005). Disruption of fusion results in mitochondrial heterogeneity and dysfunction. *Journal of Biological Chemistry*, 280(28):26185–26192.

Chu, C. T., Ji, J., Dagda, R. K., Jiang, J. F., Tyurina, Y. Y., Kapralov, A. A., Tyurin, V. A., Yanamala, N., Shrivastava, I. H., Mohammadyani, D., Qiang Wang, K. Z., Zhu, J., Klein-Seetharaman, J., Balasubramanian, K., Amoscato, A. A., Borisenko, G., Huang, Z., Gusdon, A. M., Cheikhi, A., Steer, E. K., Wang, R., Baty, C., Watkins, S., Bahar, I., Bayır, H., and Kagan, V. E. (2013). Cardiolipin externalization to the outer mitochondrial membrane acts as an elimination signal for mitophagy in neuronal cells. *Nature Cell Biology*, 15(10):1197–1205.

Cogliati, S., Enriquez, J. A., and Scorrano, L. (2016). Mitochondrial Cristae: Where Beauty Meets Functionality. *Trends in Biochemical Sciences*, 41(3):261–273.

Cottet-Rousselle, C., Ronot, X., Leverve, X., and Mayol, J. F. (2011). Cytometric assessment of mitochondria using fluorescent probes. *Cytometry Part A*, 79 A(6):405–425.

De Wever, O., Hendrix, A., De Boeck, A., Westbroek, W., Braems, G., Emami, S., Sabbah, M., Gespach, C., and Bracke, M. (2010). Modeling and quantification of cancer cell invasion through collagen type I matrices. *International Journal of Developmental Biology*, 54(5):887–896.

Deas, E., Wood, N. W., and Plun-Favreau, H. (2011). Mitophagy and Parkinson's disease: The PINK1-parkin link. *Biochimica et Biophysica Acta - Molecular Cell Research*, 1813(4):623–633.

Delettre, C., Griffoin, J. M., Kaplan, J., Dollfus, H., Lorenz, B., Faivre, L., Lenaers, G., Belenguer, P., and Hamel, C. P. (2001). Mutation spectrum and splicing variants in the OPA1 gene. *Human Genetics*, 109(6):584–591.

Delettre, C., Lenaers, G., Griffoin, J. M., Gigarel, N., Lorenzo, C., Belenguer, P., Pelloquin, L., Grosgeorge, J., Turc-Carel, C., Perret, E., Astarie-Dequeker, C., Lasquellec,

L., Arnaud, B., Ducommun, B., Kaplan, J., and Hamel, C. P. (2000). Nuclear gene OPA1, encoding a mitochondrial dynamin-related protein, is mutated in dominant optic atrophy. *Nature Genetics*, 26(2):207–210.

DeVay, R. M., Dominguez-Ramirez, L., Lackner, L. L., Hoppins, S., Stahlberg, H., and Nunnari, J. (2009). Coassembly of Mgm1 isoforms requires cardiolipin and mediates mitochondrial inner membrane fusion. *Journal of Cell Biology*, 186(6):793–803.

Duvezin-Caubet, S., Koppen, M., Wagener, J., Zick, M., Israel, L., Bernacchia, A., Jagasia, R., Rugarli, E. I., Imhof, A., Neupert, W., Langer, T., and Reichert, A. S. (2007). OPA1 Processing Reconstituted in Yeast Depends on the Subunit Composition of the m-AAA Protease in Mitochondria. *Molecular Biology of the Cell*, 18(9):3582–3590.

Epand, R. F., Schlattner, U., Wallimann, T., Lacombe, M.-L., and Epand, R. M. (2007). Novel lipid transfer property of two mitochondrial proteins that bridge the inner and outer membranes. *Biophysical Journal*, 92(1):126–37.

Ernster, L. and Schatz, G. (1981). Mitochondria : A Historical Review. *The Journal of Cell Biology*, 91:227–255.

Fiedorczuk, K., Letts, J. A., Degliesposti, G., Kaszuba, K., Skehel, M., and Sazanov, L. A. (2016). Atomic structure of the entire mammalian mitochondrial complex I. *Nature*, 538(7625):1–21.

Folch, J., Lees, M., and Stanley, G. H. S. (1957). A simple method for the isolation and purification of total lipides from animal. *Journal of Biological Chemistry*, (226):497–509.

Fritah, A., Saucier, C., De Wever, O., Bracke, M., Bièche, I., Lidereau, R., Gespach, C., Drouot, S., Redeuilh, G., and Sabbah, M. (2008). Role of WISP-2/CCN5 in the maintenance of a differentiated and noninvasive phenotype in human breast cancer cells. *Molecular and Cellular Biology*, 28(3):1114–23.

Gout, I., Dhand, R., Hiles, I. D., Fry, M. J., Panayotou, G., Das, P., Truong, O., Totty, N. F., Hsuan, J., Booker, G. W., Campbell, I. D., and Waterfield, M. D. (1993). The GTPase dynamin binds to and is activated by a subset of SH3 domains. *Cell*, 75(1):25–36.

Griparic, L., Kanazawa, T., and van der Bliek, A. M. (2007). Regulation of the mitochondrial dynamin-like protein Opa1 by proteolytic cleavage. *The Journal of Cell Biology*, 178(5):757–764.

Griparic, L. and Van Der Bliek, A. M. (2005). Assay and properties of the mitochondrial dynamin related protein Opa1. *Methods in Enzymology*, 404(05):620–631.

Gustafsson, C., Govindarajan, S., and Minshull, J. (2004). Codon bias and heterologous protein expression. *Trends in Biotechnology*, 22(7):346–353.

Hermann, M.-R., Jakobson, M., Colo, G. P., Rognoni, E., Jakobson, M., Kupatt, C., Posern, G., and Fassler, R. (2016). Integrins synergise to induce expression of the MRTF-A-SRF target gene ISG15 for promoting cancer cell invasion. *Journal of cell science*, 129(7):1391–1403.

Hinckelmann, M.-V., Virlogeux, A., Niehage, C., Poujol, C., Choquet, D., Hoflack, B., Zala, D., and Saudou, F. (2016). Self-propelling vesicles define glycolysis as the minimal energy machinery for neuronal transport. *Nature Communications*, 7:1–13.

Horvath, S. E. and Daum, G. (2013). Lipids of mitochondria. *Progress in Lipid Research*, 52(4):590–614.

Huang, W., Cen, S., Kang, X.-L., Wang, W.-F., Wang, Y., and Chen, X. (2016). TGF-beta1-induced Fascin1 promotes cell invasion and metastasis of human 786-0 renal carcinoma cells. *Acta Histochemica*, 118(2):144–151.

Huberts, D. H. E. W. and van der Klei, I. J. (2010). Moonlighting proteins: An intriguing mode of multitasking. *Biochimica et Biophysica Acta*, 1803(4):520–525.

Ingerman, E. and Nunnari, J. (2006). A continuous, regenerative coupled GTPase assay for dynamin-related proteins. *Methods in Enzymology*, 404(1995):611–619.

Ishihara, N., Fujita, Y., Oka, T., and Mihara, K. (2006). Regulation of mitochondrial morphology through proteolytic cleavage of OPA1. *The EMBO Journal*, 25(13):2966–2977.

Jacobus W and Evans, J. (1977). Nucleoside Diphosphokinase of Rat Heart Mitochondria. *The Journal of Biological Chemistry*, 252(12):4232–4241.

Jeffery, C. J. (1999). Moonlighting proteins. *Trends in Biochemical Sciences*, 24(1):8–11.

Jeffery, C. J. (2003). Moonlighting proteins: Old proteins learning new tricks. *Trends in Genetics*, 19(8):415–417.

Jevševar, S., Gaberc-Porekar, V., Fonda, I., Podobnik, B., Grdadolnik, J., and Menart, V. (2005). Production of nonclassical inclusion bodies from which correctly folded protein can be extracted. *Biotechnology Progress*, 21(2):632–639.

Jin, S. M. and Youle, R. J. (2012). PINK1- and Parkin-mediated mitophagy at a glance. *Journal of Cell Science*, 125(Pt 4):795–799.

Kagan, V. E., Bayir, H. A., Belikova, N. A., Kapralov, O., Tyurina, Y. Y., Tyurin, V. A., Jiang, J., Stoyanovsky, D. A., Wipf, P., Kochanek, P. M., Greenberger, J. S., Pitt, B., Shvedova, A. A., and Borisenko, G. (2009). Cytochrome c/cardiolipin relations in mitochondria: a kiss of death. *Free Radical Biology & Medicine*, 46(11):1439–1453.

Kagan, V. E., Chu, C. T., Tyurina, Y. Y., Cheikhi, A., and Bayir, H. (2014). Cardiolipin asymmetry, oxidation and signaling. *Chemistry and Physics of Lipids*, 179:64–69.

Kagan, V. E., Jiang, J., Huang, Z., Tyurina, Y. Y., Desbourdes, C., Cottet-Rousselle, C., Dar, H. H., Verma, M., Tyurin, V. A., Kapralov, A. A., Cheikhi, A., Mao, G., Stolz, D., St. Croix, C. M., Watkins, S., Shen, Z., Li, Y., Greenberg, M. L., Tokarska-Schlattner, M., Boissan, M., Lacombe, M.-L., Epand, R. M., Chu, C. T., Mallampalli, R. K., Bayır, H., and Schlattner, U. (2016). NDPK-D (NM23-H4)-mediated externalization of cardiolipin enables elimination of depolarized mitochondria by mitophagy. *Cell Death and Differentiation*, 23:1140–51.

Kagan, V. E., Tyurin, V. A., Jiang, J., Tyurina, Y. Y., Ritov, V. B., Amoscato, A. A., Osipov, A. N., Belikova, N. A., Kapralov, A. A., Kini, V., Vlasova, I. I., Zhao, Q., Zou, M., Di, P., Svistunenko, D. A., Kurnikov, I. V., and Borisenko, G. G. (2005). Cytochrome c acts as a cardiolipin oxygenase required for release of proapoptotic factors. *Nature Chemical Biology*, 1(4):223–232.

Kane, J. F. (1995). Effects of rare codon clusters on high-level expression of heterologous proteins in Escherichia coil. *Current Opinion in Biotechnology*, 6(suppl 7):494–500.

Kaufmann, S. H. and Hengartner, M. O. (2001). Programmed cell death: Alive and well in the new millennium. *Trends in Cell Biology*, 11(12):526–534.

Kroemer, G., Dallaporta, B., and Resche-Rigon, M. (1998). The mitochondrial death/life regulator in apoptosis and necrosis. *Annu Rev Physiol*, 60:619–642.

Kubli, D. A. and Gustafsson, Å. B. (2012). Mitochondria and mitophagy: The yin and yang of cell death control. *Circulation Research*, 111(9):1208–1221.

Kulasingam, V. and Diamandis, E. P. (2013). Fascin-1 is a novel biomarker of aggressiveness in some carcinomas. *BMC Medicine*, 11:1–3.

Kumar, N., Jain, V., Singh, A., Jagtap, U., Verma, S., and Mukhopadhyay, A. (2015). Genome-wide endogenous DAF-16/FOXO recruitment dynamics during lowered insulin signalling in C. elegans. *Oncotarget*, 6(39):41418–41433.

Lacombe, M.-l., Milon, L., Munier, A., Mehus, J. G., and Lambeth, D. O. (2000). The Human Nm23 / Nucleoside Diphosphate Kinases. *Journal of Bioenergetics and Biomembranes*, 32(3):247–258.

Lacombe, M. L., Tokarska-Schlattner, M., Epand, R. F., Boissan, M., Epand, R. M., and Schlattner, U. (2009). Interaction of NDPK-D with cardiolipin-containing membranes: Structural basis and implications for mitochondrial physiology. *Biochimie*, 91(6):779–783.

Laemmli, U. K. (1970). Cleavage of structural proteins during the assembly of the head of bacteriophage T4. *Nature*, 227(5259):680–685.

Landes, T., Emorine, L. J., Courilleau, D., Rojo, M., Belenguer, P., and Arnauné-Pelloquin, L. (2010). The BH3-only Bnip3 binds to the dynamin Opa1 to promote mitochondrial fragmentation and apoptosis by distinct mechanisms. *EMBO reports*, 11(6):459–465.

Leonard, M., Song, B. D., Ramachandran, R., and Schmid, S. L. (2005). Robust colorimetric assays for dynamin's basal and stimulated GTPase activities. *Methods in Enzymology*, 404(1991):490–503.

Li, S., Yao, Y., Xu, R., Pesenti, S., Cottet-Rousselle, C., Rieusset, J., Tokarska-Schlattner, M., Liao, K., Schlattner, U., and Rousseau, D. (2014). ATAD3 is a limiting factor in mitochondrial biogenesis and adipogenesis of white adipocyte-like 3T3-L1 cells. *Molecular and Cellular Biology*, (April):1–46.

Li, X.-X., Tsoi, B., Li, Y.-f., Kurihara, H., and He, R.-r. (2015). Cardiolipin and its different properties in mitophagy and apoptosis. *The Journal of Histochemistry and Cytochemistry*, 63(5):301–11.

Liu, R. and Chan, D. C. (2015). The mitochondrial fission receptor Mff selectively recruits oligomerized Drp1. *Molecular Biology of the Cell*, 26:4466–4477.

Liu, X., Kim, C. N., Yang, J., Jemmerson, R., and Wang, X. (1996). Induction of apoptotic program in cell-free extracts: Requirement for dATP and cytochrome c. *Cell*, 86(1):147–157.

Lu, Y.-C., Chang, J. T., Liao, C.-T., Kang, C.-J., Huang, S.-F., Chen, I.-H., Huang, C.-C., Huang, Y.-C., Chen, W.-H., Tsai, C.-Y., Wang, H.-M., Yen, T.-C., You, G.-R., Chiang, C.-H., and Cheng, A.-J. (2014). OncomiR-196 promotes an invasive phenotype in oral cancer through the NME4-JNK-TIMP1-MMP signaling pathway. *Molecular cancer*, 13:1–14.

Lukanidin, E. and Sleeman, J. P. (2012). Building the niche: the role of the S100 proteins in metastatic growth. *Seminars in Cancer Biology*, 22(3):216–225.

MacVicar, T. and Langer, T. (2016). OPA1 processing in cell death and disease – the long and short of it. *Journal of Cell Science*, 129:2297–2306.

Mannella, C. a., Pfeiffer, D. R., Bradshaw, P. C., Moraru, I. I., Slepchenko, B., Loew, L. M., Hsieh, C. E., Buttle, K., and Marko, M. (2001). Topology of the mitochondrial inner membrane: dynamics and bioenergetic implications. *IUBMB life*, 52(3-5):93–100.

Milon, L., Meyer, P., Chiadmi, M., Munier, A., Johansson, M., Karlsson, A., Lascu, I., Capeau, J., Janin, J., and Lacombe, M. L. (2000). The human nm23-H4 gene product is a mitochondrial nucleoside diphosphate kinase. *Journal of Biological Chemistry*, 275(19):14264–14272.

Milon, L., Rousseau-Merck, M. F., Munier, A., Erent, M., Lascu, L., Capeau, J., and Lacombe, M. L. (1997). nm23-H4, a new member of the family of human nm23/nucleoside diphosphate kinase genes localised on chromosome 16p13. *Human Genetics*, 99(4):550–557.

Monaghan, R. M. and Whitmarsh, A. J. (2015). Mitochondrial Proteins Moonlighting in the Nucleus. *Trends in Biochemical Sciences*, 40(12):728–735.

Nagaraj, R., Sharpley, M. S., Chi, F., Braas, D., Zhou, Y., Kim, R., Clark, A. T., and Banerjee, U. (2017). Nuclear Localization of Mitochondrial TCA Cycle Enzymes as a Critical Step in Mammalian Zygotic Genome Activation. *Cell*, 168(1):210–223.

Nawrocki Raby, B., Polette, M., Gilles, C., Clavel, C., Strumane, K., Matos, M., Zahm, J. M., Van Roy, F., Bonnet, N., and Birembaut, P. (2001). Quantitative cell dispersion analysis: new test to measure tumor cell aggressiveness. *International Journal of Cancer*, 93(5):644–52.

Nguyen, T. and Mege, R. M. (2016). N-Cadherin and Fibroblast Growth Factor Receptors crosstalk in the control of developmental and cancer cell migrations. *European Journal of Cell Biology*, 95(11):415–426.

Olichon, A., Elachouri, G., Baricault, L., Delettre, C., Belenguer, P., and Lenaers, G. (2007). OPA1 alternate splicing uncouples an evolutionary conserved function in mitochondrial fusion from a vertebrate restricted function in apoptosis. *Cell Death and Differentiation*, 14(4):682–92.

Olichon, A., Emorine, L. J., Descoins, E., Pelloquin, L., Brichese, L., Gas, N., Guillou, E., Delettre, C., Valette, A., Hamel, C. P., Ducommun, B., Lenaers, G., and Belenguer, P. (2002). The human dynamin-related protein OPA1 is anchored to the mitochondrial inner membrane facing the inter-membrane space. *FEBS Letters*, 523(1-3):171–176.

O'Rourke, B. (2010). From bioblasts to mitochondria : ever expanding roles of mitochondria in cell physiology. *Frontiers in Physiology*, 1:1–4.

Osman, C., Voelker, D. R., and Langer, T. (2011). Making heads or tails of phospholipids in mitochondria. *Journal of Cell Biology*, 192(1):7–16.

Otzen, D. (2011). Protein-surfactant interactions: A tale of many states. *Biochimica et Biophysica Acta - Proteins and Proteomics*, 1814(5):562–591.

Ovadi, J. and Srere, P. A. (2000). Macromolecular compartmentation and channeling. *International Review of Cytology*, 192:255–280.

Parsons, M. J. and Green, D. R. (2010). Mitochondria in cell death. *Essays in Biochemistry*, 47:99–114.

Patocs, A., Zhang, L., Xu, Y., Weber, F., Caldes, T., Mutter, G. L., Platzer, P., and Eng, C. (2007). Breast-cancer stromal cells with TP53 mutations and nodal metastases. *The New England Journal of Medicine*, 357(25):2543–2551.

Perkins, D. N., Pappin, D. J. C., Creasy, D. M., and Cottrell, J. S. (1999). Probability-based protein identification by searching sequence databases using mass spectrometry data. *Electrophoresis*, 20(18):3551–3567.

Pernas, L. and Scorrano, L. (2016). Mito-Morphosis: Mitochondrial Fusion, Fission, and Cristae Remodeling as Key Mediators of Cellular Function. *Annual Review of Physiology*, 78(1):505–531.

Pieri, L., Chafey, P., Le Gall, M., Clary, G., Melki, R., and Redeker, V. (2016). Cellular response of human neuroblastoma cells to ??-synuclein fibrils, the main constituent of Lewy bodies. *Biochimica et Biophysica Acta - General Subjects*, 1860(1):8–19.

Prévilon, M., Le Gall, M., Chafey, P., Federeci, C., Pezet, M., Clary, G., Broussard, C., François, G., Mercadier, J.-J., and Rouet-Benzineb, P. (2013). Comparative differential proteomic profiles of nonfailing and failing hearts after in vivo thoracic aortic constriction in mice overexpressing FKBP12.6. *Physiological Reports*, 1(3):1–27.

Qin, X., Zhang, H., Zhou, X., Wang, C., Zhang, H., Zhang, X., and Ye, L. (2007). Proliferation and migration mediated by Dkk-1/Wnt/beta-catenin cascade in a model of hepatocellular carcinoma cells. *Translational Research*, 150(5):281–294.

Quan, A. and Robinson, P. J. (2006). Rapid purification of native dynamin I and colorimetric GTPase assay. *Methods in Enzymology*, 404(05):556–569.

Quirós, P. M., Mottis, A., and Auwerx, J. (2016). Mitonuclear communication in homeostasis and stress. *Nature Reviews Molecular Cell Biology*, 17(4):213–226.

Rosano, G. L. and Ceccarelli, E. A. (2014). Recombinant protein expression in Escherichia coli: Advances and challenges. *Frontiers in Microbiology*, 5:1–17.

Rouser, G., Fkeischer, S., and Yamamoto, A. (1970). Two dimensional then layer chromatographic separation of polar lipids and determination of phospholipids by phosphorus analysis of spots. *Lipids*, 5(5):494–496.

Rudolph, R. and Lilie, H. (1996). In vitro folding. *FASEB Journal*, 10(1):49–56.

Samant, S. A., Zhang, H. J., Hong, Z., Pillai, V. B., Sundaresan, N. R., Wolfgeher, D., Archer, S. L., Chan, D. C., and Gupta, M. P. (2014). SIRT3 Deacetylates and Activates OPA1 To Regulate Mitochondrial Dynamics during Stress. *Molecular and Cellular Biology*, 34(5):807–819.

Sambrook, J., Fritsch, E. F., and Maniatis, T. (1989). *Molecular cloning a Laboratory manual second Edition vols. 1 2 and 3*. Greene Publishing Associates and John Wiley & Sons, New York.

Sazanov, L. A. (2015). A giant molecular proton pump : structure and mechanism of respiratory complex I. *Nature Reviews Molecular Cell Biology*, 16(6):375–388.

Schein, C. H. and Noteborn, M. H. M. (1988). Formation of Soluble Recombinant Proteins in Escherichia Coli is Favored by Lower Growth Temperature. *Bio/Technology*, 6(3):291–294.

Schindelin, J., Rueden, C. T., Hiner, M. C., and Eliceiri, K. W. (2015). The ImageJ ecosystem: An open platform for biomedical image analysis. *Molecular Reproduction and Development*, 82:518–529.

Schlattner, U., Tokarska-Schlattner, M., Epand, R. M., Boissan, M., Lacombe, M.-L., Klein-Seetharaman, J., and Kagan, V. E. (2015). Mitochondrial NM23-H4/NDPK-D: a bifunctional nanoswitch for bioenergetics and lipid signaling. *Naunyn-Schmiedeberg's Archives of Pharmacology*, 388(2):271–8.

Schlattner, U., Tokarska-Schlattner, M., Ramirez, S., Tyurina, Y. Y., Amoscato, A. A., Mohammadyani, D., Huang, Z., Jiang, J., Yanamala, N., Seffouh, A., Boissan, M., Epand, R. F., Epand, R. M., Klein-Seetharaman, J., Lacombe, M.-L., and Kagan, V. E. (2013a). Dual dunction of mitochondrial Nm23-H4 protein in phosphotransfer and intermembrane lipid transfer: a cadiolipin-dependent switch. *Journal of Biological Chemistry*, 288(1):111–121.

Schlattner, U., Tokarska-Schlattner, M., Rousseau, D., Boissan, M., Mannella, C., Epand, R., and Lacombe, M.-L. (2014). Mitochondrial cardiolipin phospholipid trafficking: the role of membrane contact site complexes and lipid transfer proteins. *Chemistry and Physics of Lipids*, 179:32–41.

Schlattner, U., Tokarska-Schlattner, M., and Wallimann, T. (2013b). *Metabolite Channeling: Creatine Kinase Microcompartments*. Elsevier Inc., Zürich.

Schneider, C. a., Rasband, W. S., and Eliceiri, K. W. (2012). NIH Image to ImageJ: 25 years of image analysis. *Nature Methods*, 9(7):671–675.

Segawa, K. and Nagata, S. (2015). An Apoptotic 'Eat Me' Signal: Phosphatidylserine Exposure. *Trends in Cell Biology*, 25(11):639–650.

Seifert, M., Welter, C., Mehraein, Y., and Seitz, G. (2005). Expression of the nm23 homologues nm23-H4, nm23-H6, and nm23-H7 in human gastric and colon cancer. *The Journal of Pathology*, 205(5):623–632.

Shevchenko, A. and Shevchenko, A. (2001). Evaluation of the efficiency of in-gel digestion of proteins by peptide isotopic labeling and MALDI mass spectrometry. *Analytical Biochemistry*, 296(2):279–283.

Shoushtari, A. N., Szmulewitz, R. Z., and Rinker-Schaeffer, C. W. (2011). Metastasis-suppressor genes in clinical practice: lost in translation? *Nature reviews. Clinical Oncology*, 8(6):333–342.

Singh, A., Upadhyay, V., Upadhyay, A. K., Singh, S. M., and Panda, A. K. (2015). Protein recovery from inclusion bodies of Escherichia coli using mild solubilization process. *Microbial Cell Factories*, 14(1):1–10.

Singh, S. M. and Panda, A. K. (2005). Solubilization and refolding of bacterial inclusion body proteins. *Journal of Bioscience and Bioengineering*, 99(4):303–10.

Skotheim, R. I., Autio, R., Lind, G. E., Kraggerud, S. M., Andrews, P. W., Monni, O., Kallioniemi, O., and Lothe, R. A. (2006). Novel genomic aberrations in testicular germ cell tumors by array-CGH, and associated gene expression changes. *Cellular Oncology*, 28(5-6):315–326.

Söderberg, O., Gullberg, M., Jarvius, M., Ridderstråle, K., Leuchowius, K.-J., Jarvius, J., Wester, K., Hydbring, P., Bahram, F., Larsson, L.-G., and Landegren, U. (2006). Direct observation of individual endogenous protein complexes in situ by proximity ligation. *Nature Methods*, 3(12):995–1000.

Song, Z., Chen, H., Fiket, M., Alexander, C., and Chan, D. C. (2007). OPA1 processing controls mitochondrial fusion and is regulated by mRNA splicing, membrane potential, and Yme1L. *Journal of Cell Biology*, 178(5):749–755.

Soubannier, V., McLelland, G. L., Zunino, R., Braschi, E., Rippstein, P., Fon, E. A., and McBride, H. M. (2012). A vesicular transport pathway shuttles cargo from mitochondria to lysosomes. *Current Biology*, 22(2):135–141.

Srere, P. (1987). Complexes Of Sequential Metabolic Enzymes. *Annual Review of Biochemistry*, 56(1):89–124.

Sriram, G., Martinez, J. A., McCabe, E. R. B., Liao, J. C., and Dipple, K. M. (2005). Single-gene disorders: what role could moonlighting enzymes play? *American Journal of Human Genetics*, 76(6):911–24.

Stafa, K., Tsika, E., Moser, R., Musso, A., Glauser, L., Jones, A., Biskup, S., Xiong, Y., Bandopadhyay, R., Dawson, V. L., Dawson, T. M., and Moore, D. J. (2014). Functional interaction of Parkinson's disease-associated LRRK2 with members of the dynamin GTPase superfamily. *Human Molecular Genetics*, 23(8):2055–2077.

Steeg, P. S., Kopper, L., Thorgeirsson, U. P., Talmadge, E., Liotta, L. a., and Sobep, M. E. (1988). Tumor metastasis, the process by which cells leave a tumor and colonize distant sites, is the major cause of death. *Journal of the Nation Cancer Institute*, 88:200–204.

Stroud, D. A., Surgenor, E. E., Formosa, L. E., Reljic, B., Frazier, A. E., Dibley, M. G., Osellame, L. D., Stait, T., Beilharz, T. H., Thorburn, D. R., Salim, A., and Ryan, M. T. (2016). Accessory subunits are integral for assembly and function of human mitochondrial complex I. *Nature*, 538(7623):1–17.

Studier, F. W. and Moffatt, B. A. (1986). Use of bacteriophage T7 RNA polymerase to direct selective high-level expression of cloned genes. *Journal of Molecular Biology*, 189(1):113–30.

Tatsuta, T., Scharwey, M., and Langer, T. (2014). Mitochondrial lipid trafficking. *Trends in Cell Biology*, 24(1):44–52.

Tokarska-Schlattner, M., Boissan, M., Munier, A., Borot, C., Mailleau, C., Speer, O., Schlattner, U., and Lacombe, M.-L. (2008). The nucleoside diphosphate kinase D (NM23-H4) binds the inner mitochondrial membrane with high affinity to cardiolipin and couples nucleotide transfer with respiration. *The Journal of Biological Chemistry*, 283(38):26198–207.

Traut, T. W. (1994). Physiological concentrations of purines and pyrimidines. *Molecular and Cellular Biochemistry*, 140(1):1–22.

Van Wuytswinkel, O., Savino, G., and Briat, J. F. (1995). Purification and characterization of recombinant pea-seed ferritins expressed in Escherichia coli: influence of N-terminus deletions on protein solubility and core formation in vitro. *The Biochemical Journal*, 305:253–61.

Vasina, J. A. and Baneyx, F. (1997). Expression of Aggregation-Prone Recombinant Proteins at Low Temperatures: A Comparative Study of the Escherichia coli cspAandtacPromoter Systems. *Protein Expression and Purification*, 9(2):211–218.

Wai, T. and Langer, T. (2016). Mitochondrial Dynamics and Metabolic Regulation. *Trends in Endocrinology & Metabolism*, 27(2):105–117.

Wang, C. and Youle, R. J. (2009). The role of mitochondria in apoptosis. *Annual Review of Genetics*, 43:95–118.

Wasilewski, M., Chojnacka, K., and Chacinska, A. (2017). Protein trafficking at the crossroads to mitochondria. *Biochimica et Biophysica Acta - Molecular Cell Research*, 1864(1):125–137.

Xu, Z.-Y., Chen, J.-S., and Shu, Y.-Q. (2010). Gene expression profile towards the prediction of patient survival of gastric cancer. *Biomedicine & Pharmacotherapy*, 64(2):133–9.

Zala, D., Hinckelmann, M. V., Yu, H., Lyra Da Cunha, M. M., Liot, G., Cordelières, F. P., Marco, S., and Saudou, F. (2013). Vesicular glycolysis provides on-board energy for fast axonal transport. *Cell*, 152(3):479–491.

Zhang, H., Han, Y., Tao, J., Liu, S., Yan, C., and Li, S. (2011). Cellular repressor of E1A-stimulated genes regulates vascular endothelial cell migration by the ILK/AKT/mTOR/VEGF(165) signaling pathway. *Experimental Cell Research*, 317(20):2904–2913.

Zhang, J. (2015). Teaching the basics of autophagy and mitophagy to redox biologists - mechanism and experimental approaches. *Redox Biology*, 4:242–259.

List of Figures

List of Tables

Résumé : Les nucléosides diphosphate kinases (NDPK) sont essentielles pour la génération des nucléosides triphosphates (NTPs) en utilisant l'ATP et des NDPs. L'isoforme mitochondriale de NDPK (NDPK-D), située dans l'espace intermembranaire des mitochondries, possède deux modes de fonctionnement. Dans le premier mode ("phosphotransfert"), la protéine a une activité de kinase comme les autres enzymes NDPK. Dans ce mode de fonctionnement, NDPK-D produit du GTP pour la protéine optique atrophy 1 (OPA1), une GTPase impliquée dans la fusion des mitochondries, et de l'ADP pour le translocateur à adénine (ANT) et l'ATPase mitochondriale pour la régénération d'ATP. Le second mode de fonctionnement est appelé « transfert de lipide » et est lié à la capacité de la protéine à se lier aux phospholipides anioniques, particulièrement la cardiolipine (CL). Dans ce mode NDPK-D peut réticuler les deux membranes mitochondriales et transférer CL de la membrane interne vers la membrane externe des mitochondries, pouvant servir de signal pour la mitophagie et l'apoptose. Ce travail a pour objectif d'étudier plus en détails ces différentes fonctions de NDPK-D. En utilisant des cellules HeLa exprimant de façon stable la protéine sauvage, kinase inactive (mutation H151N) ou incapable de se lier aux lipides (mutation R90D) et des cellules épithéliales de poumons de souris, nous montrons *(i)* une grande proximité entre NDPK-D et OPA1 qui conduit au channeling de GTP par NDPK-D pour OPA1, *(ii)* le rôle essentiel de NDPK-D pour l'externalisation de CL vers la surface des mitochondries pendant la mitophagie, servant de signal de reconnaissance pour le complexe LC3-II-autophagosomes afin d'éliminer les mitochondries endommagées, *(iii)* la possible inhibition de l'externalisation de CL par la présence de complexes NDPK-D/OPA1, et *(iv)* un phénotype pro-métastatique des cellules HeLa exprimant la NDPK-D mutée (H151N ou R90D), caractérisé par un fort potentiel invasif et migratoire, un profil protéique altéré, et des modifications au niveau structural et fonctionnel du réseau mitochondrial. Finalement, une première stratégie d'expression et de purification de la protéine OPA1 entière a été établie pour de futures études in vitro des complexes NDPK-D/OPA1.

Mots-clés : mitochondrie, signalisation de lipides, transfert lipidique, apoptose, mitophagie

Abstract: The nucleoside diphosphate kinases (NDPK) are essential for generation of nucleoside triphosphates (NTPs) using ATP and NDPs. The mitochondrial NDPK isoform (NDPK-D) located in the mitochondrial intermembrane space is found to have two modes of function. First, the phosphotransfer mode in which the protein has a kinase activity like other NDPK enzymes. In this mode, NDPK-D produces GTP for the optic atrophy 1 protein (OPA1), a GTPase involved in mitochondrial fusion, and ADP for the adenylate translocator (ANT) and the mitochondrial ATPase for ATP regeneration. The second mode of function is called lipid transfer and is related to the capacity of NDPK-D to bind anionic phospholipids, especially cardiolipin (CL). In this mode, the protein can cross-link the two mitochondrial membranes and transfer CL from the inner to the outer mitochondrial membrane, which can serve as a signal for mitophagy and apoptosis. This work aims to study these NDPK-D functions in more detail. With the use of HeLa cells stably expressing the wild-type, kinase inactive (H151N mutation) or lipid binding deficient (R90D mutation) NDPK-D and mouse lung epithelial cells, we show *(i)* the close proximity between NDPK-D and OPA1 that leads to GTP channeling from NDPK-D to OPA1, *(ii)* the essential role of NDPK-D for CL externalization to the mitochondrial surface during mitophagy, serving as a recognition signal for LC3-II-autophagosomes to eliminate damaged mitochondria, *(iii)* the possible inhibition of CL externalization due to the presence of NDPK-D/OPA1 complexes, and *(iv)* a pro-metastatic phenotype of HeLa cells expressing either of the NDPK-D mutants (H151N or R90D), characterized by high invasive and migratory potential, altered proteomic profile and changed mitochondrial network structure and function. Finally, a first bacterial expression and purification strategy for full-length OPA1 has been established for future in vitro studies of NDPK-D/OPA1 complexes.

Keywords: mitochondria, lipid signaling, lipid trafficking, mitophagy, apoptosis